Australian Government
Bureau of Meteorology

The Centre for Australian Weather and Climate Research
A partnership between CSIRO and the Bureau of Meteorology

CSIRO

Sydney Particle Study- Stage-II

Martin Cope, Melita Keywood, Kathryn Emmerson, Ian Galbally, Kate Boast, Scott Chambers, Min Cheng, Suzanne Crumeyrolle, Erin Dunne, Rosemary Fedele, Rob Gillett, Alan Griffiths, James Harnwell, Jack Katzfey, Dale Hess, Sarah Lawson, Branka Miljevic, Suzie Molloy, Jenny Powell, Fabienne Reisen, Zoran Ristovski, Paul Selleck, Jason Ward, Chuanfu Zhang, Jianrong Zeng

June 2014

www.cawcr.gov.au

QUT Queensland University of Technology
Brisbane Australia

ansto

SINAP 中国科学院上海应用物理研究所
Shanghai Institute of Applied Physics, Chinese Academy of Sciences

Enquiries should be addressed to:
Martin Cope
Project Manager
CSIRO Marine and Atmospheric Research
+61 3 92394647
Martin.Cope@csiro.au

ISBN: 978-1-4863-0359-5

Copyright and Disclaimer

Important Disclaimers

EXECUTIVE SUMMARY

The Sydney Particle Study represents the most comprehensive observation and modelling study of fine particles (with an aerodynamic diameter of less than 2.5 microns) undertaken in Australia. It has leveraged the skills of seven partner organisations (CSIRO, NSW OEH, NSW EPA, ANSTO, QUT, BOM, SINAP) to construct and implement observational and modelling frameworks for investigating the characteristics of particles in Sydney. In so doing, the study was aimed at providing an improved understanding and a quantitative model of the particle sources which contribute to population exposure in the Sydney region. The development of such a capability is a crucial aid to developing State and National policy for reducing the levels of population exposure to fine particles.

The Study included two observational programs (running for approximately one month each), based at Westmead (26 kilometres to the west of the Sydney CBD), which were targeted at characterising particles under summer and autumn conditions. The summer observation program identified sea salt (34%) and organic matter (OM; primary and secondary; 34%) as being the major components of $PM_{2.5}$, with secondary inorganic aerosol (15%), soil (11%) and elemental carbon (6%) also being present in significant amounts. A limited isotopic analysis of the OM carbon (based on six samples) indicated that up to 70% of the analysed carbon is modern- thus secondary organic aerosol formed from biogenic sources. The autumn observation program saw a much reduced sea salt contribution (5%) and an increased contribution from organic matter (57%). The contribution from elemental carbon was also larger (16%) while the secondary inorganic aerosol contribution was the same (15%).

A modelling framework was developed for the Study, consisting of prognostic meteorological modelling capability, a natural and anthropogenic emissions inventory, chemical transport modelling capability, and a methodology for calculating population exposure and health impacts. The framework was used to model both observation periods in detail.

Two meteorological models were used in the framework, CCAM and TAPM, and were assessed to have good agreement with observations. Use of both CCAM and TAPM in this way provided an 'ensemble' for the results. Despite using a simple top-down approach to speciating the anthropogenic total $PM_{2.5}$ emissions into particle components, the modelling

framework was able to simulate most of the significant particle processes identified by the observation programs including sea salt emissions, wood heater emissions, secondary inorganic aerosol production, primary organic aerosol emissions and secondary organic aerosol production from anthropogenic and biogenic precursors. In terms of proportions to compare with the observations mentioned above, in summer the models predicted sea salt (27% CCAM, 19% TAPM), organic matter (OM; primary and secondary; 36% CCAM, 40% TAPM) and for secondary inorganic aerosol (20% CCAM and 21% TAPM%) as being very well predicted compared to the observed proportions. Elemental carbon and soil fractions were less well predicted. In autumn the models predicted the reduced proportion of the sea salt contribution (15% TAPM, 9% TAPM), but the magnitudes were higher than observed. The models under-predicted the organic matter and over-predicted the secondary inorganic aerosol component. However the total mass concentration of $PM_{2.5}$ for seven urban monitoring stations nearby was well predicted to within 20% by both CCAM and TAPM.

The study has culminated with the provision of the data, modelling tools and associated training to the OEH air quality modellers, who will then be well placed to contribute aerosol modelling capability to the science and policy development required for NSW air policy and the National Plan for Clean Air.

ACKNOWLEDGEMENTS

We wish to thank Suzanne Quigley (formerly of NSW OEH) for having the vision to undertake this project; also thanks to Alan Betts for providing the network air quality and meteorological data. Thank you to Nick Agapides from NSW EPA for providing the GMR air emissions inventory and lots of helpful advice. We also thank the staff and management of Westmead Hospital for assistance during the field campaigns.

Contents

1. INTRODUCTION 6

2. BACKGROUND 7

2.1 Health effects 8

3. OBSERVATION AND MODELLING FRAMEWORKS 10

3.1 Observation Framework 10

3.2 Modelling Framework 12

3.2.1 Meteorological modelling 13

3.2.2 Chemical Transport Modelling 13

3.2.3 Emissions 15

4. RESULTS 18

4.1 Summary of meteorological and air quality conditions 18

4.1.1 SPS1 - Summer 2011 18

4.1.2 SPS2 - Autumn 2012 19

4.2 Model performance for the Sydney region 21

4.2.1 Near surface wind and temperature, precipitation 21

4.2.2 Vertical profiles of temperature and wind; mixing depths 29

4.2.3 Observed and modelled NO_x, NO_2, O_3 and $PM_{2.5}$ 36

4.3 Source and chemical contributions of $PM_{2.5}$ at Westmead 41

4.4 Processes- observations and modelling 51

4.4.1 Sea salt 51

4.4.2 Biomass burning 57

4.5 Secondary inorganic particles- sulphate, nitrate and ammonium 67

4.6 Carbon 77

4.6.1 Elemental Carbon 77

4.6.2 Organic Aerosol 77

4.6.3 Observations Of Organic Aerosol Precursors 79

4.6.4 Observed and Modelled VOC Precursor Ratios 81

4.6.5 Secondary Organic Aerosol 86

4.6.6 Aerosol Mass Spectrometer 94

4.7 Particle Growth Events 96

5. CONCLUSIONS AND RECOMMENDATIONS 100

A1. Sampling and analysis methodologies 107

A1.1 Sampling equipment 107

A1.1.1 ANSTO $PM_{2.5}$ ASP sampler 107

A1.2 Analysis techniques 107

A1.2.1 Ion beam analysis (IBA) techniques 107

A1.2.2 Ion chromatography 108

A1.2.3 Organic carbon (OC) and Elemental carbon (EC) analysis 108

A1.2.4 Carbonyls 109

A1.2.5 Volatile organic compounds 110
A1.2.6 Gravimetric Mass Measurement 110
A1.3 Data quality: Analysis 111
A1.3.1 NATA Accreditation 111
A1.3.2 Blank Filters 112
A1.3.3 Ion Balance 112
A1.3.4 WMO Laboratory Inter-comparison 113
A1.3.5 Comparison of Species from IC and IBA analysis 115
A2. OBSERVED AND MODELLED VERTICAL TEMPERATURE AND WIND PROFILES 116
A3. ANSTO RADON AND LIDAR OBSERVATIONS- SPS2 117
A3.1 Radon measurements 117
A3.1.1 Methods 117
A3.1.2 Hourly observations 117
A3.2 Lidar observations 119
A3.2.1 Methods 119
A3.2.2 Boundary layer detection 119
A3.2.3 Clouds and precipitation 121
A3.3 References 122
A4. AEROSOL MASS SPECTROMETER (AMS) 123
A4.1 Instrument Description 123
A4.2 Summary of results 123
A4. PROJECT PAPERS 129
A5. WOODHEATER CASE STUDY 130
A6. POSTER AND ORAL PRESENTATIONS 133
A7. GLOSSARY AND ABBREVIATIONS 136
A8. REFERENCES 145

THE SYDNEY PARTICLE STUDY- STAGE-II

1. INTRODUCTION

The relationship between particle mass (as PM_{10} and $PM_{2.5}$) and health outcomes such as decreased lung function, increased respiratory symptoms, increased chronic obstructive pulmonary disease, increased cardiovascular and cardiopulmonary disease, and increased mortality is now well established. This is well recognised by policy makers in Australia where the Council of Australian Governments has agreed that the initial focus of a new National Plan for Clean Air should be on particles, with the first stage of development being 1/ a health risk assessment; 2/ construction of an exposure reduction framework; 3/ development of emission reduction options and 4/ the undertaking of a cost benefit analysis. As such a quantitative understanding of the sources and sinks of particles within the target airsheds is an essential requirement for achieving the goals of the National Plan for Clean Air.

The NSW Office of the Environment and Heritage (OEH) has been pro-active in undertaking, in collaboration with CSIRO, ANSTO and QUT, the subject of this report- the Sydney Particle Study- comprising two field studies (conducted in February 2011 and April, May 2012), and a program of particle model development and application. During the field studies, observations of particles, particle precursor gases and other relevant environmental data were carried out at the Westmead Air Quality Station within the Sydney basin. The modelling task has seen the coupling of a three-dimensional gas-aerosol chemical transport model with the OEH air emissions inventory and the simulation of key particle processes identified by the field campaigns. The study will culminate with the provision of the data, modelling tools and associated training to the OEH air quality modellers, who will then be well placed to contribute aerosol modelling capability to the science and policy development required for the National Plan for Clean Air.

A summary of outcomes from the first field study (here-in called SPS1) and the related modelling is given in Keywood et al. (2012). In this report we present an analysis of data and modelling based on the second study period (here-in called SPS2), and additionally combine the results of SPS2 (representative of autumn conditions) with those observed in SPS1

(representative of summer conditions). We begin this report by briefly revisiting the sources and sinks of particles and the related health effects. In Section 3 we go on to describe the observational and modelling frameworks. Section 4 begins by summarising the meteorological and air quality conditions observed in SPS1 and SPS2. This is then followed (in Section 4.2) by a brief review of the performance of the modelling framework in simulating key meteorological and air quality parameters within the Sydney airshed for the two study periods. An analysis of the PM_{10} and $PM_{2.5}$ precursor characteristics and our ability to model such characteristics comprises the remainder of Section 4. Conclusions are drawn in Section 5 and the appendices contain more complete descriptions of some data analysis; outputs presented to science and policy communities during the study, together with an application of the modelling framework to investigate the health effects of wood heater usage in Sydney.

A historical perspective is that the first study of this type, the "1969 Pasadena Smog Aerosol Study" (Hidy 1972) was concerned with determining what aerosol was within the air and what were its physical and chemical properties and origin all for one location. This study is concerned with verifying emissions inventories, chemical transformation processes that produce aerosol and validation a model that will have predictive power for urban aerosol across the whole domain of the city and surrounding regions.

2. BACKGROUND

The material that makes up particles in the atmosphere (also called aerosol) comes from two sources. It can be directly emitted into the atmosphere in the solid phase and this is called primary particulate of which examples are wind-blown dust, fly ash and sea salt. There is also material emitted into the atmosphere in gaseous form that is subsequently oxidized and passes from the gas phase to the particulate phase either condensing on existing particles or forming new particles by nucleation: this particulate material is called secondary. Examples of secondary particulate include sulfate particles in power station plumes, much of the organic particles in smog, and a proportion of particles formed in smoke plumes as they traverse the landscape away from the fire. These processes are illustrated in Figure 1. Quantifying the contributions of primary and secondary particles from key sources is central to the development of control strategies for the reduction of population exposure and the incidence of particle-related mortality and morbidity.

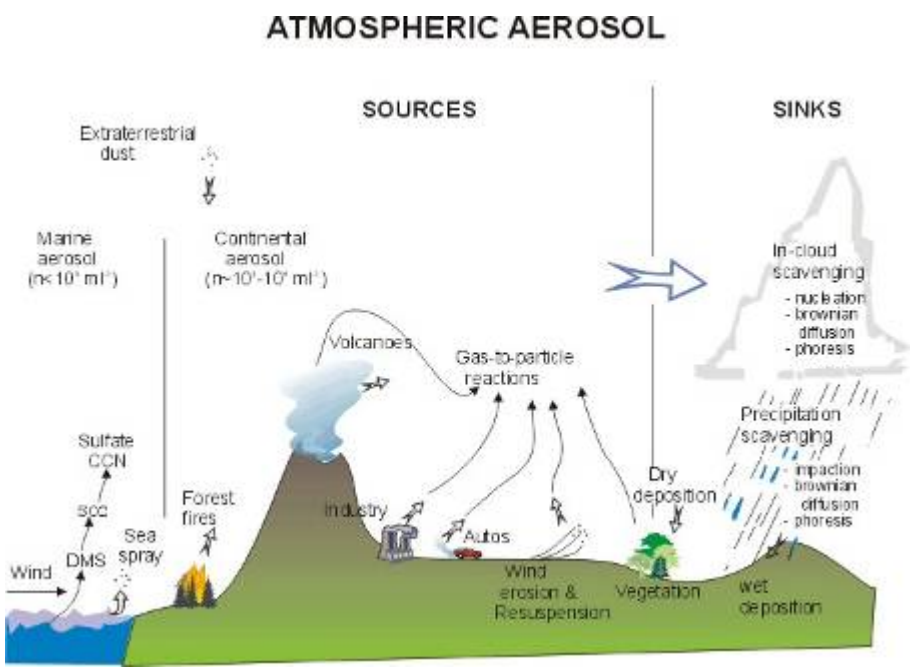

Figure 1. The source of atmospheric particles are natural (sea-salt, dust, biomass burning, volcanoes, biogenic secondary organic aerosol) and man-made (dust, biomass burning, vehicle emissions, secondary organic and inorganic aerosol). Source- http://www.ems.psu.edu/~lno/Meteo437/Aerosol.jpg.

2.1 Health effects

The relationship between particle mass (as PM_{10} and $PM_{2.5}$) and health outcomes such as decreased lung function, increased respiratory symptoms, increased chronic obstructive pulmonary disease, increased cardiovascular and cardiopulmonary disease, and increased mortality is well established (Pope and Dockery, 2006). However, health effects are difficult to quantify given the wide range of metrics associated with particulate matter. Particles can span 4 orders of magnitude in size between 1 nm to 10s of mm. Particles can be present in vast numbers; surface areas; be different shapes (such as spherical, angular); be wholly liquid based or feature some crystalline elements; and span a wide range of chemical complexity, according to source regions and transport. The composition of particles affects the toxicity.

(Ruckerl et al., 2011) showed a linear relationship between increasing PM_{10} concentrations and risk to health, with no threshold below which adverse health effects are not seen. Certain groups of the population are deemed to be more at risk, such as the very young, the elderly and unborn children. However given the widespread nature of particle exposure, the greatest health cost-benefits are seen from a population weighted focus on mitigation, concentrating on reducing exposure in densely populated cities.

Recent thinking has linked the smaller $PM_{2.5}$ fraction with health effects because smaller particles are able to find their way deeper into the lungs (Pope et al., 2002;Pope et al., 2009). However the coarse fraction should not be ignored as it still shows a strong association with asthma and obstructive pulmonary disease (Brunekreef and Forsberg, 2005). Smaller ultrafine particles are also important as they have large surface areas per unit mass, which enables increased surface contact with lung tissue, and as a surface for chemical reaction. It has long been known that the urban source of ultrafine particles scales directly with population (Ayers et al., 1982). The largest source of ultra fine particles in urban areas is from motor vehicles, nucleating from the tail pipe emissions which cool very quickly upon release (Kumar et al., 2010). Roadside particle number concentrations are typically in the range 10^4–10^5 cm^{-3} (Kumar et al., 2011).

Studies linking individual components to health effects cite black carbon (Janssen et al., 2011), coal and oil combustion and sources from vehicles as having a stronger effect than that of PM mass (Laden et al., 2000;Tsai et al., 2000). Of the inorganic compounds, sulfate shows the most common association with asthma (Tsai et al., 2000;Ostro et al., 2011) possibly because the acidity enables further reaction of organic gases (Grahame and Schlesinger, 2005). Metals in particulate matter are also deleterious to health; in particular links have been found with nickel, vanadium, lead and zinc, causing cardiac function changes (Chen and Lippmann, 2009). Other studies examined the purely carcinogenic properties of arsenic, chromium and polycyclic aromatic hydrocarbons present in particles (Harrison et al., 2004).

The relationship between particle concentrations and health impacts is well recognised by state- and federal air quality authorities. Current legislation is based on a mass metric, but an exposure overlay is expected in future. Critical to the new legislation will be the averaging time over which exposure takes place. Further scientific research is needed to better understand the causes of elevated particle concentrations, and to help develop and implement policies to reduce the sources of particles where possible.

3. OBSERVATION AND MODELLING FRAMEWORKS

3.1 Observation Framework

The observations of the Sydney Particle Study (SPS) were carried out in two stages at the Westmead Air Quality Station by teams of scientists from CSIRO, OEH, ANSTO, QUT and SINAP. The Stage I (SPS-I) program was conducted in summer 2011 (from 5 February to 7 March 2011) and the stage-II (SPS-II) was in autumn 2012 (from 16 April to 14 May 2012). Both SPS-I and SPS-II programs involved a comprehensive suite of measurements of atmospheric gases and aerosols in order to better understand the source, the chemical composition and the size distribution of the aerosol and gas-phase secondary aerosol precursors in Sydney.

The sampling program included the measurement of particles, criteria and acid/alkaline gases, speciated VOCs, radon and meteorological parameters. Measurement of particles involved continuous or semi-continuous measurements of aerosol number size distributions, aerosol mass, aerosol light scattering and aerosol composition. Gas-phase secondary aerosol precursors were measured by integrated or continuous measurements of criteria gases (NOx, CO, SO2 and ozone), acid/alkaline gases (NH_3, SO_2, HCl and HNO_3) and speciated VOCs (including carbonyls). Continuous measurements of meteorological parameters temperature, relative humidity (RH) and wind speed/direction were made during the measurement campaigns.

The integrated samples of particles, VOCs and acid/alkaline gas were collected during two periods of each day for most of the measurements; a morning sample was collected between 05:00 and 10:00 and an afternoon sample was collected between 11:00 and 19:00 each day. A third VOCs (adsorbent tube/DNPH sampling) sample was collected overnight between 19:00 and 05:00. A summary of the instruments used, the measurement description and the frequency of the measurement for observations in SPS-I and SPS-II is given in Table 1. A more complete description of the sampling and analysis methodologies is given in Appendix A1.

Table 1. Equipment used at Westmead. Contains descriptions of the instrument used, the measurement description and the frequency of the measurement in SPS1 and SPS2 observations

	Instrument	Measurement	Frequency
Particles	SMPS nano, SMPS (long column) and APS	Size distribution (number) 3-150nm, 15 – 750nm, and 300nm-10 µm	Continuous
	MOUDI	Size resolved mass (12 stage) 0.056µm – 10 µm;	Integrated 2 sample/day on 4 days
	HiVol MOUDI	Size resolved chemistry (6 stage), OC/EC, sugars (incl. Levo.), water soluble ions (0.125 – 10 µm)	Integrated (2 samples/day) on all days
	HiVol $PM_{2.5}$	$PM_{2.5}$, OC/EC, sugars (incl. Levo.), water soluble ions	Integrated (2 samples/day) on all days
	PM2.5 ASP Sampler (ANSTO) (SPS-II only)	$PM_{2.5}$ elemental analysis^	Integrated (2 samples/day) on all days
	RAAS (SPS-I only)	TSP mass, elemental analysis	Integrated (2 samples/day) on all days
	AMS (SPS-I only)	Particle composition as function of size >500nm[#]	Continuous during 2 select periods
	Nephelometer	Light scattering*	continuous
	TEOM (Env NSW)	PM10*	continuous
Criteria gas	Ecotech, Teco analysers	CO, NO, NO_2, NO_y, NO*, NO_y,* O_3*, SO_2*	continuous
Acid/alkaline gas	Gas filter sampler	NH_3, SO_2, HNO_3	Integrated (2 samples/day) on all days
VOCs	PTRMS and adsorbent tube/DNPH sampling	VOCs (incl. carbonyls)	Continuous (PTRMS) and Integrated (3 samples/ day on all days)
Radon	Radon sampler	Radon^	continuous
Meteorology	Met station	Temp*, RH*, wind speed/direction*	continuous

[*]OEH, ^ANSTO, [#]QUT

3.2 Modelling Framework

Figure 2 shows a schematic diagram of the modelling framework used for SPS1 and SPS2. The system comprises a prognostic meteorological modelling capability, an air emissions inventory, chemical transport and particle dynamics modelling capability, and output processing suitable for the estimation of population health effects and similar metrics. The schematic diagram demonstrates how the system is coupled with both the emissions and the chemical transport model being forced by the meteorology.

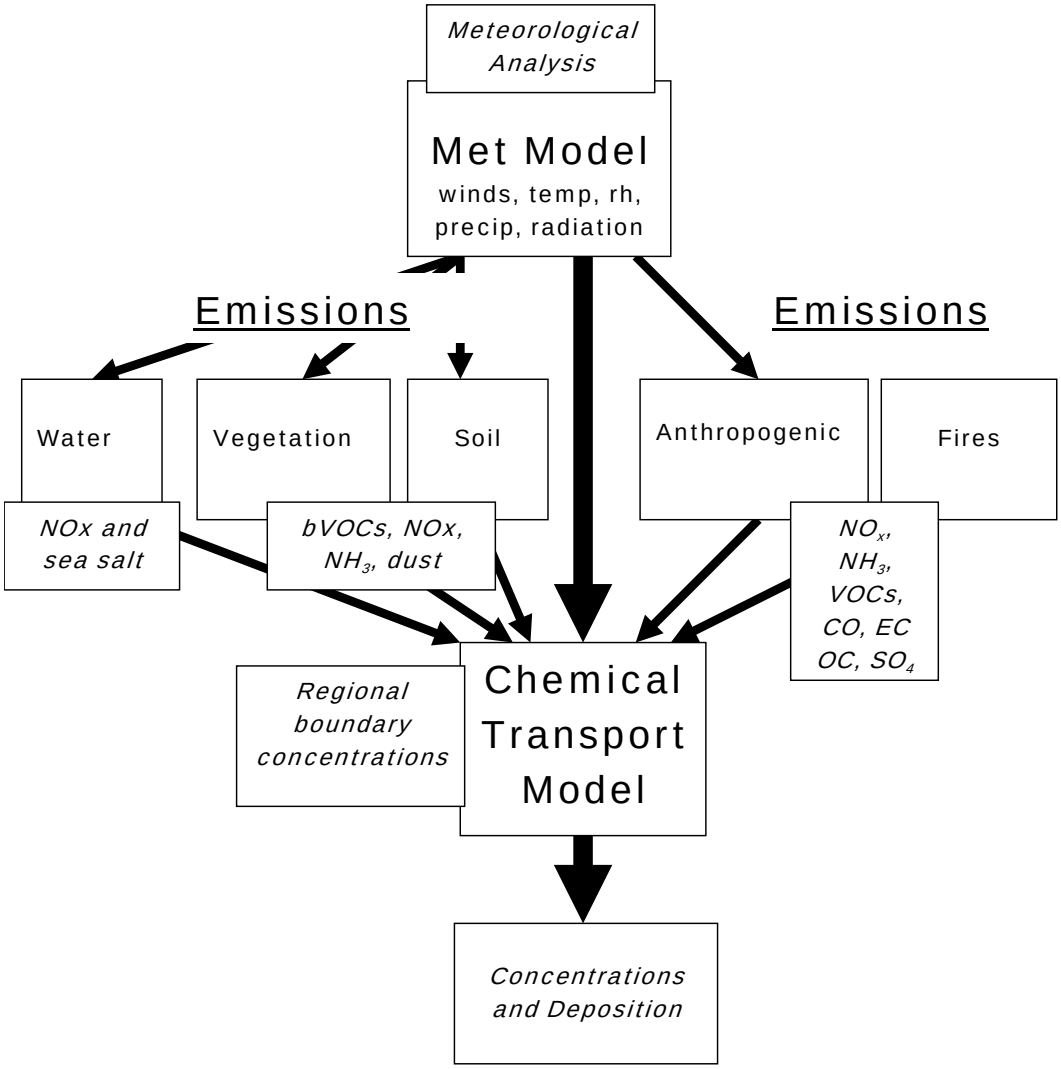

Figure 2. Schematic diagram summarising the SPS particle modelling system. Note VOC -volatile organic carbon; bVOC biogenic component of the same; EC- elemental carbon; OC- organic carbon; NO_x oxides of nitrogen; NH_3 ammonia; SO_4 sulfate.

3.2.1 METEOROLOGICAL MODELLING

Prognostic meteorological modelling was used for the prediction of meteorological fields including wind velocity, temperature, and water vapour mixing ratio (including clouds), radiation and turbulence. The meteorological fields force key components of the emissions and the chemical transport model. Because the accurate prediction of the meteorology is critical for chemical transport modelling, we have generated meteorological fields using two prognostic models- TAPM (Hurley, 2008), a limited area, nest-able, three-dimensional Eulerian numerical weather and air quality prediction system; and CCAM, a global stretched grid atmospheric simulation model (McGregor and Dix, 2008). Note that the framework has the capacity to use meteorological fields generated by the Unified Model[1]. High resolution (1.5 km) forecasts from the Bureau of Meteorology Strategic Enhancement Project[2] have been stored for the period of SPS2, and it is planned to report on these simulations at a later date.

3.2.2 CHEMICAL TRANSPORT MODELLING

The chemical transport and particle dynamics modelling was undertaken by the CSIRO Chemistry Transport Model (CTM; (Cope et al., 2004)). The CTM is a three-dimensional Eulerian chemical transport model with the capability of modelling the emission, transport, chemical transformation, wet and dry deposition of a coupled gas and aerosol phase atmospheric system. The chemical transformation of gas-phase species was modelled using an extended version of the Carbon Bond 5 mechanism (Sarwar et al., 2008) with updated toluene chemistry (Sarwar et al., 2011). The mechanism was also extended to include the gas phase precursors for secondary (gas and aqueous phase) inorganic and organic aerosols. Secondary inorganic aerosols were assumed to exist in thermodynamic equilibrium with gas phase precursors and were modelled using the ISORROPIA-II model (Fountoukis and Nenes, 2007). Secondary organic aerosol (SOA) was modelled using the Volatility Basis Set approach (VBS; (Donahue et al., 2006)). The VBS configuration is similar to that described in Tsimpidi et al (2010). The production of S-VI in cloud water was modelled using the approach described in Seinfeld and Pandis (1998).

[1] http://www.metoffice.gov.uk/research/modelling-systems/unified-model
[2] http://www.bom.gov.au/australia/radar/about/srep.shtml

The CTM can be configured to run in a single moment, multi-component, sectional configuration, or in a two moment, multi-component, multi-modal configuration. The latter uses the Global Model of Aerosol Processes model; (Mann et al., 2010) to simulate particle nucleation, coagulation and condensational growth. The results presented in this report are based on the single moment modelling only which was undertaken for a single particle size - $PM_{2.5}$. The single moment modelling approach has been used initially because, as discussed in the next section, the NSW EPA air emissions do not currently include detailed particle size and component information. However note that an initial attempt was made to add this capability to the inventory and the complete two-moment system was used to investigate particle growth events as discussed in Section 4.7.

Figure 3 shows a typical limited area nested grid system used by the CTM for modelling particles in Sydney. Note that the Australia-wide domain is used to simulate the transport of large scale processes such as windblown dust, sea salt aerosol, managed and unmanaged wildfires. Meteorological fields for this continental-scale modelling were generated from CCAM. CCAM-CTM simulations were undertaken for all but the inner 1 km spaced domain (although CCAM has now also been run at this resolution). Because TAPM is formulated for a horizontally uniform spatial domain without curvature, the maximum domain size is limited to approximately 1000 x 1000 km and thus the TAPM-CTM simulations did not include a continental-scale domain. Instead, the TAPM-CTM outer domain was forced with 15 minute chemical boundary conditions generated on the CCAM-CTM Australia-wide domain. In this way the large scale processes could also be included in the TAPM-CTM simulations. TAPM-CTM was run down to 1 km grid spacing over Sydney.

CCAM-CTM and TAPM-CTM were both run for the period of the two particle observation experiments plus a spin up period of 3–5 days prior to the start of each experiment. CCAM generated meteorological fields using a cycle of initialising the model from a global NCEP analysis, undertaking a 48 hour forecast, stepping forward 24 hours and then repeating the cycle. The second 24 hours of each 48 hour forecast was then used to drive the CTM. In the case of TAPM, the model was run continuously, nested within a GASP or NCEP analysis. The model was also nudged to the near-surface wind vector observations of the Bureau of Meteorology automatic weather station network. Note that TAPM was not nudged to wind observations of the OEH air quality network as we wished to assess the model performance using this data set.

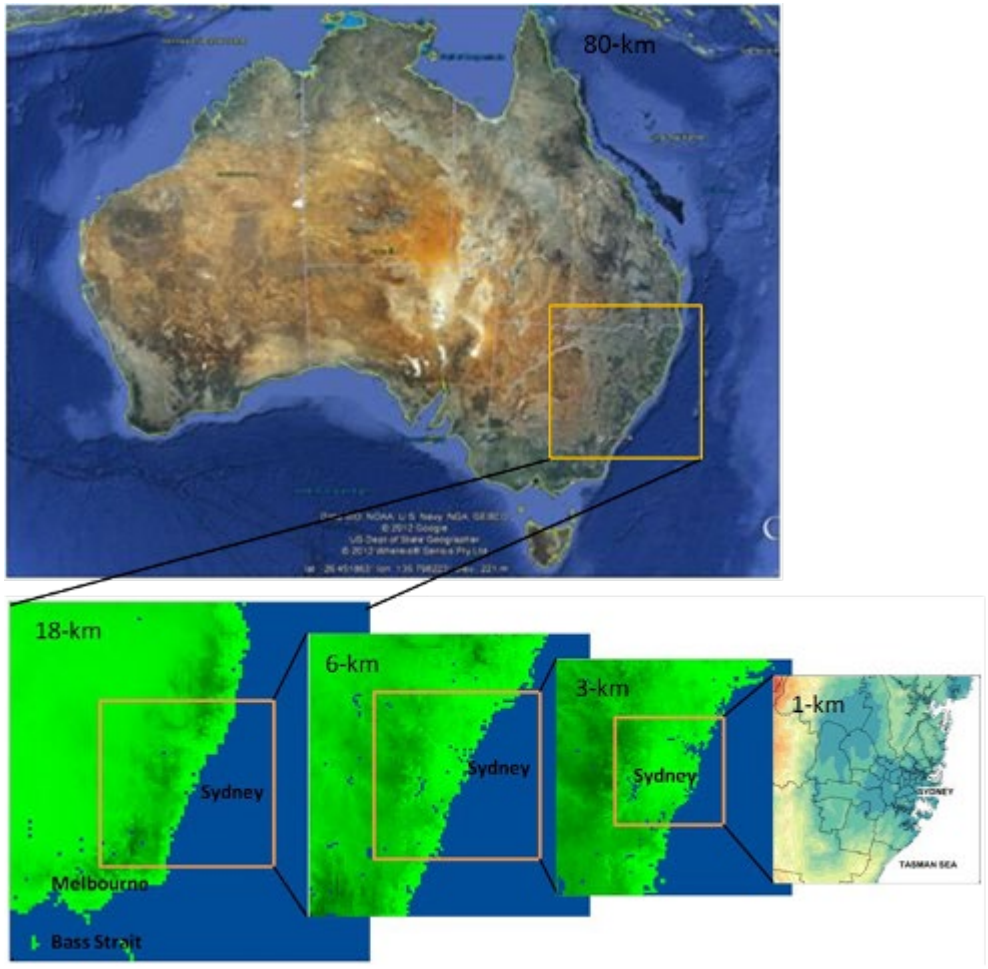

Figure 3. One of the chemical transport modelling domains used for the Sydney Particle Study.

3.2.3 EMISSIONS

ANTHROPOGENIC EMISSIONS. Emissions from roadway, domestic, commercial and industrial sources for the Sydney Greater Metropolitan Region (GMR) were provided by the NSW Department of Environment, Climate Change and Water (now NSW EPA); (DECCW, 2007). These emissions were provided as area sources (i.e. an emission rate from the surface of a 1 km x 1 km area) or point sources (i.e. a specific location with stack properties including the height and radius of the stack, the temperature of the effluent and its velocity). Species in the inventory include NO_x, CO, volatile organic compounds, SO_2 and $PM_{2.5}$. Emissions from the DECCW inventory are based on the year 2003.

Note that NSW EPA has recently published an air emissions inventory for 2008. However the related model-ready data files could not be supplied in time for inclusion in this study. However it was possible to incorporate some significant changes to motor vehicle emissions resulting from emission trends between 2003 and 2008, and the use of a new methodology developed for calculating mobile source emissions. These changes were applied as domain-level scaling factors to the 2003 motor vehicle emissions inventory.

The NSW EPA inventory is currently configured to provide VOC emissions for the Carbon Bond 4 mechanism (while the modelling system is running the CB05 mechanism with an extended set of VOC species). Additionally the inventory currently gives total $PM_{2.5}$ while the model requires emissions of elemental carbon, organic carbon, sulphate, lumped 'other' species and also ammonia (as a precursor for ammonium sulphate and nitrate). Because the inventory files are only available as three lumped source groups (all motor vehicles; all commercial-domestic sources; elevated industrial sources), it is not possible to undertake a detailed bottom up speciation of emissions as required for the CB05 VOCs and the $PM_{2.5}$ mass components. Instead we have adopted a top-down approach based on the Victorian Port Phillip Control Region Air Emissions inventory (which does include a bottom up CB05 speciation for motor vehicles, and $PM_{2.5}$ speciation for all sources) to derive spatially invariant lumped emission factors for the additional species required by the SPS modelling system. These emission factors are shown in Table 2.

NATURAL AND BIOGENIC EMISSIONS. The modelling framework includes methodologies for estimating emissions of sea salt aerosol (Gong, 2003); emissions of windblown dust (Lu and Shao, 1999); gaseous and aerosol emissions from managed and unmanaged wild fires (Meyer et al., 2008); emissions of VOC from vegetation (Azzi et al., 2012) and emissions of nitric oxide and ammonia from vegetation and soils. Emissions from all but the wildfires are calculated inline in the CTM at each time step using the current meteorological fields.

Table 2. Ratios of key gaseous and particle emission components used for the speciation of $PM_{2.5}$, NH_3 and three Carbon Bond 5 organic species.

	NH_3:NO_x	OC25:PM25	EC25:PM25	OT25:PM25	ASO4:PM25	IOLE:OLE	ALDX:ALD	ETHA:PAR
vpx	0.050	0.267	0.086	0.569	0.078	0.185	0.340	0.085
vlx	0.000	0.244	0.143	0.142	0.031	0.491	0.650	0.123
vdx	0.002	0.524	0.392	0.056	0.028	0.374	0.145	0.000
vpv	0.000	0.000	0.000	0.000	0.000	0.808	0.000	0.000
mv	0.024	0.430	0.283	0.239	0.048	0.474	0.153	0.027
gse	1.048	0.391	0.202	0.206	0.200			
whe	0.000	0.619	0.102	0.051	0.228			
pse	0.024	0.235	0.316	0.171	0.278			

Notes:

Data from Delaney and Marshall (2011)

OC25 – organic carbon in the $PM_{2.5}$ size fraction, EC25 – elemental carbon in the $PM_{2.5}$ fraction, OT25 – 'other' particles in the $PM_{2.5}$ fraction, ASO4 – sulphate aerosol, IOLE – internal olefin carbon bond, OLE – terminal olefin carbon bond, ALDX – high molecular weight aldehydes, ALD – acetaldehyde, ETHA – ethane, PAR – higher molecular weight paraffins.

vpx- Petrol vehicle exhaust; vlx- LPG vehicle exhaust; vdx- Diesel vehicle exhaust; vpv- Petrol vehicle evaporative emissions; mv- lumped motor vehicle total; gse commercial-domestic (excluding wood heaters); whe- wood heaters; pse- elevated industrial sources.

4. RESULTS

As noted in the introduction, two observation experiments were carried out at the Westmead Air Quality Station, the first in summer 2011 (5 February and 7 March 2011) and the second in autumn 2012 (April to May 2012). The research team included members of CSIRO, OEH, ANSTO, QUT and SINAP and was led by CSIRO. The sampling programs were designed to generate observations which could be used to better understand the chemical composition, and size distribution of the Sydney $PM_{2.5}$ aerosol, together with the chemical composition of gas-phase secondary aerosol precursors. No equivalent study has occurred before in Australia.

4.1 Summary of meteorological and air quality conditions

4.1.1 SPS1 - SUMMER 2011

Meteorological conditions during SPS1 were not significantly different from the long-term average for the Sydney region (although a La Niña weather pattern was present at the time). February 2011 was mainly dry with north-westerly winds being prevalent due to a series of high pressure systems progressing across the state (BoM, 2011). There was significant rain in the south of NSW until February 6th which was likely influenced by the presence of tropical cyclones Anthony and Yasi in the north of Australia. At Westmead there was 35.4 mm of rain in the month from 6 January to 5 February 2011. The average maximum temperature for the month was 0.7°C above the normal (30.2°C). As there were no extreme high temperature days, photochemical activity was observed to be moderate rather than high.

Table 3 lists the NEPM averaging periods and the ambient air quality standards (AAQS), or the investigation levels; the maximum concentrations observed at Westmead, and this concentration as a fraction of the NEPM; and a comparison of how concentrations observed across all the NSW air quality monitoring stations compare with the NEPM. The bottom half of the table contains guideline NEPMs which are being tested with a view to making an enforceable target.

Maximum 1 hour concentrations of nitrogen dioxide (NO_2) have been peaking around 50 ppb in the last few years (OEH, 2010). The maximum 1 hour concentration observed at Westmead is approximately half of this, and well below the NEPM concentration of 120 ppb. The observed maximum hourly SO_2 concentrations were comparable with the peaks of 8–12% of

the NEPM AAQS routinely measured in NSW. Toluene and the xylenes are usually found at concentrations less than 5% of the NEPM investigation level, and this was also observed at Westmead. NSW OEH considers concentrations of PM_{10} less than 33 $\mu g/m^3$ as low (OEH, 2010) and the maximum observed concentration of Westmead just falls within this category. Wind speeds and mixing rates have been calculated for SPS1. Data is presented as average (min,max). For SPS1 the wind speeds were 1.3 (0.02, 6.5) m/s with mixing rates of 13.6 (4.6, 22.5) g/kg.

4.1.2 SPS2 - AUTUMN 2012

The SPS2 sampling period at Westmead was characterised by warmer than average temperatures across the Sydney region. Average maximums measured at Observatory Hill were 1.2 and 1.5°C above the April (22.4°C) and May (19.4°C) long term averages respectively. However, as would be expected, this is considerably lower than the temperatures experienced during SPS1 in summer 2011. A coastal low pressure trough caused significant rainfall during April, with the bulk of rain falling between the 17th and 19th. Although April experienced above average rainfall, there were fewer rain days (9 at Observatory Hill) compared with the long term average (13 days). In contrast, May experienced the longest dry spell since 2002, with below average rainfall and the fewest cloudy days (3 days) on record.

Peak concentrations of key NEPM pollutants at Westmead all fell comfortably within the NEPM guidelines, although $PM_{2.5}$ reached a peak of nearly 95% of the NEPM concentration. The concentration of PM_{10} in SPS2 (33.0 $\mu g/m^3$) is very close to that of SPS1 (32.7 $\mu g/m^3$), and on the borderline of what is considered a low concentration by NSW OEH. $PM_{2.5}$ was approximately one third higher during SPS2. Peak ozone concentrations at Westmead were similar during both sampling periods, and were 60 – 70% of the NEPM concentrations. This fell towards the upper end of the range for the general NSW % of NEPM.

For SPS2 the wind speeds and mixing rates were lower and with narrower ranges than for SPS1. Again, data is presented as average (min,max). Wind speeds were 1.2 (0.03, 4.6) m/s with mixing rates of 9.0 (3.8, 15.3) g/kg during SPS2.

CO, NO_2, toluene and xylenes were somewhat higher during SPS2, approximately 1.5 – 3 times as much as SPS1. All these pollutants are products of car exhaust (although NO_2 is also produced photochemically) and the higher concentrations may be a result of calmer conditions during autumn with less mixing of the atmosphere.

Table 3. NEPM levels, Westmead highest concentrations and other NSW observations for SPS1 and SPS2

Pollutant	Averaging period	NEPM concentration	Max Observed concentration at Westmead		Westmead % of NEPM		Average NSW monitoring stations[a] % of NEPM	
			SPS1	SPS2	SPS1	SPS2	SPS1	SPS2
Carbon monoxide	8 hours	9000 ppb	276 ppb	887.5 ppb	3.1	9.9	<30	
Nitrogen dioxide	1 hour	120 ppb	26.1 ppb	40 ppb	21.8	33.3	~50	~31
Sulphur dioxide	1 hour	200 ppb	13.8 ppb	9 ppb	6.9	4.5	8-12	2 – 18
Photochemical oxidants (as ozone)	1 hour	100 ppb	60.7 ppb	66 ppb	60.7	66	[b]	44 – 72
	4 hours	80 ppb	56 ppb	53.5 ppb	70	66.9	[b]	49 – 71
Particles as PM_{10}	1 day	50 µg/m^3	32.7 µg/m^3	33.0 µg/m^3	65.4	66	[b]	54 – 104
Particles as $PM_{2.5}$	1 day	25 µg/m^3	17.7 µg/m^3	23.7 µg/m^3	70.8	94.8	[b]	
Formaldehyde	1 day	40 ppb	2.8 ppb	2.7 ppb	7	6.8	11[c]	
Toluene	1 day	1000 ppb	3.1 ppb	4.7 ppb	0.3	0.5	2	
Xylenes (sum)	1 day	250 ppb	1.7 ppb	3.3 ppb	0.7	1.3	4	

[a] data from NSW Office of Environment and Health.
[b] difficult to ascertain as NEPMs can be exceeded due to dust and bushfire events, and due to the meteorology.
[c] Formaldehyde was measured for the first time in NSW over 1 year.

4.2 Model performance for the Sydney region

The two observation experiments were by necessity focussed on the chemical and meteorological characteristics of air masses passing over the Westmead site. However before the modelling system could be used to investigate the particle processes identified from the observations, it was necessary to determine how the system performed in simulating the meteorological and air quality characteristics across the Sydney region as a whole. In this section, we provide a summary of this assessment.

4.2.1 NEAR SURFACE WIND AND TEMPERATURE, PRECIPITATION

Following a recommendation from OEH, we reviewed the performance the CCAM and TAPM predictions of near-surface wind and temperature using data from Randwick, Prospect and St. Mary's monitoring stations. These were selected on the basis of being well exposed sites which were representative of near-coastal, urban, and outer urban conditions in the Sydney region. We also looked at near-surface moisture (mixing ratio) and precipitation- here using Bureau of Meteorology observations at Mascot airport, Bankstown Air Port and Badgery's Creek.

By way of example, Figure 4 and Figure 5 show the hourly time series of observed and modelled wind speed, wind direction and dry bulb temperature for SPS1 and SPS2 respectively, for St Marys monitoring station. Figure 6 shows the observed and modelled frequency distributions for wind speed, temperature and mixing ratio. Note that output from the 3 km spaced model domains have been used for this comparison. It can be seen that the two models perform quite differently at this site, with TAPM predicting higher maximum wind speeds and CCAM predicting lower minimum temperatures, particularly during SPS2. The wind direction predictions are comparable for both models, and qualitatively match the observed variation reasonably well. The frequency distributions in Figure 6 suggest that CCAM is performing a little better than TAPM at this site, certainly with respect to simulating the frequency of light winds and minimum temperatures.

Figure 7 shows the fractional bias of each model at all three sites and demonstrates that by far the largest bias is associated with the 10 m wind speed. This is not an unexpected finding as the observed near surface wind speed is most sensitive to sub-grid scale variations in land use and the associated impact on surface roughness, stability and hence the vertical wind profile.

It is interesting to note too, that the larger wind speed biases are generally associated with SPS2 and may be associated with the weaker forcing present in autumn compared to summer and hence the presence of less organised (and more difficult to model) flow patterns. Neither model stands out as being substantially better or worse in the simulating these near surface variables.

Figure 8 shows the observed and modelled hourly precipitation time series for SPS1 and SPS2 together with the frequency distributions. The plots are for Mascot airport and demonstrate that very little rain was observed in SPS1, and that rainfall was present at the commencement of SPS2. The observed frequency distributions indicate that rainfall was experienced less than 10% of the time. The models on the other hand predict that rain fall was experienced about twice as often as observed, and that the majority of this was in the range 0.2–5 mm h^{-1}. Thus the models tend to drizzle more than was observed. Note that the prediction of too much precipitation can lead to under prediction of the concentrations of hydrophilic particles.

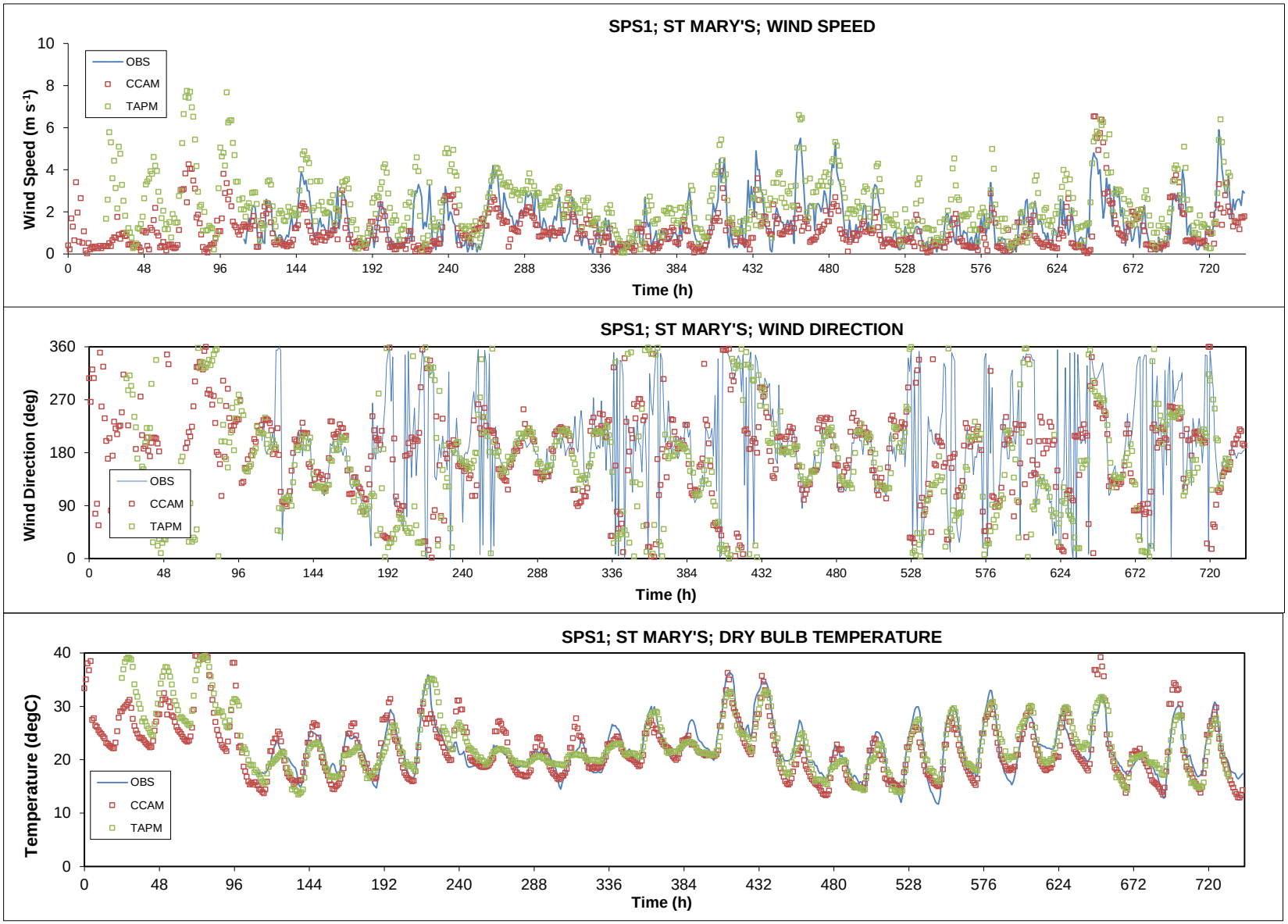

Figure 4. Hourly time series of observed and modelled (top) wind speed; (middle) wind direction; (bottom) temperature for the first study period. The observation site is St Mary's air quality monitoring station.

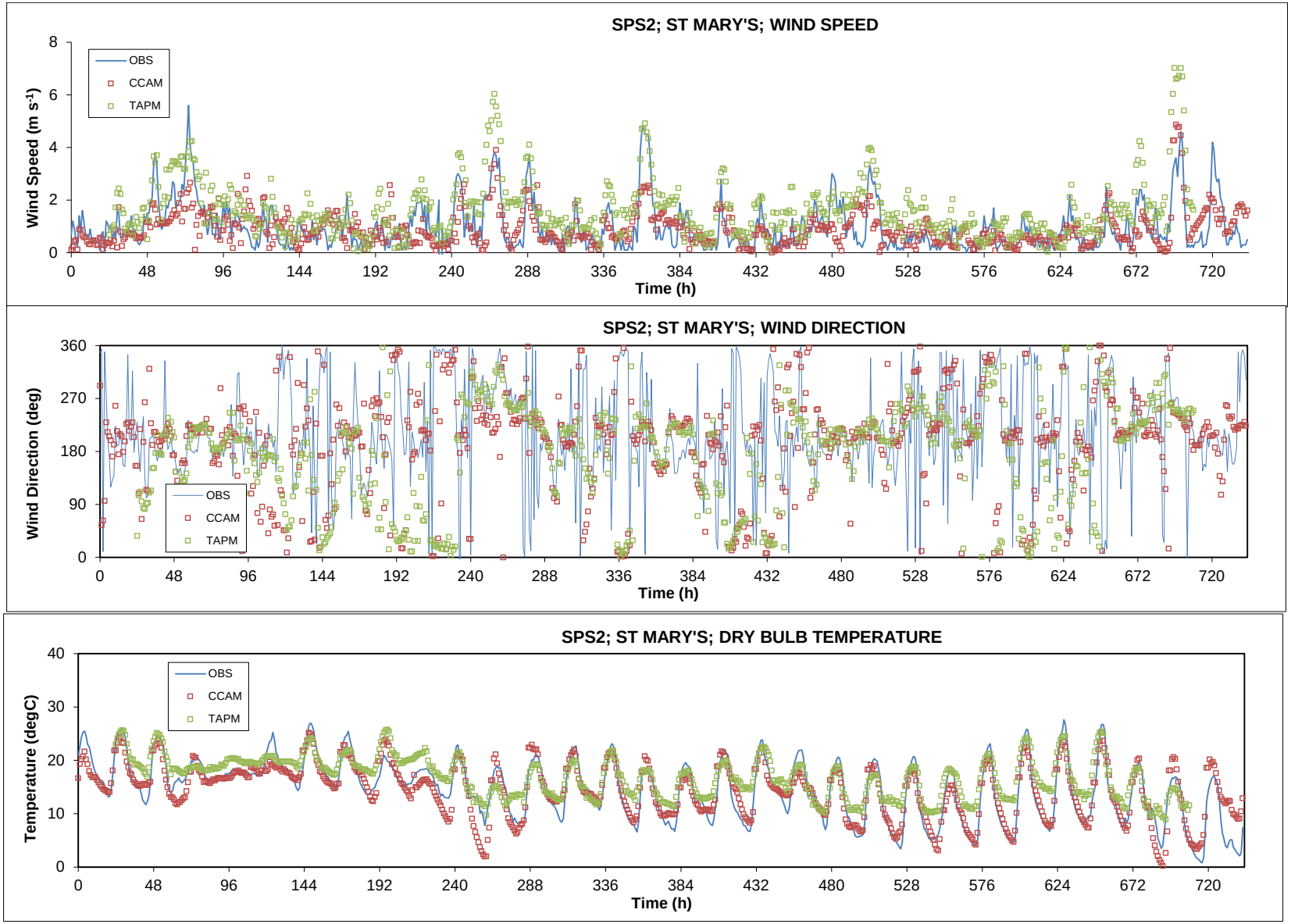

Figure 5. Hourly time series of observed and modelled (top) wind speed; (middle) wind direction; (bottom) temperature for the second study period. The observation site is St Mary's air quality monitoring station.

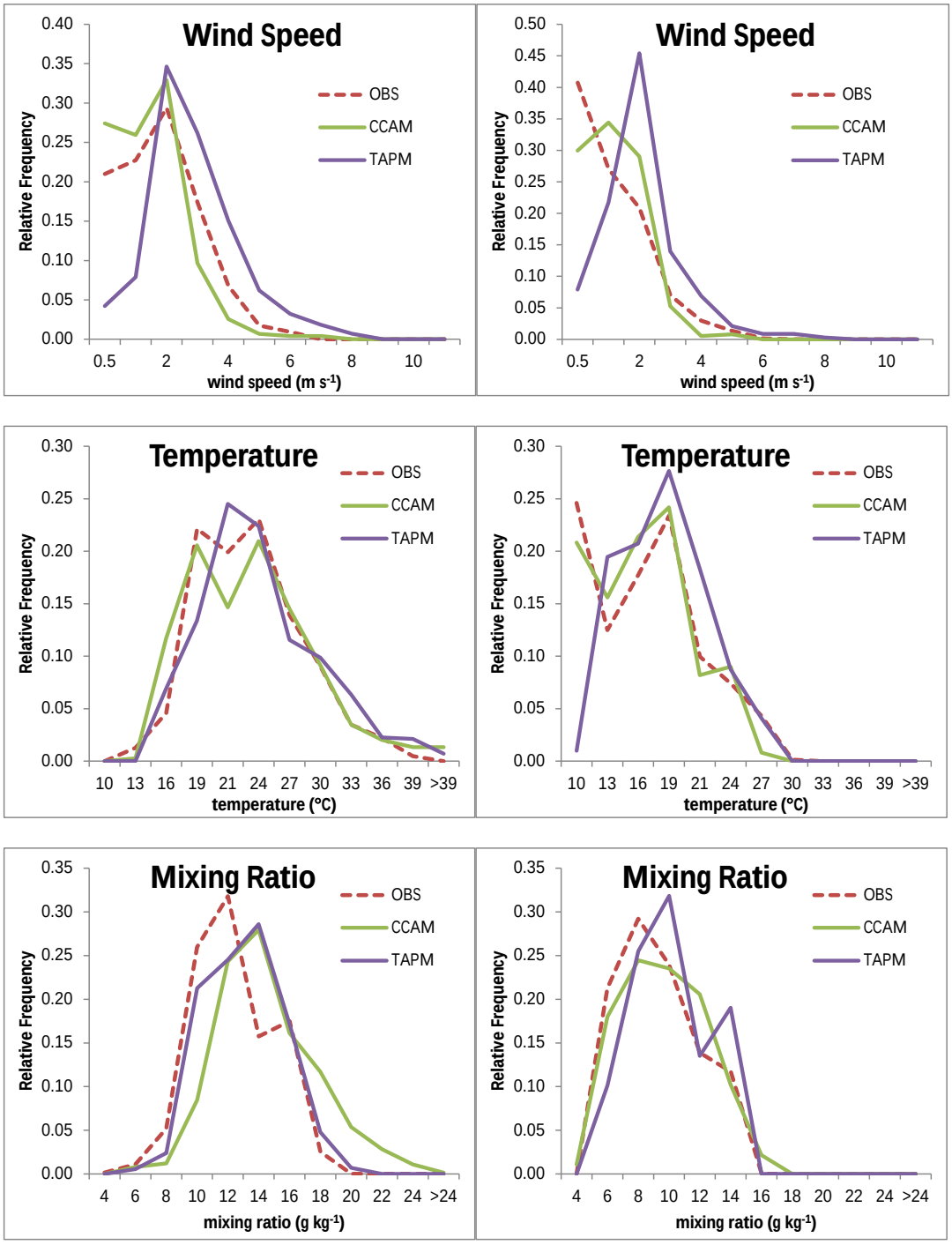

Figure 6. Observed and modelled frequency distributions of hourly wind speed, temperature and water vapour mixing ratio for (left) the first study period SPS1 and (right) the second study period SPS2.

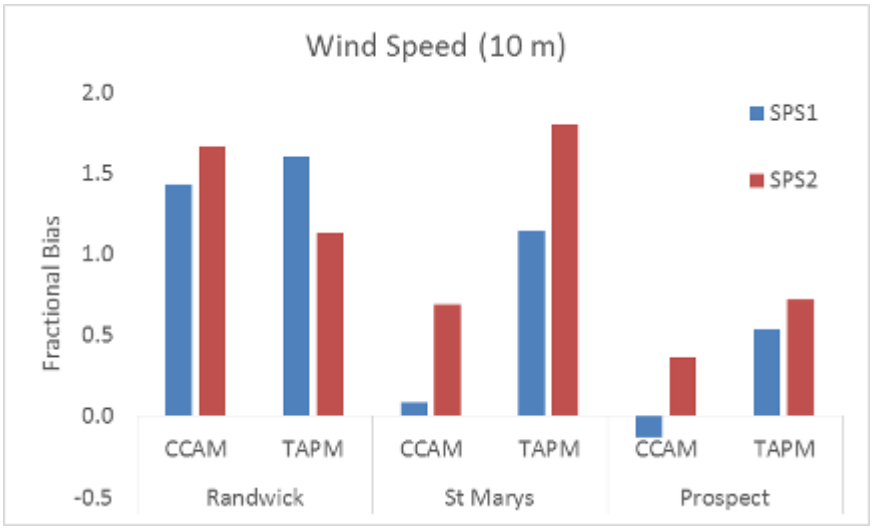

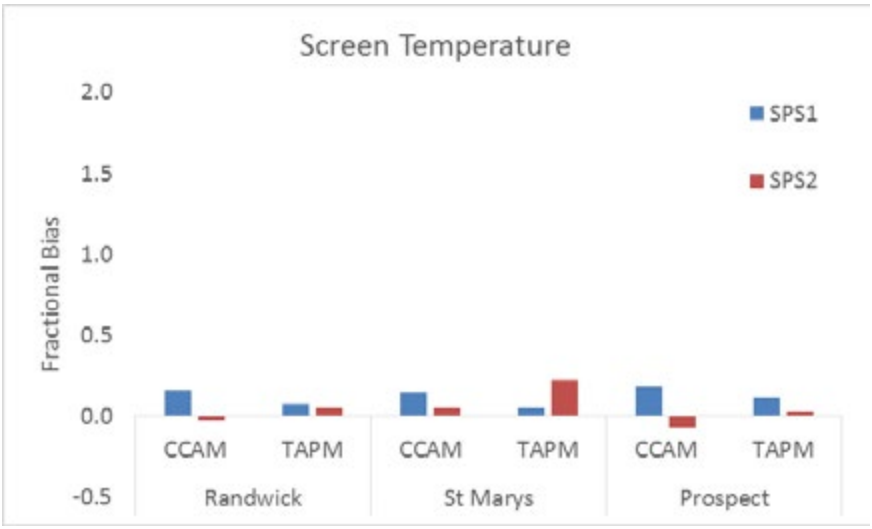

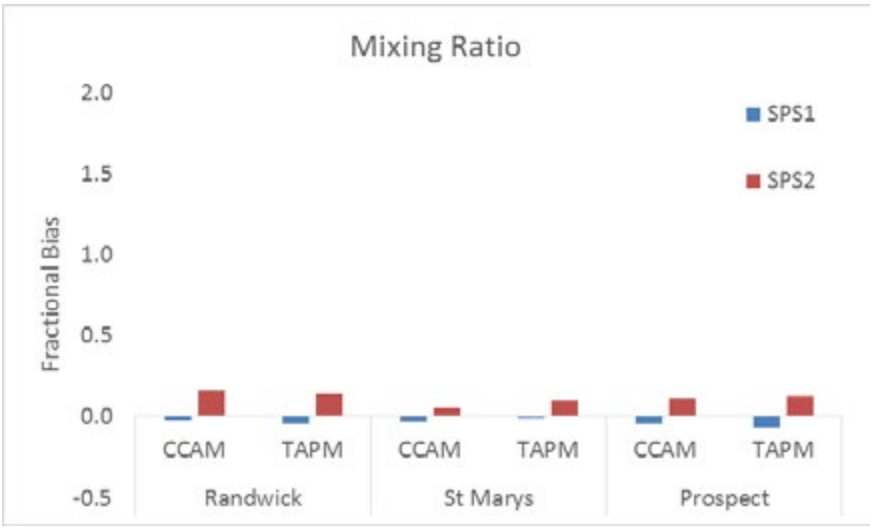

Figure 7. Plots of fractional bias for (top) wind speed; (middle) temperature; bottom (water vapour mixing ratio). The fractional bias is shown for three air quality observation sites and for both meteorological models.

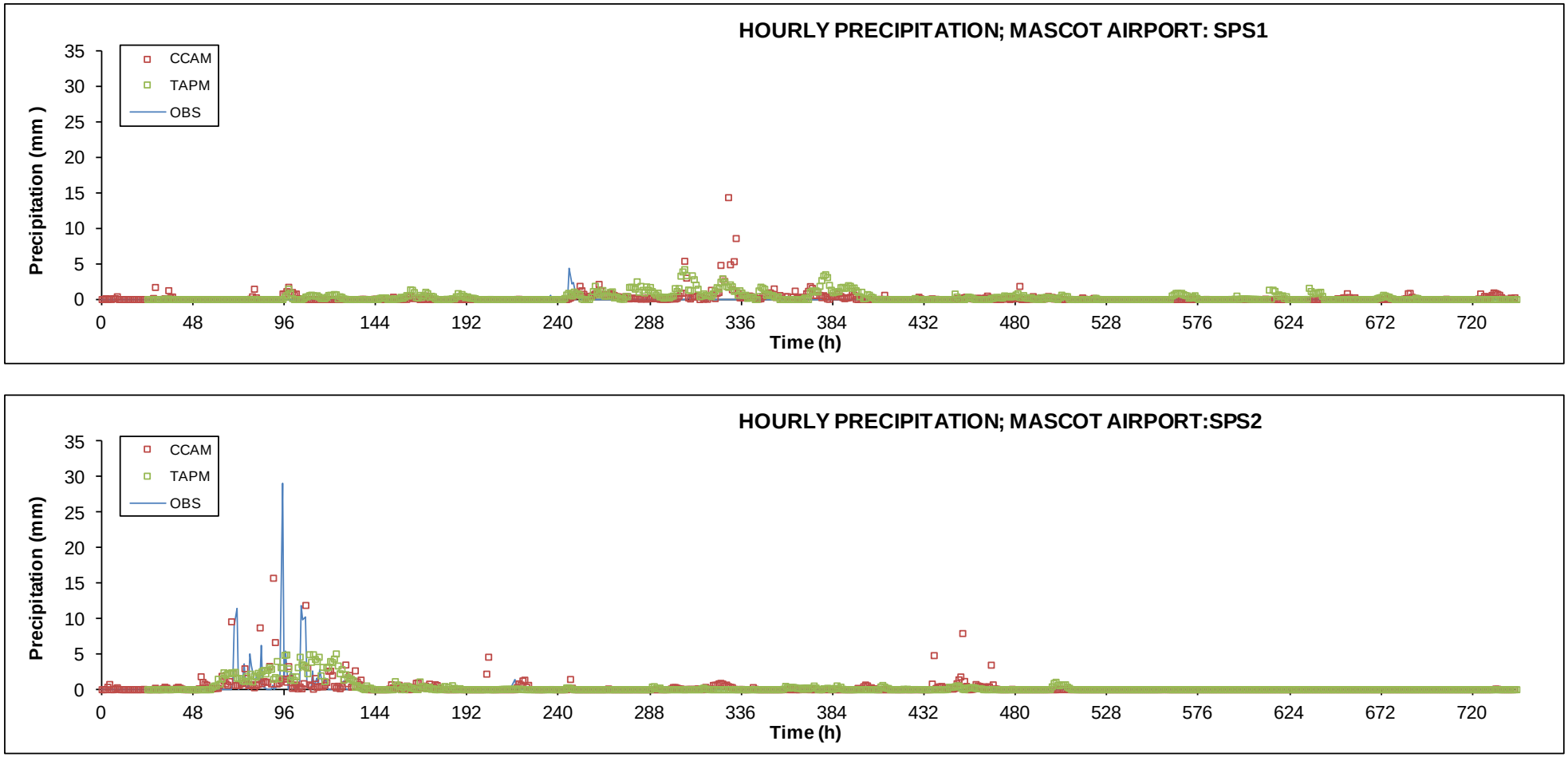

Figure 8. Precipitation. Observed and modelled hourly time series precipitation for Mascot airport top- SPS1, bottom- SPS2.

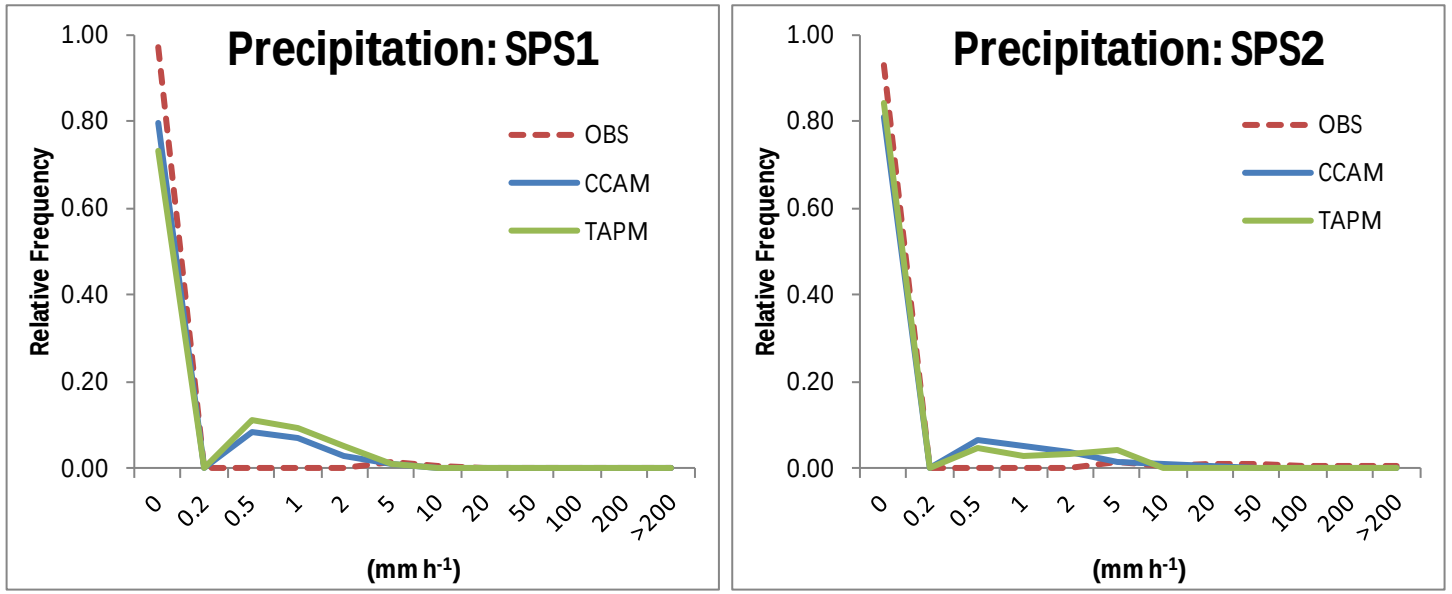

Figure 8- cont....Frequency distributions for SPS1 and SPS2 observed and modelled data.

4.2.2 VERTICAL PROFILES OF TEMPERATURE AND WIND; MIXING DEPTHS

In addition to the near-surface meteorological observations, we have also leveraged automated weather reports obtained from commercial aircraft (AMDAR data) to investigate model skill in simulating vertical profiles of temperature and wind velocity. The temperature profile gives an indication of the boundary layer height- and hence the turbulent mixing depth. The wind velocity provides a measure of the pollutant ventilation and mean transport direction.

The AMDAR data used are measured during take-offs and landings at Sydney Airport, and consist of point samples with an averaging time of 1 second or less. The profiles shown are measured over a period of 5–10 minutes; individual flights are identified by their starting time. The estimated temperature accuracy is 0.5 K and the estimated vector wind accuracy is 1.8 m/s. We also extended the profiles to the surface layer using surface wind and temperature data measured at Westmead and/or Earlwood.

The meteorological models, TAPM and CCAM, provide temperatures and winds at the mean height of the vertical model levels averaged over the grid volume and the time step (a few minutes). Note however that no attempt has been made to interpolate the model temperatures and winds to the flight trajectories. Hence the model profiles are valid at a particular location and the AMDAR profiles are valid along the aircraft flight trajectory. When the atmospheric conditions are spatially homogeneous, the AMDAR and model profiles should agree.

Days and times of interest for secondary aerosol formation are often times of meteorological complexity. However our analysis of the observed and modelled wind and temperature profiles under such conditions suggests that the meteorological models can cope with this complexity except when flows are in transition. For example, the presence of non-steady meso-scale systems, such as an advancing sea breeze circulation, may cause the profiles to disagree for some hours. Because the interaction between synoptic-scale flow and meso-scale circulations is complex, meteorological models may not represent the dynamics correctly (the sea breeze may not penetrate inland far enough, or may be late in arriving, etc.). These defects, or merely the timing of the switch over from convective to stable conditions, can lead to disagreement in the profiles, so that interpretation of the comparison results requires care.

These defects could affect elements of the pollutant exposure at the given locations. We illustrate this point with the following examples taken from SPS1 and SPS2.

For SPS1, we used modelled vertical profiles for a column located close to Earlwood and selected the period 9–11 February for analysis. This was done to coincide with the first observation period of the QUT aerosol mass spectrometer and because some interesting particle growth events were observed during this time. A complete set of observed and modelled vertical profiles is given in Appendix A2.

As an example, Figure 9 shows the vertical potential temperature profiles at 0600 UTC (1700 DST) and 0700 UTC (1800 DST) on 11th February 2011. This was a period of transition from unstable to stable conditions, and thus is a good test of the models' ability to simulate the timing of this process. In this case it can be seen that TAPM has not captured the extent of the cooling in the lower boundary layer at 0600 UTC while CCAM has modelled this situation very well. However TAPM begins to better match the observed cooling at 0700 UTC and this improvement continues into the evening (see Appendix A2).

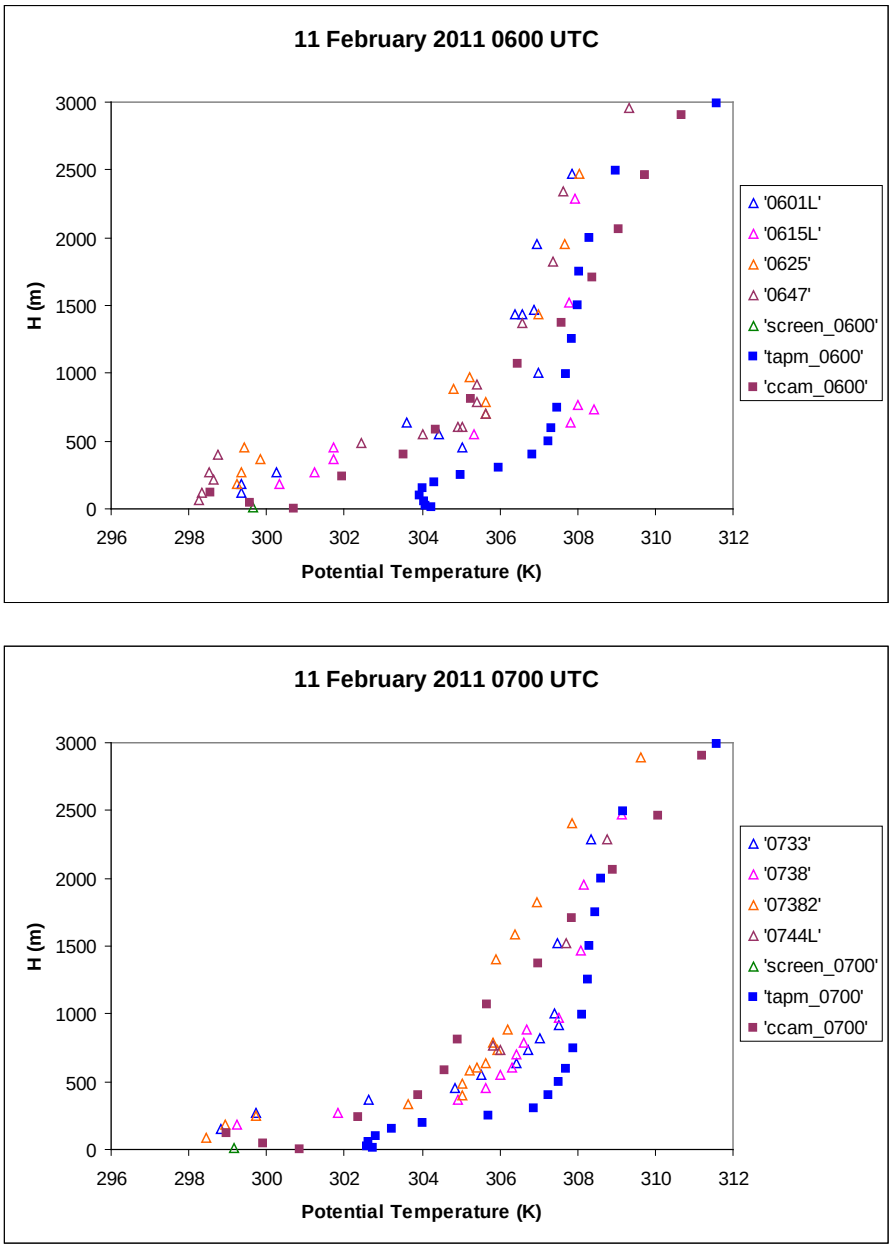

Figure 9. Observed and modelled vertical profiles of potential temperature for hours 6 and 7 UTC (17 and 18 DST) 11th February 2011.

For SPS2, we chose Westmead as the analysis location for vertical profiles because lidar backscatter measurements were made there by ANSTO and these provide an alternative method of observation of the boundary layer height. Here we have focussed on 8th May 2012 because $PM_{2.5}$ concentrations were observed to be elevated at some network sites on this day and also because ANSTO has provided an analysis of the lidar observations for this day (Appendix A3).

Figure 10 shows the convective boundary-layer height, as determined by the lidar backscatter measurements of ANSTO, is approximately 900 m at 1500 EST (0500 UTC; 1600 DST) on 8 May 2012 at Westmead. Figure 11 shows the observed and modelled vertical potential temperature profiles for the same time. It can be seen that TAPM predicts a convective boundary-layer height between 900 – 1000 m, in agreement with the ANSTO measurements. On the other hand, the AMDAR aircraft measurements show a stable boundary layer except for the lowest 90 m. The calculated vertical potential temperature profile from CCAM agrees with these measurements and places the height of the near-surface convective layer at 130 m in agreement with the AMDAR measurements.

Thus at 0500 UTC, TAPM maintains the convective conditions whereas the AMDAR data indicate cooling is occurring in the lower boundary layer. The surface observations are from Westmead. TAPM matches the observed screen temperature better than CCAM does.

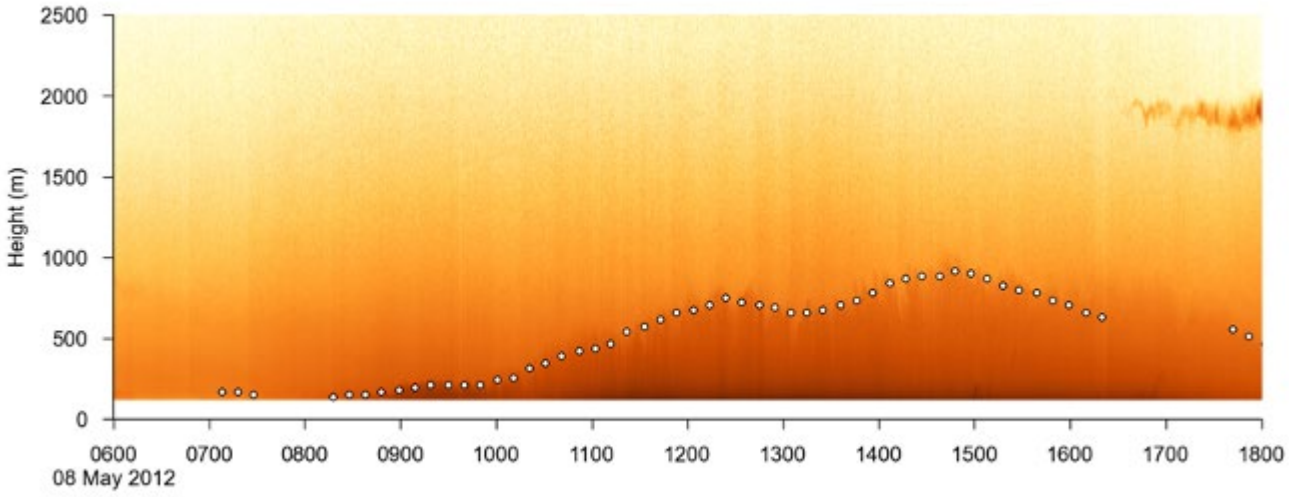

Figure 10. Range-normalised lidar backscatter (indicated by shading, dark colours indicate more signal) for the 8th May 2012, along with the boundary layer height retrieved every 10 minutes during the day (hours are in EST).

The spatial plot of surface winds for a 15 hour period commencing hour 12 (EST) 8th May 2012 (Figure 12) demonstrates how CCAM has not correctly matched the balance between synoptic scale and meso-scale forcing during this period. This has resulted in the model not predicting the generation and inland propagation of a weak sea breeze, nor the low level jet apparent in Figure 12 (an issue also common to TAPM at this time). A comparison of the observed screen temperature at Westmead, and the lower part of the aircraft temperature profiles (at Mascot) demonstrate the strong spatial inhomogeniety of the temperature fields at hour 15 EST. Here, the model errors may result from uncertainties in prescribing synoptic forcing and/or soil

moisture. However, our experience is that although such errors can occur in any of the current state-of-the-art weather prediction models (and this has been the focus of the discussion above), in general the models are able to simulate the observed meteorology with good skill.

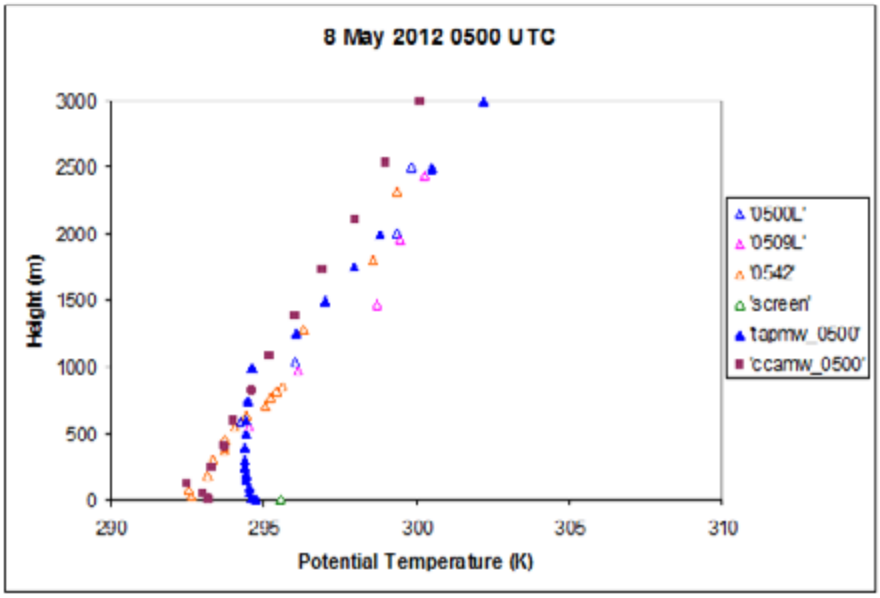

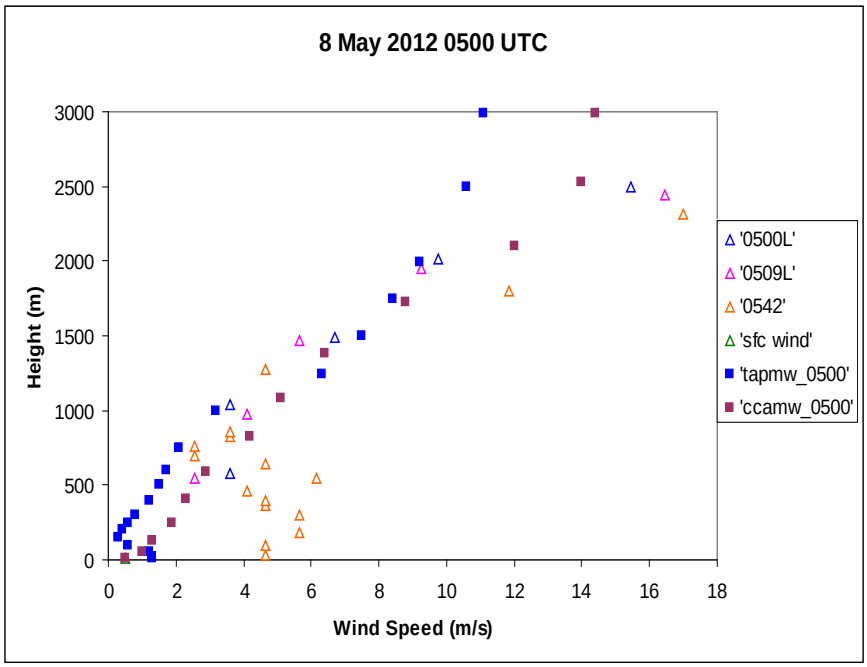

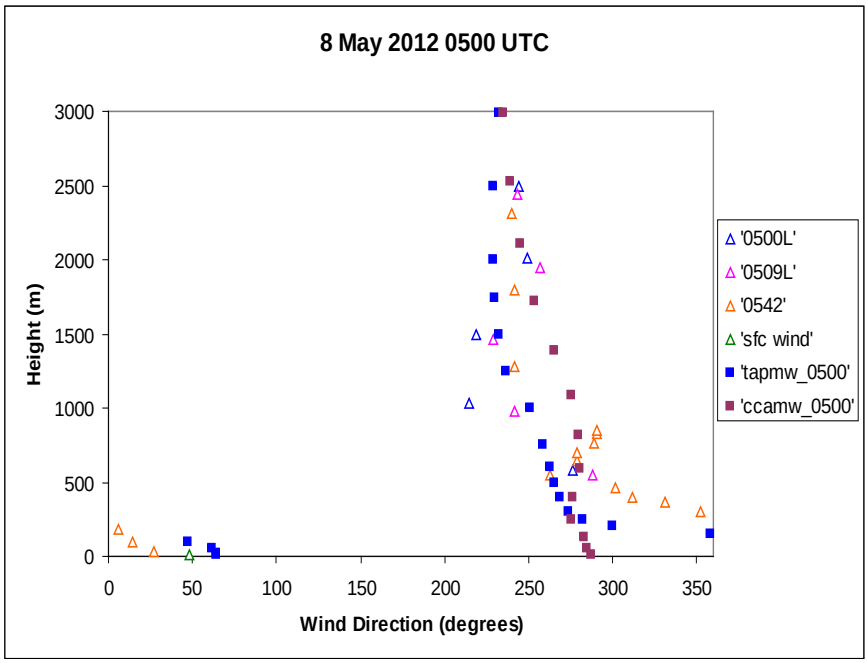

Figure 11. Observed and modelled vertical profiles of potential temperature, wind speed and wind direction for hour 5 UTC (15 LST) 8th May 2012.

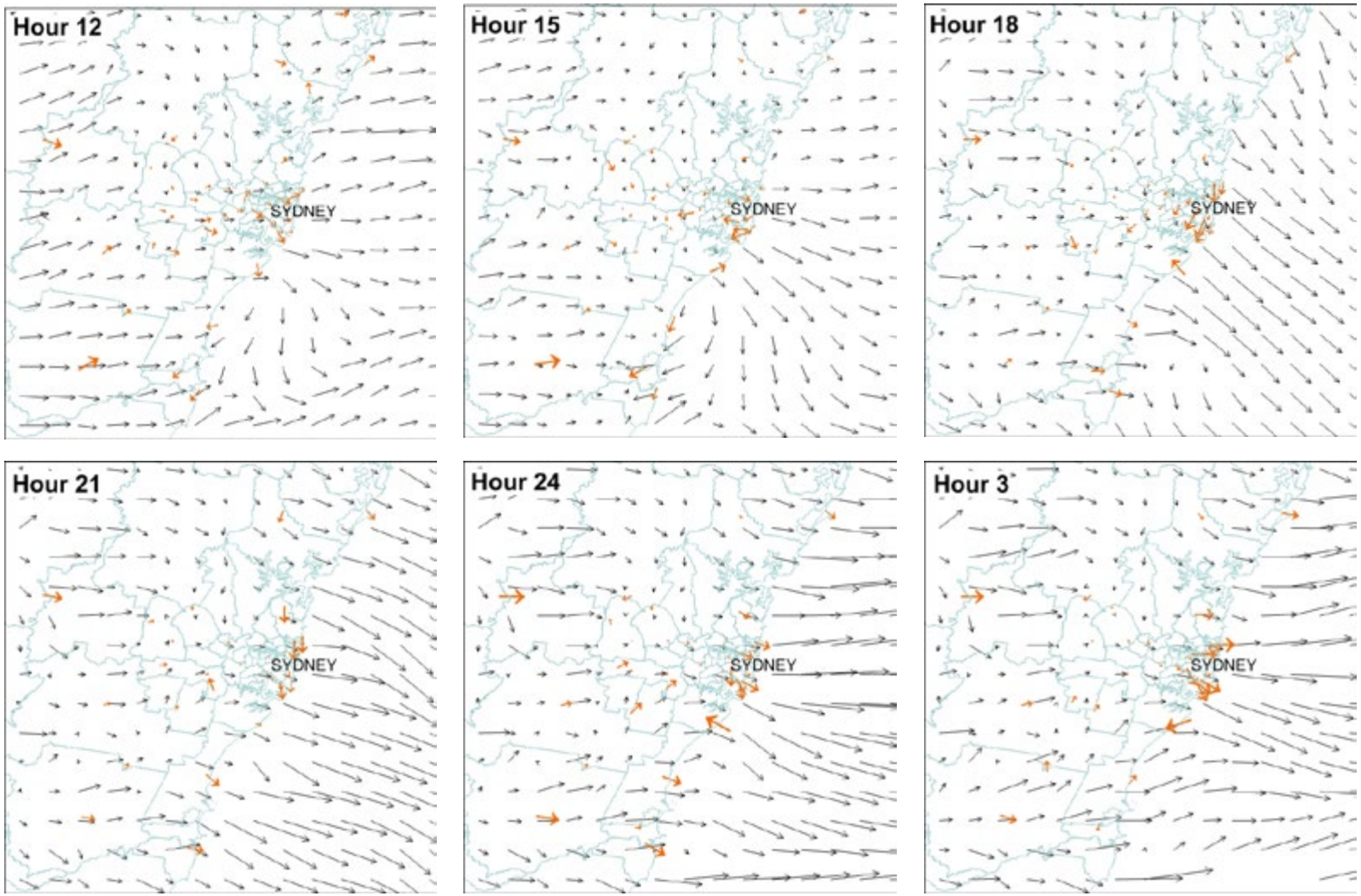

Figure 12. Observed and modelled near-surface winds at hours 12, 15, 18, 21, 24 EST on 8th May 2012; also hour 3 on 9th May 2012. The modelled winds have been generated on the 3 x 3 km^2 spaced grid and are for a CCAM simulation.

4.2.3 OBSERVED AND MODELLED NO_X, NO_2, O_3 AND $PM_{2.5}$

In this section we summarise the performance of TAPM-CTM and CCAM-CTM for the pollutants routinely observed by the OEH monitoring network. Here we focus on monitoring stations which are located on the TAPM-CTM 1 km inner grid- Randwick; Earlwood; Rozelle; Lindfield; Chullora; Prospect; Liverpool. By way of example, the plots below in Figure 13 show the observed and modelled 1-h time series for pollutants observed at Chullora- selected because Chullora observes directly $PM_{2.5}$ using a TEOM.

It is interesting to contrast the difference between the (summer) SPS1 period and the (autumn) SPS2 period. For example, it can be seen that the observed peak NO_x concentrations for SPS2 are up to double those observed in SPS1- a direct consequence of lower solar insolation and ventilation rates, and possibly also because the rain present at the beginning of SPS2 would have led a larger partitioning of the incident radiation into latent heat rather than sensible heat- thus leading to reduced levels of sensible heating. While the models have captured some of the increases in peak NO_x in SPS2, they have not been able to capture the total change in the peak concentrations. This may result from insufficient resolution in the model close to the surface (the first CTM layer is 20 m deep).

The models have done a better job at capturing the increase in NO_2 – with the highest concentrations again observed and modelled to occur in SPS2. This is an interesting outcome as the majority of the observed NO_2 is likely to be photochemically produced (rather than directly emitted), perhaps indicating that the reduction in solar insolation (and hence photochemical reactivity) is more than compensated by the reduction in ventilation rate.

Both models have done quite well at modelling the changes in ozone concentrations between SPS1 and SPS2, although this is a robust outcome which is strongly forced by the different levels of insolation between summer and autumn.

As may be expected, the $PM_{2.5}$ is the most challenging pollutant to simulate. Here the modelled $PM_{2.5}$ is generated by adding up the CTM internal $PM_{2.5}$ components from all of the simulated anthropogenic and natural source groups (note however that wildfires have not been modelled at this stage). Nevertheless, the framework's ability to simulate $PM_{2.5}$ is quite promising- capturing the variation in baseline concentrations (which possibly reflect the change from oceanic to continental sources) and also capturing many of the observed $PM_{2.5}$ peaks. It should also be noted that the breakdown of $PM_{2.5}$ sources which makes up the $PM_{2.5}$

concentrations varies strongly between seasons (dominated by sea salt in the summer; contributed to by wood heaters in the latter half of SPS2).

Figure 14 summarises the differences between model performance for $PM_{2.5}$ for SPS1 and SPS2 and suggests that for total $PM_{2.5}$, there is little difference between the performances of the two modelling frameworks. This is also the case for the other pollutants considered in this section, with the highest Index of Agreement not being biased to either of the model configurations.

In summary, we have found that TAPM-CTM and CCAM-CTM have performed quite well in modelling the concentrations of the ubiquitous air pollutants across the Sydney region. It will be interesting at a future date to incorporate the 2008 inventory, and in particular to investigate how the revised motor vehicle emissions methodology influences the model performance.

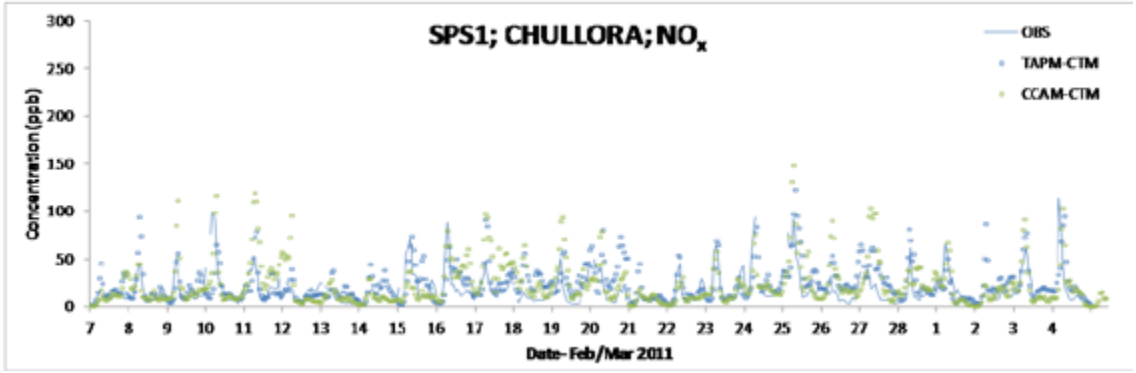

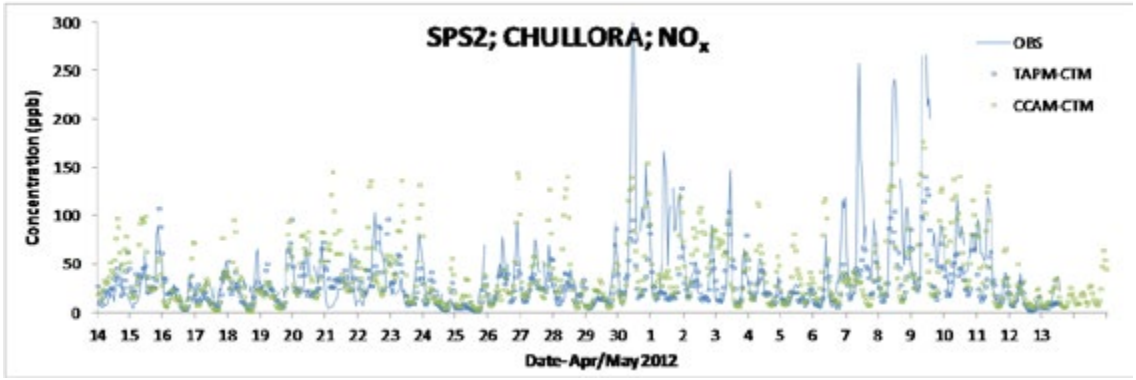

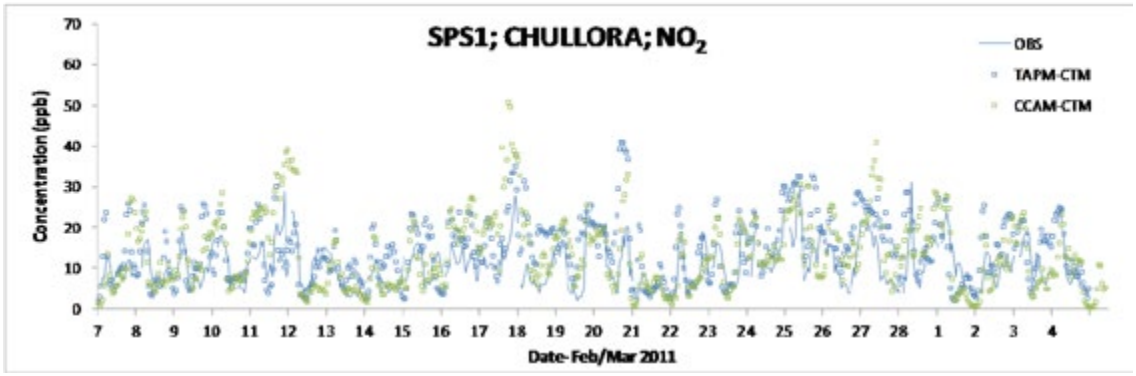

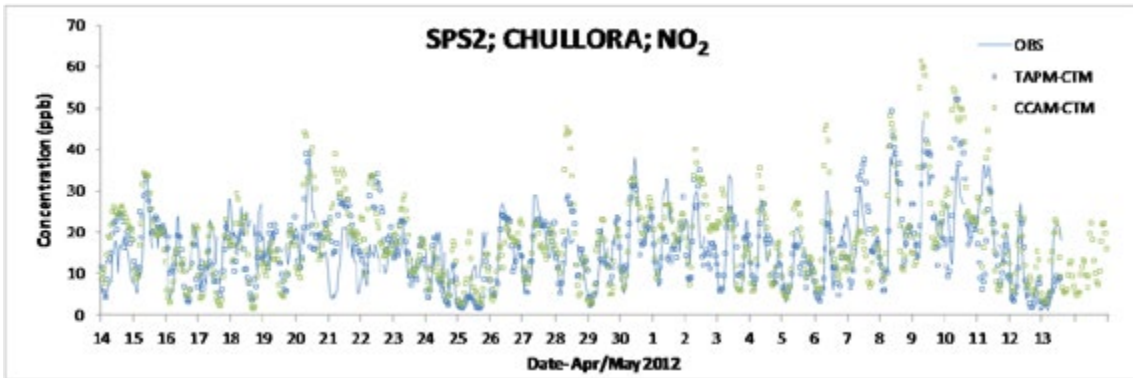

Figure continues →

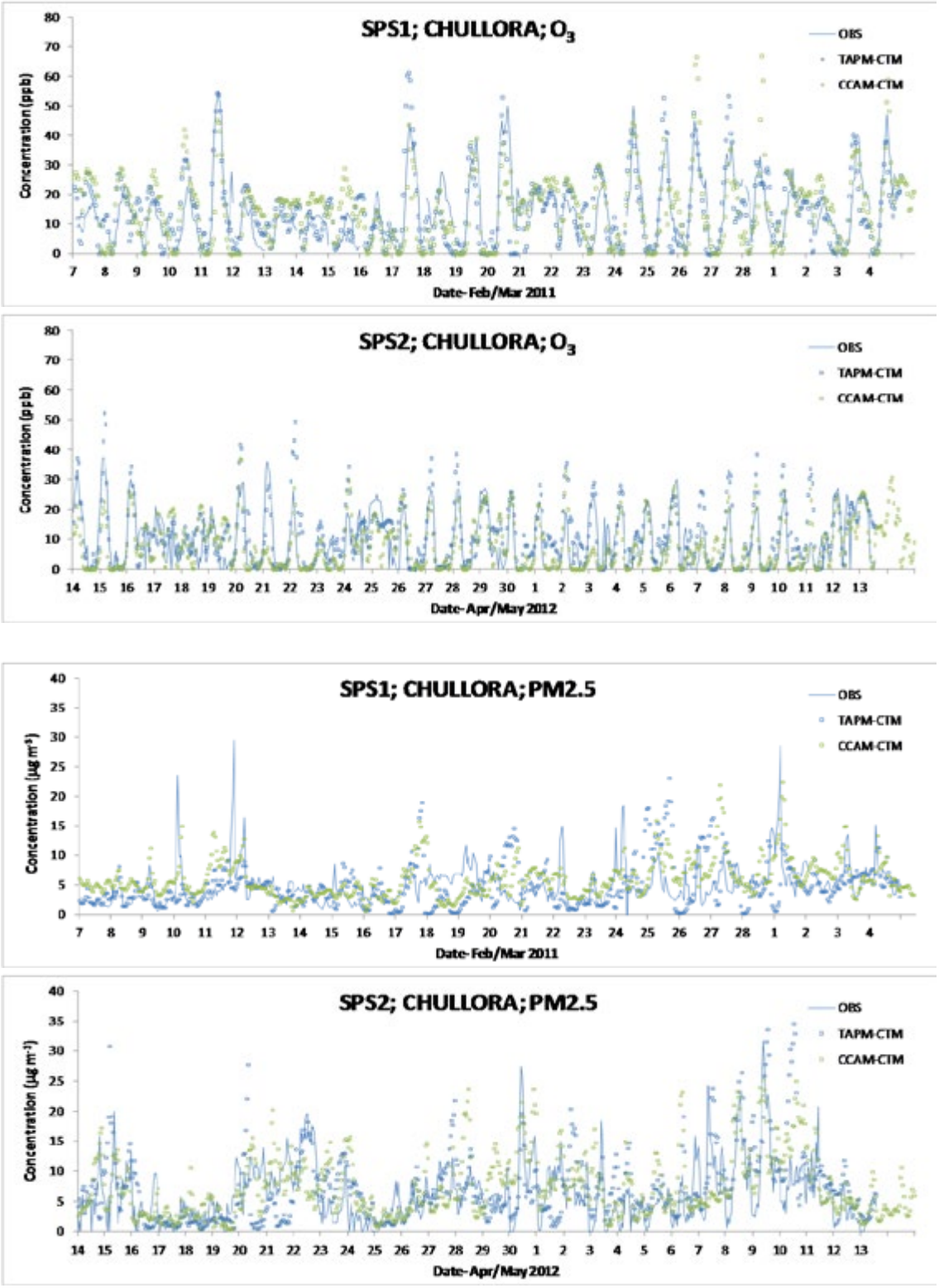

Figure 13. Time series in NOx, NO_2, O_3, and $PM_{2.5}$ at Chullora for both the SPS1 and SPS2 campaigns.

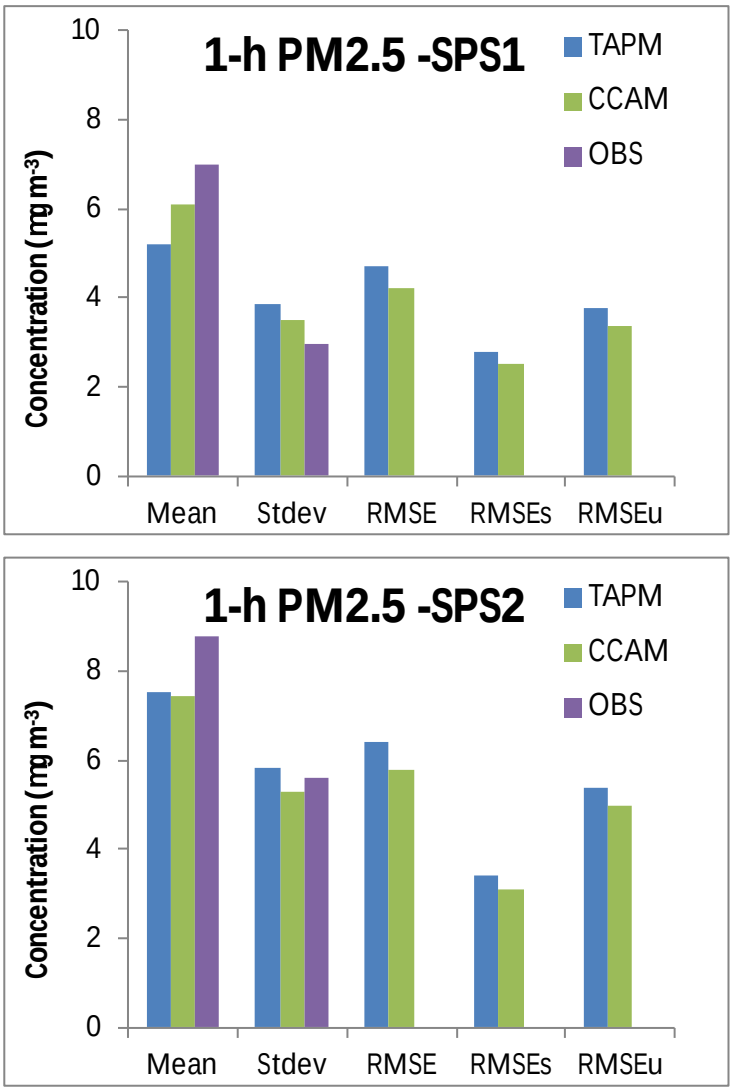

Figure 14. Comparison of statistical metrics between the modelled and observational data for $PM_{2.5}$ concentrations. Top plot is for SPS1, middle plot is SPS2, whilst the lower plot shows the index of agreement between the CCAM and TAPM models.

4.3 Source and chemical contributions of $PM_{2.5}$ at Westmead

The chemical composition of particles is determined by the source of the particles (or precursor gases) and subsequent chemical transformations in the atmosphere or within the particles themselves. This means that the chemical composition of the particles can in some instances indicate the source of the particles. This is relatively straight forward when a unique tracer is measured in the particle chemical composition, such as in the case of levoglucosan, a tracer for smoke (Simoneit et al., 1999; Simoneit 2002). In other cases ratios of species may indicate a specific source. For example within 100 km of the coast [Na+/Mg2+] of 1.17 is characteristic of a sea salt contribution to the aerosol (Cainey et al., 1999), and [Si/Al] of 3.08 indicates an Australian crustal dust source (Radhi et al., 2010). However many compounds have a number of different sources (e.g. EC from biomass burning, industrial emissions, and vehicle emissions). In this case receptor models can be used to quantify source contributions at a site. These are mathematical models that rely on the internal variability of the data to determine factor profiles and their contributions to each sample. These factor profiles are related back to specific sources, such as burning or diesel emissions. At a minimum, a hundred or more samples from many locations and/or one location over a long time period are needed for this type of receptor modelling (Norris et al. 2008).

During both SPS1 and SPS2 approximately 60 samples were collected for the measurement of aerosol chemical composition, 30 of these in the mornings and 30 in the afternoons. This number of samples is too low to carry out a rigorous source apportionment analysis using receptor modelling methodologies. Instead we use marker species to develop a qualitative assessment of sources (Table 4). Note that a number of chemical species are derived from several sources (e.g. organic matter (OM) from vehicle emissions, secondary organic aerosol, and biomass burning), while others such as levoglucosan are derived from a single source (biomass burning).

Table 4. Source components and their marker species

Dominant sources	Marker Species
Soil*	Non sea salt Calcium (Ca), Silicon (Si), Iron (Fe), Aluminium (Al), Titanium (Ti)
Organic Matter (OM) – Vehicles, Industry, Biomass Burning (BB), secondary organic aerosol (SOA)	Organic Carbon
Elemental Carbon (EC)- Vehicles, Industry, BB	EC
Sea Salt	Sodium, Chloride, Magnesium
Secondary Inorganic Aerosol (SIA)	Non sea salt Sulfate (SO_4), Ammonium (NH_4), Nitrate (NO_3)
Biomass Burning (BB)	Levoglucosan

*nss Ca used in SPS1 and Si, Fe, Al, Ca and Ti used in SPS2

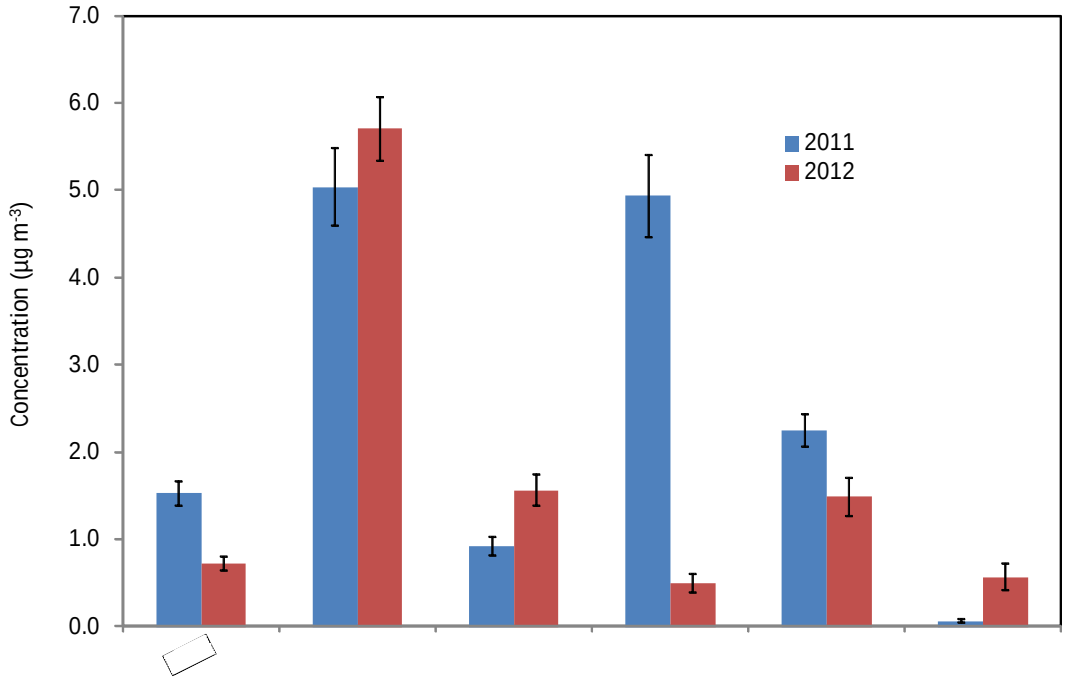

Figure 15. Average concentrations of chemical marker species (indicative of sources) during the summer 2011 (SPS1) and autumn 2012 (SPS2) measurement periods. Error bars represent standard error. Species/markers that are significantly different between the measurement periods are soil (p=<<<<0.05), EC (p=0.002), fresh sea salt (p=<<<<0.05) and aged sea salt (p=<<<<0.05)

Figure 15 compares the average concentrations of the different source components for each measurement campaign. Soil components, sea salt components and SIA components have significantly greater concentrations during the SPS1 summer period in 2011, while EC and BB are significantly greater during the SPS2 autumn period in 2012.

The relative contribution each source makes to the total chemical mass (i.e. derived from summing all the measured chemical components) for each sampling period is shown in Figure 16. BB has not been included as its chemical mass is included in OM and EC. During SPS2, OM makes a greater contribution (p<<<<0.05) (57%) than during SPS1 (34%) and EC is also greater (p<<<<0.05) during SPS2 (16% compared with 6% during summer). The contribution of SIA is not significantly different between the periods, while the contribution of sea salt is significantly greater (p <<<<0.05) during SPS1. Soil also makes significantly greater contribution (p=0.001) during SPS1.

In summary both the absolute concentrations and the relative contributions of a number of sources differ between SPS1 and SPS2 with soil and sea salt being greater in SPS1 and EC being greater in SPS2. Organic matter has the largest mass fraction. The absolute concentration of

OM does not differ between the sampling periods although its relative contribution to the chemical mass is greater during SPS2.

Figure 16 and Figure 17 shows the observed and modelled % contributions to the total $PM_{2.5}$ mass from the SPS1 and SPS2 campaigns respectively.

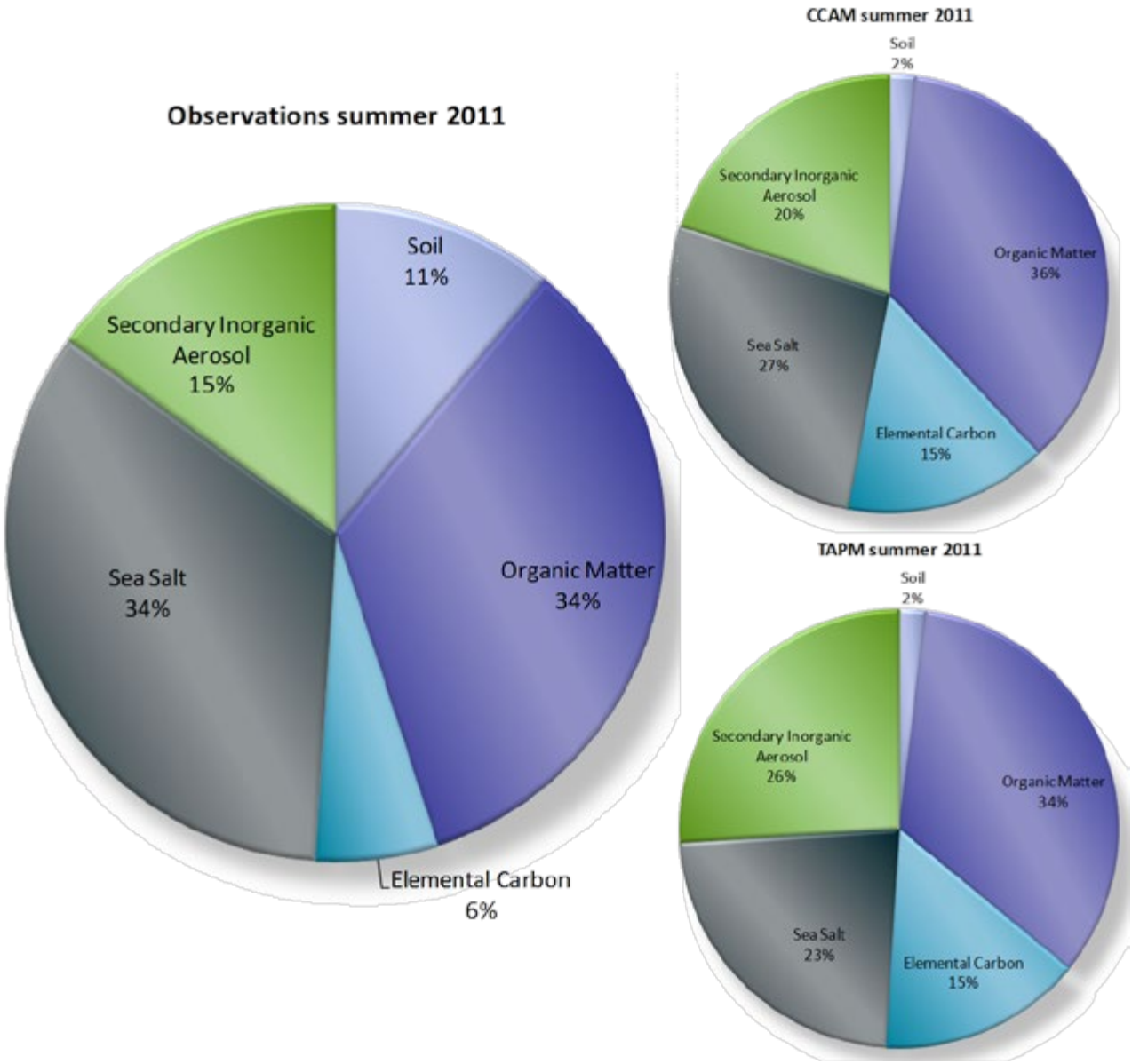

Figure 16. Pie charts showing the percentage contribution of chemical source groups to SPS1 campaign average $PM_{2.5}$ concentration. Left- the observed contribution; right- the contribution estimated from chemical transport modelling.

During SPS1 (Figure 16) the observations show that organic matter (34%) and sea salt (34%) dominated the total particle mass concentrations, which both models have captured well.

However both models have over-predicted the relative contribution of elemental carbon, slightly over-predicted the secondary inorganic fraction and under-estimated the soil fraction.

Figure 17 shows there is much less sea salt (~5% in the observations during SPS2) than was present in at Westmead during SPS1. The CCAM and TAPM models predict a slightly higher fractional sea salt contribution (15% and 9%, respectively) than was observed in SPS2.

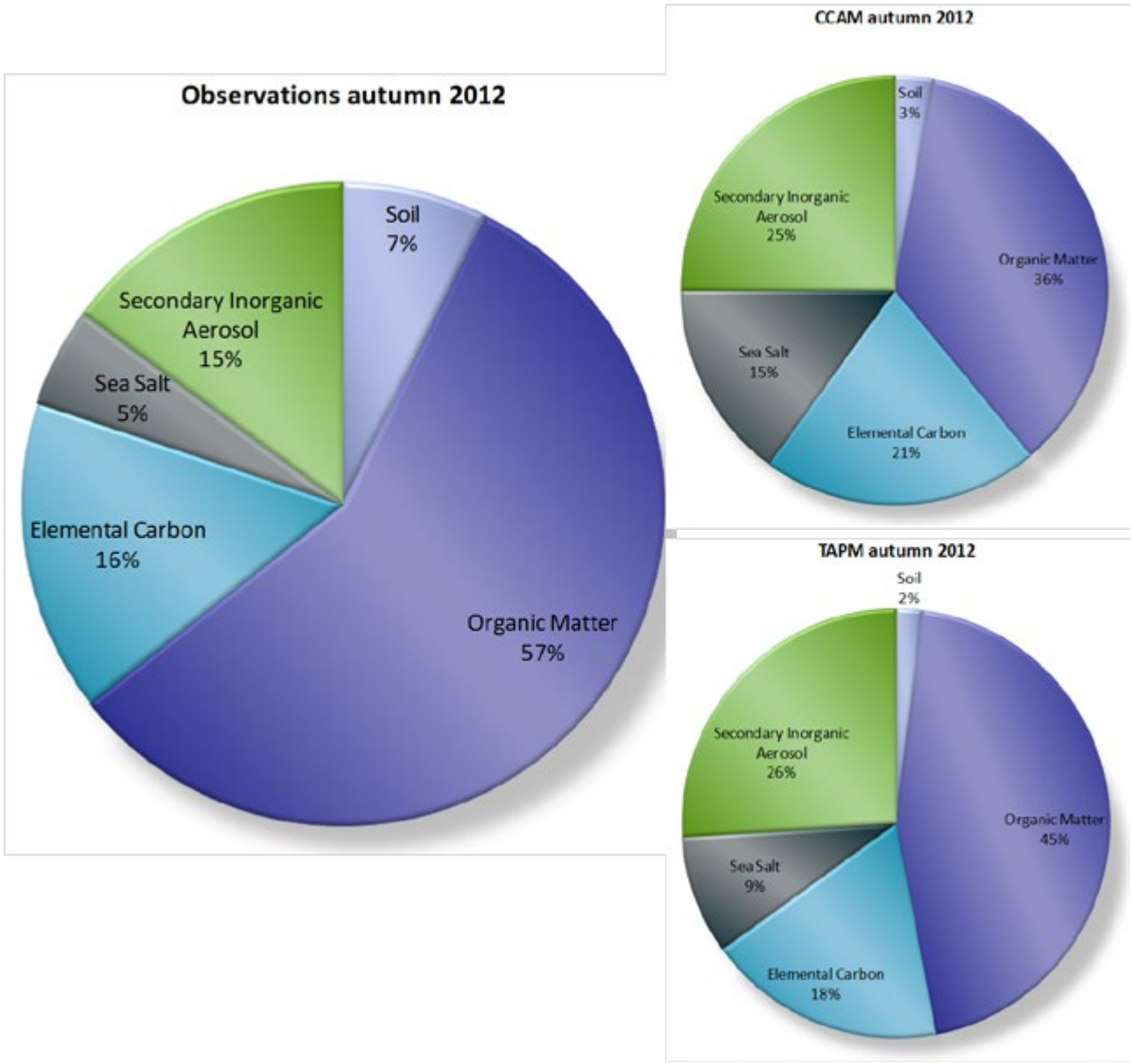

Figure 17. Pie charts showing the percentage contribution of chemical source groups to SPS2 campaign average $PM_{2.5}$ concentration. Left- the observed contribution; right- the contribution estimated from chemical transport modelling.

The SPS2 campaign was dominated by organic matter (58%) and elemental carbon (16%); both models under-predict the organic matter and over-predict the elemental carbon. Of the inorganic species, both models have high contributions from nitrate aerosol, as was the case in the SPS1 results. The modelled proportions of nitrate relate to the concentrations of sea salt, as sodium prefers to bond with nitrate than sulfate. Thus CCAM predicts higher nitrate concentrations because the model predicts more sea salt.

Figure 16 and Figure 17 show the breakdown of $PM_{2.5}$ by chemical breakdown as compared to the observations; however we note that there is a significant proportion of particulate material in the model labelled as 'Other'. The 'Other' particles contain metals, paved road-dust (note the large fraction of other included in the motor vehicle emissions- Table 2 labelled OT25:PM2.5) and other mechanically generated material. A fraction of the 'Other' component may also contain some soil derived material. The correct apportionment of this 'Other' component will be the subject of future work. In Figure 18 we show how inclusion of the 'other' component (up to 30%) affects the percentages of the model bulk chemical contributions to the $PM_{2.5}$. Running two different meteorological models helps diagnose modelling issues given they are running exactly the same emission inventories, chemistry and processes. We are also able to separate the organic matter into primary and secondary species which allows us to identify whether the carbon results from directly emitted processes or from photochemistry occurring in situ. In both seasons, the CCAM model simulated sea salt contribution is approximately double those of TAPM, due to the stronger wind speeds predicted by CCAM over water. The TAPM model tends to predict more carbon than CCAM, especially from secondary organic matter. Both models predict similar soil, ammonium, nitrate and sulfate aerosol.

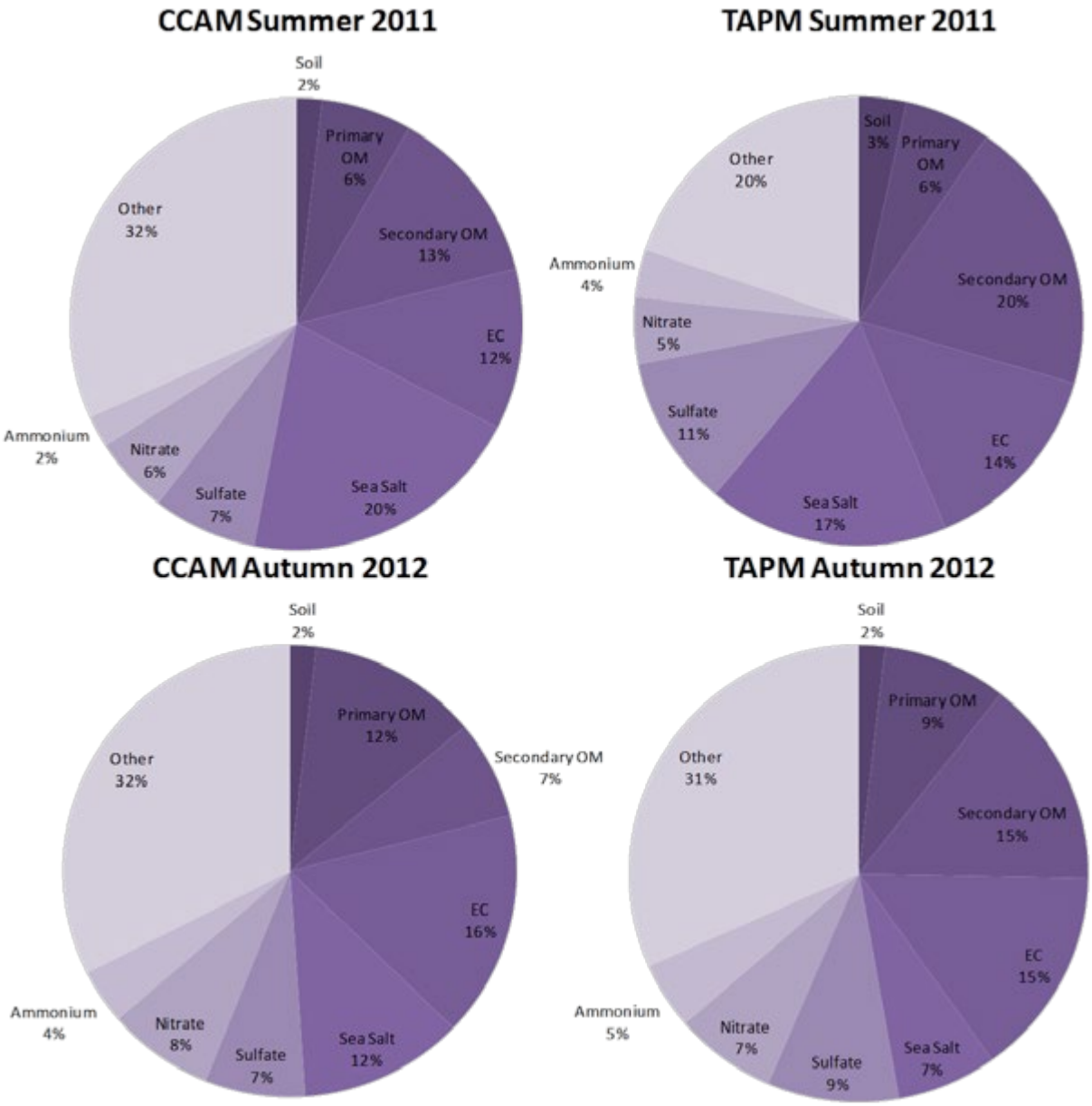

Figure 18. Pie charts to show the CCAM and TAPM contributions to $PM_{2.5}$ broken down by chemical constituent for the summer SPS1 (top) and autumn SPS2 (bottom) campaigns.

Figure 19 shows the observed and modelled morning and afternoon breakdown of $PM_{2.5}$ into chemical components for the summer 2011 campaign. In the observations it can be seen that sea salt concentrations are similar in the morning and afternoon, and that organic carbon (OC) and secondary inorganic aerosol concentrations are greater in the afternoons while elemental carbon (EC) is greater in the morning. The morning and afternoon mean concentrations for OC and EC are significantly different (at a 95% confidence). Our analysis suggests that the EC is

reduced in the afternoon because EC is a primary particulate source, and enhanced levels of atmospheric ventilation in the afternoon lead to lower concentrations. On the other hand, elevated concentrations of OC in the afternoon suggest the presence of a significant secondary source.

The modelled morning and afternoon variation in $PM_{2.5}$ component concentrations exhibits some variation from the observed. For example both models predict more EC during the afternoon. CCAM predicts more sea salt in the afternoon whereas TAPM predicts more during the morning. However the modelled $PM_{2.5}$ component concentrations are less than 50% of the observed. This may result from uncertainties in the particle speciation used for the emissions, and/or too much washout from rainfall (recall the propensity of CCAM and TAPM to over-drizzle). In fact we have tested the sensitivity of the sea salt concentration predictions to wet deposition and confirmed that the wash-out process is a significant sink for sea salt $PM_{2.5}$. Additionally, errors in the modelled ventilation rates may also be a contributing factor, however recall from Figure 14 that the two modelling systems predict monthly mean total $PM_{2.5}$ concentrations which lie within 10–15% of the observed. This suggests that perhaps uncertainties in our current top-down methodology may be contributing to errors in the anthropogenic $PM_{2.5}$ mass components at least.

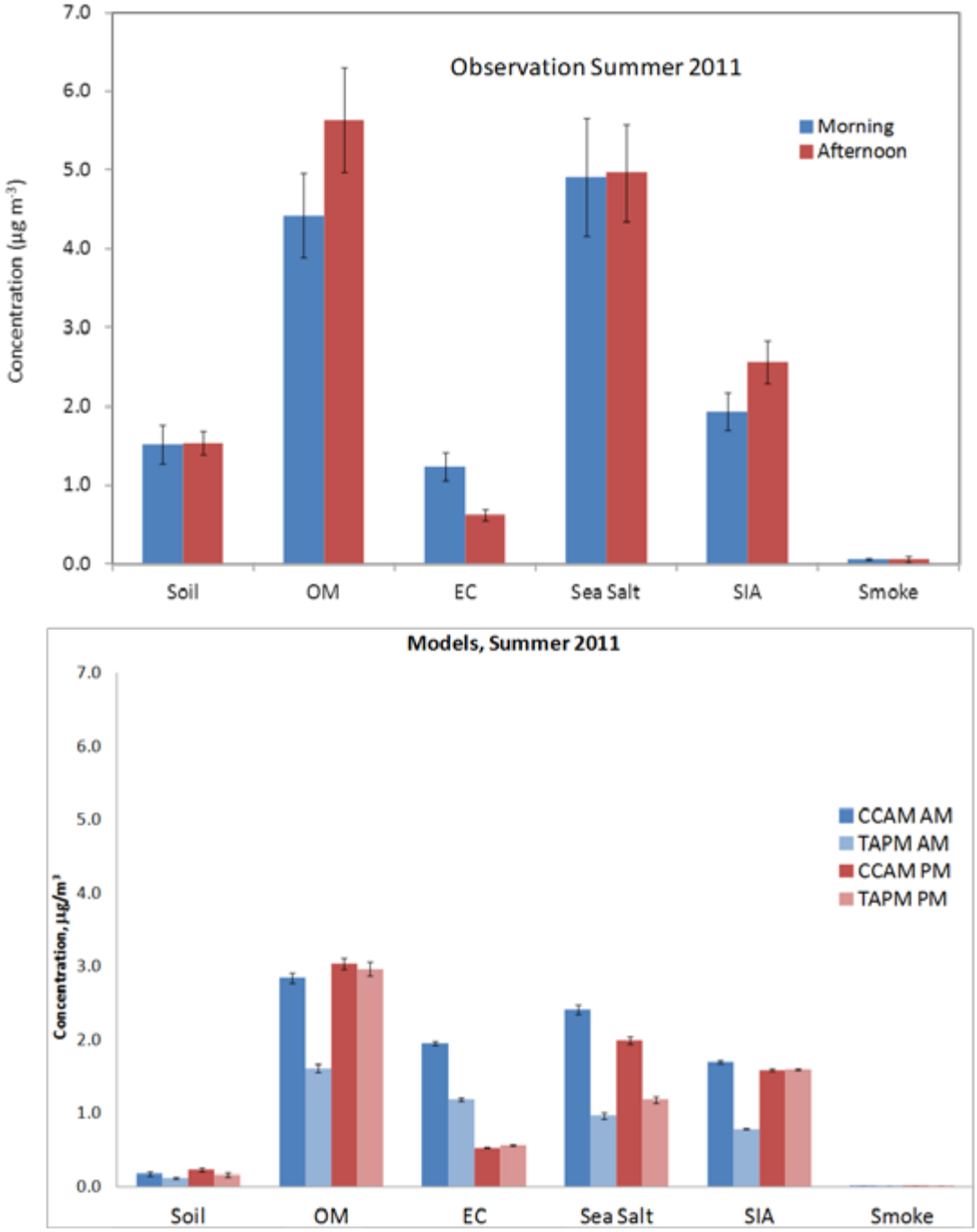

Figure 19: SPS1 Summer 2011. Top- Observed campaign average morning and afternoon concentrations of the major aerosol components measured in integrated samples of $PM_{2.5}$. Bottom- modelled campaign average concentrations.

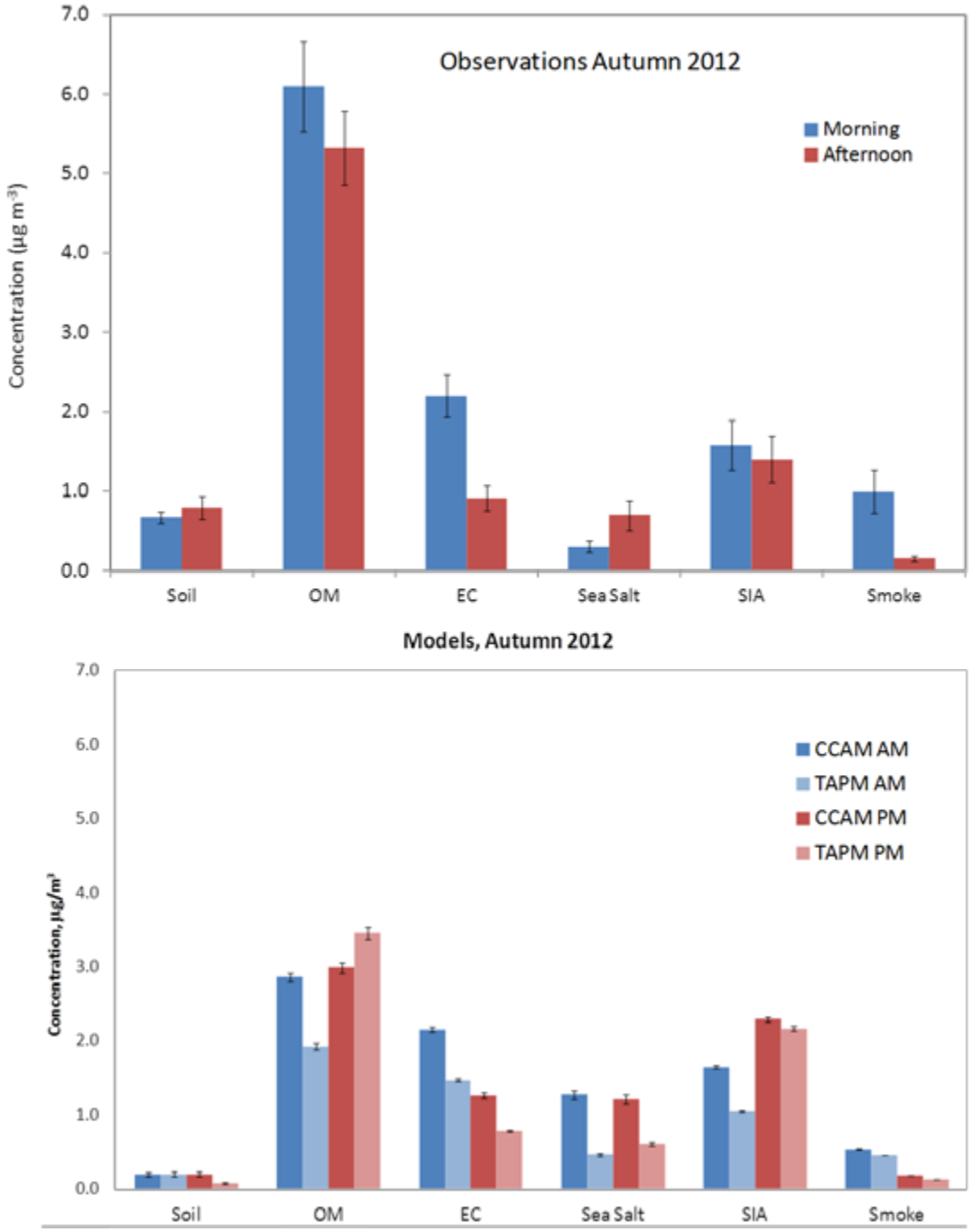

Figure 20: SPS2 Autumn 2012. Top- Observed campaign average morning and afternoon concentrations of the major aerosol components measured in integrated samples of $PM_{2.5}$. Bottom- modelled campaign average concentrations.

Figure 20 shows the morning and afternoon breakdown for the SPS2 campaign. Whilst there is a general model under-prediction across all the species, CCAM does marginally better then TAPM when it comes to morning and afternoon differences. The observations show more

organic matter present in the morning than the afternoon which CCAM predicts but which TAPM does not. CCAM also captures the correct AM/PM split in EC, but does not capture the differences for sea salt or SIA.

4.4 Processes- observations and modelling

In this section we investigate some of the individual processes with lead to particle formation during SPS1 and SPS2.

4.4.1 SEA SALT

Sea salt aerosol emissions are caused by wave-breaking in the open ocean and from coastal surf breaks, as shown in Figure 21. The magnitude of the open ocean sea salt fluxes is a strong function of the surface shear stress and hence the near-surface wind speed.

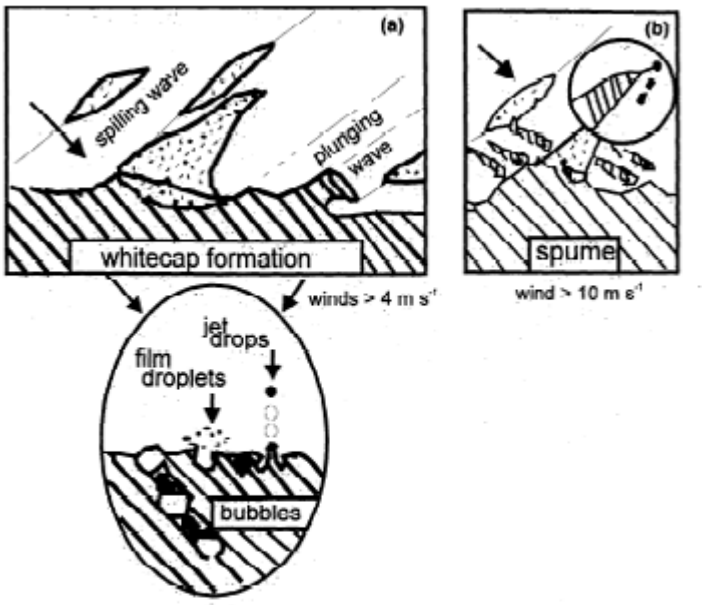

Figure 21. Mechanism for sea salt aerosol generations (adapted from Monahan et al (1986). Two mechanisms are presented (a) indirect production by bubbles and (b) direct production by spumes. Taken from (Gong et al., 1997).

The modelling framework parameterises sea salt emissions according to the approach in Gong et al (2003) for the open ocean and from Clarke et al. (2003) for the wave breaking mechanism. The parameterisations result in a sea salt aerosol flux such as that shown in Figure 22, where the peak in the sea salt flux occurs in particles sized at 0.2 mm in radius.

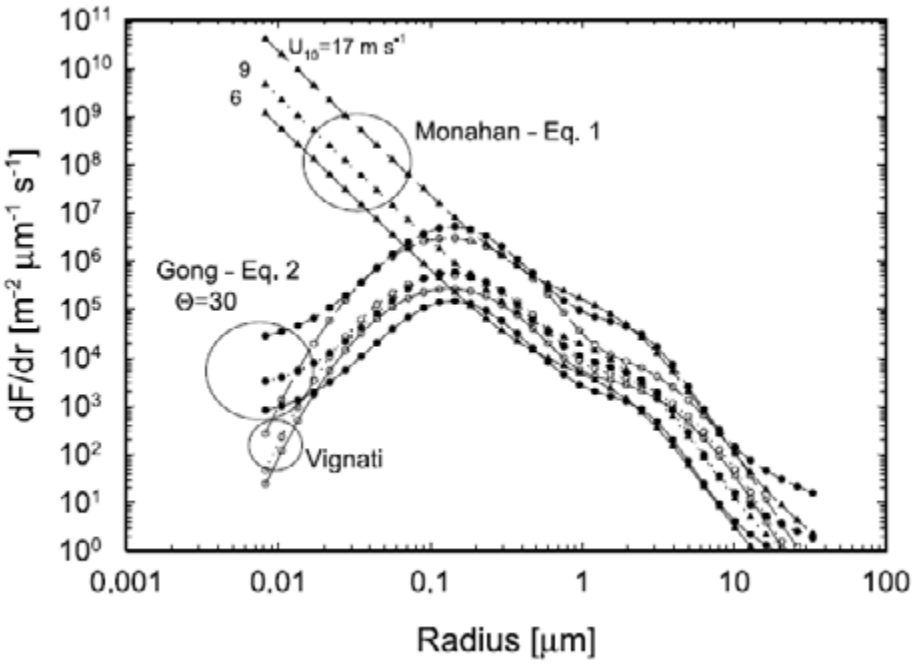

Figure 22. Sea salt flux as a function of particle size from three source functions: (1) Monahan (solid triangle), (2) Gong-Monahan (solid circle) and (3) Vignati (open circle) at three wind speeds (solid line, 6 m s-1, (dotted line, 9 m/s), and (dashed line, 17 m/s). Relative humidity (RH) is 80%. Taken from (Gong, 2003).

Figure 23 shows the daily concentrations of $PM_{2.5}$ sea salt observed at Westmead, together with observations of radon and a radon-based interpretation of air parcel origin for both SPS1 and SPS2. It can be seen that the sea salt concentrations are inversely correlated with radon concentrations during 2011, thus confirming the oceanic source of the sea salt. Note the extremely high concentration of sea salt observed on the 3rd March 2011. This event is confirmed from coincident measurements of high PM_{10} at Westmead. However PM_{10} observations from the OEH network for this day do not provide evidence for a concentrated sea salt plume advecting inland from the coast within the surface layer. The cause of this event is still under investigation. During SPS2 the radon measurements show only one event where an oceanic fetch could be diagnosed; this is corroborated by the much lower concentrations of sea salt observed at Westmead in 2012 (also shown in the % contribution of sea salt to the $PM_{2.5}$ in Figure 17). In SPS2 there were more periods where a continental fetch dominated than in SPS1 and this is the reason why there is much less sea salt in the models for SPS2.

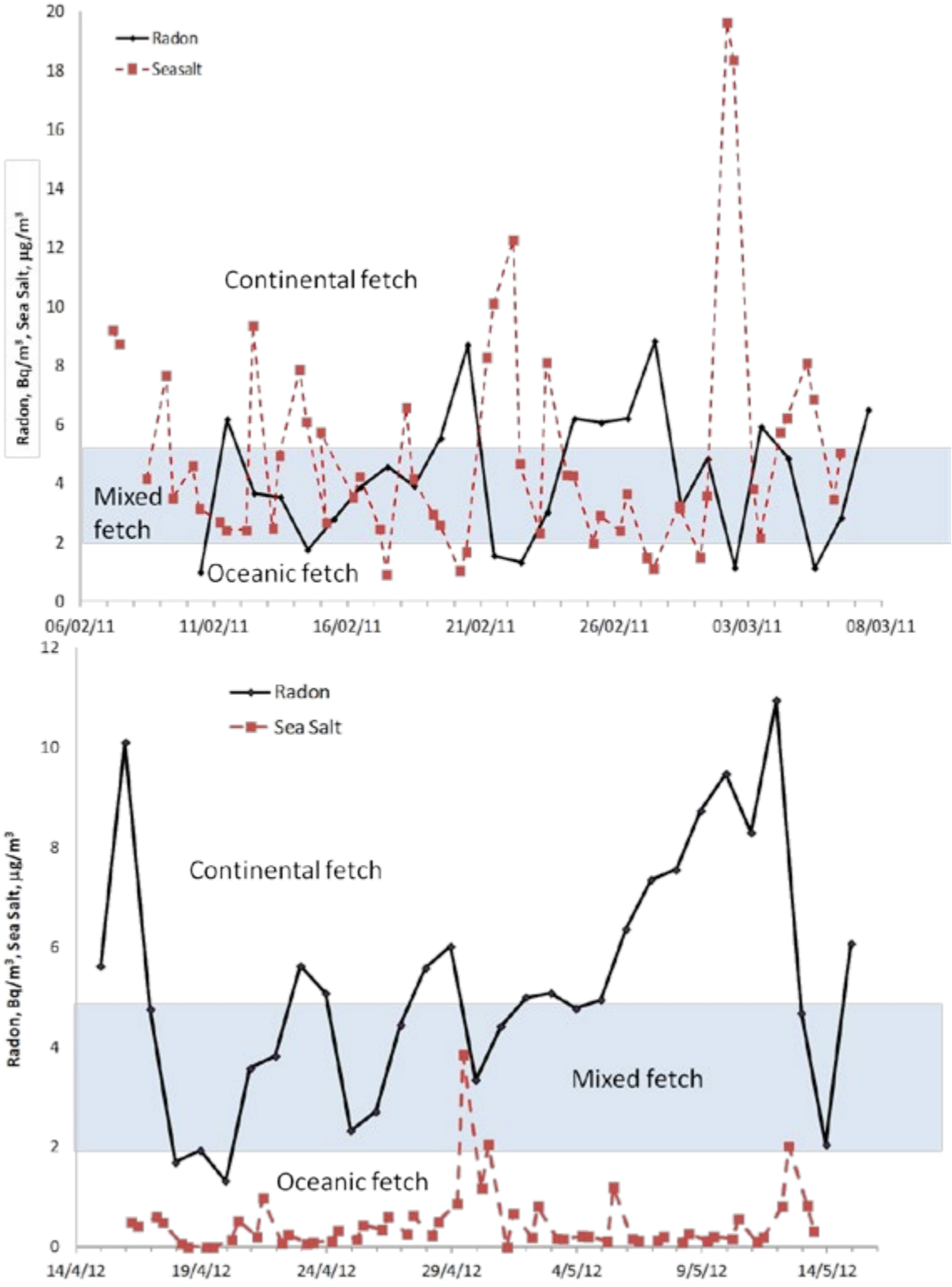

Figure 23. The time series of daily sea salt concentration together with radon measurements which give the air parcel history over land/ocean. Top plot refers to SPS1, bottom plot to SPS2.

Figure 24 shows the results of an inverse modelling simulation of $PM_{2.5}$ sea salt concentrations for a summer month. The inverse simulation is an example of a technique which can be used to identify the source regions which contribute to the sea salt observed in Sydney. It was not possible to run an inverse modelling situation for 2011 at the time of this report, therefore the results should be treated as indicative of likely source regions. Figure 24 suggests that sea salt emissions from as far away as the Southern Ocean can influence the observed sea salt. This is not entirely surprising given the distances other natural sources, i.e. soil dust are known to travel in Australia. Given that sea salt makes up a large proportion of $PM_{2.5}$, it important that consideration is given to the health impacts of chemicals within the sea salt aerosol, e.g. as the sea salt ages chemically (Song and Carmichael, 1999), when assessing the impact of total $PM_{2.5}$ on the NSW population.

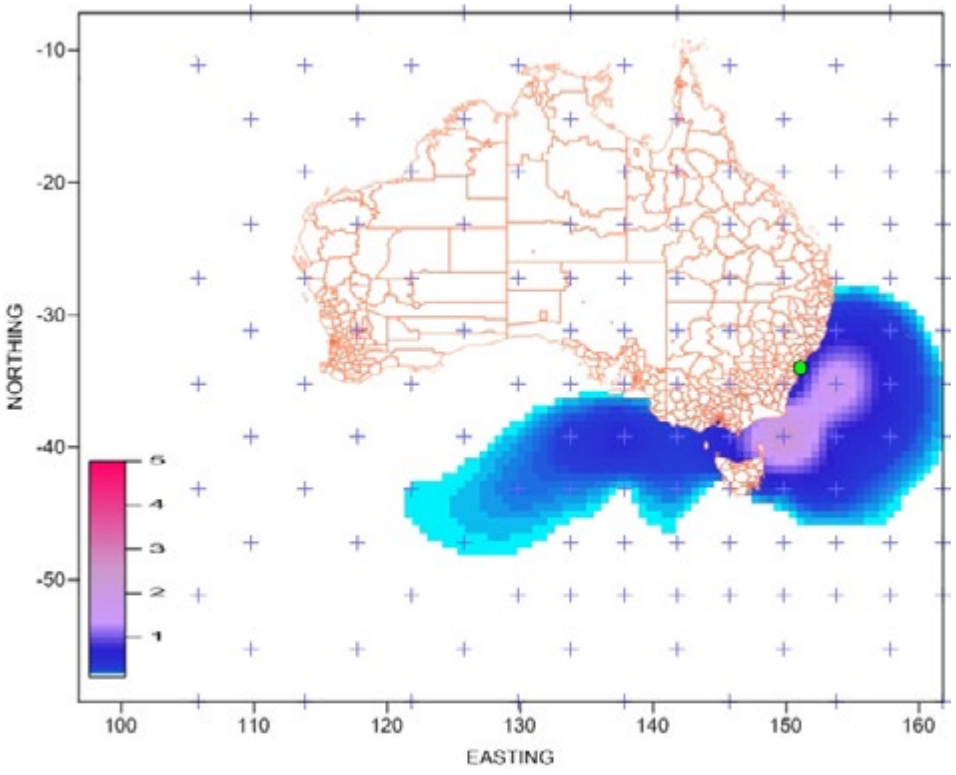

Figure 24. Example of the percentage contribution of oceanic source regions to sea salt $PM_{2.5}$ in Sydney

In particular, the modification of sea salt particles via condensation of acidic gases could result in significant human exposure to particulate matter in coastal regions. However sea salt particles cannot be controlled, and as such are not included in the reporting of particulate

matter for health effects. There is currently debate as to whether the contribution of particles from natural sources should be included.

Figure 25 shows the modelled and observed relationship between sodium and chloride for both campaigns.

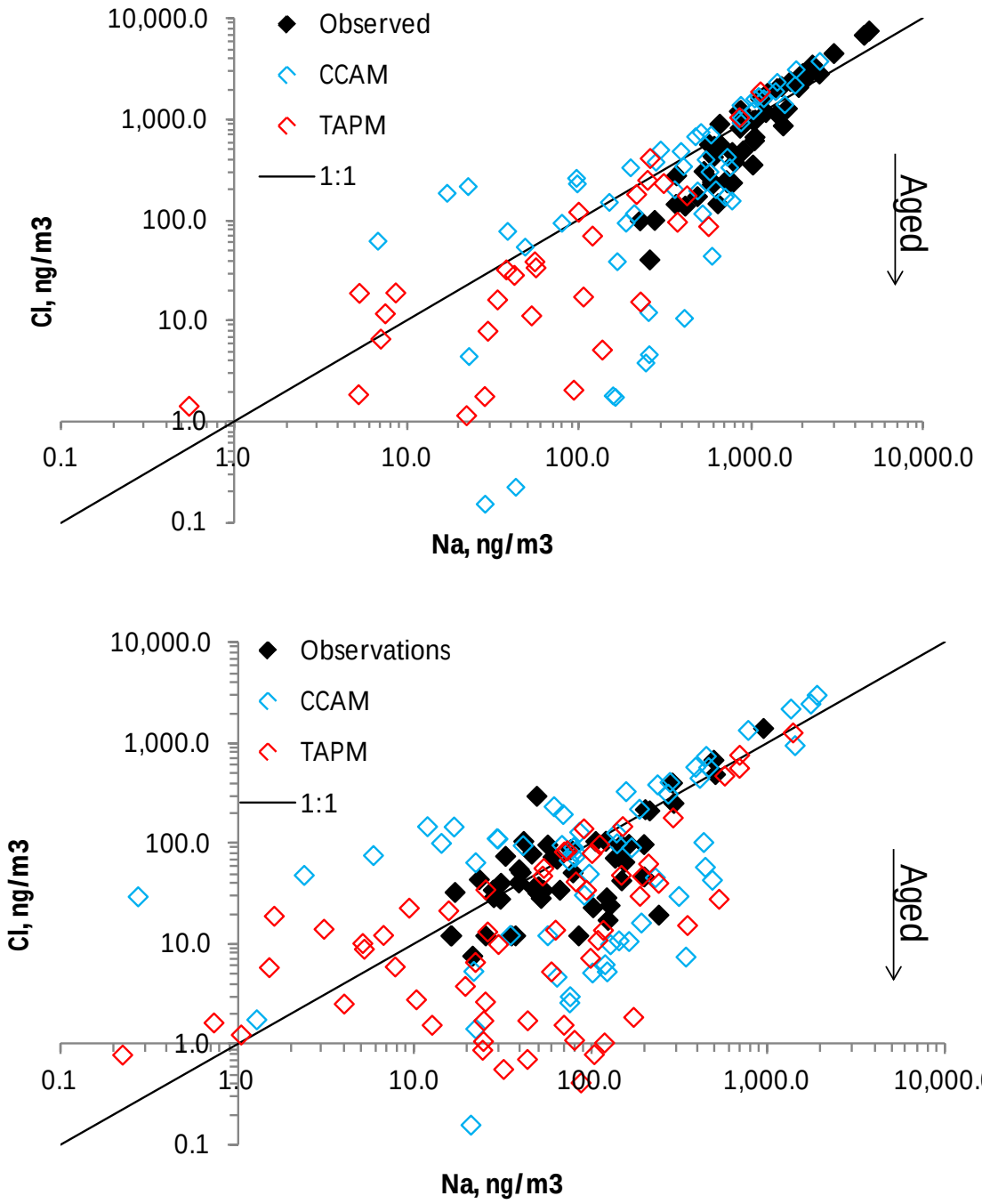

Figure 25. Scatter plot on a logarithmic scale to show the relationship between the modelled and observed sodium and chloride concentrations. The top plot is from SPS1; the bottom plot is from SPS2.

In SPS1 (top plot) the observations show higher concentrations of both sodium and chloride. In SPS2 the concentrations of sodium and chloride are an order of magnitude lower than those measured in SPS1. The rate at which chloride is driven off the sea salt aerosol gives an indication of the amount of ageing in the particle. The 1:1 line roughly defines the point at which ageing occurs; points which lie below this line have undergone some chemical ageing. The observed points show there is more ageing when concentrations of chloride fall below 500 ng/m^3 in summer. The model can also show concentrations below the limit of detection for the observations (which is 10 ng/m^3). There is certainly more spread in the observed data for SPS2 than for SPS1 campaign; in the model there is spread for both periods. Both models are showing a higher proportion of fresh sea salt in SPS2 than in SPS1.

Figure 26 shows the observed and modelled contributions from sea salt to $PM_{2.5}$ as time series for both campaigns. The first plot shows that in some cases for the observations, notably during SPS1 on March 2nd 2011, all of the $PM_{2.5}$ is composed of sea salt. The highest ratio that either model can produce is around 50%, with CCAM producing more than TAPM owing to the higher wind speed predictions in the model. During the autumn SPS2 campaign sea salt makes up nearly all the observed $PM_{2.5}$ on 29th April 2012. However for the most of SPS2 the observed sea salt ratio is under 10%. This is more of a background level of sea salt which the models do much better at predicting. Again CCAM is higher than TAPM, especially during the first few days of SPS2.

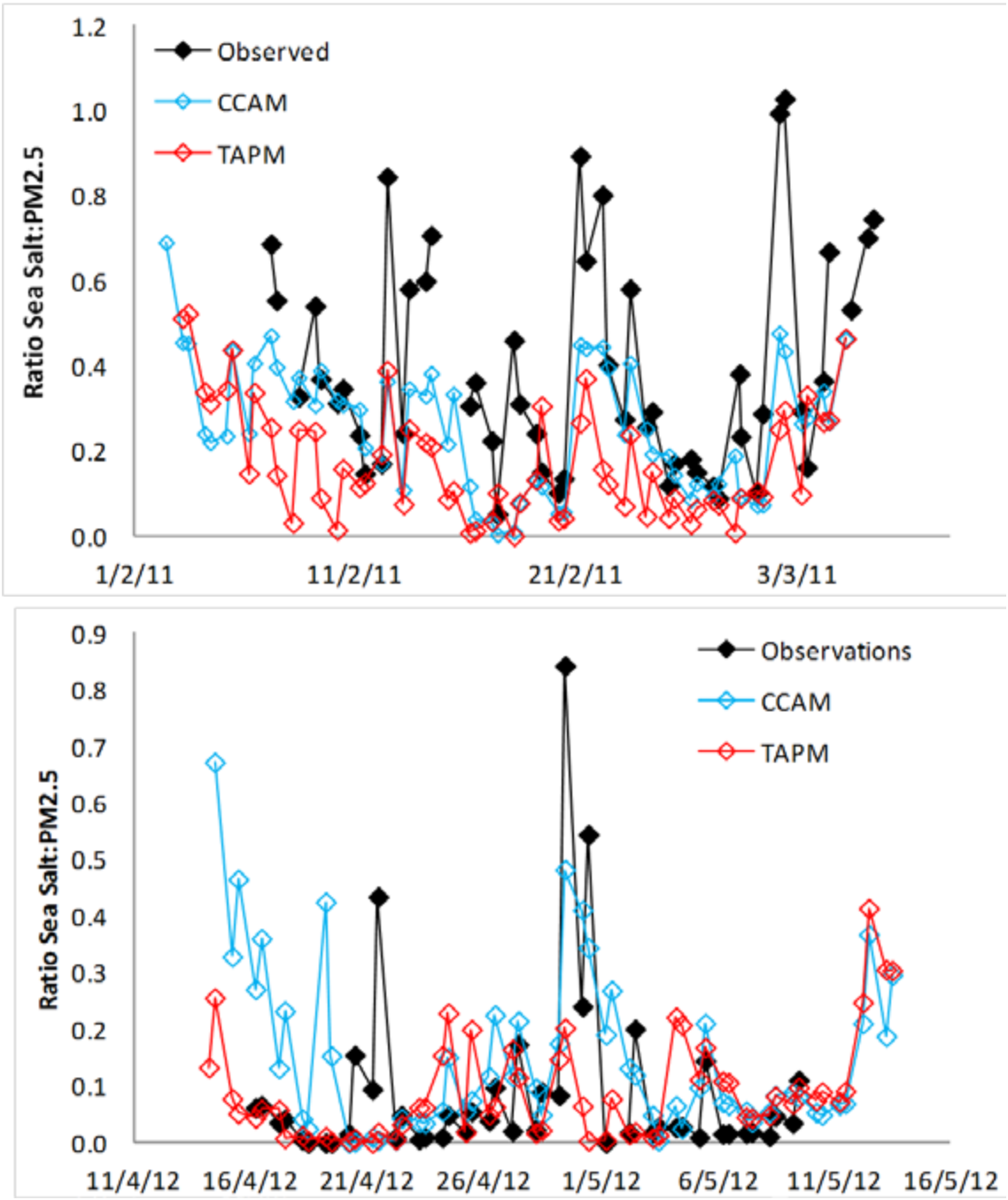

Figure 26. Time series plot to show ratio of sea salt to total $PM_{2.5}$ contributions between the model and observations. Top plot refers to summer 2011; the bottom to autumn 2012.

4.4.2 BIOMASS BURNING

One of the purposes of the Sydney Particle Study is to identify the presence of wood smoke at Westmead, and if present, to assess its impact on the observed particle size distribution and chemistry. Scheduling of the observation experiments in summer and autumn thus provided

an opportunity for capturing plumes from wildfires (managed and natural) and from domestic wood combustion. We are fortunate that particulate matter from biomass combustion can be discriminated from other sources by particle size and chemical composition, and with regard to the latter, produces a unique tracer- the sugar levoglucosan (Meyer et al., 2011). The lifetime of levoglucosan is on a par with many atmospheric alcohols Hoffmann et al. (2010); Hennigan et al (2010) estimate a lifetime of up to 2 days whilst Kessler et al (2010) calculate a lifetime of ~9 days (for heterogeneous oxidation). Two days is adequate time for a state-wide fire to reach Westmead; nine days would give enough time for a continental fire to reach the sample site at Westmead. Levoglucosan was measured during both of the SPS observation periods.

Figure 27 shows the observed time series for levoglucosan at Westmead for the two study periods, and indicates that wood smoke was present in both SPS1 and SPS2. With regard to the SPS1 period, small concentrations of levoglucosan were present on about 50% of the days observed. The largest wood smoke event was observed on 26th February and was found to be caused by fire management burns to the north of Sydney (Keywood et al., 2012). On the other hand, the levoglucosan mass observed in SPS2 was about a factor of seven higher than that observed in SPS1. While a large spike on levoglucosan concentration observed at the start of the second observation period is likely related to a fire management burn, the build-up of levoglucosan in the second half of this observation period is related to the onset of cooler ambient temperatures and thus is likely to have a significant wood heater component. This provides a good opportunity to test the woodheater emission algorithms in the modelling system.

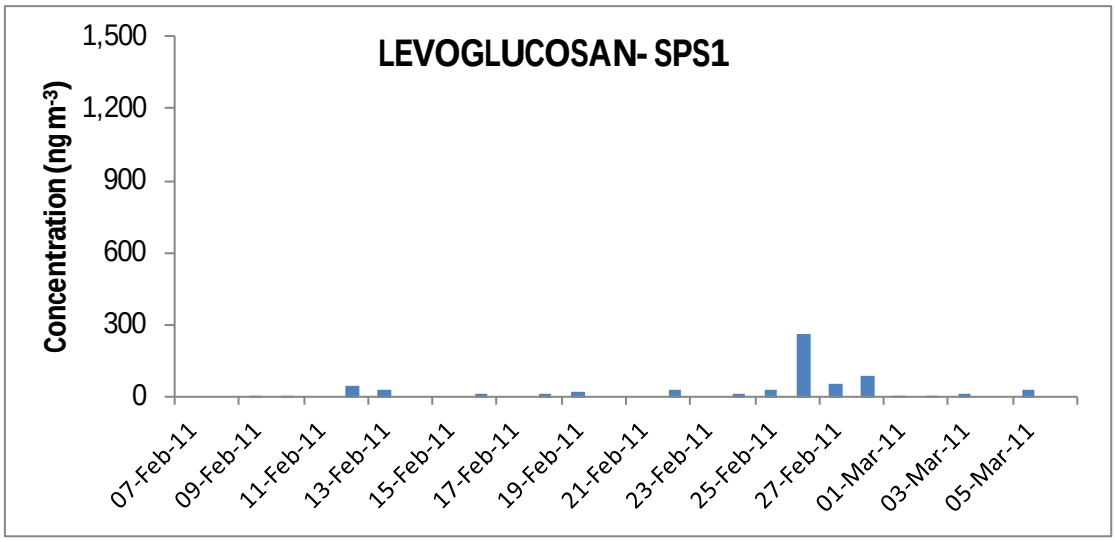

Figure continued →

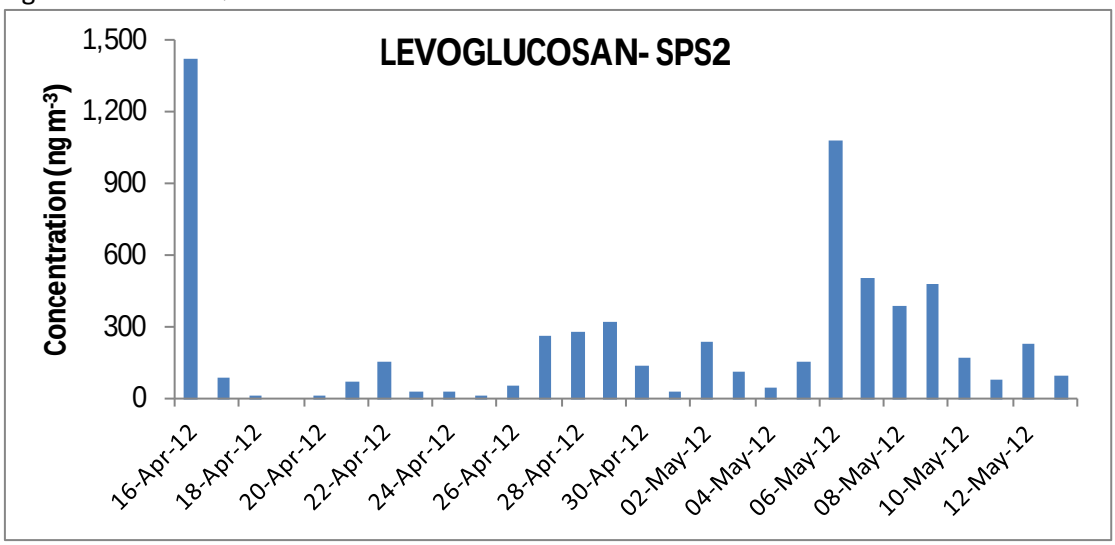

Figure 27. Time series plot of the wood smoke tracer levoglucosan as observed at the Westmead site for the two observation experiments. Note that the sampling averaging time for the observations is 6–9 hours.

Agapides (2012) provides a concise summary of the methodology used to estimate woodheater emissions for the 2008 NSW Greater Metropolitan Region air emissions inventory.

1. The emission methodology draws on the 2008 USEPA National Emissions Inventory[3]; the USEPA Emission Inventory Improvement Program[4]/ USEPA AP42[5]; and inventory approaches promoted by the Mid-Atlantic Regional Air Management Association[6]

[3] http://www.epa.gov/ttnchie1/net/2008inventory.html
[4] http://www.epa.gov/ttnchie1/eiip/
[5] http://www.epa.gov/ttnchie1/ap42/

2. An online domestic survey (Ozquest) was used to gather statistics on wood consumption, wood source, usage patterns and wood heater type.

3. The domestic survey data was scaled up to cover the entire inventoried region using ABS gridded dwelling type data.

4. Emissions were estimated from the survey, dwelling type and emission factor data.

5. Emission factors were derived from Australian and New Zealand in-service test data.

6. Wood heater temporal factors were generated using Bureau of Meteorology heating degree days and TAPM modelling of near surface temperature to derive annual emission factors. Monthly daily and hourly usage patterns were derived from the domestic survey.

Figure 29 shows the estimated annual contribution of solid fuel combustion emissions (dominated by wood heater emissions) to $PM_{2.5}$ emissions in Sydney, and demonstrates that wood heaters are the most significant source of $PM_{2.5}$ in the region. Thus the ability to be able to quantitatively model the impact of particle emissions from wood heaters is an essential requirement for a Sydney particle model. In this regard, the approach taken in this study involved the following steps.

1. Isolate the wood heater emission from the combined commercial-domestic inventories provided by NSW EPA by subtracting a January inventory (minimal wood heater emissions) from a July inventory. This yielded an estimate of weekday and weekend hourly varying emissions, here for July 2003. Figure 29 compares the diurnal emission profiles of wood heaters with the other surface based sources on the 1-km TAPM Sydney domain, and highlights the significant size of the solid fuel combustion source.

2. Generate July 2012 emissions by scaling July 2003 emissions by a wood heater performance factor (average in-service performance decreased from 13.82 to 11.33 kg PM_{10}/tonne wood over this period; Nick Agapides NSW EPA- personal communication).

[6] http://www.marama.org/technical-center/emissions-inventory/projects-overview

3. Calculate the basin-average near daily temperature for the period of SPS2. This is shown in Figure 30 where the 24-h running average observed and TAPM estimated, and a CCAM estimated fixed daily average is shown.

4. Normalise the July 2012 daily emissions by the daily average heating degree days (HDD) for July, and generate daily emissions for the study period by scaling the normalise emissions with the daily, basin average HDD for Sydney. Figure 30 shows the normalised HDD for SPS2 and demonstrates how the HDD increase in the second half of the SPS2 period correlates with the increase in levoglucosan concentrations (Figure 27). Figure 30 also demonstrates that CCAM generally estimates a higher HDD factor than TAPM. This is a direct consequence of CCAM predicting cooler overnight temperatures than TAPM (see Figure 5). In fact it was found that the modelled woodheater emissions (and hence $PM_{2.5}$ concentrations) were sensitive to the differences in the modelled near surface temperature, and thus the observed basin average temperatures and HDDs were used to force the wood heater emissions. The last plot in Figure 30 shows the result of normalising and scaling the wood heater emissions for the SPS2 study period.

5. Test the wood heater emission estimates using observed levoglucosan as a constraint (levoglucosan was added to the modelling systems for this purpose). Figure 32 shows how the modelled morning (hour 5–10 EST average) and afternoon (hour 11–19 EST average) levoglucosan concentrations vary with various woodheater emission scenarios. The base case uses the woodheater emissions normalised by HDD as described above and the inventory default diurnal emission profile (with emissions peaking around 7–9 pm) and shows strong over prediction of the afternoon concentrations and some over prediction of the morning concentrations. Total $PM_{2.5}$ concentrations within the Sydney region are also over predicted (not shown). Halving the woodheater emissions leads to improved agreement with the morning levoglucosan concentrations, however the afternoon concentrations are still over predicted. Finally, following discussions with EPA NSW (Nick Agapides- personal communication), the time of the evening peak woodheater usage was staggered back by two hours (now peaking at 10 pm), thus corresponding better to the observed later onset of the evening hourly heating degree peak in May compared to that observed in July when daily average temperatures are much cooler. This emission scenario led to

further improvements in both the modelled and observed levoglucosan and the airshed $PM_{2.5}$ (also see Figure 14).

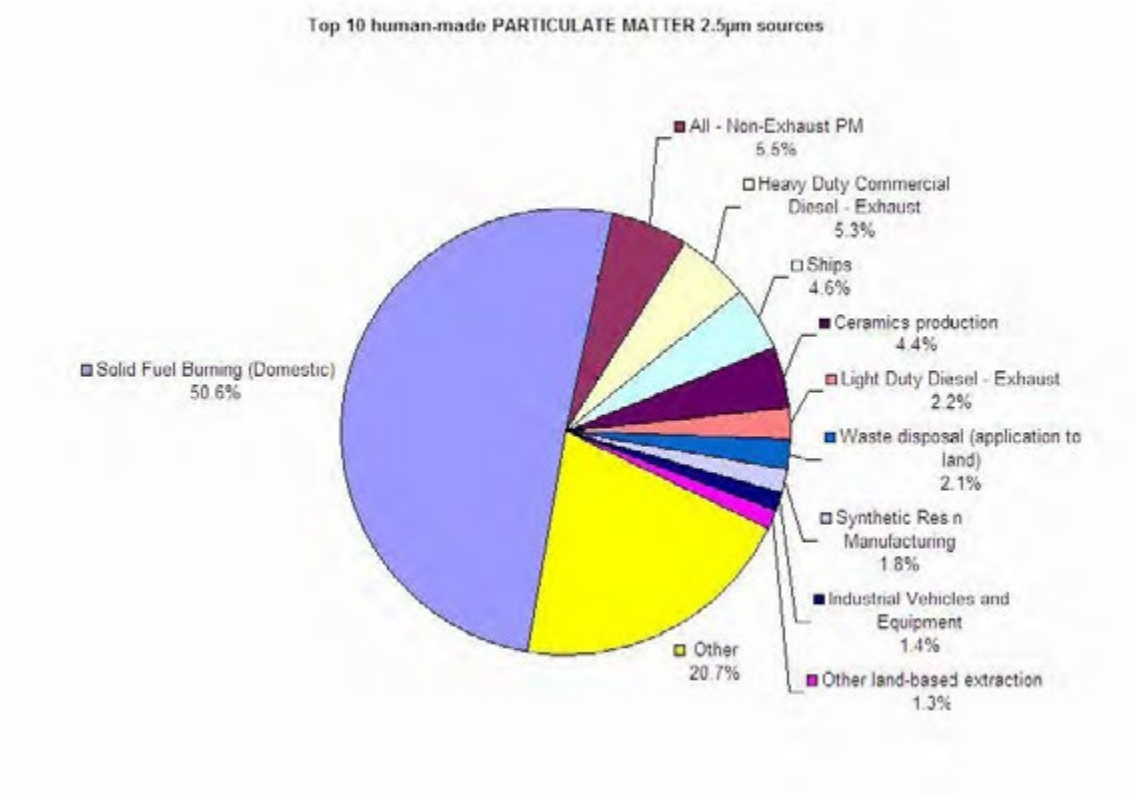

Figure 28. Top- the estimated percentage proportion on the top 10 $PM_{2.5}$ sources to the total annual $PM_{2.5}$ emissions in the Sydney region[7].

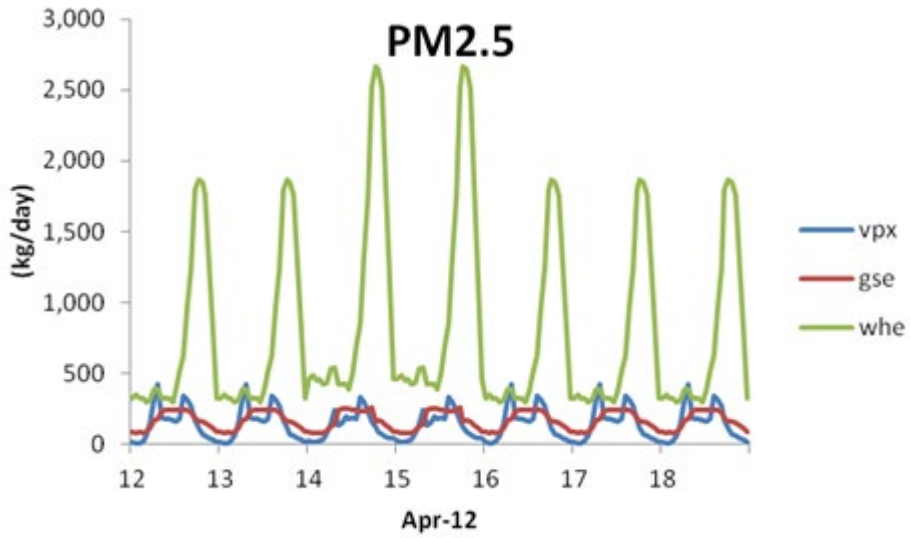

Figure 29. A comparison of the hourly $PM_{2.5}$ emissions from motor vehicles (vpx); commercial-domestic sources excluding wood heaters (gse); wood heaters (whe).

[7] http://www.environment.nsw.gov.au/resources/air/120255AEITR1NatHumanES.pdf

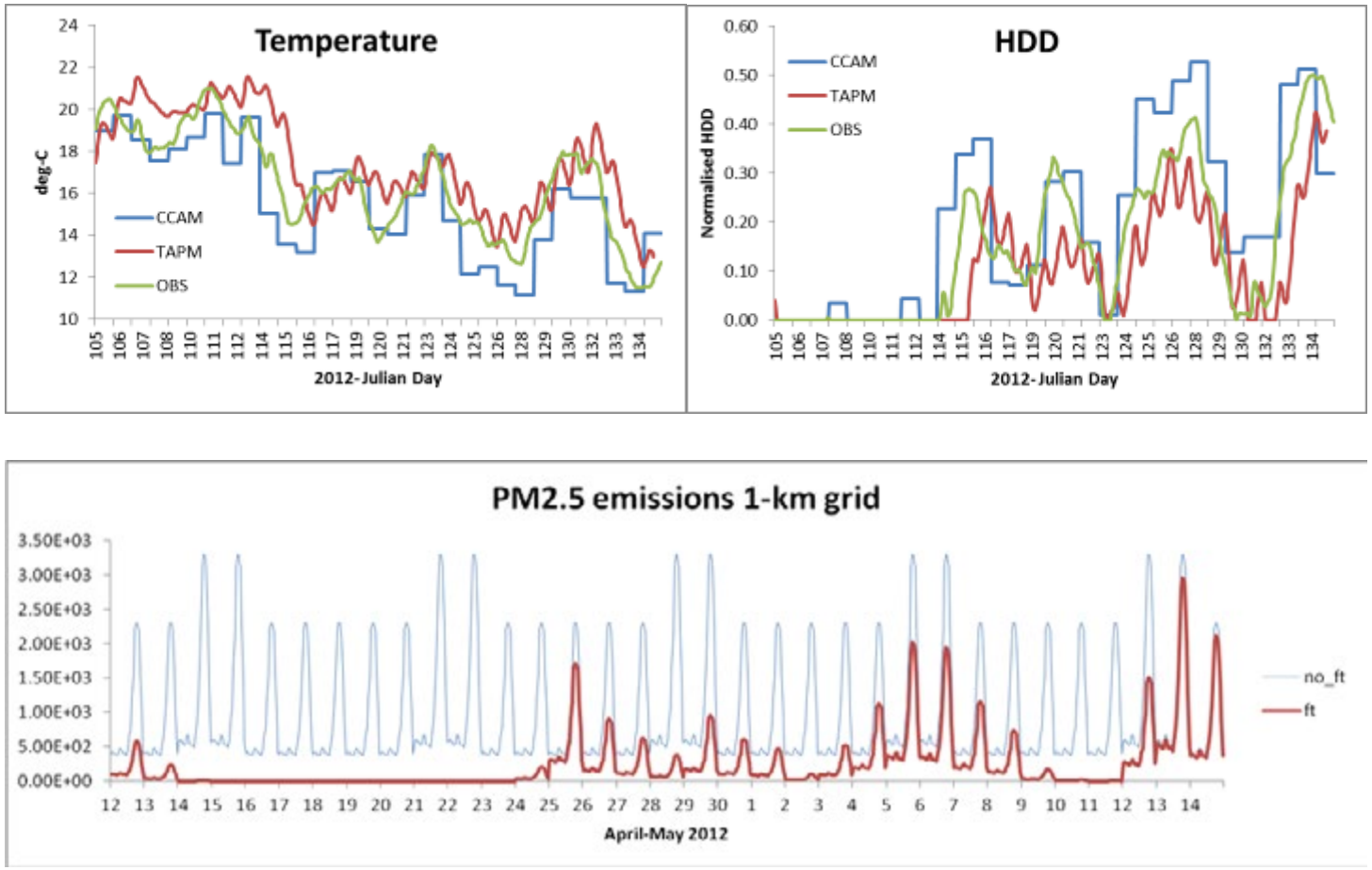

Figure 30. Top (left) observed and modelled daily average temperature for the Sydney basin for the period of SPS2. Top (right)- the observed and modelled normalised daily heating degree days for SPS2. Bottom- a comparison of the HDD scaled (ft) and unscaled (no_ft) daily wood heater emissions (kg/h) from the TAPM 1-km modelling domain..

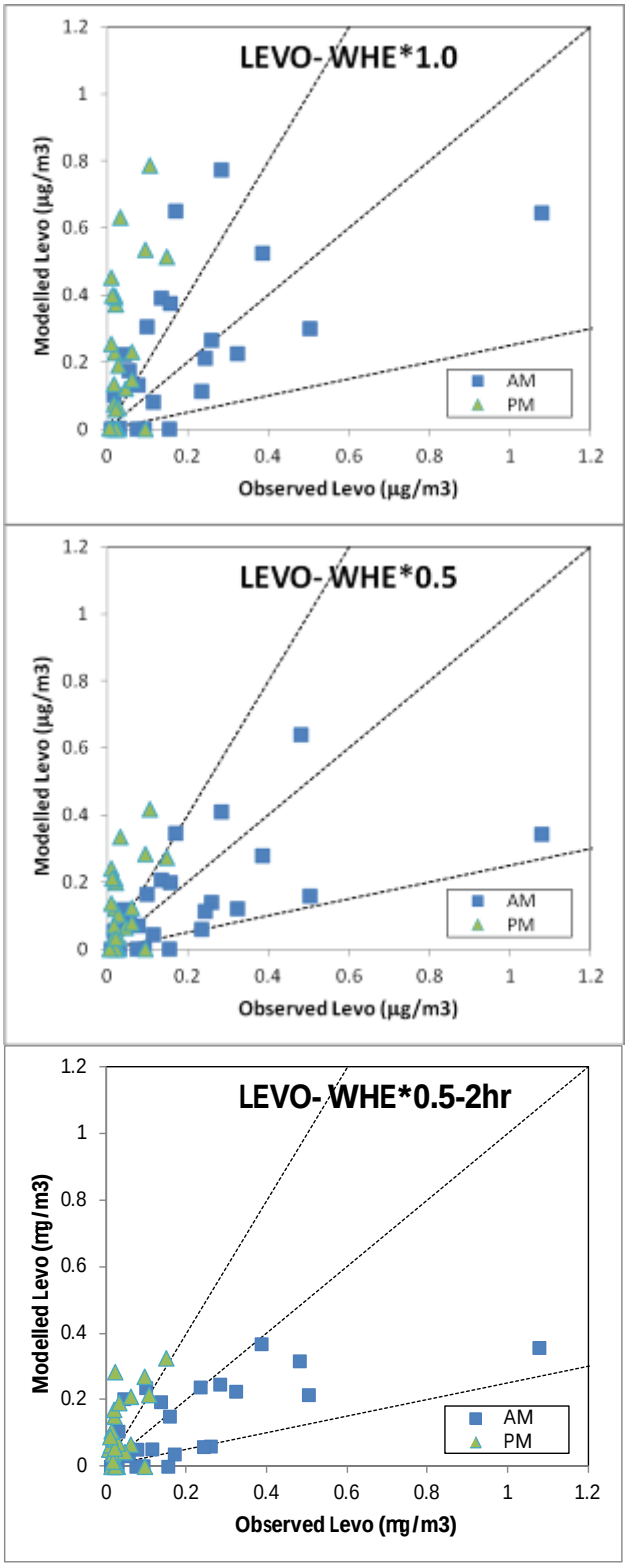

Figure 31. Modelled vs. observed levoglucosan calculated for various woodheater emission scenarios in the model in SPS2. Top- whe not scaled; middle whe emissions halved; bottom; whe emissions halved and staggered back in time by 2 hours. The dashed lines show ± factor of 2 and 1:1 agreement.

As a final check, the observed and modelled ratios of levoglucosan to $PM_{2.5}$ were analysed. Observations close to woodheater sources indicate that levoglucosan makes up about 25% of the emitted $PM_{2.5}$ (Meyer et al., 2008). If the woodheater emissions are the dominant source in Sydney over the SPS2 observation period, then it would be expected that that the observed levo:$PM_{2.5}$ ratios would fall at or below a 1:4 (25%) line (this assumes that the short-term loss rates of levoglucosan and $PM_{2.5}$ are similar). Points which fall below the line correspond to air masses where the $PM_{2.5}$ is also formed from sources other than wood combustion (and hence do not have a levoglucosan component). This is demonstrated in Figure 32 (right) where it can be seen that the morning ratios peak at about 4% (approximately), and the afternoon ratios peak at about 2%. This corresponds to wood heater emissions contributing a maximum of 16% and 8% respectively to the $PM_{2.5}$ burden in the Sydney airshed for the SPS2 observation period. Figure 32 (left) demonstrates that with the emission scaling approach described above, a similar distribution is generated by the modelling, including the differences between the morning and afternoon ratios.

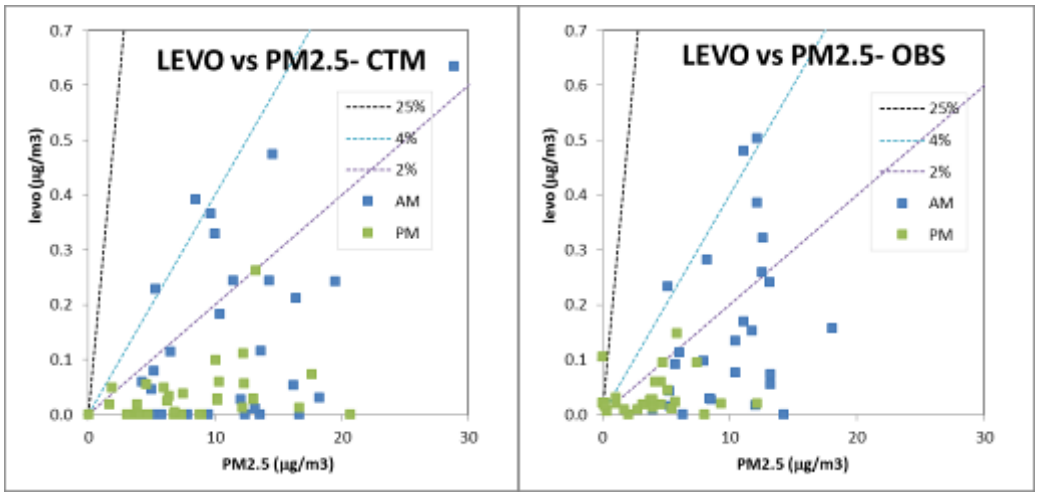

Figure 32. Left- modelled levoglucosan to $PM_{2.5}$ ratios for SPS2. Right- observed levoglucosan to $PM_{2.5}$ ratios.

Appendix A5 documents a case study which used the Sydney Particle Study modelling framework (including the woodheater emission approach described above) to assess the health impacts of wood heaters within the Sydney region. The case study highlights the need to consider all of the primary and secondary particle sources; and to correctly couple the wood heater emissions to the ambient environment. In the case study, the modelling was based on June 2004 meteorological conditions and it was estimated that wood heater emissions contributed between 10 and 30% to the $PM_{2.5}$ population exposure (with a population-weighted mean contribution of 18%).

4.5 Secondary inorganic particles- sulphate, nitrate and ammonium

Sulfate, nitrate and ammonium in fine particles are produced by chemical reactions in the atmosphere from gaseous precursors. The gaseous precursors for sulphate are sulfur dioxide (SO_2) from anthropogenic sources and volcanoes, and dimethyl sulfide (DMS) from marine plankton (note that SO_2 is produced in the oxidation pathway of DMS).

SO_2 can be oxidised in the gas phase or in the aqueous phase after SO_2 becomes dissolved in cloud droplets (aqueous production). Aqueous sulfate becomes aerosol when the cloud droplets evaporate. The sulfate in aerosol particles is present as sulfuric acid (H_2SO_4),

ammonium sulfate $(NH_3)_2SO_4$, or intermediate compounds, depending on the availability of gaseous ammonia to neutralize the sulfuric acid formed from SO_2.

The gaseous precursor for nitrate is nitrogen dioxide (NO_2) from anthropogenic sources. NO_2 is oxidised to form nitric acid (HNO_3) which is a weak acid compared to H_2SO_4. Thus any ammonium will preferentially neutralise H_2SO_4, however in the case of excess ammonium, ammonium nitrate (NH_4NO_3) may form in the fine particle range. In addition, HNO_3 may condense onto coarse sea salt aerosol, due to the weakly basic nature of sodium chloride, resulting in loss of Cl from the coarse aerosol as discussed in Section 4.4.1.

As discussed above oxidation can occur in both the gas and liquid phases. In this work the gas phase oxidation is simulated using ISORROPIA-iia which calculates the composition and phase state of an ammonia-sulfate-nitrate-chloride-sodium-(calcium-potassium-magnesium)-water inorganic aerosol in thermodynamic equilibrium with gas phase precursors (Fountoukis and Nenes 2007). Table 5 lists the reactions and physical constants used in ISORROPIA-iia. Aqueous phase oxidation is simulated in this work using an in-cloud sulfate processing algorithm incorporated into CTM (based on Seinfeld and Pandis). However Figure 33 shows there is little sensitivity of gaseous sulphate to cloud chemistry and hence aqueous phase oxidation processes were not modelled. Although aqueous phase conversion of sulfur dioxide to sulfate within cloud water droplets is very fast, during this study cloud processing was limited by the absence of suitable clouds.

Table 5. Equilibrium and temperature dependence constants used in ISORROPIA II. Taken from (Fountoukis and Nenes, 2007).

Reaction	Equilibrium Constant Expression	K^0 (298.15 K)	$\frac{\Delta H^0(T_0)}{RT_0}$	$\frac{\Delta c_p^0}{R}$	Units
$Ca(NO_3)_{2(s)} \leftrightarrow Ca^{2+}_{(aq)} + 2NO^-_{3\,(aq)}$	$\left[Ca^{2+}\right]\left[NO_3^-\right]^2 \gamma^2_{Ca^{2+}} \gamma^2_{NO_3^-}$	$\mathbf{6.067\times10^5}$	$\mathbf{-11.299}$♣	–	$mol^3\,kg^{-3}$
$CaCl_{2(s)} \leftrightarrow Ca^{2+}_{(aq)} + 2Cl^-_{(aq)}$	$\left[Ca^{2+}\right]\left[Cl^-\right]^2 \gamma_{Ca^{2+}} \gamma^2_{Cl^-}$	$\mathbf{7.974\times10^{11}}$	$\mathbf{-14.087}$♣	–	$mol^3\,kg^{-3}$
$CaSO_4.2H_2O_{(s)} \leftrightarrow Ca^{2+}_{(aq)} + SO^{2-}_{4(aq)} + 2H_2O$	$\left[Ca^{2+}\right]\left[SO_4^{2-}\right] \gamma_{Ca^{2+}} \gamma_{SO_4^{2-}} a_w^2$	$\mathbf{4.319\times10^{-5}}$	–	–	$mol^2\,kg^{-2}$
$K_2SO_{4(s)} \leftrightarrow 2K^+_{(aq)} + SO^{2-}_{4(aq)}$	$\left[K^+\right]^2\left[SO_4^{2-}\right] \gamma^2_{K^+} \gamma_{SO_4^{2-}}$	$\mathbf{1.569\times10^{-2}}$	$\mathbf{-9.589}$	$\mathbf{45.807}$	$mol^3\,kg^{-3}$
$KHSO_{4(s)} \leftrightarrow K^+_{(aq)} + HSO^-_{4\,(aq)}$	$\left[K^+\right]\left[HSO_4^-\right] \gamma_{K^+} \gamma_{HSO_4^-}$	$\mathbf{24.016}$	$\mathbf{-8.423}$	$\mathbf{17.964}$	$mol^2\,kg^{-2}$
$KNO_{3(s)} \leftrightarrow K^+_{(aq)} + NO^-_{3\,(aq)}$	$\left[K^+\right]\left[NO_3^-\right] \gamma_{K^+} \gamma_{NO_3^-}$	$\mathbf{0.872}$	$\mathbf{14.075}$	$\mathbf{19.388}$	$mol^2\,kg^{-2}$
$KCl_{(s)} \leftrightarrow K^+_{(aq)} + Cl^-_{(aq)}$	$\left[K^+\right]\left[Cl^-\right] \gamma_{K^+} \gamma_{Cl^-}$	$\mathbf{8.680}$	$\mathbf{-6.167}$	$\mathbf{19.953}$	$mol^2\,kg^{-2}$
$MgSO_{4(s)} \leftrightarrow Mg^{2+}_{(aq)} + SO^{2-}_{4(aq)}$	$\left[Mg^{2+}\right]\left[SO_4^{2-}\right] \gamma_{Mg^{2+}} \gamma_{SO_4^{2-}}$	$\mathbf{1.079\times10^5}$	$\mathbf{36.798}$	–	$mol^2\,kg^{-2}$
$Mg(NO_3)_{2(s)} \leftrightarrow Mg^{2+}_{(aq)} + 2NO^-_{3\,(aq)}$	$\left[Mg^{2+}\right]\left[NO_3^-\right]^2 \gamma_{Mg^{2+}} \gamma^2_{NO_3^-}$	$\mathbf{2.507\times10^{15}}$	$\mathbf{-8.754}$♣	–	$mol^3\,kg^{-3}$
$MgCl_{2(s)} \leftrightarrow Mg^{2+}_{(aq)} + 2Cl^-_{(aq)}$	$\left[Mg^{2+}\right]\left[Cl^-\right]^2 \gamma_{Mg^{2+}} \gamma^2_{Cl^-}$	$\mathbf{9.557\times10^{21}}$	$\mathbf{-1.347}$♣	–	$mol^3\,kg^{-3}$
$HSO^-_{4(aq)} \leftrightarrow H^+_{(aq)} + SO^{2-}_{4(aq)}$	$\frac{\left[H^+\right]\left[SO_4^{2-}\right]}{\left[HSO_4^-\right]} \frac{\gamma_{H^+}\gamma_{SO_4^{2-}}}{\gamma_{HSO_4^-}}$	$\mathbf{1.015\times10^{-2}}$	$\mathbf{8.85}$	$\mathbf{25.14}$	$mol\,kg^{-1}$
$NH_{3(g)} \leftrightarrow NH_{3(aq)}$	$\frac{\left[NH_{3(aq)}\right]}{\left[P_{NH_{3(aq)}}\right]} \gamma_{NH_{3(aq)}}$	$\mathbf{5.764\times10^1}$	$\mathbf{13.79}$	$\mathbf{-5.39}$	$mol\,kg^{-1}\,atm^{-1}$
$NH_{3(aq)} + H_2O_{(aq)} \leftrightarrow NH^+_{4(aq)} + OH^-_{(aq)}$	$\frac{\left[NH_4^+\right]\left[OH^-\right]}{\left[NH_{3(aq)}\right]a_w} \frac{\gamma_{NH_4^+}\gamma_{OH^-}}{\gamma_{NH_{3(aq)}}}$	$\mathbf{1.805\times10^{-5}}$	$\mathbf{-1.50}$	$\mathbf{26.92}$	$mol\,kg^{-1}$
$HNO_{3(g)} \leftrightarrow H^+_{(aq)} + NO^-_{3(aq)}$	$\frac{\left[H^+\right]\left[NO_3^-\right]}{P_{HNO_3}} \gamma_{H^+}\gamma_{NO_3^-}$	$\mathbf{2.511\times10^6}$	$\mathbf{29.17}$	$\mathbf{16.83}$	$mol^2\,kg^{-2}\,atm^{-1}$
$HNO_{3(g)} \leftrightarrow HNO_{3(aq)}$♠	$\frac{\left[HNO_{3(aq)}\right]}{\left[P_{HNO_3}\right]} \gamma_{HNO_{3(aq)}}$	$\mathbf{2.1\times10^5}$	$\mathbf{29.17}$	$\mathbf{16.83}$	$mol\,kg^{-1}\,atm^{-1}$
$HCl_{(g)} \leftrightarrow H^+_{(aq)} + Cl^-_{(aq)}$	$\frac{\left[H^+\right]\left[Cl^-\right]}{P_{HCl}} \gamma_{H^+}\gamma_{Cl^-}$	$\mathbf{1.971\times10^6}$	$\mathbf{30.20}$	$\mathbf{19.91}$	$mol^2\,kg^{-2}\,atm^{-1}$
$HCl_{(g)} \leftrightarrow HCl_{(aq)}$◇	$\frac{\left[HCl_{(aq)}\right]}{\left[P_{HCl}\right]} \gamma_{HCl(aq)}$	$\mathbf{2.5\times10^3}$	$\mathbf{30.20}$	$\mathbf{19.91}$	$mol\,kg^{-1}\,atm^{-1}$
$H_2O_{(aq)} \leftrightarrow H^+_{(aq)} + OH^-_{(aq)}$	$\frac{\left[H^+\right]\left[OH^-\right]}{a_w} \gamma_{H^+}\gamma_{OH^-}$	$\mathbf{1.010\times10^{-14}}$	$\mathbf{-22.52}$	$\mathbf{26.92}$	$mol^2\,kg^{-2}$
$Na_2SO_{4(s)} \leftrightarrow 2Na^+_{(aq)} + SO^{2-}_{4(aq)}$	$\left[Na^+\right]^2\left[SO_4^{2-}\right] \gamma^2_{Na^+} \gamma_{SO_4^{2-}}$	$\mathbf{4.799\times10^{-1}}$	$\mathbf{0.98}$	$\mathbf{39.75}$	$mol^3\,kg^{-3}$
$(NH_4)_2\,SO_{4(s)} \leftrightarrow 2NH^+_{4(aq)} + SO^{2-}_{4(aq)}$	$\left[NH_4^+\right]^2\left[SO_4^{2-}\right] \gamma^2_{NH_4^+} \gamma_{SO_4^{2-}}$	$\mathbf{1.817\times10^0}$	$\mathbf{-2.65}$	$\mathbf{38.57}$	$mol^3\,kg^{-3}$
$NH_{4(s)}Cl \leftrightarrow NH_{3(g)} + HCl_{(g)}$	$P_{NH_3} P_{HCl}$	$\mathbf{1.086\times10^{-16}}$	$\mathbf{-71.00}$	$\mathbf{2.40}$	atm^2
$NaNO_{3(s)} \leftrightarrow Na^+_{(aq)} + NO^-_{3(aq)}$	$\left[Na^+\right]\left[NO_3^-\right] \gamma_{Na^+} \gamma_{NO_3^-}$	$\mathbf{1.197\times10^1}$	$\mathbf{-8.22}$	$\mathbf{16.01}$	$mol^2\,kg^{-2}$
$NaCl_{(s)} \leftrightarrow Na^+_{(aq)} + Cl^-_{(aq)}$	$\left[Na^+\right]\left[Cl^-\right] \gamma_{Na^+} \gamma_{Cl^-}$	$\mathbf{3.766\times10^1}$	$\mathbf{-1.56}$	$\mathbf{16.90}$	$mol^2\,kg^{-2}$
$NaHSO_{4(s)} \leftrightarrow Na^+_{(aq)} + HSO^-_{4(aq)}$	$\left[Na^+\right]\left[HSO_4^-\right] \gamma_{Na^+} \gamma_{HSO_4^-}$	$\mathbf{2.413\times10^4}$	$\mathbf{0.79}$	$\mathbf{14.75}$	$mol^2\,kg^{-2}$
$NH_4NO_{3(s)} \leftrightarrow NH_{3(g)} + HNO_{3(g)}$	$P_{NH_3} P_{HNO_3}$	$\mathbf{4.199\times10^{-17}}$	$\mathbf{-74.735}$	$\mathbf{6.025}$	atm^2
$NH_4HSO_{4(s)} \leftrightarrow NH^+_{4(aq)} + HSO^-_{4(aq)}$	$\left[NH_4^+\right]\left[HSO_4^-\right] \gamma_{NH_4^+} \gamma_{HSO_4^-}$	$\mathbf{1.383\times10^0}$	$\mathbf{-2.87}$	$\mathbf{15.83}$	$mol^2\,kg^{-2}$
$(NH_4)_3\,H\,(SO_4)_{2(s)} \leftrightarrow 3NH^+_{4(aq)} + HSO^-_{4(aq)} + SO^{2-}_{4(aq)}$	$\left[NH_4^+\right]^3\left[SO_4^{2-}\right]\left[HSO_4^-\right] \times \gamma^3_{NH_4^+} \gamma_{SO_4^{2-}} \gamma_{HSO_4^-}$	$\mathbf{2.972\times10^1}$	$\mathbf{-5.19}$	$\mathbf{54.40}$	$mol^5\,kg^{-5}$

* Compiled by: Kim and Seinfeld (1995) and Kim et al. (1993) unless otherwise indicated; Reactions with constants in bold are new in ISORROPIA II.

♣ Compiled by: Kelly and Wexler (2005)

♠ The equilibrium constant K_{1b} of the reaction $HNO_{3(aq)} \overset{K_{1b}}{\longleftrightarrow} H^+_{(aq)} + NO^-_{3(aq)}$ is calculated from K_1 and K_{1a} of the reactions $HNO_{3(g)} \overset{K_1}{\longleftrightarrow} H^+_{(aq)} + NO^-_{3(aq)}$ and $HNO_{3(g)} \overset{K_{1a}}{\longleftrightarrow} HNO_{3(aq)}$, respectively: $K_{1b} = K_1 / K_{1a}$

◇ The equilibrium constant K_{2b} of the reaction $HCl_{(aq)} \overset{K_{2b}}{\longleftrightarrow} H^+_{(aq)} + Cl^-_{(aq)}$ is calculated from K_2 and K_{2a} of the reactions $HCl_{(g)} \overset{K_2}{\longleftrightarrow} H^+_{(aq)} + Cl^-_{(aq)}$ and $HCl_{(g)} \overset{K_{2a}}{\longleftrightarrow} HCl_{(aq)}$, respectively: $K_{2b} = K_2 / K_{2a}$

– Data not available

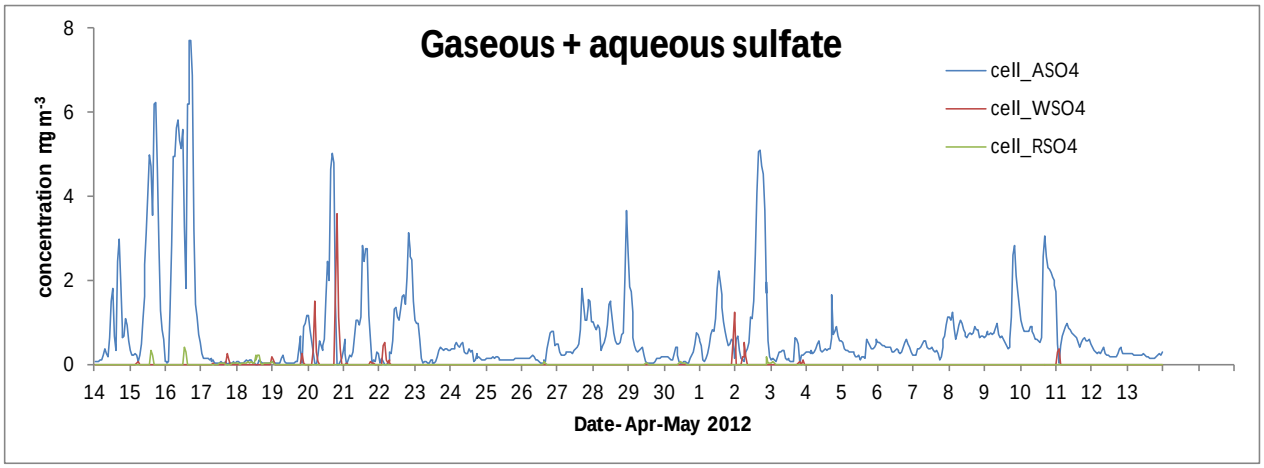

Figure 33. Plot shows the time series (for SPS2) of modelled dry sulfate (ASO4), cloud water sulfate (WSO4) and rain water sulfate (RSO4)

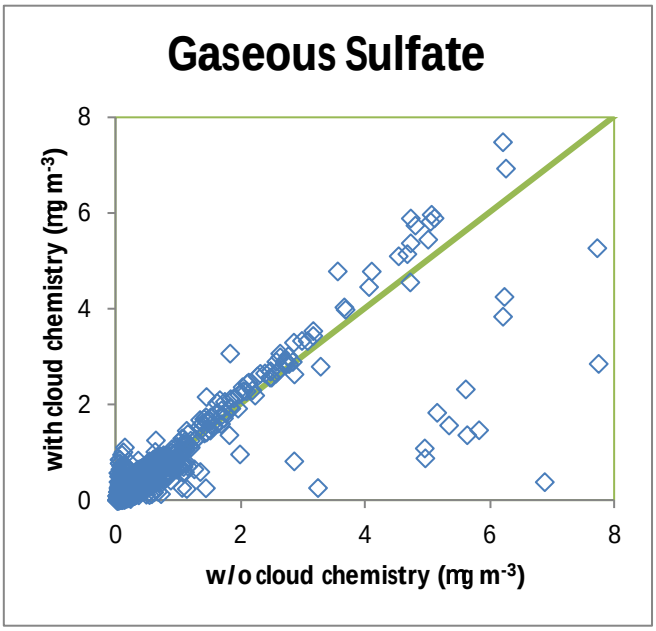

Figure 34. Plot shows the difference in the gas phase sulfate concentrations when sulfate production in cloud water and cloud rain are included.

Previously, Figure 16 showed that the inorganic compounds comprised 15% of the measured $PM_{2.5}$ aerosol mass at Westmead during SPS1. The most common form of these inorganic aerosols is ammonium sulfate and ammonium nitrate and thus ammonia is an additional precursor of these aerosols. The sources of these precursor gases within the Sydney airshed are mainly anthropogenic although oxides of nitrogen and ammonia may also be emitted from natural sources such as soils.

Sulfur dioxide is converted to sulfuric acid and hence to sulfate aerosol through gas-phase radical chemistry which is primarily driven by volatile organic compounds (aqueous phase conversion of sulfur dioxide to sulfate within cloud water droplets is much faster, but is limited by the presence of suitable clouds as noted above). Note that approximately 3% of SO_x is also directly emitted as sulfate, and thus sulfate is both a primary and a secondary aerosol. Sulfate is also present in sea salt (comprising approximately 8% of the dry mass of sea salt aerosol).

Oxides of nitrogen are converted to nitric acid which can then combine with ammonia to partition into the aerosol phase as ammonium nitrate. However, while ammonium sulfate is non-volatile and remains in the aerosol phase, ammonium nitrate may partition between the gas- and aerosol phases depending on temperature and other environmental factors.

Figure 35 compares the observed time series of sulfate and nitrate measured by the aerosol mass spectrometer (AMS) and from filter measurements for SPS1. The concentration peaks observed on 11th February correspond to a day of moderate photochemistry.

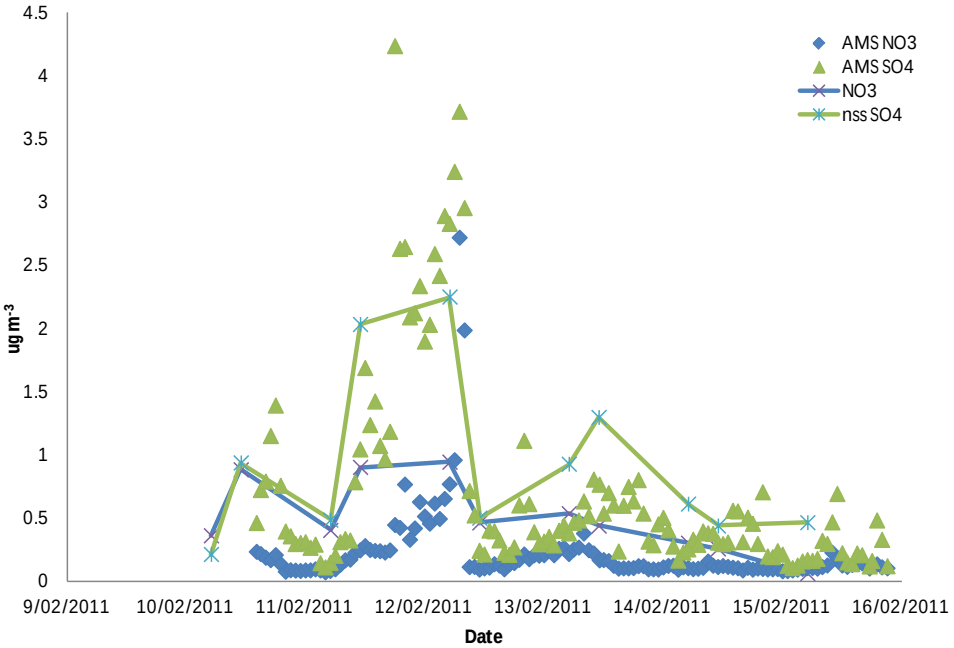

Figure 35. Time series of AMS and $PM_{2.5}$ filter data for sulfate and nitrate particles for SPS1. Note the difference in the averaging time as the cartridge data only make 2 measurements per day.

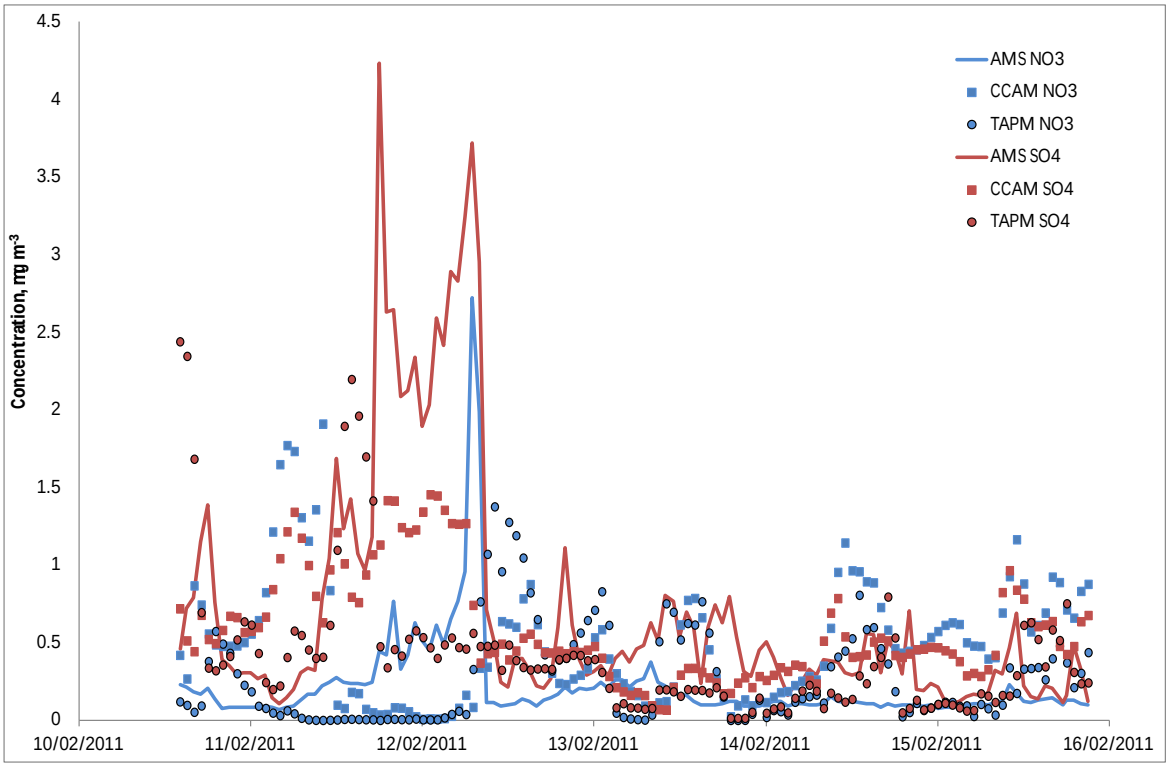

Figure 36. Time series of the AMS and modelled data for sulphate and nitrate particles. The averaging period is the same for both datasets

Figure 36 compares the modelled and observed sulfate and nitrate of a 7 day period in SPS1. We see that the modelled estimate of sulfate aerosol is under-predicted whilst the nitrate contribution is over-predicted. We test two hypotheses; that either there is not enough SO_2 being emitted or that the assumption of 3% transfer of SO_2 to SO_4 aerosol is not enough. We discount the fact that the chemical reaction rate to form SO_4 may not be fast enough, as the rate in both models is similar to the kinetic rate data from the Jet Propulsion Laboratory (JPL, 2011).

To test the SO_2 emissions we compare the modelled and observed SO_2 at Westmead for SPS2 (in Figure 37). If there are not enough SO_2 emissions then we expect the modelled SO_2 scatter points to systematically fall below the 1:1 line. The observed SO_2 generally stays below 10 $\mu g/m^3$ whilst both models exceed this on a few occasions. These tend to be in the afternoon for CCAM and morning or afternoon for TAPM. The lack of significant model bias indicates that the models and observations are similar >10 $\mu g/m^3$, and suggests that there are enough SO_2 present in the models.

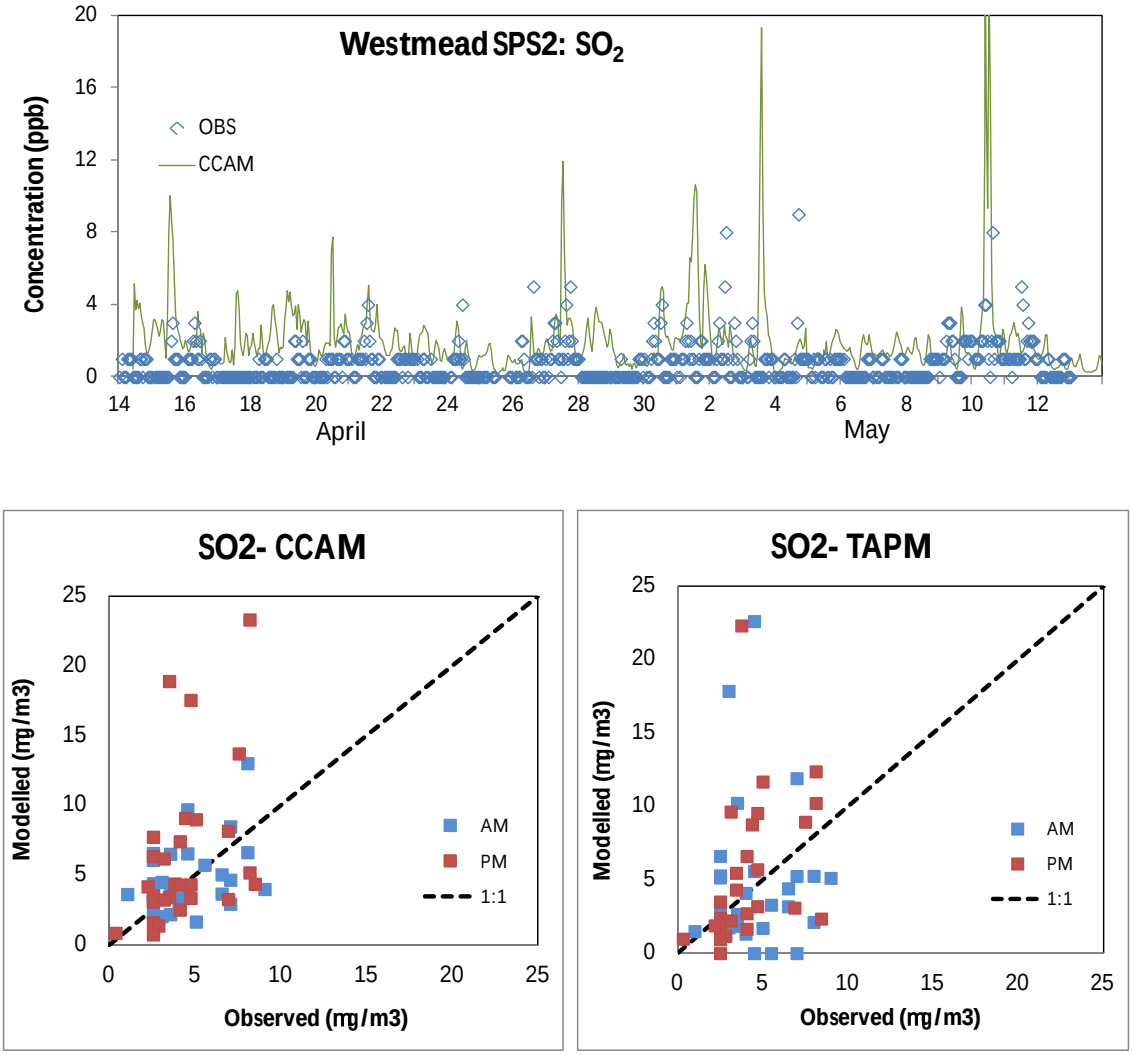

Figure 37. Top- time series of observed and modelled 1-h SO_2 concentration at Westmead for SPS2. Bottom- scatter plots of observed and modelled (left- CCAM; right- TAPM) for SPS2.

To test the proportion of sulfur residing in the gas and aerosol phases, we now compare the ratio of SO_4 to the total SOx concentration; that is the sum of gas and aerosol phase sulfate together in Figure 38. We plot a dashed line at SO_4=5% of the SOx to help indicate the relationships. This line approximately bounds the minimum SO_4:SOx ratio. Both models and the observations have the majority of their points at or above the 5% line suggesting that the emitted SO_4 fraction is about 5% of the total sulphur. Points which lie above the 5% line represent chemistry occurring in the model and observations, or localised particulate emission events not in the emissions inventory such as ship plumes.

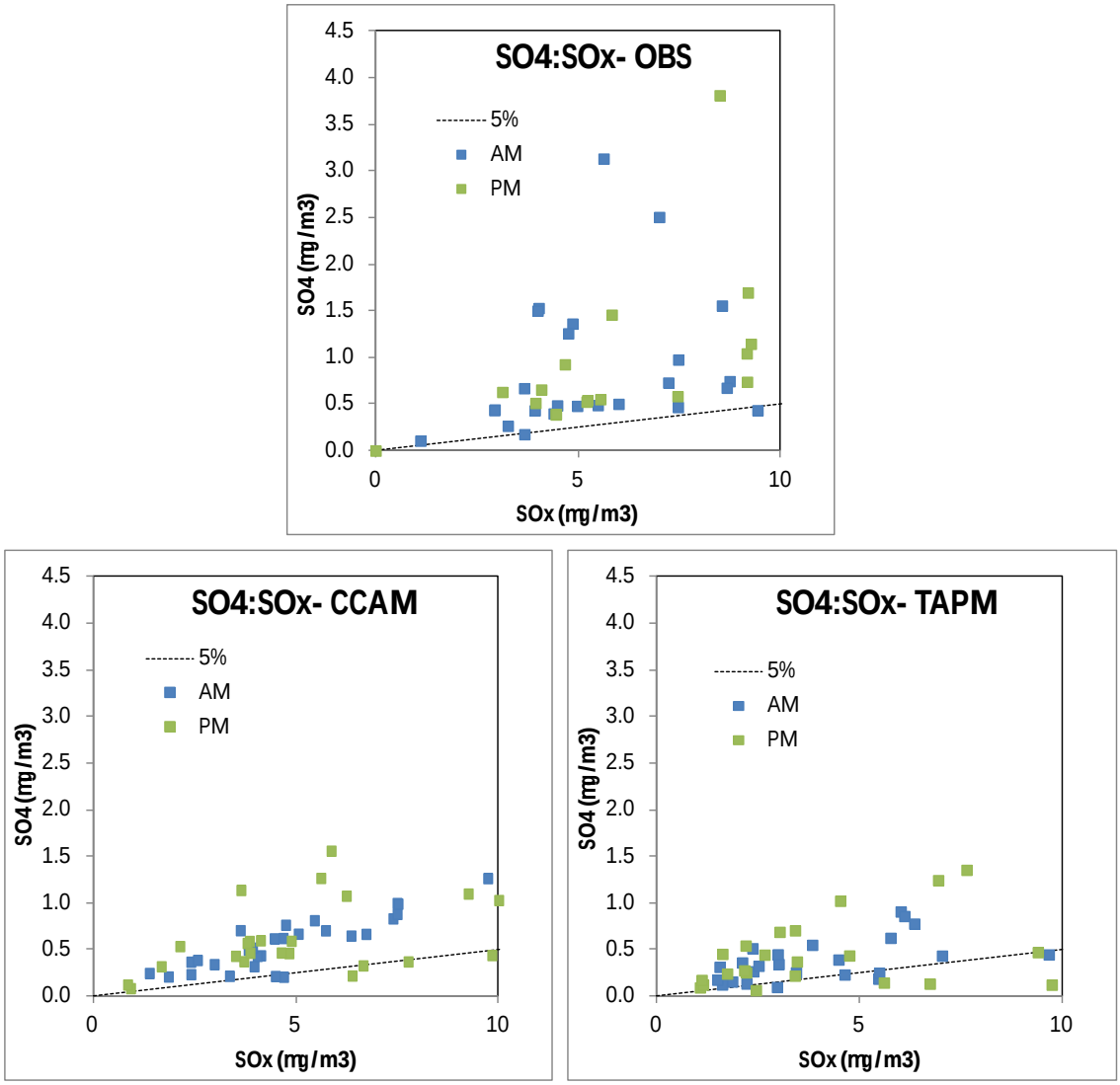

Figure 38. Scatter plots to show ratio of SO_4 to total SOx between the observations (top) and both models (underneath) for the autumn SPS2 campaign.

Figure 39 shows the observed and modelled ratio of particulate NO_3 (NIT) to the sum of the gas phase HNO_3 and particulate NO3 (NITx) for SPS2. We plot a 100% line on each of the plots for reference. The plots show that slightly more gas phase NITx resides in the models, especially in the afternoon, than is observed.

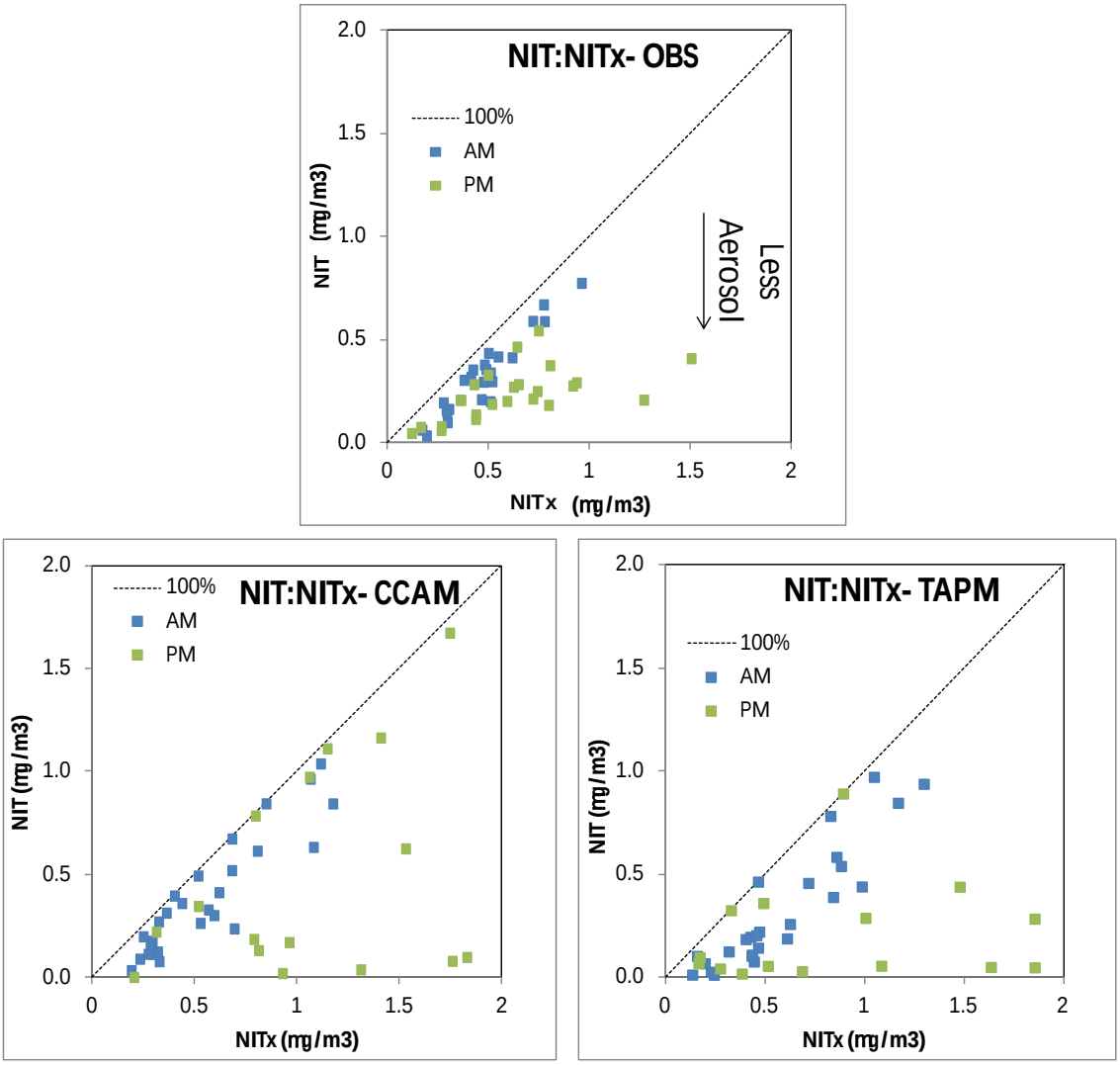

Figure 39. Scatter plots to show ratio of NO_3 to total NITx between the observations (top) and both models (underneath) for the autumn SPS2 campaign.

Figure 40 shows the observed and modelled ratio of particulate ammonium (NH4) to the sum of the gas phase ammonia and particulate ammonium (NHx) for SPS2. We plot a 50% line on each of the plots for reference. The observations show most of the points fall just underneath this line demonstrating that the aerosol phase ammonium makes up around 40% of the total NHx. In the case of both models the aerosol phase proportion is less than observed, particularly for TAPM where the great majority (up to 80%) of the NHx still resides in the gas phase. We conjecture if there was more sulphate available then more of the NHx would form aerosol. The modelled concentrations of NHx are larger than those observed particularly for

TAPM. This may be as a result of the uncertainties introduced from the top-doen speciation methodology used to generate NH_3 in the inventory.

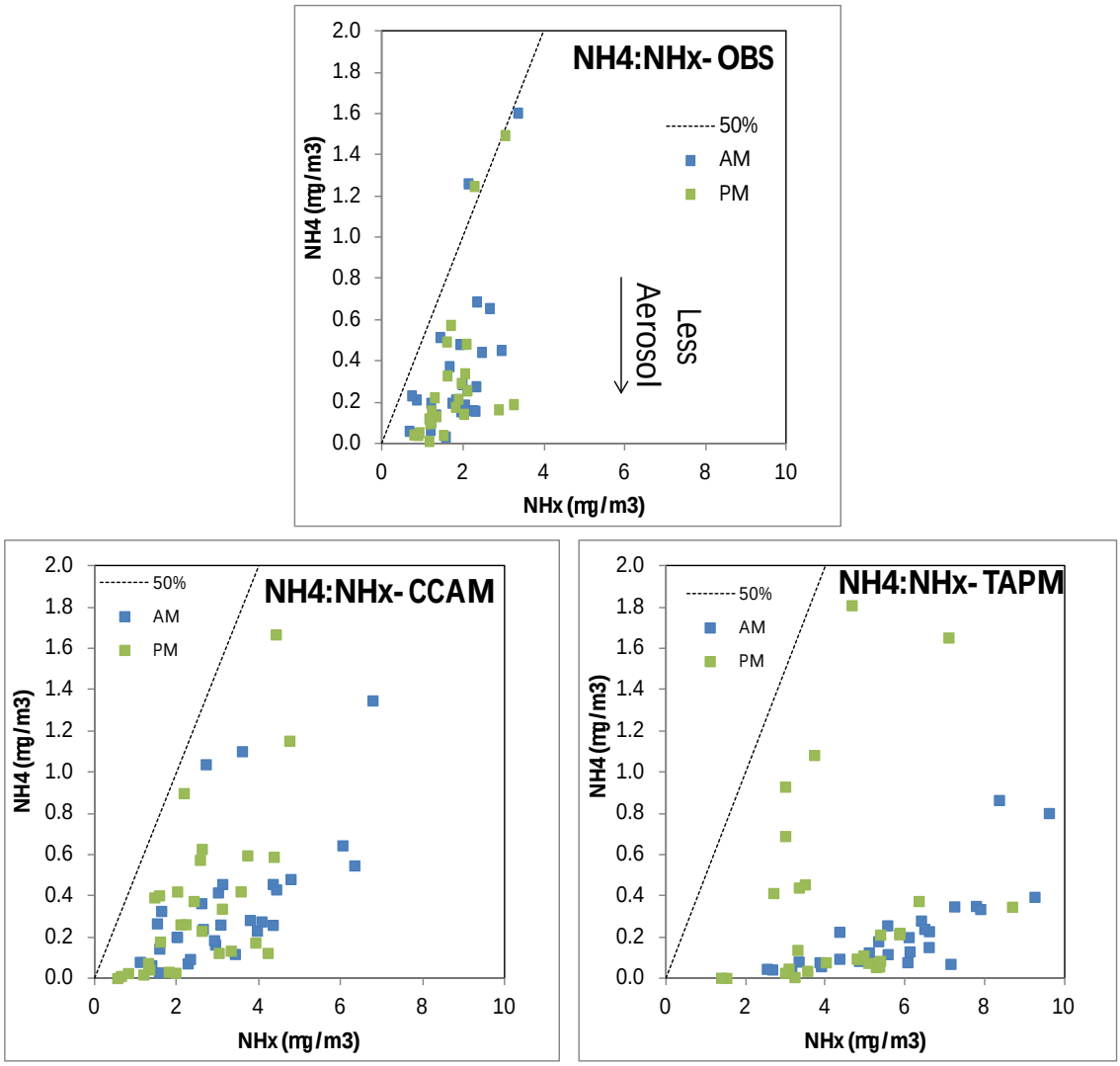

Figure 40. Scatter plots to show ratio of NH_4 to total NHx between the observations (top) and both models (underneath) for the autumn SPS2 campaign.

Because the precursors of sulfate and nitrate are mainly anthropogenic, options are available to control these inorganic aerosols, with the most straightforward approach being to reduce the sulfur content of fuels. The control of nitrates is more complex given that nitrate production is driven by the concentrations of NO_X, VOCs and NH_3 and the relationship between nitrate production and these precursors are non-linear.

4.6 Carbon

In this study, three forms of carbon are observed. These are: volatile organic compounds present in the gas phase; organic carbon particles that can come from either primary or secondary sources, and in the case of secondary sources arise from the oxidation of volatile organic compounds in the atmosphere (Goldstein and Galbally 2007), and elemental or black carbon which arises from primary sources, primarily combustion (Bond et al. 2004).

4.6.1 ELEMENTAL CARBON

From the pie charts shown in Figure 16 and Figure 17, it can be seen that the EC makes up 6% and 16% of the mass of observed $PM_{2.5}$ for SPS1 and SPS2, respectively. The models yield too much in SPS1 (15% and 15% for CCAM and TAPM respectively) and do well in SPS2 (21% and 18% for CCAM and TAPM respectively). Because EC is a primary emission, is non-volatile, non-reactive and generally has a low background concentration, the relationship between emission rate and concentration is approximately linear. Thus vehicle emission controls should lead to a small but robust reduction in EC loading. Note however that there may also be periods of time when the Sydney airshed is impacted by EC emitted from other sources such domestic wood combustion, and biomass burning plumes from control burns and bushfires.

4.6.2 ORGANIC AEROSOL

Primary organic aerosol (POA) is directly emitted into the atmosphere in the solid phase, e.g. organic particles in car exhaust. There are also organic gases emitted into the atmosphere that are subsequently oxidized and transfer from the gas phase to the particulate phase by either condensing on existing particles or by nucleating to form new particles. Common organic gases which react to form particles include toluene, xylene and monoterpenes for example. This organic particulate material is called secondary organic aerosol. Examples are the haze over the Blue Mountains and the Brown Haze in Sydney. A schematic of organic aerosol formation is shown in Figure 41.

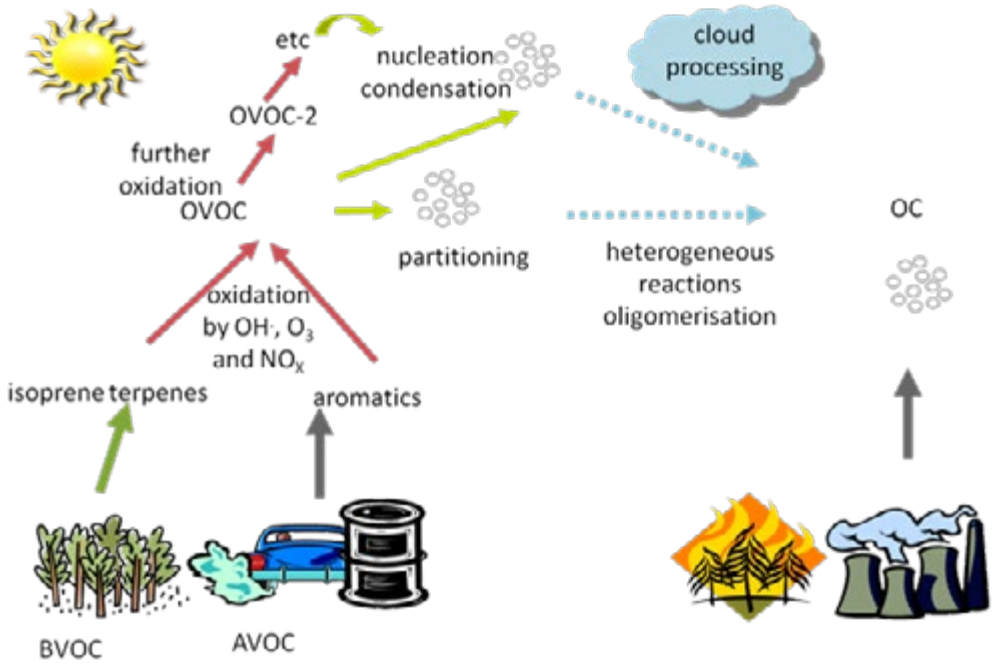

Figure 41. Schematic diagram showing the formation of secondary organic aerosol from the oxidation of biogenic and anthropogenic VOCs

As secondary organic material becomes more oxidised, or 'aged', the compound becomes less volatile (Goldstein and Galbally, 2007) and either nucleates to form new particles or condenses out upon existing particles. In either case the process leads to the growth in mass of secondary organic aerosol. Figure 42 demonstrates how carbon is aged in the modelling framework, by means of splitting the carbon mass into a number of 'volatility bins'. As the carbon is oxidised most of it moves to bins of lower volatility. However there are reverse reactions due to both further oxidation and also the inherent partitioning between the vapour and particulate phase of any compound, which causes some SOA to return to the vapour phase. These processes are represented in the model.

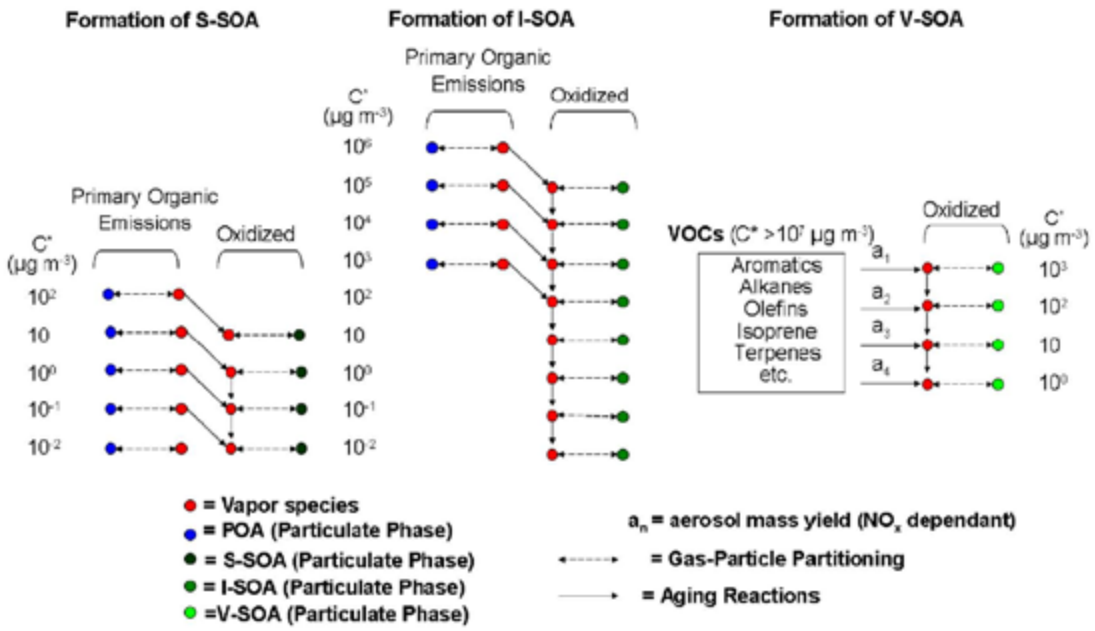

Figure 42. How the model treats semi-volatile OC. Taken from (Tsimpidi et al., 2010).

4.6.3 OBSERVATIONS OF ORGANIC AEROSOL PRECURSORS

A Proton Transfer Mass Spectrometer (PTR-MS) was utilized to determine the real-time volatile organic compound (VOC) composition and concentration at Westmead from 19th February – 7th March 2011. Twenty one anthropogenic and biogenic VOCs were observed with the continuous monitoring. A total of 50 VOCs were identified between the PTR-MS and the integrated (multi hour adsorbent tube and DNPH cartridge) sampling. These VOCs were examined along with the AMS organic aerosol to identify the possible precursors to secondary organic aerosol. The hourly averaged organic aerosol mass concentrations from the AMS and the VOC concentrations from the PTR-MS were compared for different times of the day and Table 6 presents these selected for correlation coefficients of 0.7 or greater. For the early morning hours of 04:00 to 10:00 biogenic monoterpenes, emitted primarily by trees, have the largest correlation (R = 0.71). During the day from 11:00 to 15:00 biogenic isoprene and its oxidation products, formic acid along with ambient temperature which is a major driver of biogenic emissions, have the largest correlations (R = 0.81, 0.72, 0.90 respectively). Isoprene is emitted from plants, primarily trees. Isoprene emissions increase with both sunlight and temperature. Isoprene has a short life in the atmosphere and so its oxidation products are also a good measure of its emissions. During the evening and night from 18:00 to 23:00

anthropogenic pollutants as reflected by acetonitrile emitted almost exclusively from biomass burning, and nitrogen oxides, emitted from fossil fuel and biomass combustion have the highest correlations (R = 0.79, 0.72 respectively). This indicates that even during the course of a typical day there are a variety of VOC sources of secondary organic aerosol.

Table 6. Correlation coefficients for the relationship between hourly average aerosol organic mass and some VOCs, NO_X and temperature for SPS1. The hourly averages for each variable were grouped according to time of day into morning (4am – 10am), afternoon (11am – 3pm) and night (6pm – 11pm).

	Morning	Afternoon	Night
Isoprene + oxidation products	0.53	**0.81**	0.35
Monoterpenes	**0.71**	0.11	0.16
Acetonitrile	0.12	0.07	**0.79**
Formic acid	0.40	**0.72**	0.65
Temperature	0.28	**0.90**	0.48
NOx	0.44	-0.37	**0.72**

Evidence of these correlations can be seen in Figure 43 which shows the time series of the mass loading of organic aerosol and selected PTRMS results for the period 19-24 February 2011. It can be seen that the AMS organic mass loadings are elevated for the period midday 19th – early 20th of February and that this peak was related to isoprene and its oxidation products and monoterpenes. This is an example of secondary organic aerosol attributed primarily from oxidation of biogenic VOC precursors. A second peak in organic aerosol was observed on the 23rd February and this peak was associated primarily with aromatic VOCs. This is an example where the organic aerosol may be attributed to primary organic aerosol emitted from anthropogenic sources or secondary aerosol formed from VOCs emitted from anthropogenic sources.

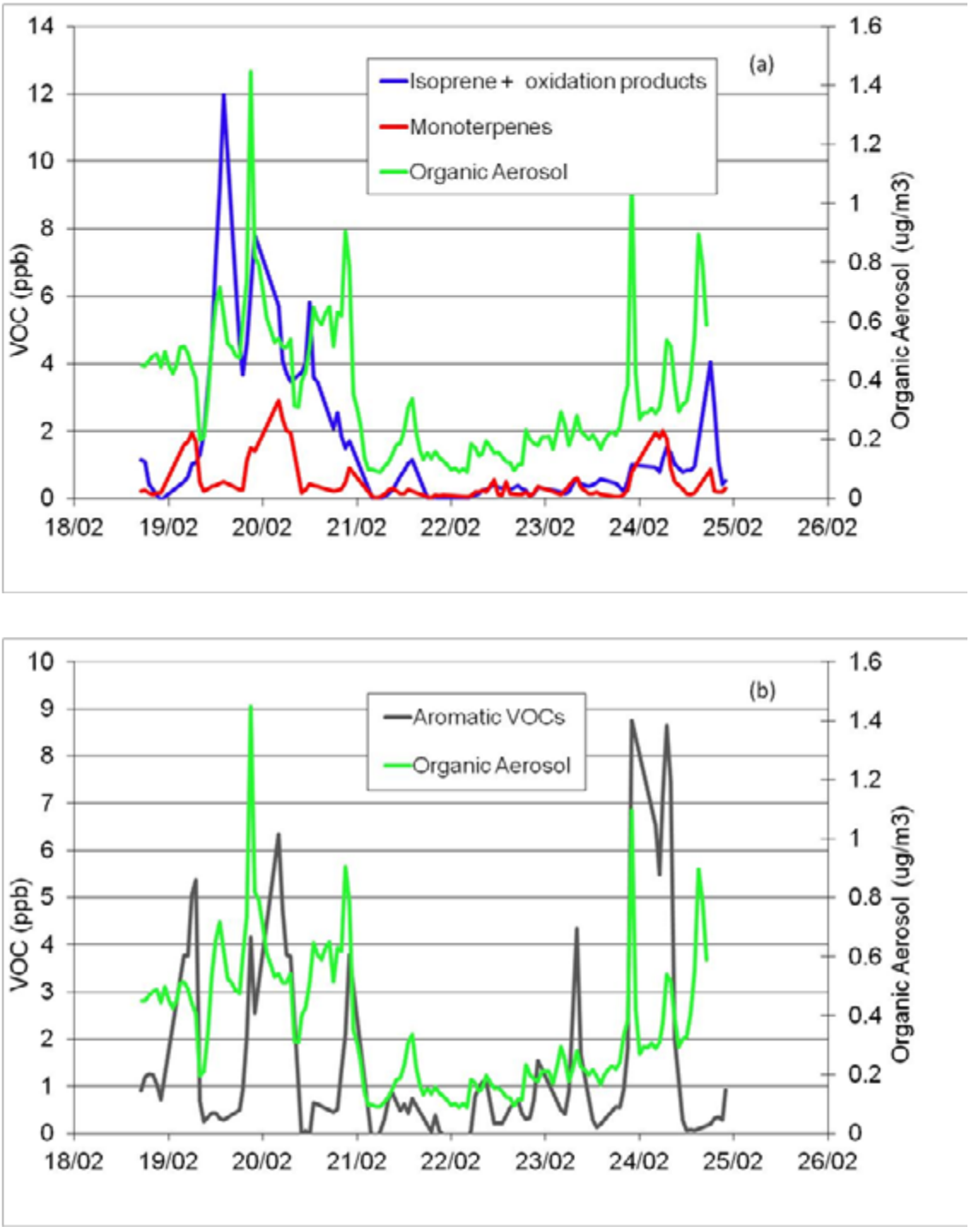

Figure 43. The observed organic aerosol and (a) biogenic isoprene and monoterpenes and (b) anthropogenic aromatic hydrocarbons observed at Westmead during SPS1.

4.6.4 OBSERVED AND MODELLED VOC PRECURSOR RATIOS

In Figure 44 the ratio of toluene to xylene determined by two independent measurement methods at Westmead and the modelled ratio using the Sydney emissions inventory are

compared for SPS1. For this aspect of the inventory good agreement between the observations and the inventory are observed.

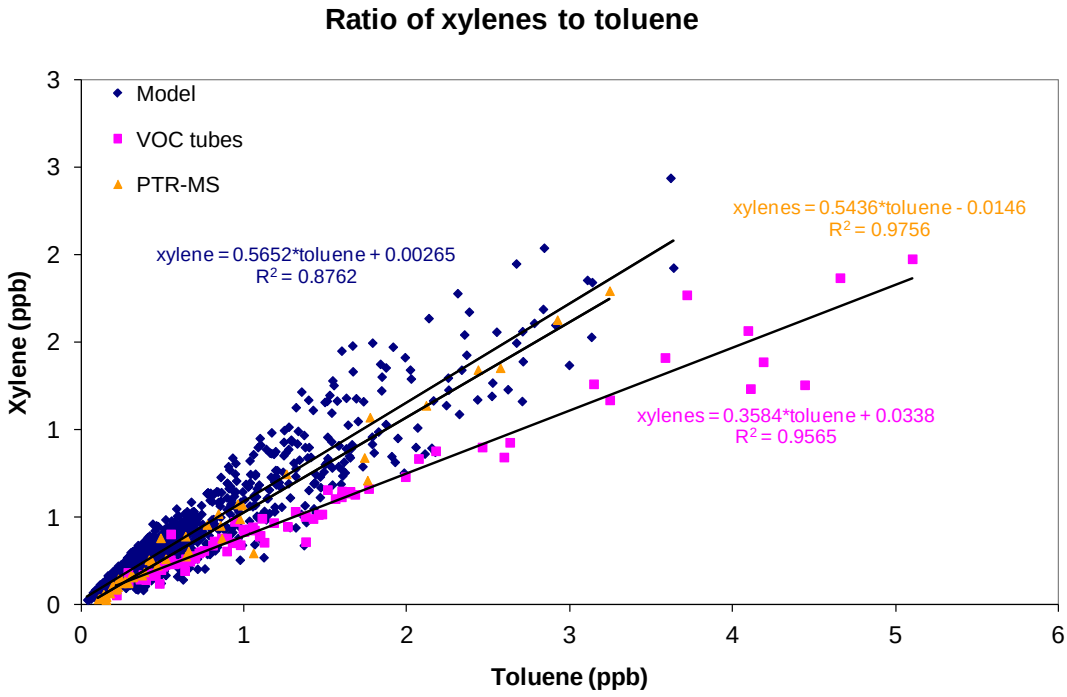

Figure 44 Scatter plot showing the relationship between toluene and xylene in the inventory/model and two independent sets of observations at Westmead during SPS1.

Observed ratios of benzene and toluene at a number of different atmospheric environments are shown in Figure 45, and suggests that pure woodsmoke contains a much greater proportion of benzene than toluene. In heavy traffic (the grey bars) environments the benzene:tolunene ratio is above 0.5 whilst in urban environments (the blue bars) the ratio is generally less than 0.5. Figure 46 shows a plot of benzene and toluene for SPS2 for both models and the measurements. The observations show that as the concentration of toluene increases, the concentration of benzene stabilises. This plateau presumably arises because of the influence of domestic and commercial sources of toluene at higher concentrations. The sources (solvents, paints etc) contain toluene but only very low levels of benzene. This is not the case in the models which show increasing benzene with increasing concentrations of toluene.

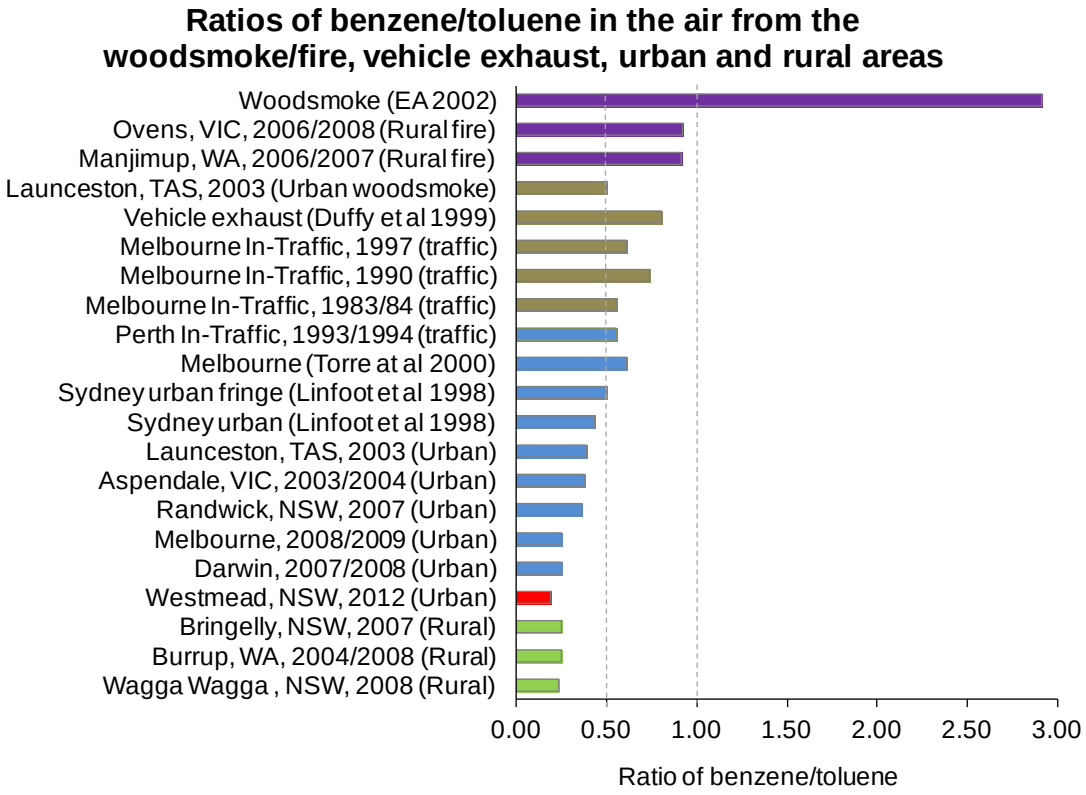

Figure 45. The benzene:toluene ratio in the observations at Westmead (shown in red) compared with other urban and rural observations. The colours refer to conditions relating to fire (purple), traffic (grey), urban areas (blue) and rural (green).

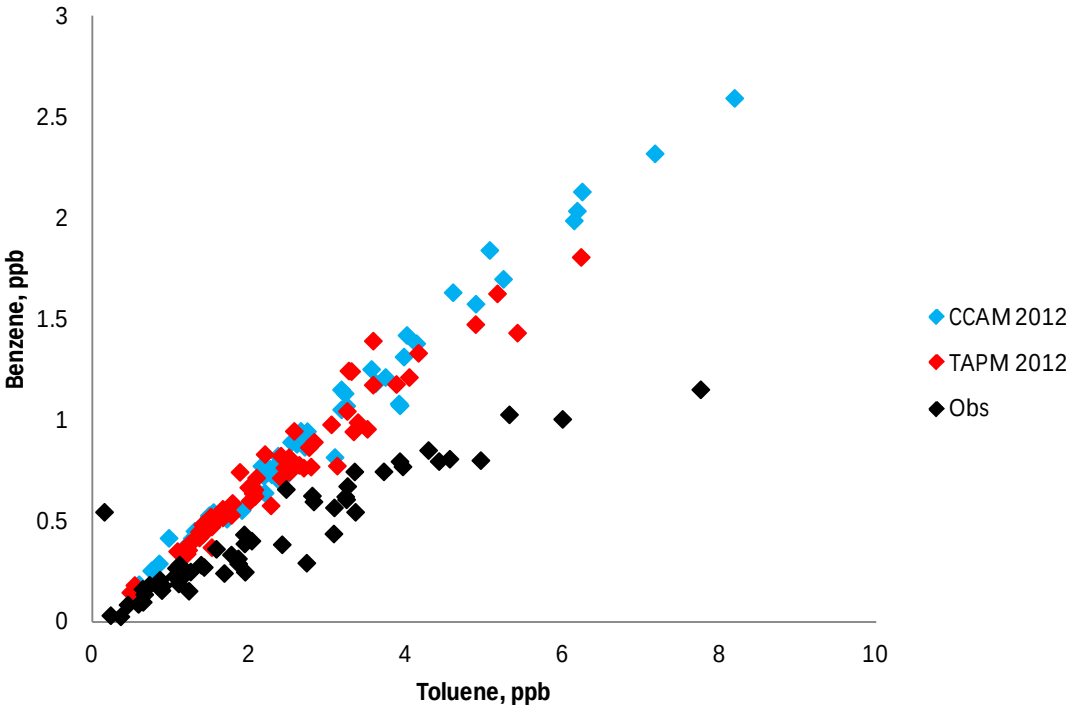

Figure 46. Modelled and observed benzene and toluene during SPS2.

Figure 47 examines the modelled and observed ratio of the reaction products of the biogenic VOC isoprene to its sum of isoprene and oxidation products (methacrolein and methylvinyl ketone). This ratio is a measure of the photochemical ageing of isoprene emissions within the air. While there are additional products of isoprene oxidation including formaldehyde, both the observations and models have treated these separately. Formaldehyde is not included because it has multiple other sources in the urban atmosphere. In SPS1 the models are showing more isoprene plus oxidation products are present than in the observations, indicating perhaps an overestimate of the isoprene emissions during this period. The observed ratios overlap indicating that the combination of air chemistry, meteorology and location of isoprene sources is similar in the models and the observations. Both models are closer to the observations during SPS2, with CCAM performing particularly well. Perhaps with the weaker solar strength in autumn, the isoprene emissions are represented more accurately. Again it appears, particularly for CCAM that the combination of air chemistry, meteorology and location of isoprene sources is similar in the models and the observations.

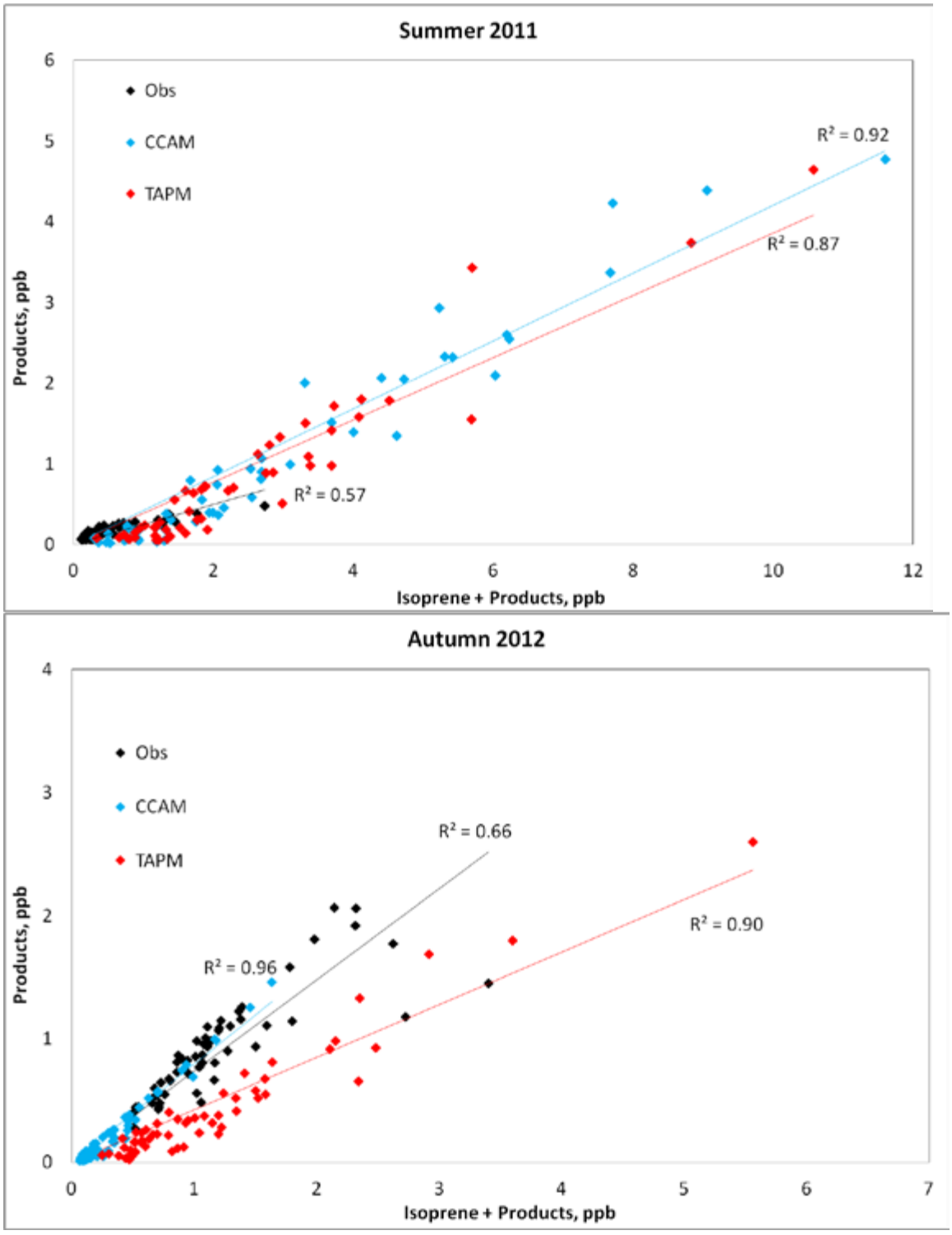

Figure 47. Ratio of the products of the isoprene reaction to isoprene + products during SPS1 (top) and SPS2 (bottom). In the observations and models the products used here are methacrolein and methyl vinyl ketone. In the model these products are described as 'ISPD'.

4.6.5 SECONDARY ORGANIC AEROSOL

We have calculated the secondary component of the observed organic aerosol using the OC:EC ratio method (Keywood et al., 2012).The program of collecting samples in the morning and afternoon means the OC/EC_{pri} for motor vehicle emissions can be readily determined from the morning OC/EC sample ratios in the case where motor vehicles are the only source of OC_{pri} in the morning. This is the case for the Summer SPS1 campaign, however during the Autumn SPS2 campaign, significant concentrations of levoglucosan the tracer for biomass burning, were measured in the morning samples with the morning levoglucosan concentrations being greater than the afternoon samples of each day. Biomass burning smoke includes primary OC. The higher levoglucosan concentrations measured in the morning of the Autumn SPS2 samples is due to the low dispersion rate in the surface air before sunrise, resulting in a build-up of pollutants. Thus the contribution of smoke OCpri should be accounted for when determining the SOA concentration using the EC tracer method for these samples.

We can determine the OC/EC_{pri} for the biomass burning source using the OC/EC measured in samples with levoglucosan concentrations in the greatest 75^{th} percentile. For the afternoon samples the levoglucosan/OC ratio averages 1% and ranges between 0 and 7%, therefore making it unnecessary to determine the contribution of OC/EC_{pri} from smoke to the afternoon samples. For the morning samples the levoglucosan/OC comprises between 0-15% (median 5%), so the contribution of biomass burning OC/EC_{pri} is more significant.

Intuitively this makes sense since the biomass burning smoke present in the morning samples results from the build up of smoke overnight and some of this smoke may be aged (with SOA being present). For the analysis presented here though we focus on SOA generated in the afternoons, and because of the low levoglucosan concentrations in the afternoon, we do not account for OC/ECpr from biomass burning in this analysis.

Figure 48 shows the OC and EC concentrations measured in the morning and afternoons of both measurement campaigns. The slope of the lower envelope line of the OC/EC relationship determined in the morning samples represents the OC/ECpri for motor vehicle emissions. Figure 48 shows that the OC/EC pri for motor vehicles is similar for each measurement campaign (Summer SPS1 1.21, Autumn SPS2 1.0), and are similar to that used in other published studies for motor vehicle sources (ranging from 0.7 for the City Link Tunnel (Keywood et al., 2011) to 2.2 for light duty petrol vehicles in Los Angeles (Hildemann et al.,

1991)). Figure 48 also shows the OC and EC concentrations predicted by CCAM and TAPM for the morning and afternoon periods of SPS1 and SPS2. In both campaigns the model AM points sit below the measured OC/EC_{pri} lines showing the influence of the morning rush hour through the higher EC concentrations predicted. In the afternoons of both campaigns the models predict more organic carbon as this is produced through photochemical activity. The models follow the observed data very well, both in magnitude and in the observed pattern of where the AM and PM points sit. The overall modelled OC/EC ratio is slightly lower than observed, perhaps because the models are not seeing enough OC in the mornings, due in part to the volatility of the motor vehicle emissions being uncertain.

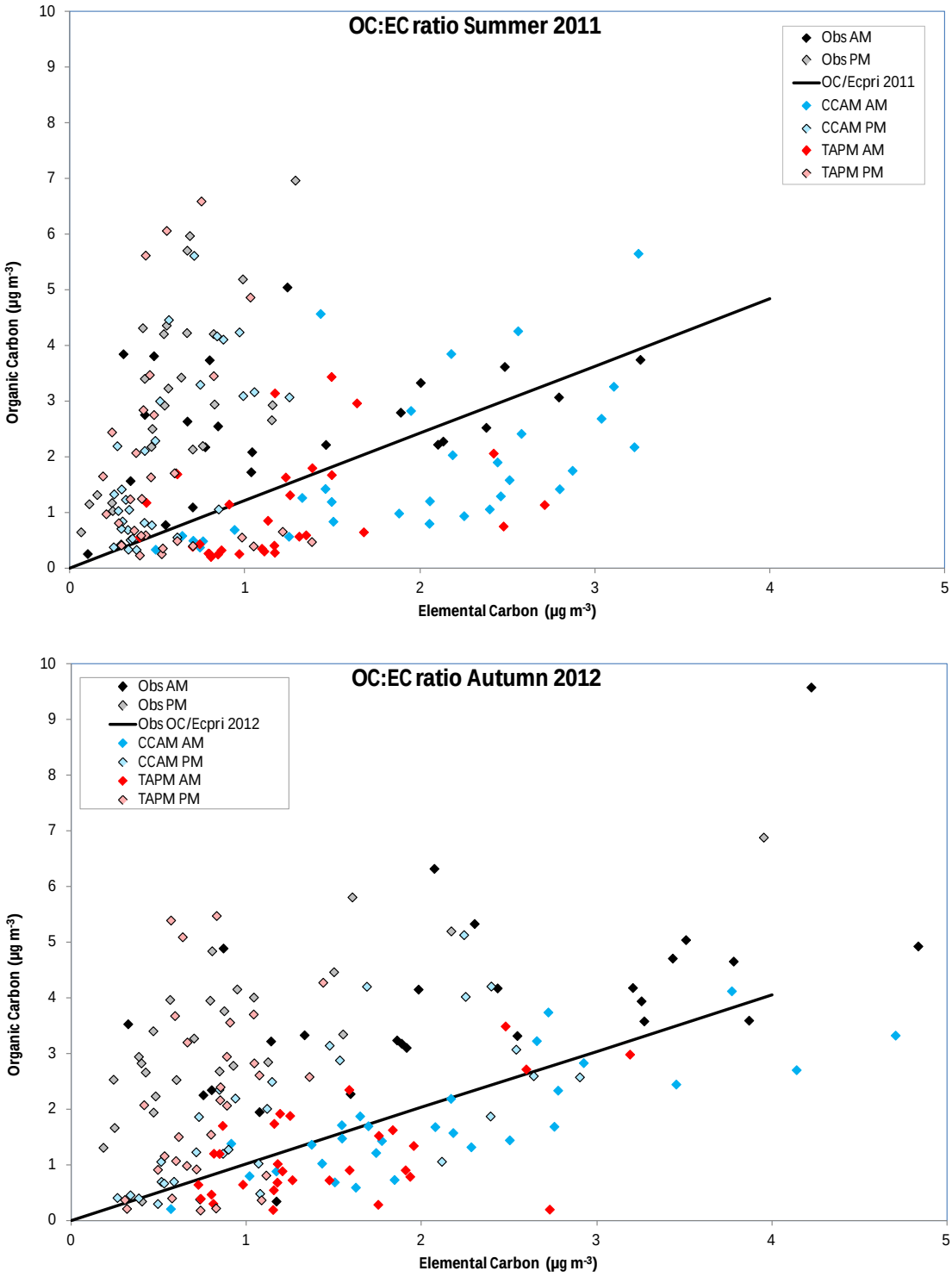

Figure 48. OC and EC concentrations measured and modelled in the morning and afternoons of both measurement campaigns.

A subset of samples from SPS1 were measured for the 14C content, and from this measurement the percentage of modern carbon making up the sample was determined. The 14C concentration in a source is dependent on the age of the carbon in that source. The half life of 14C (5730 yr) means that emissions from fossil fuel combustion contain no I4C because the geologic age of the fuel is much greater than the half-life of 14C. In contrast, for modern carbon sources 14C concentrations are similar to the atmospheric 14C concentration (Hildemann et al., 1994). Thus fossil fuel emission sources produce carbon depleted in 14C.

The percentage of modern carbon as a function of OC concentration for the samples analysed is shown in Figure 49. The afternoon samples (PM) display close to 70% modern carbon, suggesting that for these samples biogenic carbon is more significant than fossil carbon. Two of the morning samples show percent modern carbon around 30%, suggesting that for these samples fossil carbon is a greater component (as would be expected for morning vehicle emissions). Two of the morning samples also displayed percent modern carbon around 70% suggesting a biogenic contribution to the OC on these mornings. These are consistent with subsequent analysis of OA sources.

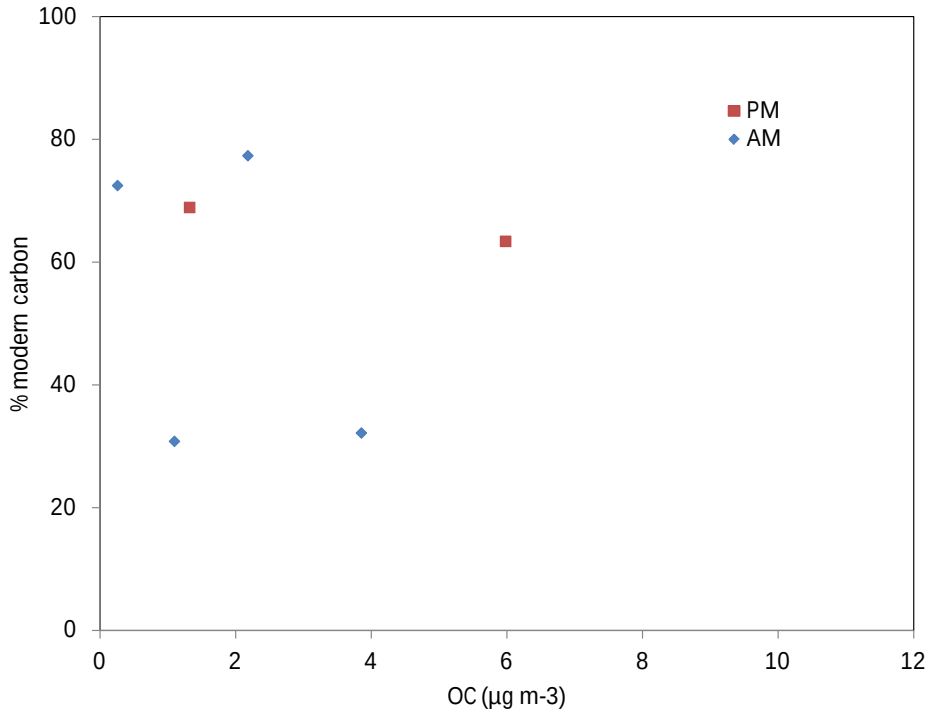

Figure 49. Percent modern carbon versus OC for selected samples from SPS1 Summer 2011 analysed for their ^{14}C content.

The model breakdown of new (secondary biogenic) and fossil based carbon (secondary anthropogenic) for SPS1 and SPS2 is shown in Figure 50. This indicates that around 50% of the modelled OC for SPS1 was secondary and of biogenic origin. POA is modelled to comprise just over 26-20% (CCAM,TAPM) of the SPS1 OC and anthropogenic SOA is modelled to comprise just over 29-25% (CCAM,TAPM) of the OC. With organic carbon comprising up to 34% of the measured $PM_{2.5}$ mass (Figure 16), the implication of the above is that approximately 25% of the OC mass (and hence 10% of the $PM_{2.5}$ mass) can be reduced through the direct control of POA emissions, and about 20% of the OC mass can be indirectly controlled through reduction in the VOC precursors which lead to secondary anthropogenic SOA production. Such precursors include toluene and the xylenes, which have been observed to generate SOA in smog chamber experiments. In autumn SPS2, the secondary biogenic carbon is reduced to 13-35% (CCAM,TAPM), whilst the primary organic component has almost doubled to 48-28% (CCAM,TAPM). This is in part due to the lower biogenic emissions at this time of year combined with the increased use of domestic woodheaters.

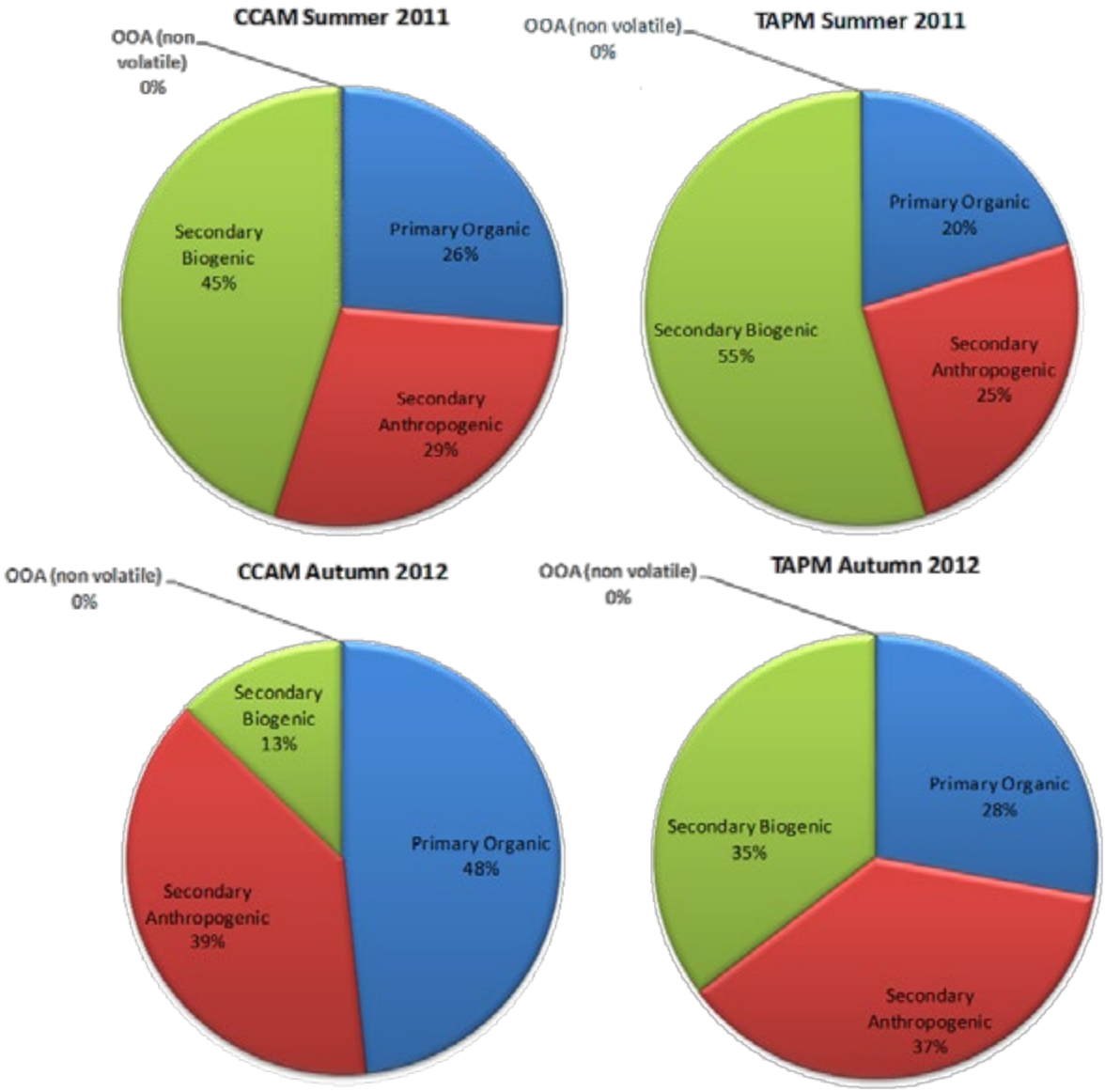

Figure 50. The breakdown of the modelled organic aerosol into primary anthropogenic, secondary anthropogenic and biogenic; non-volatile background aerosol.

Figure 51 shows the time series concentration of the SOA derived from the OC/EC ratio of the primary emissions. Also shown is the SOA concentration from the chemical transport model. The observed SOA shows a number of peaks across SPS1, with each peak corresponding to a period of moderate photochemical activity. SOA concentrations of up to 9 $\mu g/m^3$ are observed. The timing of the modelled SOA often matches those of the observed SOA and the magnitude of the modelled SOA is generally within a factor of two or better of the observed. Figure 51 also shows the modelled ratio of biogenic SOA to total SOA concentration and suggests that, at the time of the peak SOA concentrations, 60-80% of the SOA mass has a biogenic origin during SPS1. In SPS2 the observed SOA peaks at 6.5 $\mu g/m^3$, and again the

models match the timing of the peaks. TAPM predicts more SOA that CCAM during SPS2. TAPM also predicts a significantly higher percentage of biogenic SOA than CCAM for the whole campaign (50% compared to 30% for TAPM and CCAM respectively)

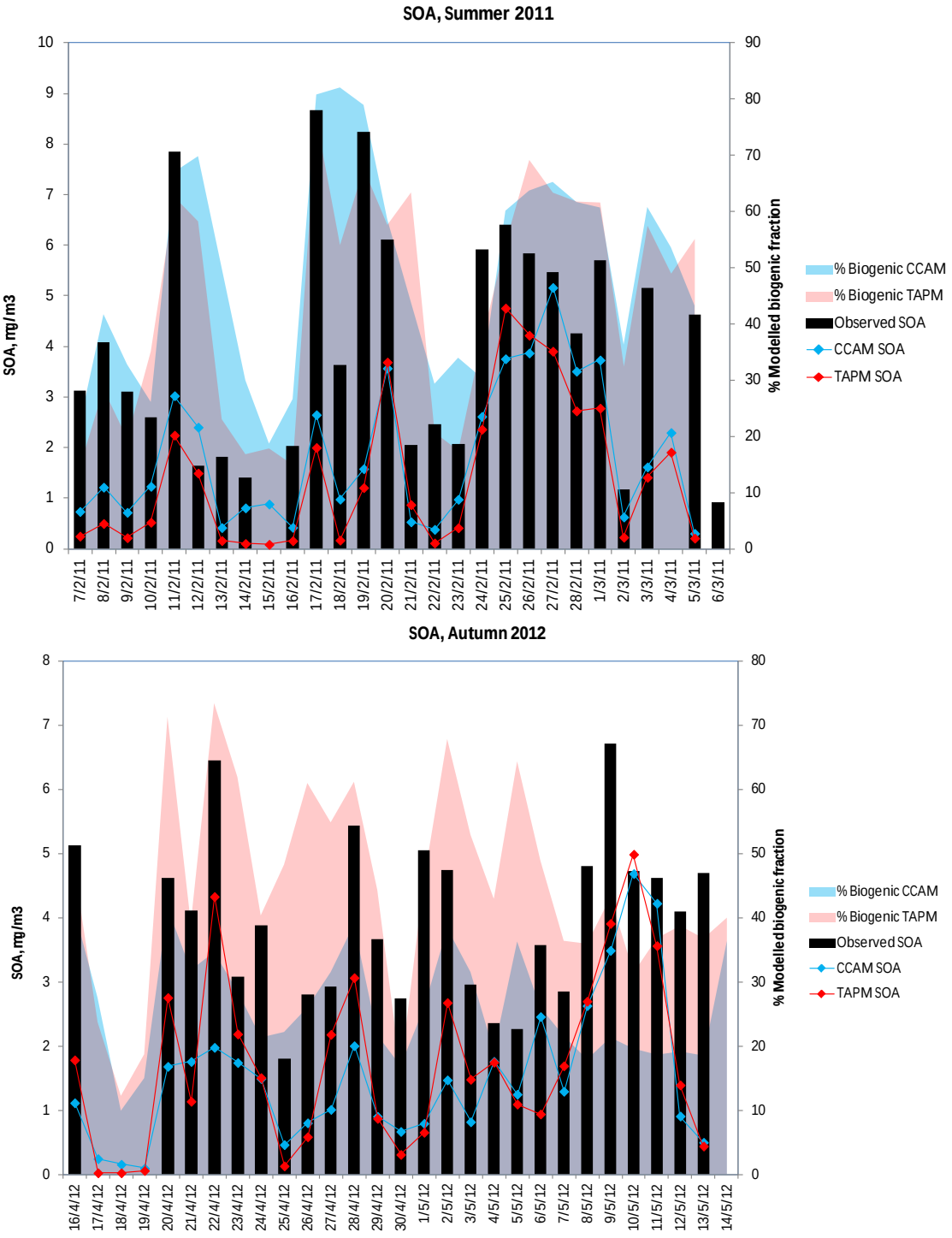

Figure 51. Time series for SPS1 and SPS2 of the observed and modelled SOA and the modelled percentage contribution of biogenic SOA to the total modelled SOA.

Table 7 shows over both studies, SPS1 and SPS2, that temperature, isoprene and the isoprene oxidation products methacrolein and methylvinylketone are the variables most closely correlated with secondary organic aerosol. There is a remarkable agreement with the estimated SOA from filter measurements and the OC measured by the AMS (R = 0.95). This would be expected on theoretical grounds, and indicates the small uncertainty in the estimated SOA.

Table 7. Correlations of estimated SOA with PM measurements (except where indicated).

	SPS1 Summer 2011	SPS2 Autumn 2012
Environmental Variables		
Temp (Max)	0.82	0.59
Solar radiation	NA	0.19
Ozone	0.82	0.34
SO2	-0.02	0.10
NH3	0.59	0.31
HCl	0.59	NA
Precursors and Indicative Tracers		
Isoprene	0.84	0.70 (PTRMS)
Monoterpenes	0.72 (AM)	0.41 (AM)
Methanol	0.83	0.48
Trimethyl benzene	0.61	0.20
Acetonitrile	0.77	0.23
Levoglucosan	0.19	0.27 (AM)
Parallel oxidation		
HNO_3	0.71	0.22
Formaldehyde	0.81	0.56
Methylglyoxal	0.81	0.55
Methacrolein and Methylvinyl ketone	0.83 (PTRMS)	0.64 (PTRMS)
Acetaldehyde	0.68	0.31
Acetone	0.72	0.36
Formic acid	0.82	0.34
Acetic acid	0.84	0.47
Related Measurements		
OC	0.83	0.85
AMS OC	0.95	NA

The chemical transport modelling, VOC observations and the ^{14}C data suggest that biogenic VOC emissions are a major precursor of the SOA during the summer period. During Autumn the primary and secondary sources of anthropogenic organic aerosol are dominant with particular influence from wood heaters. It should be noted that the modelled ratio of biogenic to anthropogenic SOA cannot be directly verified using the available suite of observations, and

thus these outcomes must be interpreted with caution. Additionally these conclusions apply only to the (summertime) conditions observed at Westmead during SPS1. The breakdown of particle composition may be quite different in other seasons- particularly the colder months where particle emissions from domestic wood combustion may be a dominant source.

4.6.6 AEROSOL MASS SPECTROMETER

An aerosol mass spectrometer, AMS, was utilized during SPS1 to determine the real-time (10 s – 10 min) size-resolved chemical composition and mass concentration of non-refractory submicron aerosol particles between 60 and 600 nm (approximately PM_1). For example, Figure 52 shows the time series of the mass loading of PM_1 for the period 10-15 February 2011. It can be seen that the AMS mass loadings are elevated for the period 9 am 11th February to 9 am 12th February, and that this peak occurred for all of the measured compounds. The OC was observed to comprise about 55% of the PM_1 mass during this time period.

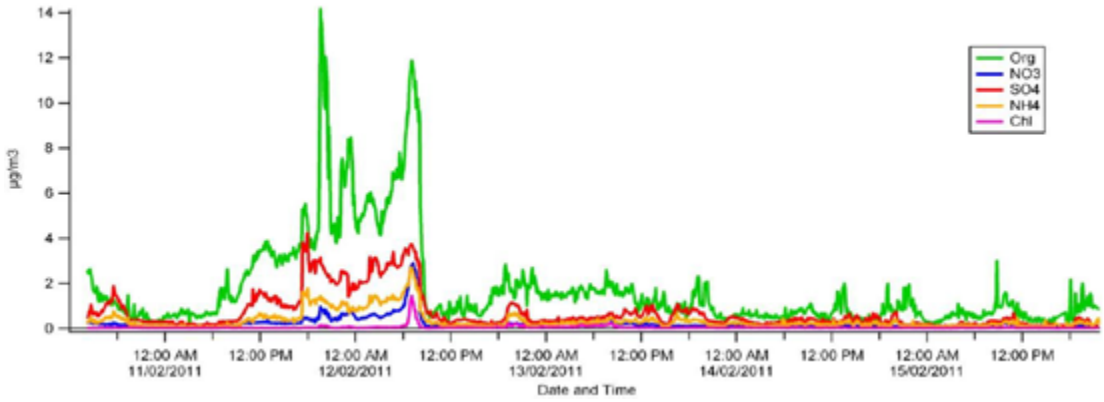

Figure 52. Time series of the mass loadings of the non-refractory PM1 species for 10th – 15th February 2011, measured with the AMS.

The modelled organic aerosol is shown in Figure 53. CCAM predicts more organic carbon than TAPM, and both models do very well at predicting the shape of the AMS time series. The models have captured the peak period between 11th and 12th February with about 80% of the observed concentration for CCAM and 50% for TAPM. Both models do a better job of capturing the magnitude of the background concentrations rather than the peak events.

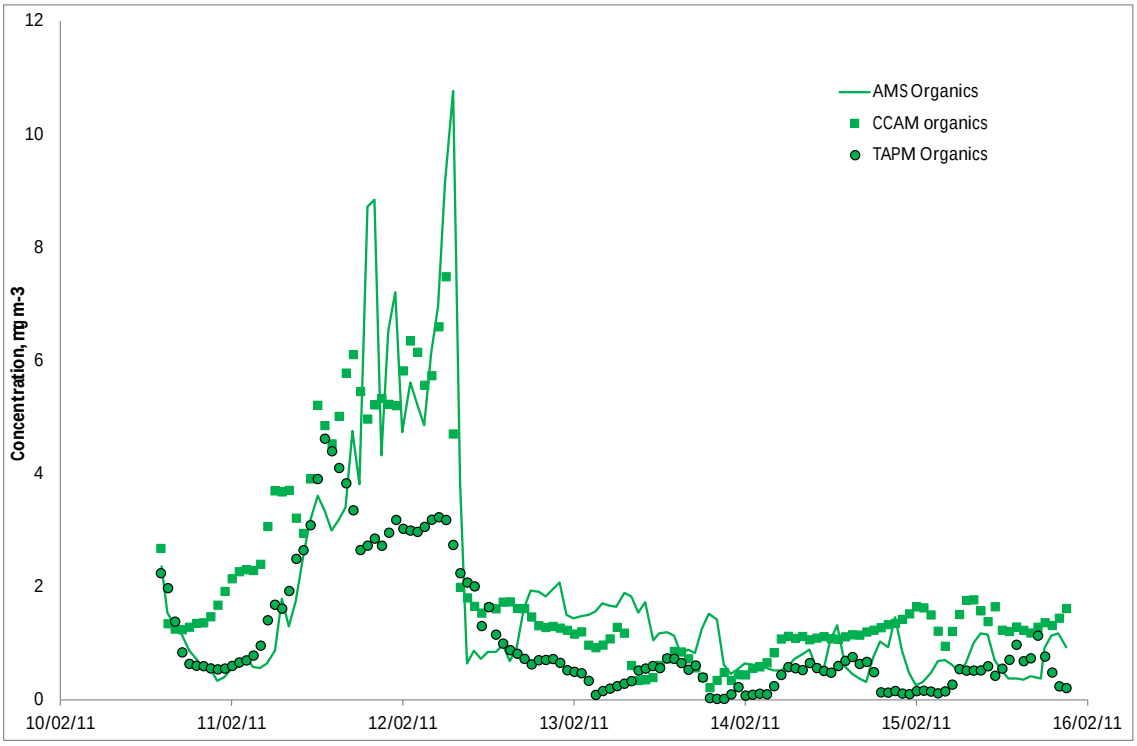

Figure 53. Comparison of the AMS time series for organic carbon and the corresponding modelled data during SPS1.

Identification of molecular ions used as markers can separate oxygenated organic species (likely to be SOA, denoted f44 in Figure 54) from hydrocarbon-like organic species (likely primary aerosol, denoted f57 in Figure 54). A value of about 0.14 for f44 indicates the presence of aged SOA, while a value of 0.07 would indicate fresher, but still oxygenated (secondary) OC. Thus secondary OC was observed for the majority of the period 10 - 15 February. Values of f57 of about 0.07 indicate the presence of primary OC. Figure 54 indicates that there was a transition from primary OC to secondary OC between 6 am and 12 pm on the 11th February, and this transition corresponded to a low peak in sulfate and organic PM1 aerosol as shown in Figure 52. The secondary y-axis in Figure 54 shows the equivalent modelled primary and secondary organic matter. The models show photochemical activity up until noon on February 12th, as denoted by the presence of secondary organic material, but after this date no secondary organic material is produced.

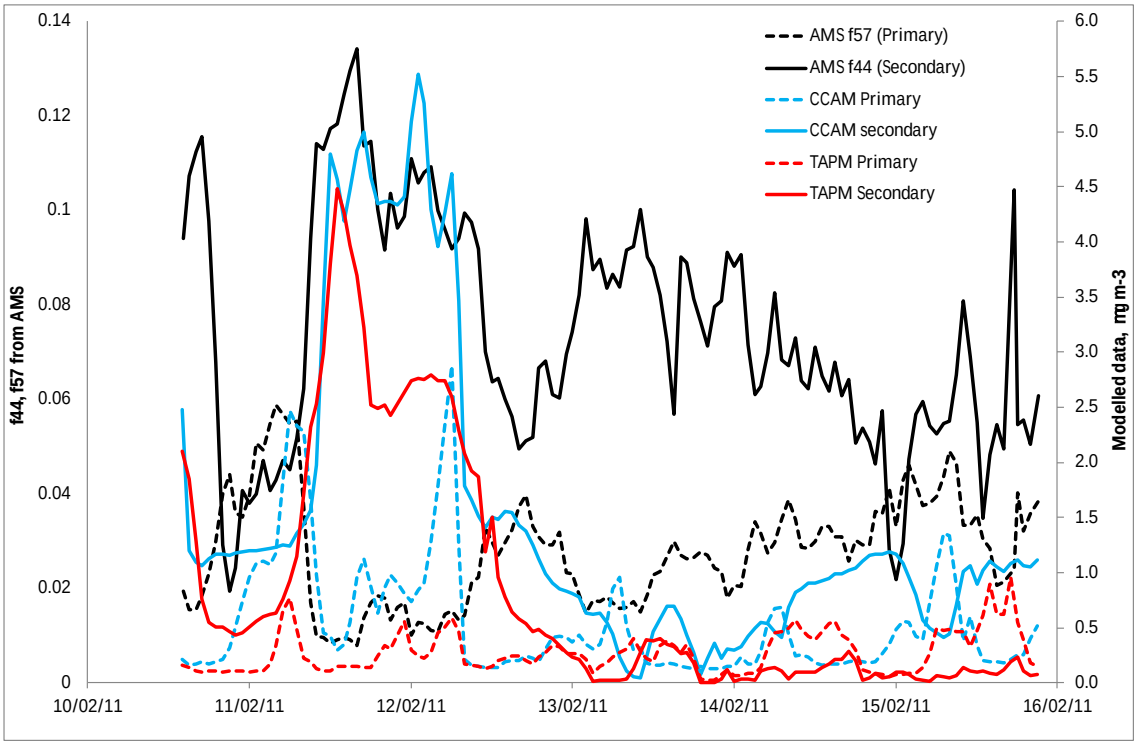

Figure 54. Time series of f44 and f57 from the AMS together with modelled primary and secondary carbon for the time period of 10 – 15 Feb 2011.

4.7 Particle Growth Events

Particles grow in the atmosphere via coagulation, condensation or gas to particle partitioning. In some instances the particles that grow are ones formed by nucleation (known as new particles) that coagulate to form larger particles. In other instances pre-existing particles may be the recipient of gas to particle partitioning particularly associated with the oxidation of volatile compounds (organic or inorganic) within the atmosphere to form products with lower volatility that preferentially partition to the particle phase.

The semi-continuous measurement of particle size distributions during the SPS1 and SPS2 allows an investigation of the growth of particles in the Sydney airshed. Two types of growth events were observed, those that progressed over a period of greater than 2 hours (prolonged event such as shown in Figure 55) and those that occurred over less than 2 hours (burst event such as shown in Figure 55).

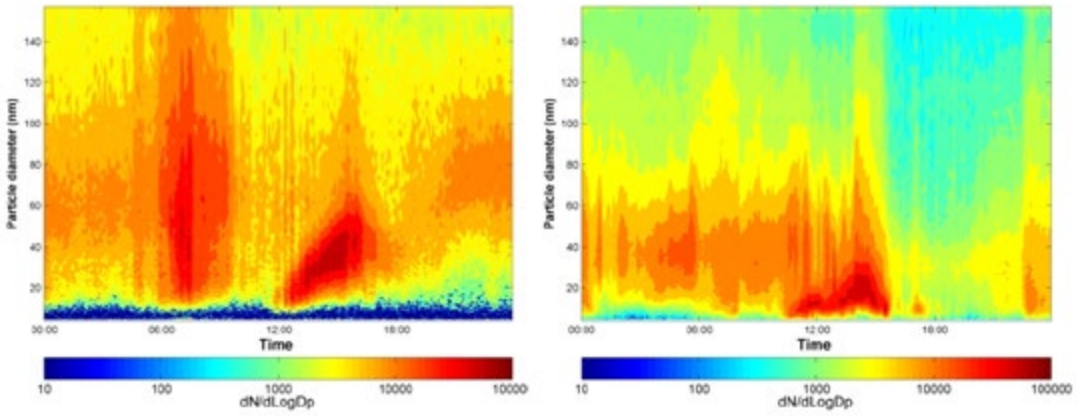

Figure 55. Typical particle size distribution measured event with the nano particle spectrometer during two different events. (a) "prolonged growth" type event on 24 February 2011 and (b) "burst" type event on 9 February 2011.

Table 8 compares the number of prolonged and burst events that occurred during SPS1 and SPS2. During both measurement programs the fraction of event days where events occurred was similar (around 50%). However during SPS1 there were more burst events, while during SPS2 there were more prolonged events.

Table 8. Number of burst and prolonged growth events that occurred during the Summer 2011 and Autumn 2012 measurement campaigns. The occurrence of an event was identified by visual inspection of the daily contour plots of size distributions (e.g. Figure 55). The ± figures represent the number of events that may be considered borderline events.

	Summer SPS1		Autumn SPS2	
	number	**fraction**	**number**	**fraction**
bursts	8±3	31%±12%	5±3	18%±11%
prolonged	5±1	19%±4%	10±3	36%±11%
no event	13±4	50%±15%	13±6	46%±21%
total	26		28	

The occurrence of growth episodes depends on various factors including emissions of precursors, composition and number concentration of the pre-existing aerosol population, meteorological parameters (in particular solar radiation, temperature, relative humidity) and photo-chemical processes (Kulmala, 2003;Kulmala et al., 2001). We compare the average values that represent a number of these factors during periods of growth events and non events in Table 9.

Table 9. Comparison of atmospheric concentrations between event and non-event days

SPS1	non event			event			
EC AM (µg/m^3)	0.87	±	0.45	1.784	±		
HNO3 PM (ppb)	0.22	±	0.19	0.680	±	0.43	0.005
HNO3 AM (ppb)	0.60	±	0.27	0.936	±	0.40	0.021
NO AM (ppb)	9.18	±	11.91	28.69	±	22.91	0.017
NOx AM (ppb)	13.85	±	12.50	33.80	±	23.68	0.018
O3 PM (ppb)	21.83	±	7.13	32.36	±	12.49	0.019
Benzene AM (ppb)	0.16	±	0.03	0.56	±	0.19	0.009
Toluene AM (ppb)	0.82	±	0.50	2.26	±	1.06	0.021
Xylenes AM (ppb)	0.43	±	0.25	1.23	±	0.59	0.020
Monoterpenes AM (ppb)	0.54	±	0.30	1.28	±	0.62	0.032
***Terpenes AM (ppb)**	0.12	±	0.09	0.27	±	0.13	0.004
SPS2	**non event**			**event**			
SO2 Max (ppb)	0.19	±	0.13	0.45	±	0.32	0.035
SO2 PM (ppb)	0.45	±	0.38	1.13	±	0.77	0.032
NH4+ AM (ng/m^3)	446	±	425	204	±	106	0.039
nssSO4 AM (ng/m^3)	1022	±	828	464	±	224	0.017
Methylglyoxal PM (ppb)	0.39	±	0.23	0.71	±	0.35	0.019

Note that the data presented in Table 9 are only those variables that showed a significant difference in mean values at 95% confidence. Table 9 suggests that during SPS1, the occurrence of a growth event is governed by NOx/O3 chemistry involving oxidation of both aromatic and monoterpene precursor compounds while during SPS2 SO_2 oxidation is the driver for particle growth. Further work will investigate how these relationships influence whether bursts or prolonged growth events occur and the role of atmospheric dynamics in determining particle growth.

The latter can be investigated further by modelling the growth events. Here we have incorporated the GLOMAP particle microphysical processes model into the CTM (Mann et al., 2010). The processes include nucleation of sulphate aerosol, condensation of vapour onto the aerosol surface, coagulation and wet/dry deposition of aerosol. GLOMAP contains 7 modes based on aerosol size distributions (nucleation mode plus Aitken, accumulation and coarse

aerosol in the soluble and insoluble distributions). Inclusion of boundary layer nucleation in the model resulted in the reproduction of the particle growth events shown in Figure 56.

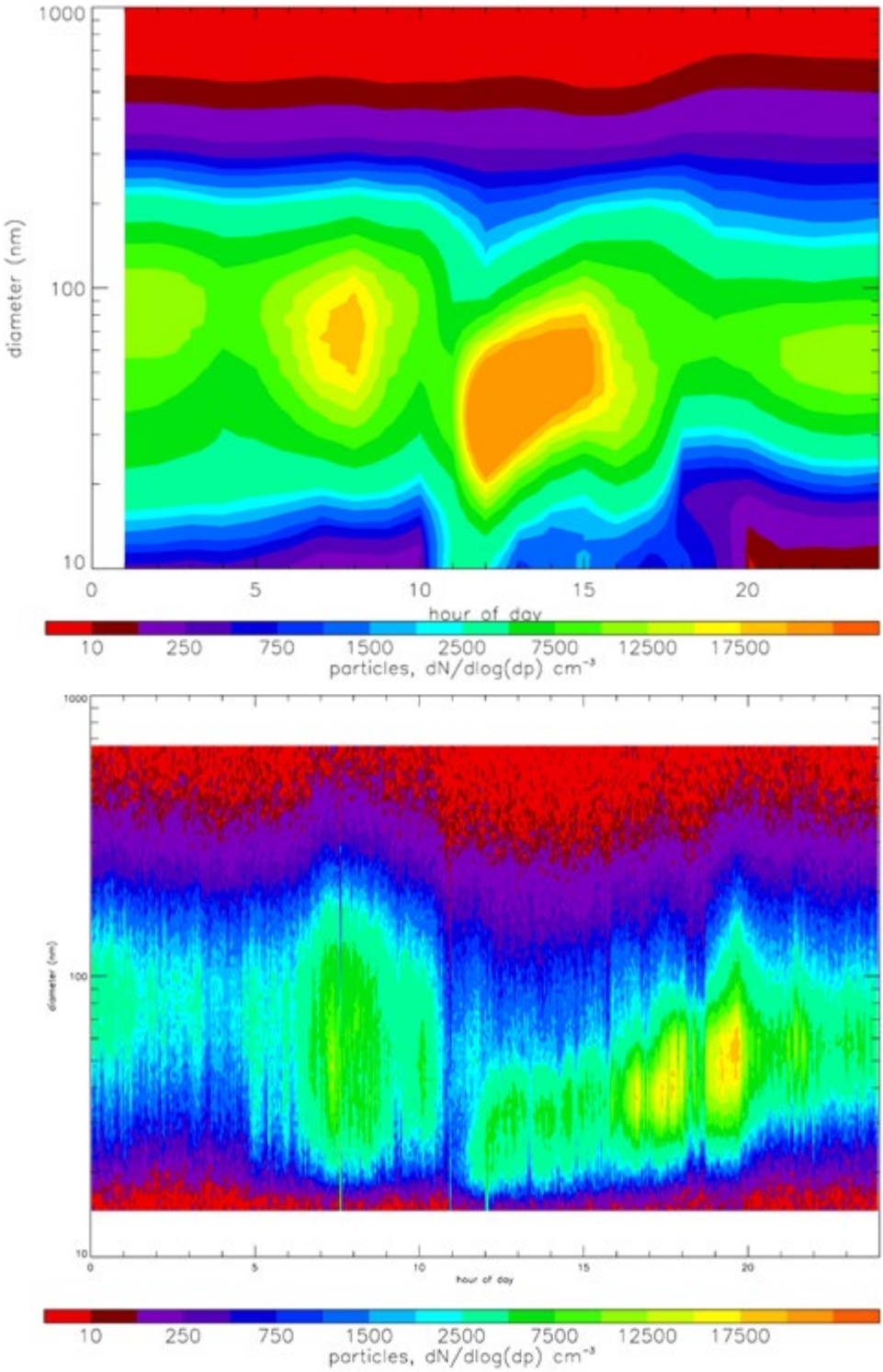

Figure 56. Comparison of particle size distribution for 1 May 2012 top) simulated with the model with boundary layer nucleation included and bottom) measured.

In the model this boundary layer nucleation is defined by the presence of SO_2 to form H_2SO_4. The model works by treating nucleation and condensation processes as being in 'competition' with each other. This competition is accounted for by splitting the model time step (300 s) into 5, looping round each process. Condensation and nucleation therefore happen at the same time. This SO_4 condensation/nucleation process is independent of NH_3 concentrations, instead being dependent on whether there is enough of a condensational sink for H_2SO_4 before passing the remainder to be nucleated. This parameterisation is solely dependent on the vapour pressure of H_2SO_4 and whether there is an available surface area of particles.

The model captures the high concentration of particles in Figure 56 between 20 nm and 100 nm associated with the morning traffic peak and the onset of the growth event at 12:00. The growth rate in the model however appears to be faster than in the observations.

While this analysis is preliminary and ongoing, we propose that the atmospheric composition and photochemical environment in the Sydney airshed is such that photochemical oxidation is a common occurrence. However in order for the oxidised products to partition to the particle phase and promote particle growth an acid catalyst is required (Gao et al., 2004). SO_2 from power plumes oxidised in the boundary layer to form H2SO4 which then nucleates forming the catalyst seeds. If this occurs in the boundary layer (dependent on amount of H_2SO_4) the regular drawdown of air from the boundary layer in the early afternoon brings these nucleated particles to the surface providing the seed particles into which the oxidised VOC products can partition and condense and further react.

5. CONCLUSIONS AND RECOMMENDATIONS

The Sydney Particle Study represents the most comprehensive observation and modelling study of fine particles undertaken in Australia. It has leveraged the skills of seven partner organisations (CSIRO, NSW OEH, NSW EPA, ANSTO, QUT, BOM, SINAP) to construct and implement observational and modelling frameworks for investigating the characteristics of particles in Sydney. In so doing, the study has aimed at providing an improved understanding and a quantitative model of the particle sources which contribute to population exposure in

the Sydney region. The development of such a capability is a crucial aid to developing State and National policy for reducing the levels of population exposure to fine particles.

The Study included two observational programs (running for approximately one month each), based at Westmead (26 kilometres to the west of the Sydney CBD), which were targeted at characterising particles under summer and autumn conditions. The summer observation program identified sea salt (34%) and organic matter (OM; primary and secondary; 34%) as being the major components of $PM_{2.5}$, with secondary inorganic aerosol (15%), soil (11%) and elemental carbon (6%) also being present in significant amounts. A limited isotopic analysis of the OM carbon (based on six samples) indicated that up to 70% of the analysed carbon is modern- thus secondary organic aerosol formed from biogenic sources. Anthropogenic and biogenic precursors to secondary organic aerosol such as toluene, the xylenes, isoprene and the terpenes were all observed at Westmead and found to correlate with observed concentrations of organic matter. The autumn observation program saw a much reduced sea salt contribution (5%) and an increased contribution from organic matter (57%). The contribution from elemental carbon was also larger (16%) while the secondary inorganic aerosol contribution was the same (15%). Radon observations were consistent with an increased frequency of continental vs. marine air mass exposure for the second study period.

The observation programs also identified the presence of wood smoke during both observation periods. However the concentrations of the wood smoke tracer- levoglucosan were seven times larger during the autumn study period. The autumn levoglucosan concentrations correlated well with decreasing daily temperatures which suggested that domestic solid fuel combustion may be the major source of the wood smoke.

Particle size distributions were measured on a semi-continuous basis during both observation programs and detected many occurrences of rapid particle growth in the 10–60 nanometre size range. Particle growth events were observed to be both prolonged (progress over of period of greater than two hours), and rapid burst events. Such nano particle events may be caused by a combination of new particle formation through nucleation, Aitken mode primary emissions, particle coagulation and gas to particle partitioning.

A modelling framework was developed for the Study, consisting of prognostic meteorological modelling capability, a natural and anthropogenic emissions inventory, chemical transport modelling capability, and a methodology for calculating population exposure and health impacts. The framework was used to model both observation periods in detail. Two meteorological models were used (CCAM and TAPM) in order to investigate the sensitivity of the modelling particle characteristics to the meteorological forcing. The chemical transport model (the CSIRO CTM) included the capability to model the major particle processes identified during the observation periods. The NSW EPA air emissions inventory included a comprehensive representation of the major sources contributing to emissions of oxides of nitrogen, sulfur dioxide, volatile organic compounds, carbon monoxide and $PM_{2.5}$. However speciated $PM_{2.5}$ is not yet available and was estimated using a top-down scaling approach.

An assessment of the meteorological models demonstrated that they generally had good skill in modelling the meteorological conditions observed during the two study periods. However the models were sometimes challenged during transition conditions, or when meso-scale and synoptic forcings were approximately in balance.

The modelling framework was able to simulate most of the major particle processes that were identified by the observation programs including sea salt emissions, wood heater emissions, secondary inorganic aerosol production, primary organic aerosol emissions and secondary organic aerosol production from anthropogenic and biogenic precursors. The framework did a relatively good job of predicting the proportions of sea salt (19–27% modelled vs. 34% observed), organic matter (36–40% vs. 34%) and secondary inorganic aerosol (20–21% vs. 15%) in the summer observation period, however over predicted the sea salt component (9–15% vs. 5%) and under predicted the OM contribution in the autumn study period (36–45% vs. 57%). Also the absolute concentrations of the major aerosol components were generally systematically under predicted. Interestingly, the average total $PM_{2.5}$ concentrations for seven urban monitoring stations were predicted with good skill (monthly mean concentrations predicted to within 20%).

One of the major areas of uncertainty in the project relate to the NSW EPA air emissions inventory. As noted previously, the inventory provided comprehensive estimates of the total $PM_{2.5}$ emissions for summed mobile sources, summed commercial-domestic sources, and

elevated industrial sources. Because it was not possible (with the exception of wood heater emissions) to easily reverse-engineer the emission data files into a finer set of source sub-categories (i.e. mobiles sources into light and heavy duty petrol vehicles; diesel vehicles; paved and unpaved road dust), $PM_{2.5}$ emission factors had to be heavily lumped and were spatially invariant. This had the potential to introduce considerable uncertainty into the estimates of the $PM_{2.5}$ component emissions. The same issue also exists for ammonia, which is a precursor for secondary inorganic aerosols. Thus it is recommended that a useful intermediate step prior to the NSW EPA developing a comprehensive bottom-up estimate of the PM2.5 component emissions would be (if possible) to provide emissions in a more disaggregated form, considering perhaps the top five (or more) emission sub-groups making up each major source category.

A top down verification of the emissions inventory is also recommended. In this regard, one of the new techniques introduced in 2012 was the use of CO_2 as a method of quantifying emission factors. This has been previously developed by CSIRO and utilized in on-road studies of motor vehicle emissions in Melbourne, Perth, Hong Kong and Bangkok. Here a variant of the method is demonstrated.

Carbon dioxide in the Sydney region will arise from biomass burning, fossil fuel combustion, including vehicular sources and also from plant and soil respiration. During the late afternoon and early evening plant and soil respiration will dominate over plant uptake by photosynthesis. In parallel with the soil emissions there will be emissions from the peak hour motor traffic and use of wood heaters. In Figure 57 we see the correlation of $PM_{2.5}$ with CO_2 levels in the late afternoon and early evening hours at Westmead. The observed CO_2 increase is contributed to by all three sources, (a) biomass burning, (b) fossil fuel combustion, including vehicular sources and (c) plant and soil respiration. The first two of these sources, biomass burning and fossil fuel combustion (including vehicular sources) contribute emissions of $PM_{2.5}$ to the atmosphere. Similar relationships are observed for CO2 with nephelometer particle scattering, PM_{10}, NOx, CO and many other VOCs.

In Figure 58 we see the correlation of three VOCs with CO_2 levels in the late afternoon and early evening hours at Westmead. The influence of soil CO_2 emissions is minimised by selecting the data for low Radon content, because Radon like CO_2 is emitted from soils. These

three compounds have the largest correlations with CO_2 for this data. These highly substituted aromatic compounds have high reaction rates in the atmosphere and are effective sources of secondary organic aerosol.

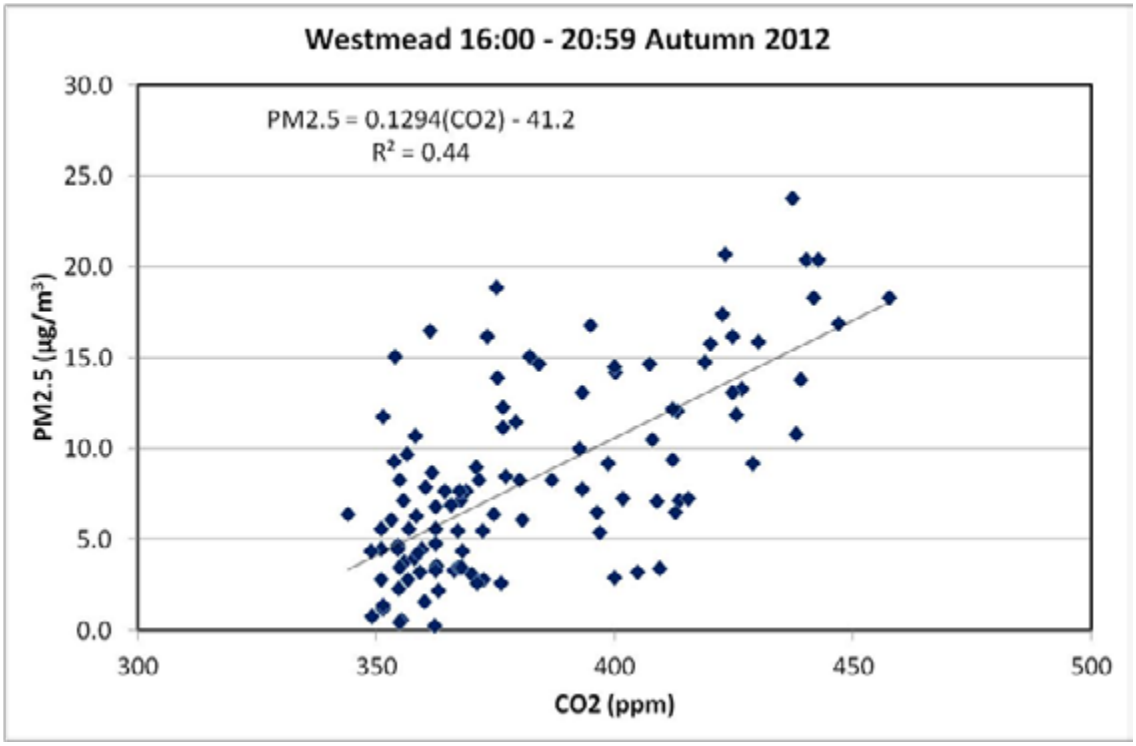

Figure 57. The relationship of $PM_{2.5}$ to carbon dioxide during 16:00 to 21:00 at Westmead in SPS2 autumn 2012.

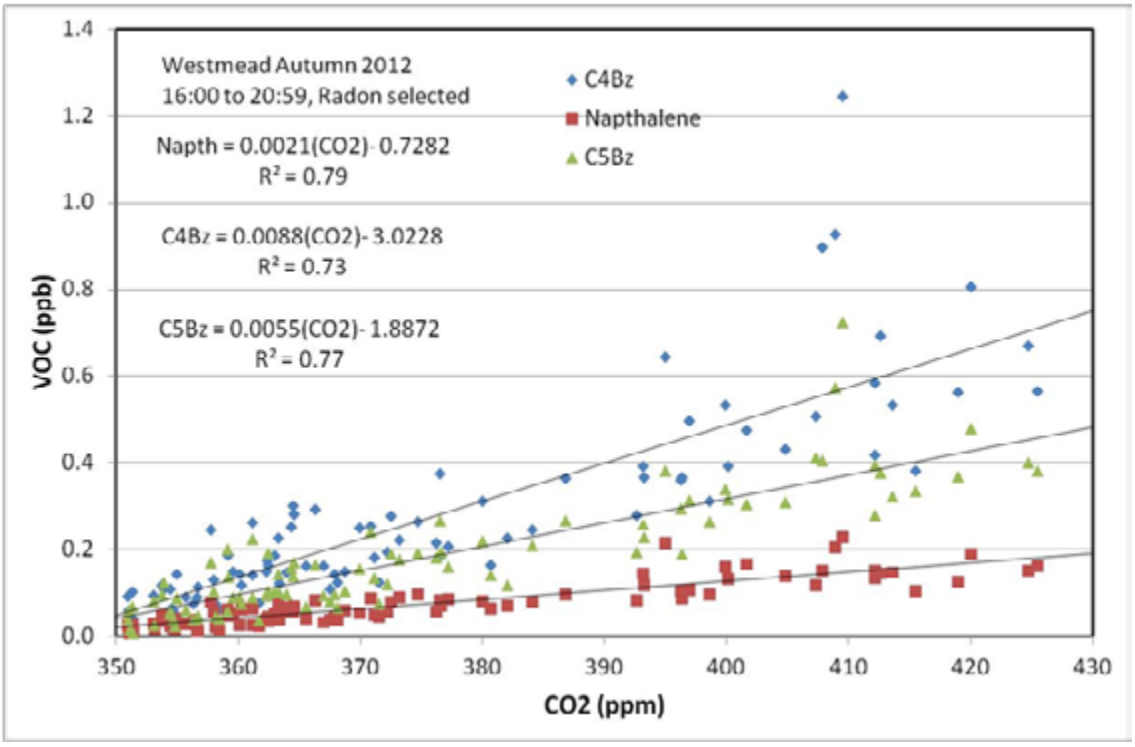

Figure 58. The relationships of Napthalene, C4 and C5 substituted benzene compounds to carbon dioxide during 16:00 to 21:00 at Westmead during SPS2 in autumn 2012.

In Table 10 we see the observed ratios of these VOCs to CO_2 from the observations shown in Figure 58, and from the GMR Sydney 2008 Emissions Inventory for on-road motor vehicles. For Napthalene and C4 substituted benzene compounds there is good agreement between inventory and observations and warrants further investigation. For C5 substituted benzene compounds the inventory suggests a factor of ten less than observed. Because these compounds are very effective at forming SOA, the correct emissions are important for accurate modelling.

Table 10. The ratio of selected VOCs to CO2 (mol mol^{-1}) from observations at Westmead in autumn 2012, between 16:00 and 20:59 selected for lower Radon, and the ratios for the same quantities for the GMR region from motor vehicles in the 2008 Inventory.

Compound	Westmead Observations	GMR 2008 MV Inventory
Napthalene	2.1×10^{-6}	1.5×10^{-6}
C4 substituted benzene	8.8×10^{-6}	6.3×10^{-6}
C5 substituted benzene	5.5×10^{-6}	4.6×10^{-7}

An additional area in which further work is recommended is to undertake observations to better characterise the organic matter component of $PM_{2.5}$ in Sydney, particularly the breakdown between primary and secondary, anthropogenic and biogenic sources. With

respect to the modelling, one of the key areas of uncertainty is the modelling of rainfall and the wet deposition of fine particles. Additionally, there is a need to model the complete size distribution of particles (including the Aitken, Accumulation and coarse modes). A component of this work would include building a capability to model the emission and growth of ultra-fine particles.

A1. SAMPLING AND ANALYSIS METHODOLOGIES

This section contains more details on how the sampling and analytical procedures were carried out.

A1.1 Sampling equipment

A1.1.1 ANSTO $PM_{2.5}$ ASP SAMPLER

The ANSTO built ASP sampling unit is a $PM_{2.5}$ cyclone type sampler based on the US EPA IMPROVE system used across North America in their National Parks air monitoring program. The cyclone operates at a flow rate of 22 L min^{-1} using a mass flow controller which results in a $PM_{2.5}$ particle size cut-off. The particles are collected on a 25mm diameter thin stretched Teflon filter masked to 17 mm diameter to increase sample thickness and improve deposit uniformity. The filters and the sampling regime are specifically designed for the ANSTO ion beam analysis (IBA) system described below. Samples were collected over the same time period and on the same days as the high volume sampler to enable comparison of data.
The sample collection rate was 100% in that all samples were returned to ANSTO for analysis.

A1.2 Analysis techniques

A1.2.1 ION BEAM ANALYSIS (IBA) TECHNIQUES

The 25 mm Teflon filters were analysed non-destructively on the ANSTO STAR 2MV accelerator using nuclear IBA techniques.
The simultaneous IBA techniques applied are:

- Proton induced X-ray emission (PIXE) – for analysis of elements from aluminium to lead in concentrations from a few ng m^{-3} upwards, as described in Cohen (1993).
- Proton induced gamma-ray emission (PIGE) – for analysis of light elements such as fluorine and sodium in concentrations above 100 ng m^{-3}, as described in Cohen (1998).
- Proton elastic scattering analysis (PESA) – for analysis of hydrogen at levels down to 20 ng m^{-3}, as described in Cohen (1996).

A full description of these methods and how they are used can be found on the ANSTO web page at www.ansto.gov.au/environment/iba together with key publications describing other fine particle studies at ANSTO.

A1.2.2 ION CHROMATOGRAPHY

A 6.25 cm^2 portion of each quartz filter was analysed for major water soluble ions by suppressed ion chromatography (IC) and for anhydrous sugars including levoglucosan by high-performance anion-exchange chromatography with pulsed amperometric detection (HPAEC-PAD). The filter portions were extracted in 10 ml of 18.2 mΩ de-ionized water. The sample is then preserved using 1% chloroform.

Anion and cation concentrations were determined with a Dionex ICS-3000 reagent free ion chromatograph. Anions were separated using a Dionex AS17c analytical column (2 x 250 mm), an ASRS-300 suppressor and a gradient eluent of 0.75 mM to 35 mM potassium hydroxide. Cations were separated using a Dionex CS12a column (2 x 250 mm), a CSRS-300 suppressor and an isocratic eluent of 20 mM methanesulfonic acid.

Anhydrous sugar concentrations were determined by HPAEC-PAD with a Dionex ICS-3000 chromatograph with electrochemical detection. The electrochemical detector utilizes disposable gold electrodes and is operated in the integrating (pulsed) amperometric mode using the carbohydrate (standard quad) waveform. Anhydrous sugars are separated using a Dionex CarboPac MA 1 analytical column (4 x 250mm) with a gradient eluent of 300 mM to 550 mM sodium hydroxide.

A1.2.3 ORGANIC CARBON (OC) AND ELEMENTAL CARBON (EC) ANALYSIS

The carbon in $PM_{2.5}$ is analysed to obtain two separate components – organic carbon and elemental carbon – because different sources emit different types of carbon. Elemental carbon is principally emitted during the combustion of fossil fuels as small, sooty particles often with other chemicals attached to their surface.

Organic carbon is the carbon in organic compounds in $PM_{2.5}$. In practice this includes most compounds that contain carbon, excluding particles that are just elemental carbon. Sources of organic carbon include traffic and industrial combustion

Elemental and organic carbon analysis was performed using a DRI Model 2001A Thermal-Optical Carbon Analyzer following the IMPROVE-A temperature protocol (Chow et al., 2007).

Laser reflectance is used to correct for charring, since reflectance has been shown to be less sensitive to the composition and extent of primary organic carbon. Prior to analysis of filter samples, the sample is baked in an oven to 910°C for 10 minutes to remove residual carbon. System blank levels are then tested until < 0.20 mg C cm^{-2} is reported (with repeat oven baking if necessary). Twice daily calibration checks are performed to monitor possible catalyst degeneration. The analyser is reported to effectively measure carbon concentrations between 0.05 – 750 mg C cm^{-2}, with uncertainties in OC and EC of ± 10%.

The IMPROVE-A carbon method measures four OC fractions at four non-oxidizing heat ramps (OC1 at 140°C, OC2 at 280°C, OC3 at 480°C, OC4 at 580°C) and three EC fractions at three oxidizing heat ramps (EC1 at 580°C, EC2 at 740°C, EC3 at 840°C). The quartz filter sample is held at the target temperature until all carbon is desorbed at that fraction. During the non-oxidizing heat ramps some of the OC can be pyrolyzed and will not desorb until the oxidized stages. The quantity of OC that was pyrolyzed (OCpyro) during the non-oxidizing heat ramps is determined based on the time the reflectance of the filter rises back up to its initial value. Total OC is then calculated from the addition of all the OC fractions plus OCpyro. Total EC is calculated from the addition of all the EC fractions minus OCpyro.

As discussed in Appendix A, analysis of the initial results showed that EC was overestimated, and for the results presented in this report did not include OCpyro in the OC fraction.

A1.2.4 CARBONYLS

Samples for the analysis of carbonyl compounds (including formaldehyde) are collected by drawing air through Supelco LpDNPH S10 air monitoring. Carbonyls are trapped on high purity silica adsorbent coated with 2,4-dinitrophenylhydrazine(2,4-DNPH), where they are converted to the hydrazone derivatives. An ozone scrubber was placed in front of the LpDNPH cartridge. The derivatives are eluted from the cartridge in 3.0 ml of acetonitrile. The analysis of carbonyls is based on EPA Method TO11A.

The acetonitrile extractions are analysed by HPLC consisting of a Dionex GP40 gradient pump, a Waters 717 autosampler, a Shimadzu System controller SCL-10A VP, a Shimadzu diode array detector SPD-M10A VP, a Shimadzu Column Oven CTO-10AS VP and Shimadzu CLASS-VP chromatography software. The compound separation is performed with a Supelco Supelcsil LC-18 column, 5 µm, 4.6 mm ID x 250 mm in length, Part No 58298. The chromatographic conditions include a flow rate of 2.0 ml min^{-1} and an injection volume of 20 µl, and detector wavelength of 360 nm. The peaks were separated by gradient elution with a mobile phase of

60% acetonitrile and 40% Milli-Q water initial conditions to 100% acetonitrile at 17min, and column temperature of 30ºC. Standard solutions were prepared from Supelco Carb Method 1004 DNPH Mix 2, and the HPLC grade acetonitrile was purchased from Merck. The water used for analysis was 18.2 mΩ.cm grade produced from a Millipore Milli-Q Advantage 10 system.

The concentrations have been blank corrected. Where the mass of carbonyl on the DNPH tube is less than the blank, half the Limit of Detection has been substituted. The method detection limit was calculated from the standard deviation of blanks collected during the study period (ISO, 1994).

A1.2.5 VOLATILE ORGANIC COMPOUNDS

AT VOC (adsorbent tube Volatile Organic Compounds) samples were collected by an automatic VOC sequencer which actively draws air through two multi-adsorbent tubes in series (Markes Carbograph 1TD / Carbopack X). The adsorbent tubes were then analysed by a PerkinElmer TurboMatrix™ 650 ATD (Automated Thermal Desorber) and a Hewlett Packard 6890A gas chromatography (GC) equipped with a Flame Ionization Detector (FID) and a Mass Selective Detector (MSD) at CSIRO Marine and Atmospheric Research (CMAR) laboratories. Certified BTEX (benzene, toluene, ethylbenzene and xylenes), TO 15/17, terpenes, alcohols and PAM gas standards were used for the calibration. The method of AT (adsorbent tube) VOC sampling and analysis in this study was compatible with ISO16017-1:2000 (ISO 2000) and according to USEPA Compendium method TO-17 (USEPA TO-17).

Samples were collected three times per day and at hours of 05:00 – 10:00, 11:00 – 19:00 and 19:00 – 05:00. For each sampling day, there was also a tube which was unopened and used as a field blank.

A1.2.6 GRAVIMETRIC MASS MEASUREMENT

Particle mass less than 10 µm in diameter (PM10) is measured by gravimetric mass determination. PM10 samples are collected using the Micro-Vol which draws air at a constant flow rate (3 L min^{-1}) through a PM10 size-selective inlet (which removes particles greater than 10 µm in diameter) and onto a 47 mm stretched Teflon filter (Pall R2PJ047, 2 µm pore size) on which particles less than 10 µm diameter are trapped. Each filter is weighed before and after sampling to determine the mass of particles collected. Gravimetric mass measurements

are performed using a Mettler UMTA2 microbalance at 30-50 % relative humidity. Electrostatic charging is reduced by the presence of static discharge sources within the balance chamber. The resolution of the balance is 0.0001 mg (0.1 µg). Each 47 mm Teflon filter is weighed repeatedly, both before and after sampling, until three weights within 0.001 mg are obtained. The detection limit was calculated from the standard deviation of 14 blanks collected during Winter/Spring and Summer/Autumn (ISO, 1994). The precisions were calculated separately during Winter/Spring and Summer/Autumn, as the % relative standard deviation, when kits were co-located at CMAR, and sampling was carried out for 7 days.

Detection limit: $<0.1\ \mu g\ m^{-3}$

Precision: 4.6 % and 1.9 % for summer and winter respectively

Resolution: N/A

Accuracy: N/A

Reference Methods

AS/NZS 3580.9.9:2006 Methods for sampling and analysis of ambient air - Determination of suspended particulate matter – PM10 low volume sampler - Gravimetric method.

ISO Standard 9168:1994(E), Air Quality – Determination of performance characteristics of measurement methods, International Organization for Standardization, Geneva, Switzerland, 18 pp, 1994.

A1.3 Data quality: Analysis

A1.3.1 NATA ACCREDITATION

The wet chemistry laboratory at CSIRO Aspendale has National Association of Testing Authority (NATA) accreditation, No 245, for IC analysis. As part of the NATA accreditation a check standard is analysed in each analysis run after the 7 calibration standards and then every 20 samples. The samples are reanalysed if:

- Two or more of the control or replicate standards exceed the ”warning” limit, which means the measured value is greater than 2 standard deviations from the true value.
- One or more control or replicate standards exceed the “recal” limit, which means the measured value is greater than 3 standard deviations from the true value.

A1.3.2 BLANK FILTERS

Blank filters were analysed throughout the study. The average of the blank concentration is subtracted from each measurement. The blanks are also used to calculate the method detection limit (MDL). We followed the Standards Australia procedures which are those of the International Standard ISO 6879 Air quality – Performance characteristics and related concepts for air quality monitoring methods. Section 5.2.7 of the Standard states that a zero sample has a 5 % probability of causing a measured concentration above the detection limit, so that:

$$MDL = t_{0.95} \acute{} \; s_{c(0)} \qquad (1)$$

where:

$S_{c(0)}$ is the standard deviation of the blanks, and

$t_{0.95}$ is value of the 1-tailed t distribution for P<0.05 (i.e. the 95 % confidence limit).

A1.3.3 ION BALANCE

The ion balance (IB) gives an indication of the aerosol chemistry data quality in that the total cation equivalents (positive charged ions) should equal the total anion equivalents (negative charged ions). The Global Atmospheric Watch Program (GAW) which is part of the World Meteorological Organisation (WMO) gives the IB equation and criteria for assessing valid data results in its technical report 160, "Manual for the GAW Precipitation Chemistry Programme". Note that a poor IB does not always indicate bad data quality. For example pH is not measured in this project and samples with high pH levels might have a poor IB due to high levels of bicarbonate; these samples usually also have high levels of calcium. Similarly, samples with low pH may have excess anions. Samples that have been flagged as invalid have been reanalysed. The IB plot for both sites is shown in Figure A 1.

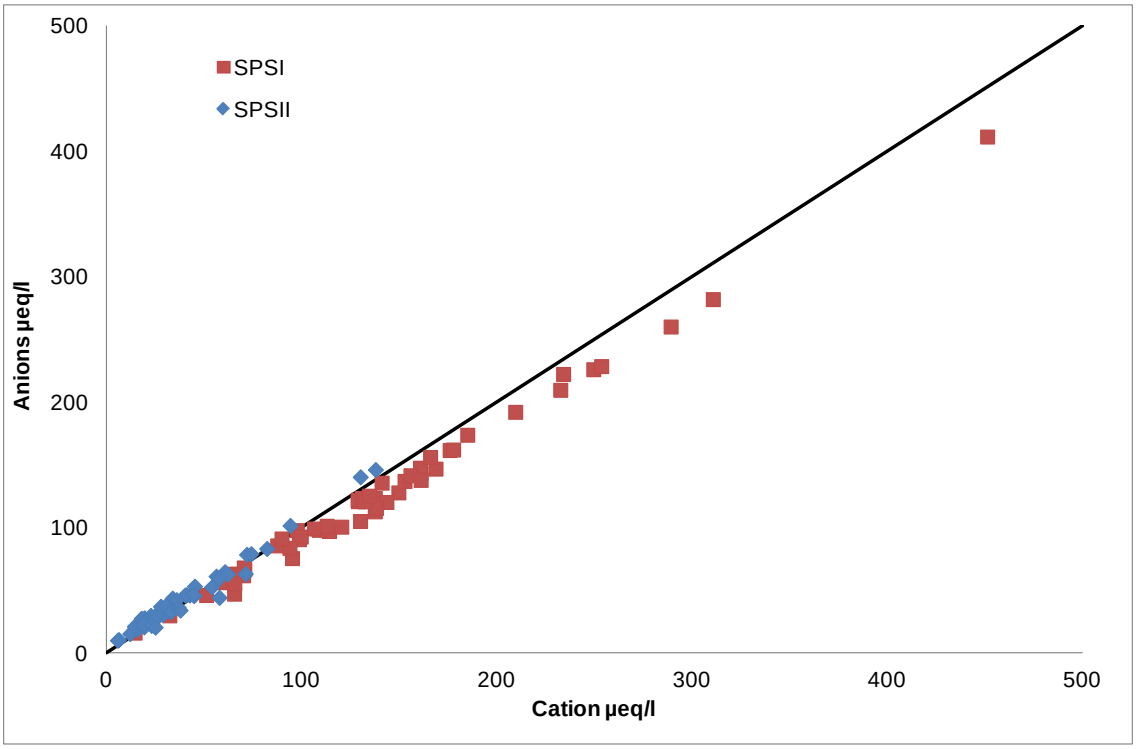

Figure A 1 Ion Balance for the ion chromatography measurements

A1.3.4 WMO LABORATORY INTER-COMPARISON

Each year the Wet Chemistry Laboratory at CMAR Aspendale participates in the WMO synthetic rainwater inter-comparison. This involves the analysis of a range of cations and anions on three separate synthetic rainwater samples two times each year. The analytical values for each sample are then compared to the true values. The results of the inter-comparison shown in figure A 2 indicate that the CMAR Aspendale Wet Chemistry Laboratory performs well in this laboratory inter-comparison. The ring diagram results for CMAR (lab id 700007) are shown for samples 1, 2 and 3. Below the results is the ring diagram overview of the current analyses and the key to the ring diagrams.

Lab 700007 Australia, LIS 2011 45 Ring Diagrams

Sample #1	Sample #2	Sample #3

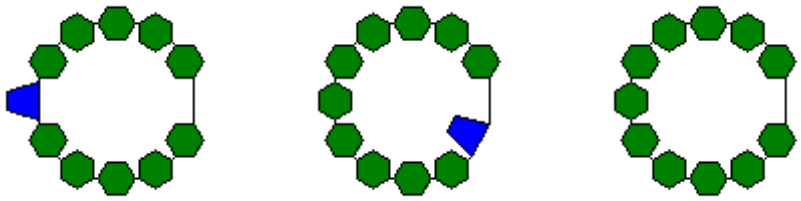

Ring Diagram Overview

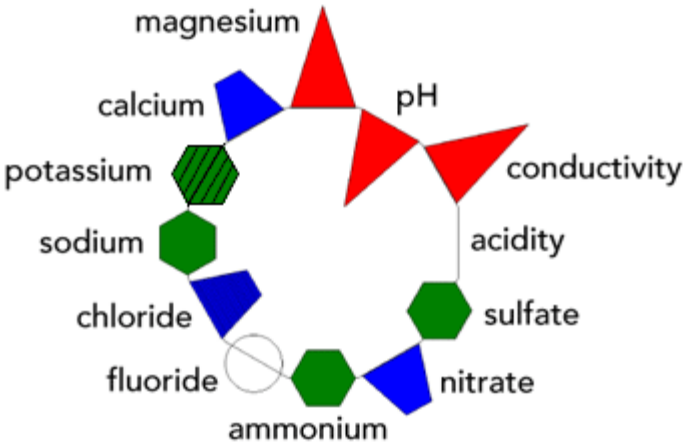

	GOOD - Green Hexagon
	Measurement is within the interquartile range (IQR), defined as the 25th to 75th percentile or middle half (50%) of the measurements. This applies to sulfate, ammonium, sodium, and potassium.
	SATISFACTORY - Blue Trapezoid
	Measurement is within the range defined by the median ± IQR/1.349. The ratio, IQR/1.349, is the non-parametric estimate of the standard deviation, sometimes called the pseudo-standard deviation. This applies to nitrate, chloride, and calcium.
	UNSATISFACTORY - Red Triangle
	Measurement is outside the range defined by the median ± IQR/1.349. This applies to pH, conductivity, and magnesium.

Figure A 2 WMO Inter-Comparison Results and ring diagram overview (see text for more details).

A1.3.5 COMPARISON OF SPECIES FROM IC AND IBA ANALYSIS

The IC and IBA have some common species which can be compared. Sulfur measured by IBA is mostly water soluble and can be compared to sulfate measured by IC (Figure A 3). The sulfur concentrations from IBA analysis should be a third of the sulfate concentrations from IC analysis to account for the difference in molecular weight of sulfur (32) and sulfate (96). The two analysis methods show very good agreement in mass concentrations and correlations.

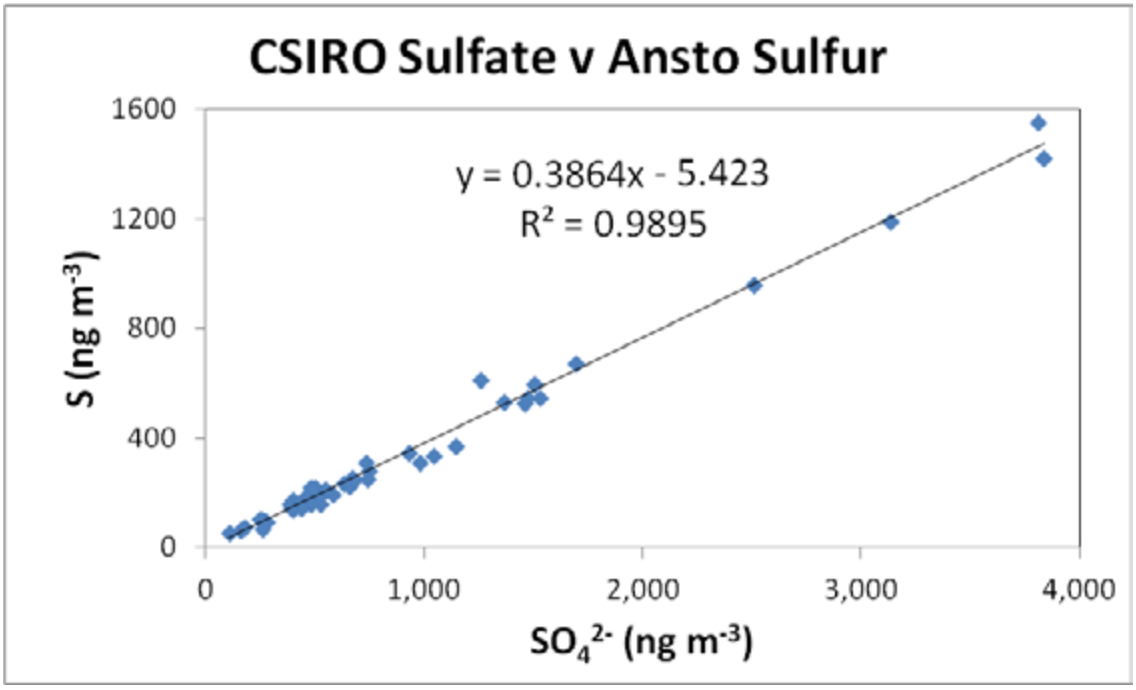

Figure A 3. Comparison of sulfur against sulfate.

A2. OBSERVED AND MODELLED VERTICAL TEMPERATURE AND WIND PROFILES

Figures relate to Feb 11th 2011 and May 9th 2012 and are plots of potential temperature, wind speed and wind direction for every hour of these days. The observed data comes from AMDAR profiles (see section 4.2.2).

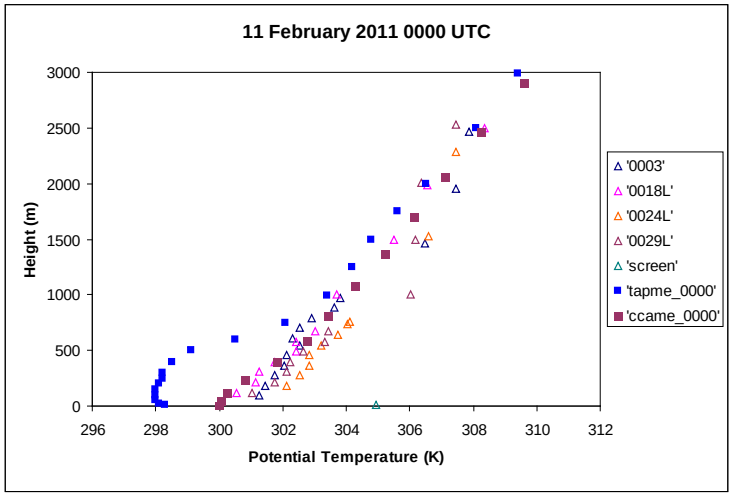

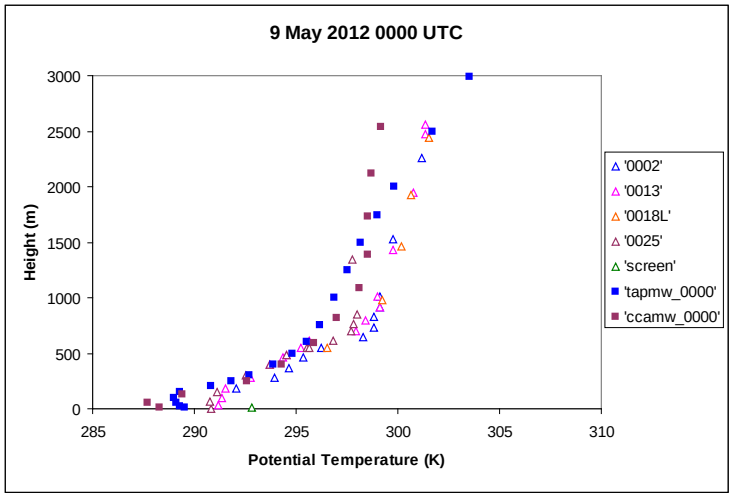

A3. ANSTO RADON AND LIDAR OBSERVATIONS- SPS2

Overview of ANSTO radon and lidar observations during the second Sydney Particle Study: April-May 2012

Alan Griffiths and Scott Chambers
Australian Nuclear Science and Technology Organisation

Australian Nuclear Science and Technology Organisation (ANSTO) conducted continuous radon and aerosol lidar measurements on the grounds of Westmead Hospital, Sydney, between 10 April and 9 May, 2012 as part of the second Sydney Particle Study led by CSIRO.

A3.1 Radon measurements

A3.1.1 METHODS

Measurements were made using a 750 L dual flow-loop two filter radon detector, which was setup to sample at 40 L min^{-1} from a height of 2 m above ground level. For information on the principle of operation of these detectors the reader is referred to Chambers *et al.*, (2011). Instrumental background checks were performed immediately before and after deployment, and an onsite calibration was performed using a Pylon 118.19 ±4% kBq Ra-226 source, traceable to NIST standards. The detector has a response time of approximately 45 minutes, and a lower limit of detection of 40-50 mBq m^{-3}.

A3.1.2 HOURLY OBSERVATIONS

A summary of the hourly radon observations at Westmead is presented in figure A4. The variability evident in the 26-day record results from the superposition of two main signals: (a) a "background" radon concentration representing the integrated influence of the radon source function over the air mass' most recent 2-week history, and (b) a concentration/dilution term resulting from diurnal changes in depth of the atmospheric boundary layer (ABL).

A third term, one which can often be neglected, is also significant for these observations. Several days of heavy rain during the first week of the campaign completely saturated the soil at and around Westmead. As a result radon emissions were suppressed, partly explaining the lower concentrations in the earlier part of the campaign.

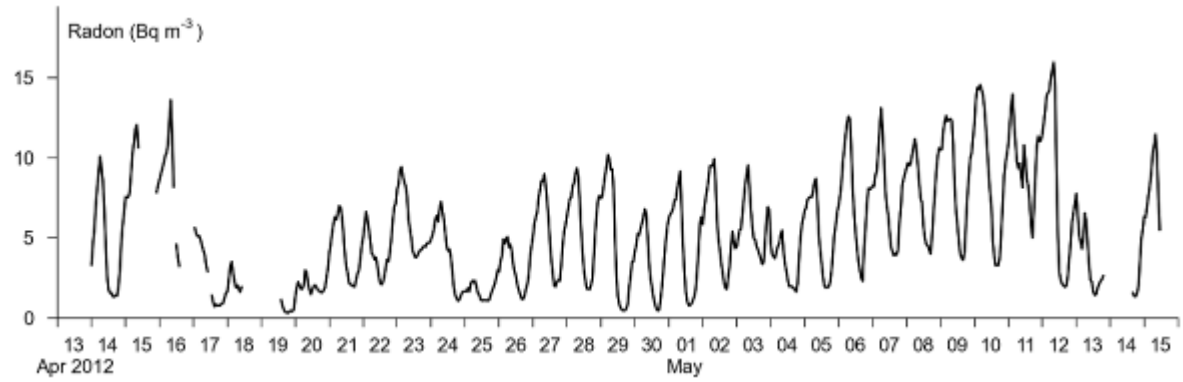

Figure A 4. Hourly radon concentration measurements at Westmead

The ABL is typically deepest, and most well mixed, in the mid-afternoon (figure A5). At this point of the diurnal cycle radon concentrations are at their lowest; fetch influences on observed radon concentration dominate over diurnal changes in mixing depth. Figure A6 summarises the daily minimum radon concentrations, which generally occur in the late afternoon. Since the radon source function is almost exclusively terrestrial, by inspecting the afternoon radon concentrations (i.e. independent of local meteorological observations) it is relatively easy to identify air masses that have had a predominantly oceanic fetch (arrived fairly directly from the east), or long-term continental fetch (arriving from the west to southwest).

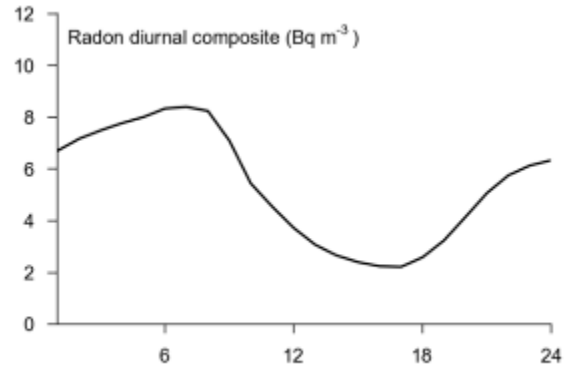

Figure A 5. Diurnal composite of hourly radon observations showing, on average, a period of steady accumulation during the night time followed by dilution after sunrise until the boundary layer grows to its deepest extent during the late afternoon.

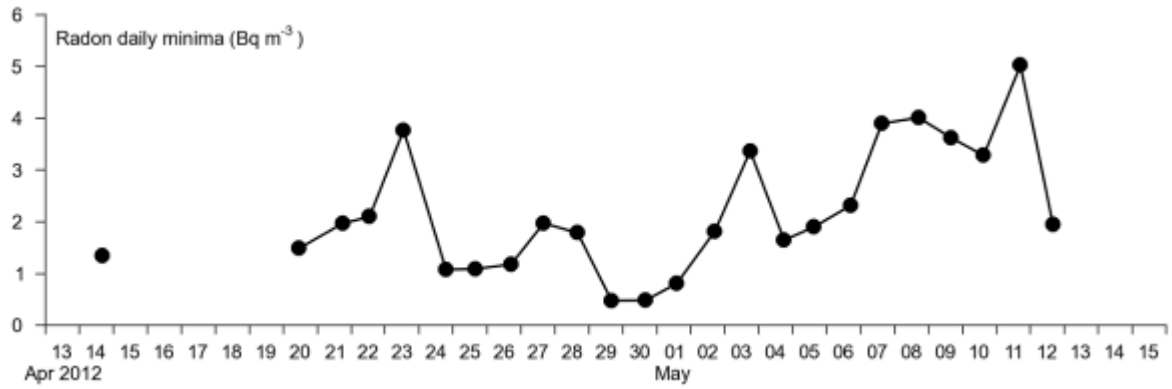

Figure A 6. Daily minimum radon concentration, which serves as an indicator of air mass history. Lowest values indicate oceanic fetch and highest values indicate continental fetch.

A3.2 Lidar observations

A3.2.1 METHODS

Observations were made using a Leosphere ALS 450 lidar (specifications in Table A 1) which measured UV light scattered back to a receiver from molecules and aerosols in the air column. The signal can be processed to obtain an estimate of cloud base, cloud top (when the clouds are optically thin enough), and boundary layer height. Further details, specific to this particular lidar system, can be found in Griffiths et. al. (2013).

Table A 1. lidar specifications.

· PBL detection frequency (typical)	· 10 min
· Spatial resolution	· 15 m
· Laser wavelength	· 355 nm
· Range min (full overlap) - max	· 0.4 to 20 km
· After overlap correction	· 0.15 to 20 km
· Temporal resolution	· 10 s

A3.2.2 BOUNDARY LAYER DETECTION

Using lidar, the depth of the boundary layer can be detected only under certain circumstances: the boundary layer top must be comfortably within the range of the lidar, i.e. deeper than about 200 m, and accompanied by a drop in aerosol abundance. These conditions are most likely to be met during the daytime on days with clear skies or in the presence fair weather cumulus.

Figures A7 and A8 show lidar signals and retrieved boundary layer heights for a fair-weather day. The profiles in Figure A show that the boundary layer is generally well mixed with a drop

in aerosol abundance at the top. Although there is also an indication of a second layer which persists near the ground throughout the day. It is relatively simple to retrieve the boundary layer height using a standard algorithm.

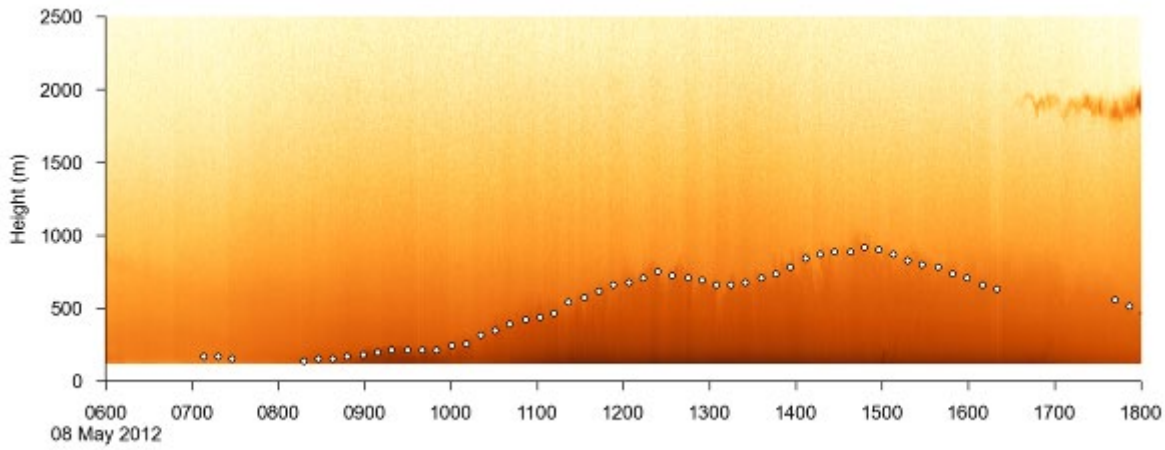

Figure A 7. Range-normalised lidar backscatter (indicated by shading, dark colours indicate more signal) along with the boundary layer height retrieved every 10 minutes during the day.

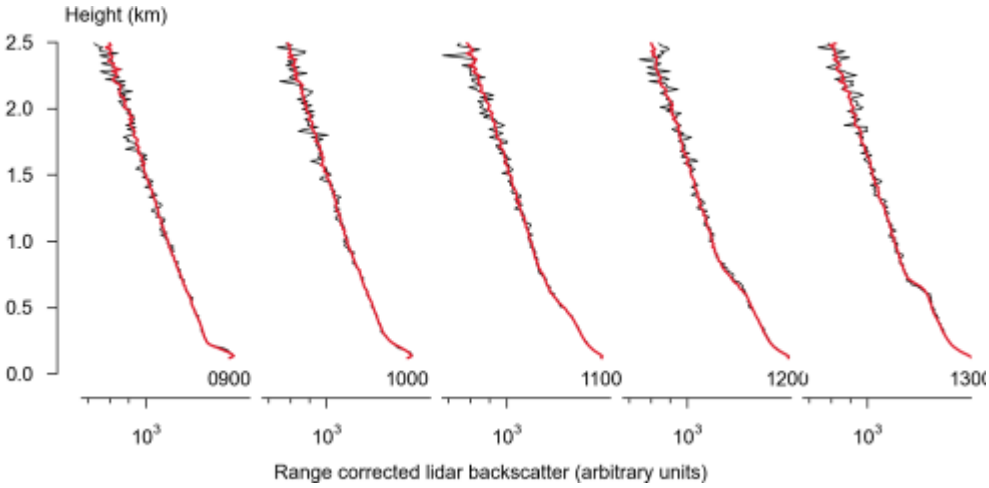

Figure A 8. Profiles of range-normalised lidar backscatter (30 second and 10 minute averages) for the clear-sky case.

Figures A9 and A10 show another clear sky day where the boundary layer can be determined from lidar, but in this case a relatively aerosol-free boundary layer is growing beneath layers of aerosol in the stratified air above. The elevated layers appear to be close to saturation, indicated by the formation of a cloud just before midday.

After the elevated layers have disappeared, having been either entrained into the boundary layer or carried away by the mean winds, the boundary layer appears more typical with the profile at 1300 (Figure A) showing a well-mixed boundary layer with a drop in aerosol abundance at the top. The active boundary layer eddies are also visible in Figure A these are the small oscillations from 1200 onward at a height of 1000 m.

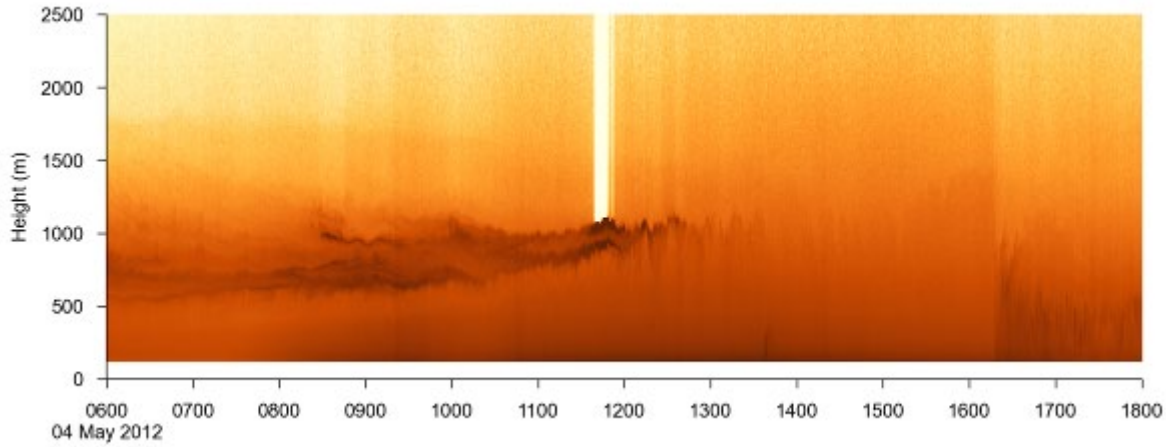

Figure A 9 Range-normalised lidar backscatter (indicated by shading, dark colours indicate more signal) on a day with clear skies but with an elevated aerosol layer.

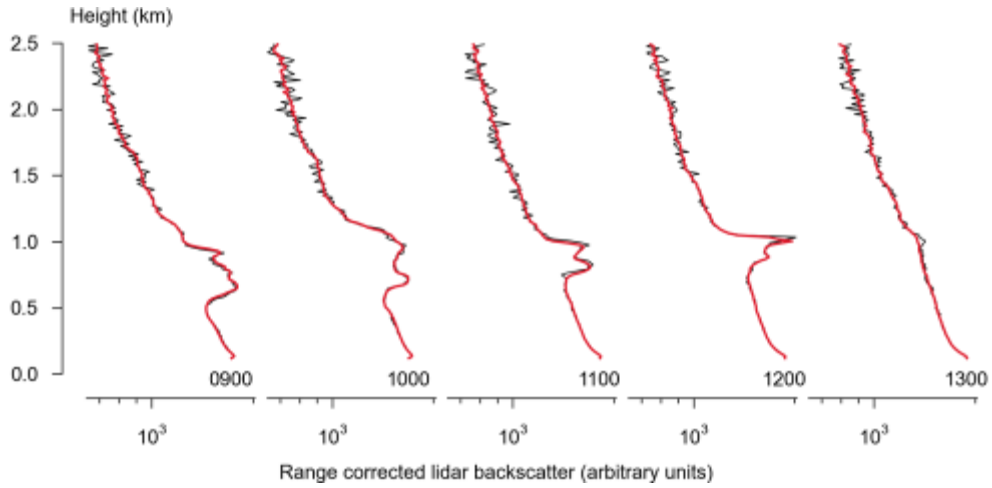

Figure A 10. Profiles of range-normalised lidar backscatter corresponding to Fig. 9.

A3.2.3 CLOUDS AND PRECIPITATION

Figures A11 and A12 show two cloudy days were observed by the lidar. In figure A11, boundary layer cloud is present throughout the day but is optically thin enough for the lidar to detect both the cloud base and cloud top. In contrast, Figure A shows deeper precipitating clouds from a convective system. Showers are visible (e.g. between 1400 and 1500) which re-evaporate before reaching the ground, or are carried sideways out of the field of view. At about 1530, a heavier shower indeed reaches the ground, attenuating the signal as a result of water pooling on the lidar windows. During periods of precipitation, a line of low backscatter is visible (called the lidar dark band as an analogy to the radar bright band) attributable to partially melted hydrometeors having fallen through the freezing level.

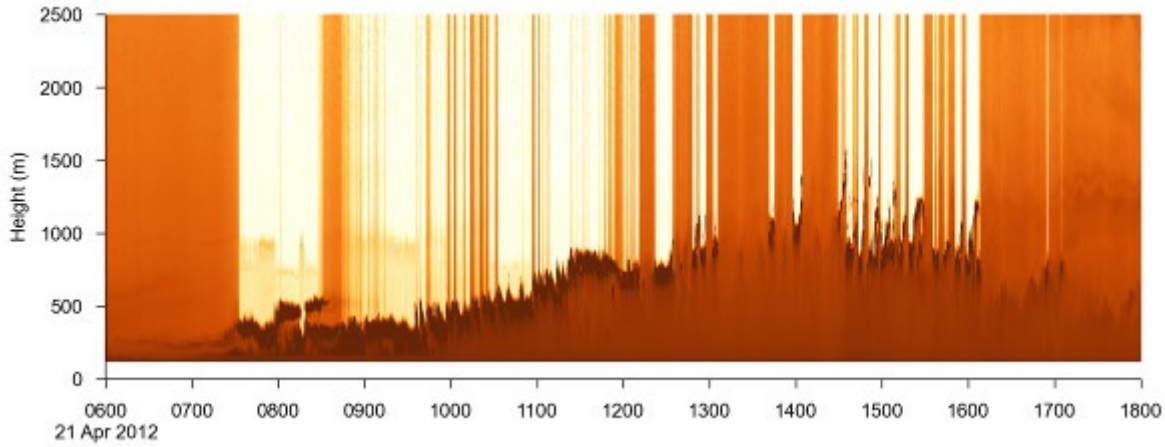

Figure A 11. Range-normalised lidar backscatter (indicated by shading, dark colours indicate more signal) on a day with boundary layer clouds.

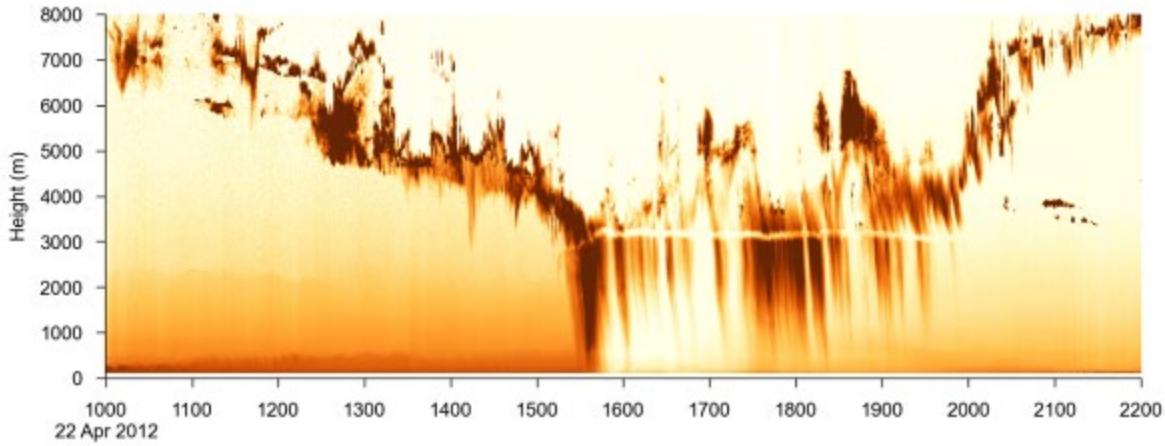

Figure A 12. Range-normalised lidar backscatter (indicated by shading, dark colours indicate more signal) on a day with precipitation falling through the freezing level.

A3.3 References

Chambers, S., A. G. Williams, W. Zahorowski, A. Griffiths and J. Crawford, 2011. Separating remote fetch and local mixing influences on vertical radon measurements in the lower atmosphere. Tellus B, pp. 17. DOI: 10.1111/j.1600-0889.2011.00565.x.

Griffiths, A. D., Parkes, S. D., Chambers, S. D., McCabe, M. F., and Williams, A. G.: Improved mixing height monitoring through a combination of lidar and radon measurements, Atmos. Meas. Tech. Discuss., 5, 6835-6866, doi:10.5194/amtd-5-6835-2012, 2012

A4. AEROSOL MASS SPECTROMETER (AMS)

Branka Miljevic and Zoran Ristovski, Queensland University of Technology, Brisbane.

A4.1 Instrument Description

Aerosol mass spectrometers are a very significant development in aerosol measurement technology in recent decades. A description of their theory and practice is presented in Jimenez et al. (2003). A compact Time-of-Flight Aerosol Mass Spectrometer (c-ToF-AMS; Aerodyne Research, Inc., Billerica, MA, USA) was used for the on-line quantification and chemical characterisation of the submicron non-refractory aerosol components. The term 'non-refractory' is assigned to those species that evaporate rapidly at 600^{o}C under high vacuum condition (~10^{-5}Pa) and in practice includes species such as ammonium sulphate and bisulphate, ammonium nitrate, ammonium chloride and organic compounds. The AMS consists of three main sections: the aerosol inlet, the particle-sizing chamber and the particle composition detection section. In the aerosol inlet section particle are sampled into the AMS through an aerodynamic lens forming a narrow particle beam of ~100 μm diameter. The aerodynamic lens has 100% transmission for particles in the size range of 60 – 600 nm and partial transmission down to 30 nm and up to 1.5 μm. When particles exit the lens and expand into high vacuum chamber they acquire size-dependent velocity. These velocities (and, thus, sizes) are determined by measuring particle time of flight between a rotating chopper wheel with a 2 radial slits and the detector. In the detection section, the particles impact onto the vaporiser, a heated, porous tungsten surface (~600^{o}C), where non-refractory aerosol components are flash vaporised and then ionized by electron impact. Positive ions generated in that way are then detected by time-of flight mass spectrometer (TOF-MS).

The c-ToF-AMS (short: AMS) was deployed at the Westmead air quality station in February 2011. The data is available for two sampling periods: 10 – 15 Feb and 18 – 24 Feb. The instrument provided submicron particle mass loadings and their composition with a time resolution of 5 min. A particle collection efficiency of 0.5 was estimated to calculate the aerosol mass concentration.

A4.2 Summary of results

Figure A13 and A14 show time series of the mass loadings of the PM_1 species as measured by the AMS for the time period of 10 – 15 Feb and 18 – 24 Feb, respectively. Note that due to instrumentation problems, mass loadings of the second time period are suspected to be lower than they should have been; however, their relative change and ratio between the distinct AMS components was not affected. It can be seen from figure A13 that the AMS mass loadings are substantially higher for the time period of 11 Feb (~9 am) – 12 Feb (~9 am).

Increase in the mass loadings for this time period is characteristic for all AMS components (organics, sulphates, etc.), meaning that their relative ratio has not changed during that time period, which is evident from figure A15. Averaging percentage of each AMS component presented in figure A15 throughout the whole sampling period gives that Org = 55% ± 10%; SO4 = 23.4% ± 7%; NO3 = 8% ± 2.5%; NH4 = 11.8% ± 3.5% and Chl = 2% ± 1%. Increase in the AMS mass loadings for the time period of 11 Feb (~10 am) – 12 Feb (~8 pm) coincides with the ozone levels, which were the highest for that time period (O_3 = 30-55 ppb). The spikes in the Org mass loadings might be due to appearance of combustion sources in the close proximity of the measurement site.

Figure A14 shows that during the time period of 19 Feb (~11am) – 20 Feb (~11:30pm) there was an increase in the organic (Org) mass loadings, whereas other AMS components remained low. It is evident from figure A16 that the percentage of organics "jumps" from ~50% to ~75% after 11 am on 19 Feb and stays around that value until midnight 20 Feb. This increase in the organic mass loadings also coincides well with the ozone levels, which were the highest for 19 and 20 Feb. In addition, it can be seen from figure A14 that there are three distinct events with sulphates and ammonium mass loadings increasing. These events were during afternoon hours on 20, 21 and 23 Feb. During those time periods the wind was blowing from SE. Such a distinct event was also observed in the afternoon hours of 11 Feb (and the wind during that period had ESE direction.

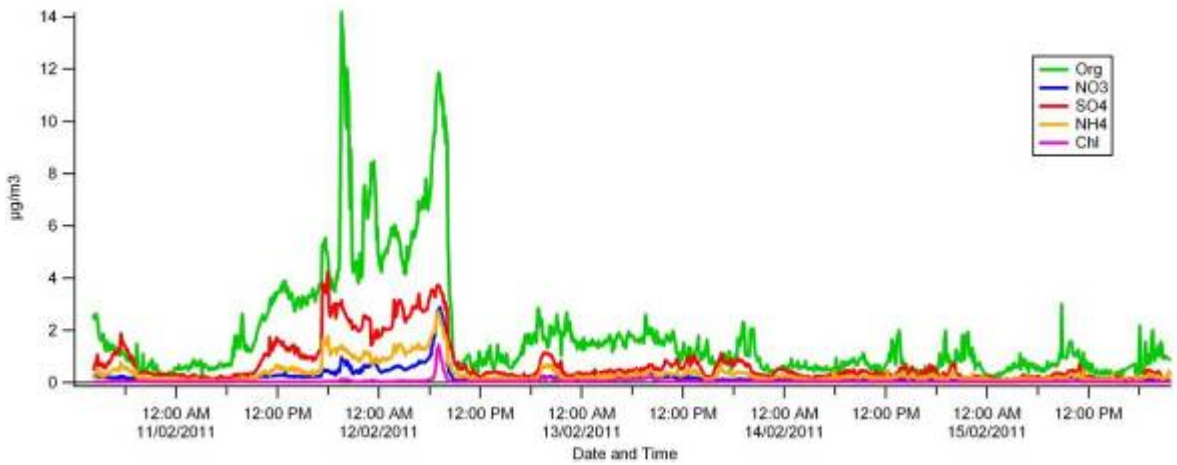

Figure A 13. Time series of the mass loadings of the non-refractory PM_1 species[8] for the time period of 10 – 15 Feb 2011.

[8] Org = organics; NO3 = nitrates; SO4 = sulphates; NH4 = ammonium; Chl = chloride

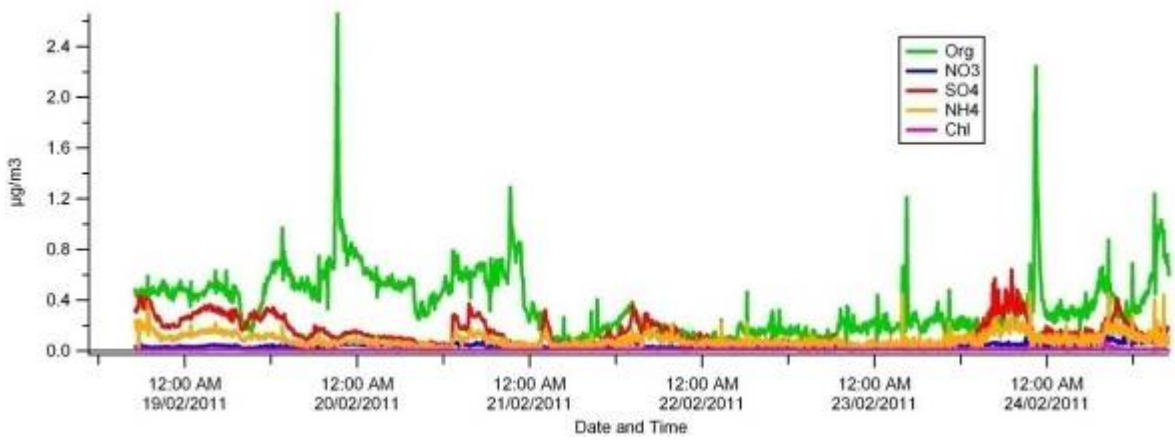

Figure A 14. Time series of the mass loadings of the non-refractory PM_1 species for the time period of 18 – 24 Feb 2011.

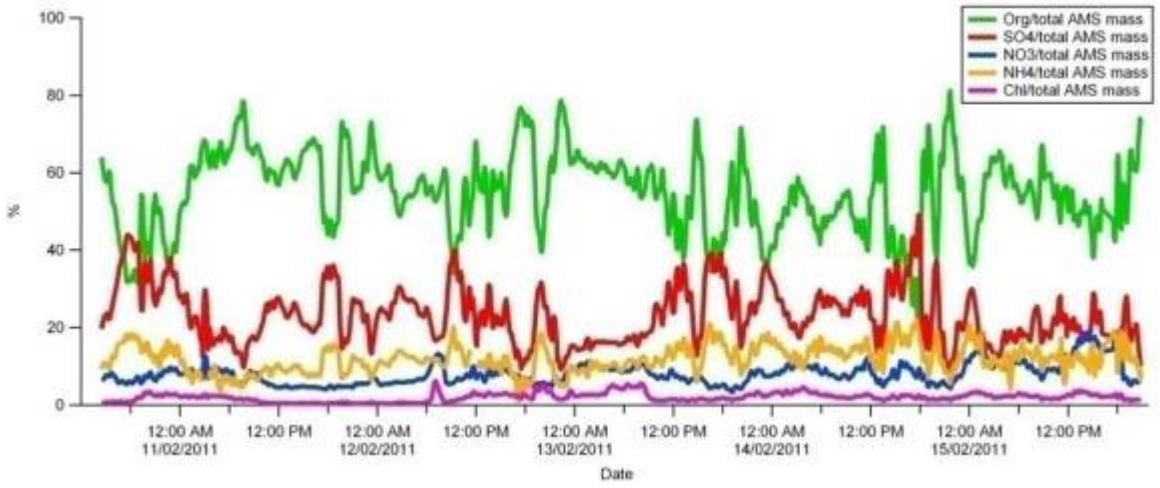

Figure A15. Time series of the percentage of the AMS measured components compared to the total mass measured by the AMS for the time period of 10 - 15 Feb 2011.

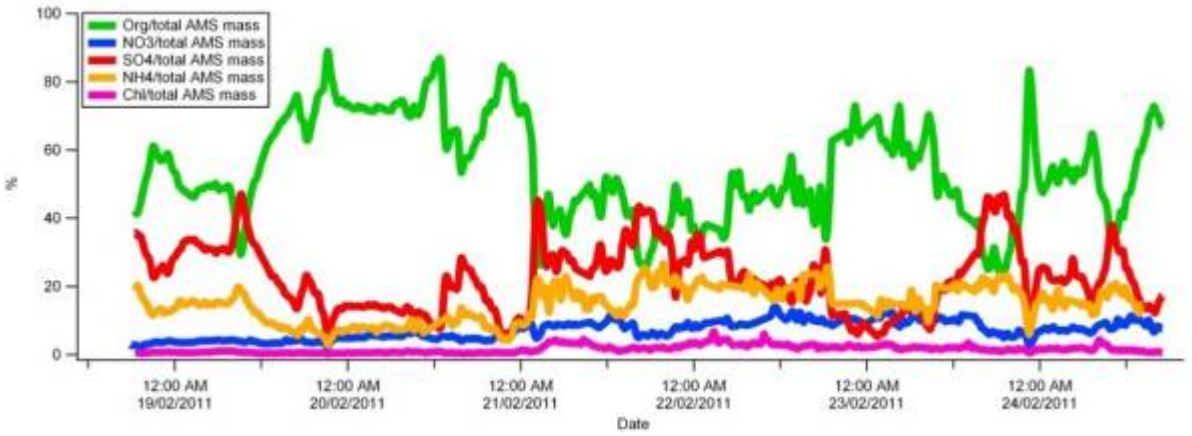

Figure A 16. Time series of the percentage of the AMS measured components compared to the total mass measured by the AMS for the time period of 18 - 24 Feb 2011.

Electron impact (EI) ionization results in significant fragmentation of molecules being analysed, which makes identification of molecular ions (i.e. exact species present in PM) impossible. Therefore, certain fragments (i.e. certain mass to charge ratios – m/z), specifically m/z44, m/z 57 and m/z60 have been proposed as markers for oxygenated organic species, hydrocarbon-like organic species and biomass combustion organic species, respectively ((Alfarra et al., 2004)). The abundance of certain peak is defined as:

$$f_{xy} = (m/z\ xy) / total\ organic\ mass$$

Based on these values one can gain more information about the nature of organic aerosol being sampled. For example, f44 ≈ 0.14 indicates that organic aerosol being sampled is oxygenated, which is typical for SOA The summary of organic tracers, species they are related to and their average values are presented in Table A 2.

Table A 2. Summary of organic tracers ((Ng et al., 2011))

Tracer (m/z)	Type of organic species	Average abundance (f_{xy}) values
43[9]	Total OA	0.05- 0.1
44	Oxygenated organic aerosol (OOA) - SOA	0.14
44	Low volatility oxygenated organics (LV-OOA)	0.16
44	Semi-volatile oxygenated organics (SV-OOA)	0.05
57	Hydrocarbon-like organic aerosol (HOA) - POA	0.07 – 0.08 (0.01 in OOA)
60, 73	Biomass burning organic aerosol (BBOA)	0.03

The time series of f43, f44 and f57 for the time periods of 10 – 15 Feb and 18 – 24 Feb are presented in figures A17 and A19, respectively. f60 was not shown as it was lower than 0.005 throughout the whole sampling periods, indicating that biomass burning did not contribute to organic aerosol sampled during those periods. It can be seen from figure A17 that there was a

[9] m/z 43 has contributions from both oxygenated ($C_2H_3O^+$) and non-oxygenated ($C_3H_7^+$) ions it is a useful tracer for total OA.

steep increase in f44 on 11 Feb around 8am from ~0.04 to ~0.12-0.14, indicating that there was an increase in oxygenated organic compounds (e.g. carboxylic acids, acyl peroxides). At the same time, there was a steep decrease in f57 (from ~0.06 to 0.01), meaning that hydrocarbon-like compounds present in the aerosol had decreased. As m/z 43 has contributions from both oxygenated and non-oxygenated ions, the values of f43 do not tend to change much. Increase in f44 (and decrease in f57) occurs around the same time as total mass loadings start to increase (figure A13).

Three time periods from 11 Feb were selected and their average mass spectra was extracted (figure A18). These periods are:

1) 11 Feb night and early morning (3:30am – 7:30am): f44 is low (~0.04) and f57 is high (~0.06). As can be seen in figure A18(1), relative abundance of signals at m/z 41,43, 55,57, 69,71, 83, 85 is quite high. These signals belong to alkyl fragments ($C_nH_{2n+1}^+$: 43,55,71,85; $C_nH_{2n-1}^+$: 41,55,69,83), which are characteristic for HOA
2) 11 Feb morning (8am – 9am): transition period – f44 starts to increase, f57 starts to decrease. Figure A18(2) shows that relative abundance of alkyl fragments starts to decrease and m/z 44 starts to increase
3) 11 Feb afternoon (12pm – 17pm): f44 is high (~0.13) and f57 is low (~0.01). It evident from figure A18(3) that relative abundance of m/z 44 is much higher than in the previous two mass spectra, whereas relative abundance of alkyl fragments is low (excluding m/z 43, which is relatively high – probably due to $C_2H_3O^+$ ions)

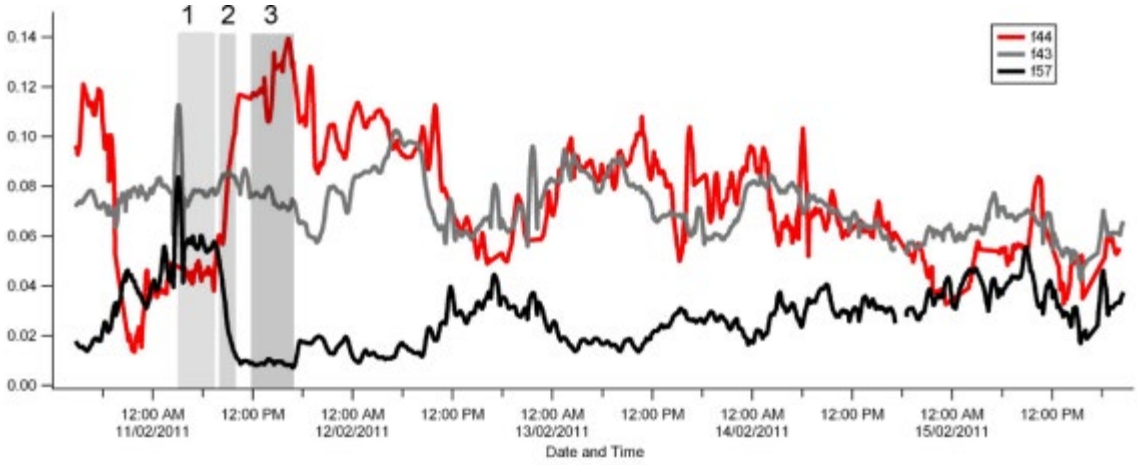

Figure A17. Time series of f43, f44 and f57 for the time period of 10 – 15 Feb 2011. Shaded areas denote periods for which average mass spectra was extracted.

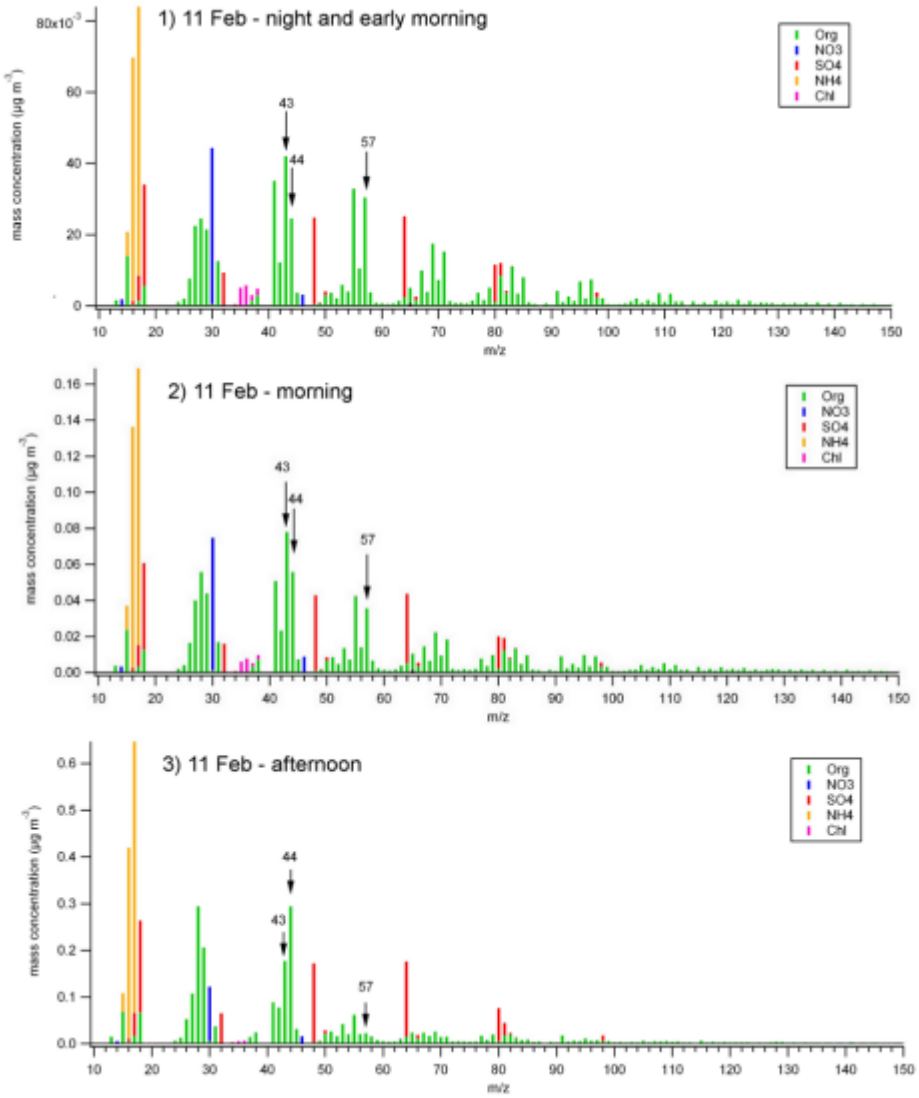

Figure A18. Average mass spectra of three time periods on 11 Feb.

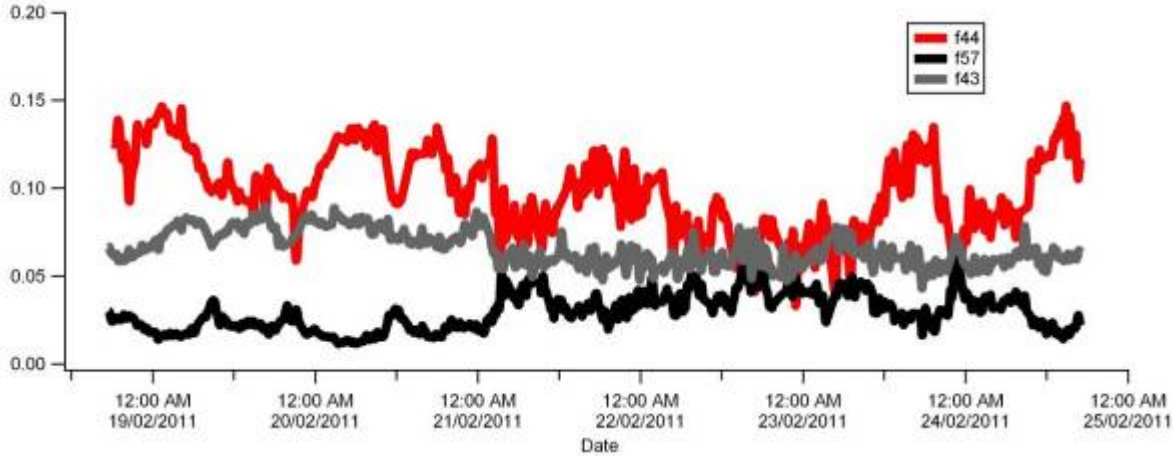

Figure A19. Time series of f43, f44 and f57 for the time period of 18 – 24 Feb 2011.

A4. PROJECT PAPERS

Publication in the International Journal of Mass Spectrometry, 2012.

International Journal of Mass Spectrometry 319–320 (2012) 40–47

Contents lists available at SciVerse ScienceDirect

International Journal of Mass Spectrometry

journal homepage: www.elsevier.com/locate/ijms

Interference in the PTR-MS measurement of acetonitrile at *m/z* 42 in polluted urban air—A study using switchable reagent ion PTR-MS

Erin Dunne[a,b,*], Ian E. Galbally[a], Sarah Lawson[a], Antonio Patti[c]

[a] Centre for Australian Weather and Climate Research, CSIRO Marine and Atmospheric Research, PMB 1, Aspendale, Vic, 3195, Australia
[b] School of Applied Science, Monash University, Gippsland, Vic., Australia
[c] Centre for Green Chemistry, Monash University, Clayton, Vic., Australia

ARTICLE INFO

Article history:
Received 30 January 2012
Received in revised form 4 May 2012
Accepted 7 May 2012
Available online 20 May 2012

Keywords:
Acetonitrile
Switchable reagent ion
PTR-MS
Mass interference
Urban air

ABSTRACT

In Proton Transfer Reaction Mass Spectrometer (PTR-MS) measurements of the atmosphere, the signal at *m/z* 42 is commonly regarded as a unique measure of acetonitrile. However, two other ions potentially contribute to the signal at *m/z* 42. These are ^{13}C isotopologues of $C_2H_5^+$ and the product ion $C_3H_6^+$ produced by reaction of NO^+ and O_2^+ (present in trace amounts in the H_3O^+ reagent gas), with a number of volatile organic compounds. Thus, there is the possibility of interference in the measurement of acetonitrile at *m/z* 42 by PTR-MS.

Interference in the measurement of acetonitrile at *m/z* 42 was quantified in urban air over 17 days in Sydney, Australia, in summer. A PTR-MS with Switchable Reagent Ion capability was used for measurements at *m/z* 41 and 42 in three different primary reagent ion modes, O_2^+, NO^+ and H_3O^+, to quantify the contribution of non-acetonitrile compounds to the signal at *m/z* 42 when the PTR-MS was operating in H_3O^+ reagent ion mode. Acetonitrile dominated the ion signal at *m/z* 42; however non-acetonitrile ions contributed 5–41% of the total ion signal at *m/z* 42. The average corrected and uncorrected acetonitrile concentrations were 120 pptv and 148 pptv respectively.

The interference in the *m/z* 42 signal was calculated from known or interpolated concentrations of compounds identified as potential interferrants. Overall the isotopologue correction is due to alkenes including isoprene with probable contributions from other compounds not measured in this study. The other component of the interference, produced by reactions of O_2^+, is due to alkanes and alkenes.

Levoglucosan, a biomass burning tracer in atmospheric particulate matter was more highly correlated with the corrected acetonitrile signal than the uncorrected acetonitrile signal.

Measurements of acetonitrile by PTR-MS at *m/z* 42 in urban air will frequently require correction because of the non-trivial concentrations of alkanes and alkenes commonly observed in urban air.

1. Introduction

Biomass burning is a major source of gases and particles to the atmosphere at concentrations that have a significant influence on atmospheric chemistry at local, regional and global scales [1]. Acetonitrile is almost exclusively emitted from biomass burning and has an atmospheric lifetime of many months [2]. Consequently, it is commonly used as a tracer for biomass burning. In the urban atmosphere measurements of acetonitrile are a useful indicator of the contribution to air quality of controlled and uncontrolled biomass burning, wood fuelled heating, and any other biomass combustion.

Proton transfer mass spectrometry (PTR-MS) observations have been useful in identifying biomass burning plumes and observing their transport and chemical processing [e.g., 3,4]. PTR-MS instruments are capable of detecting numerous VOCs including acetonitrile and other nitrogen-containing VOCs as well as oxygenated VOCs, aromatics and some alkenes [5,6] online with fast response and high sensitivity (sub-ppb). The principal of the PTR-MS is the utilization of proton transfer reactions from H_3O^+ compounds with a proton affinity (PA) > H_2O (166.5 kcal mol^{-1}) to produce charged products.

The ion detection system in a standard PTR-MS consists of a quadrupole mass spectrometer that separates the ions according to their mass/charge ratio (*m/z*) and a secondary electron multiplier (SEM) operated in count mode that detects the number of impinging ions at each *m/z* channel with a mass resolution of 1 amu. The major practical limitation of PTR-MS is its inability to distinguish between ions with the same mass to charge ratio (*m/z*) [7]. The low

* Corresponding author at: Private Bag 1, Aspendale, Vic. 3195, Australia.
Tel.: +61 3 9239 4428; fax: +61 3 9239 4444.
E-mail address: Erin.Dunne@csiro.au (E. Dunne).

1387-3806/$ – see front matter.
http://dx.doi.org/10.1016/j.ijms.2012.05.004

A5. WOODHEATER CASE STUDY

Talk given by Martin Cope to the CASANZ Technical Meeting, September 2012.

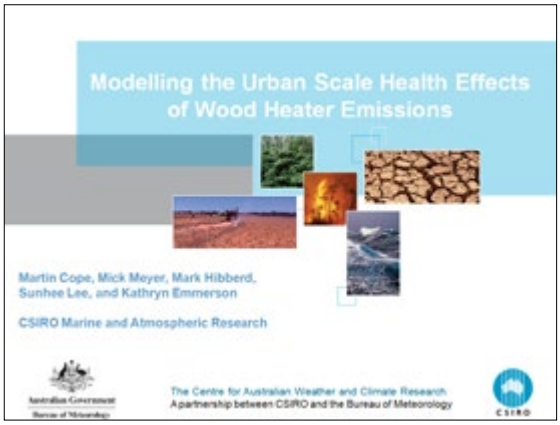

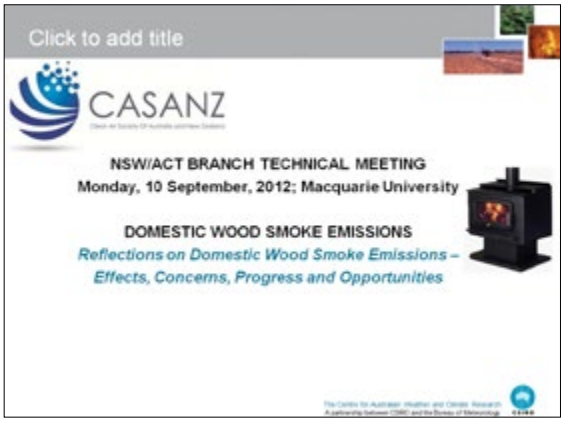

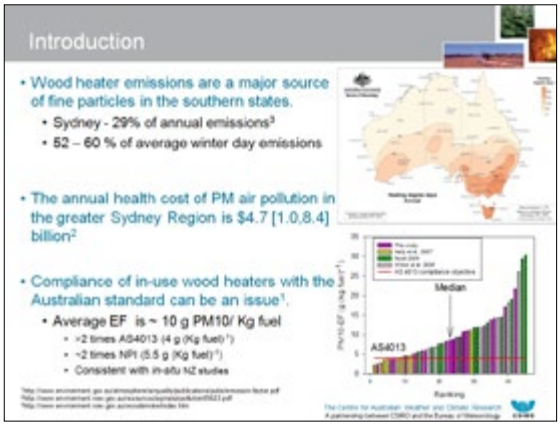

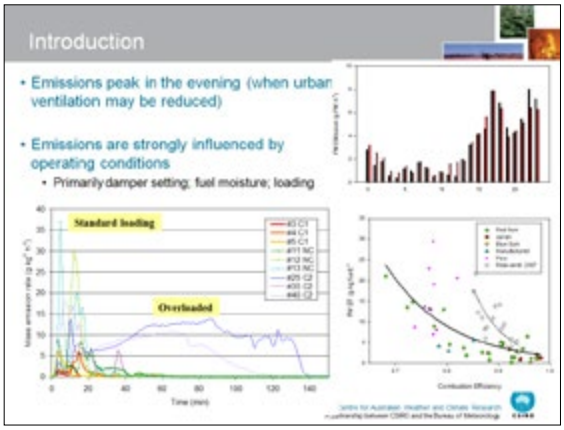

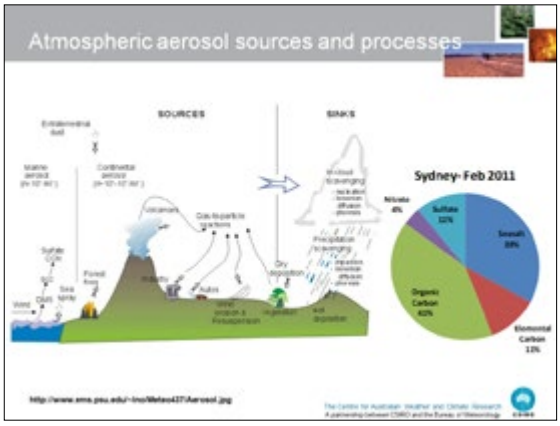

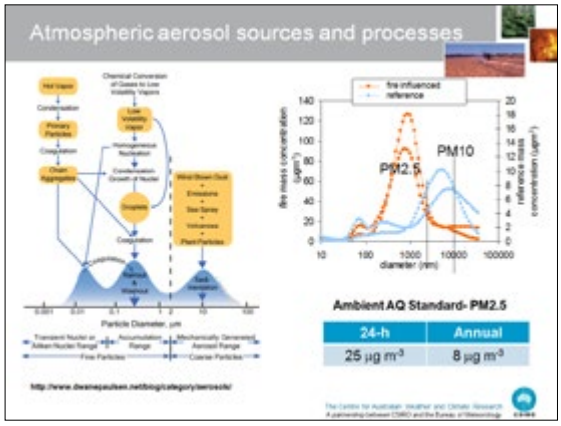

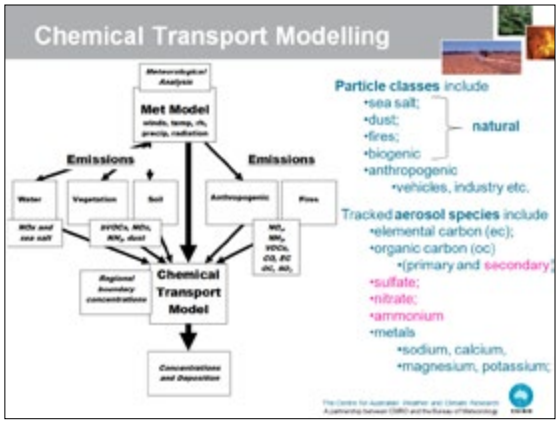
Chemical Transport Modelling
Met Model
Emissions
Emissions
Chemical Transport Model
Particle classes include
•sea salt;
•dust;
•fires;
•biogenic
natural
•anthropogenic
•vehicles, industry etc.
Tracked aerosol species include
•elemental carbon (ec);
•organic carbon (oc)
•(primary and secondary)
•sulfate;
•nitrate;
•ammonium
•metals
•sodium, calcium,
•magnesium, potassium;

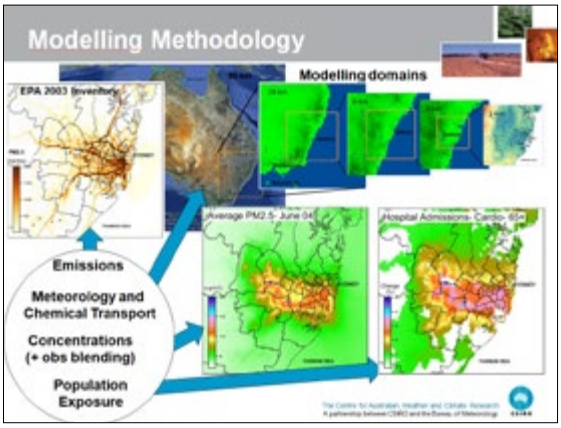
Modelling Methodology
Modelling domains
EPA 2003 inventory
Emissions
Meteorology and Chemical Transport
Concentrations (+ obs blending)
Population Exposure

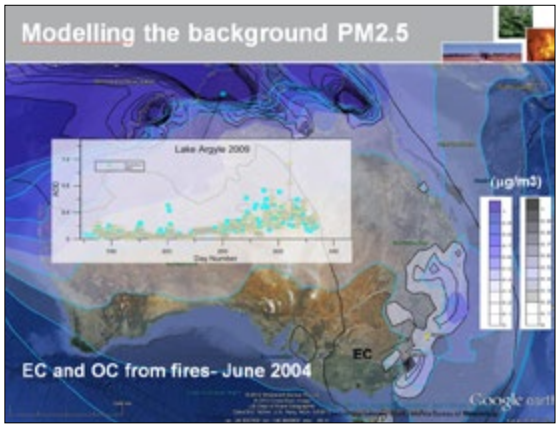
Modelling the background PM2.5
Lake Argyle 2009
(µg/m3)
EC and OC from fires- June 2004
EC

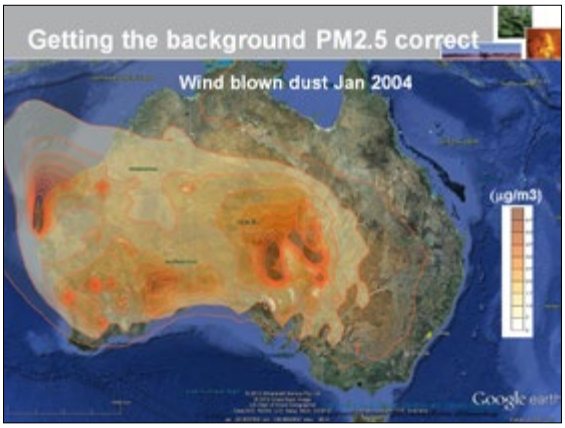
Getting the background PM2.5 correct
Wind blown dust Jan 2004
(µg/m3)

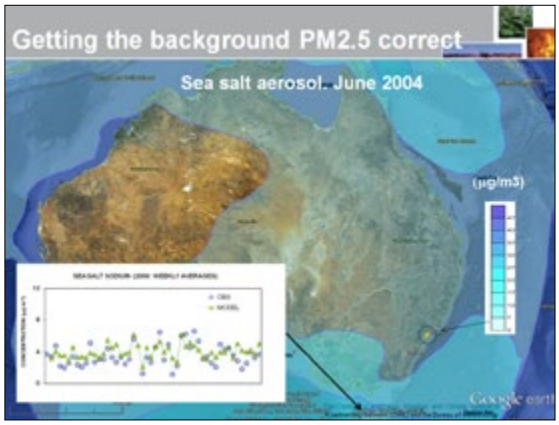
Getting the background PM2.5 correct
Sea salt aerosol. June 2004
(µg/m3)

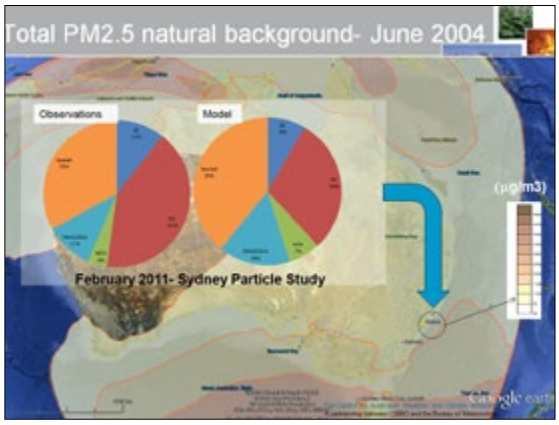
Total PM2.5 natural background- June 2004
Observations
Model
(µg/m3)
February 2011- Sydney Particle Study

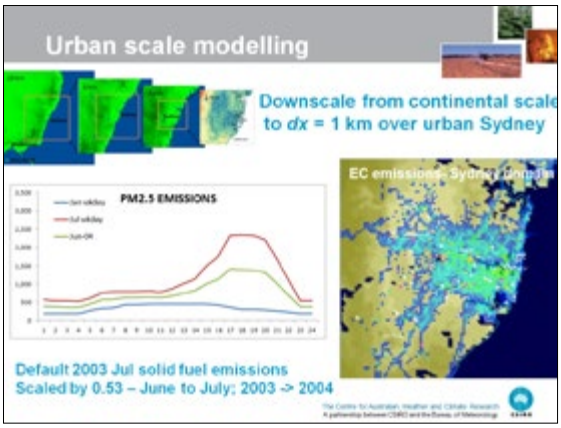
Urban scale modelling
Downscale from continental scale to dx = 1 km over urban Sydney
PM2.5 EMISSIONS
Default 2003 Jul solid fuel emissions
Scaled by 0.53 – June to July; 2003 -> 2004

Urban scale modelling

Observed[1] and modelled percentiles of 24-h PM2.5 for June 2004- for 7 OEH monitoring stations

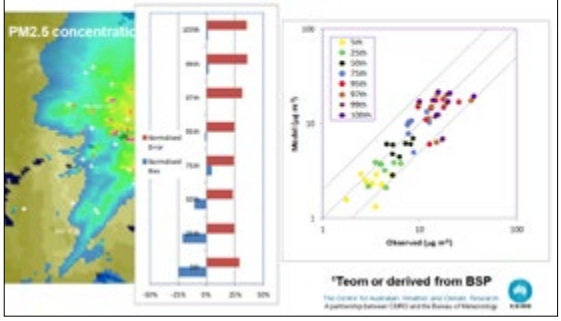

[1]Teom or derived from BSP

Modelled breakdown of PM2.5 sources

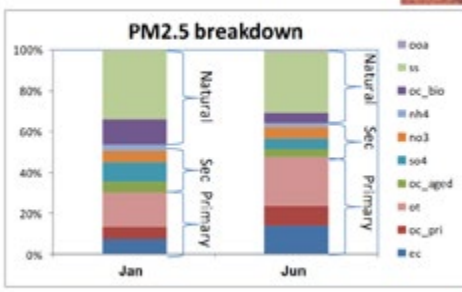

Air Quality and Health Effects

A recent EPHC study found significant increases in mortality and hospital admissions associated with increases in air pollutant concentrations in Australian and New Zealand cities.

Pollutant	15-64 years	65+ years	Cities used in analyses
Nitrogen dioxide	Total cardiovascular, All cardiac, cardiac failure, arrhythmia	Total cardiovascular, All cardiac, cardiac failure, IHD*, MI*	Auckland, Brisbane, Canberra, Christchurch, Melbourne, Perth, Sydney
Carbon monoxide	Total cardiovascular, All cardiac, cardiac failure, arrhythmia	Total cardiovascular**, All cardiac**, cardiac failure**, IHD*, MI*	Auckland, Brisbane, Canberra, Christchurch, Melbourne, Perth, Sydney
PM_{10}	-	All cardiac, cardiac failure	Brisbane, Christchurch, Melbourne, Perth, Sydney
$PM_{2.5}$	-	Total cardiovascular, All cardiac, cardiac failure, IHD*, MI*	Brisbane, Melbourne, Perth, Sydney

*IHD = ischaemic heart disease, MI = myocardial infarction
** Evidence of heterogeneity for these outcomes with Sydney results higher than the other cities, but pooled estimates for the remaining cities still significant and positive.

EPHC (2010), Expansion of the multi-city mortality and morbidity study. Final Report. Executive Summary and Summary Report. Environment Protection and Heritage Council, September 2010.
http://www.ephc.gov.au/sites/default/files/AQ_Rech_Multi-city_MM_Executive_Summary_Sept_Final_201008.pdf

Air Quality and Health Effects

$$\Delta H = H_0 (e^{\beta \Delta C} - 1) P$$

ΔH	-change in health outcome
H_0	-baseline health outcome
P	-at risk population
β	- relative risk factor
ΔC	-concentration change

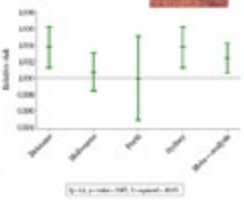

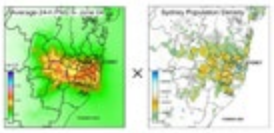

Example- city specific and meta-analysis relative risk factors of mortality (all cause; all ages) for a 1 μg/m³ increase in 24-h PM2.5 (EPHC 2010) [yearly all cause- 21k]

All Cause, All Age Mortality- June 2004

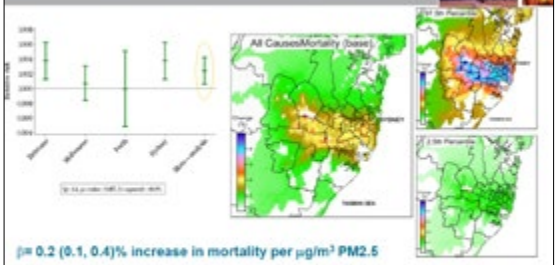

β= 0.2 (0.1, 0.4)% increase in mortality per μg/m³ PM2.5

This leads to a 1.5 (0.7, 3)% increase in base line mortality (median = 0.8, min = 0.5 max =5.9 %)

The wood combustion contribution

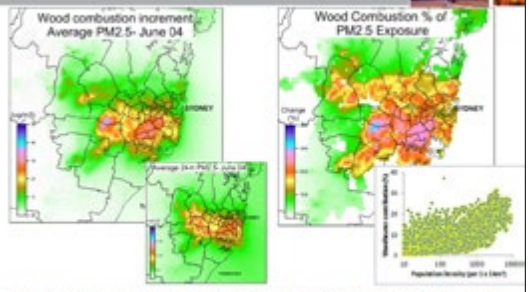

The model predicts a median contribution of 7% across the entire domain with a minimum increment of 0.4% and a maximum of 37%. Exposure increases with population density (pop-weighted exposure = 18%)

Summary

- Particle exposure is a multi-scale problem (scales from urban to continental influencing PM2.5 exposure in Sydney).
- In the cases studied, the contribution of anthropogenic primary emissions to PM2.5 exposure was 50% of less. Of course this will vary with location and time.
- For the June 2004 case study (solid fuel combustion emissions 50% of potential), a median contribution of 7% is modelled.

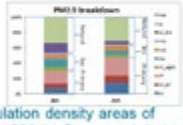

- However, the contribution scales with population density areas of maximum population density in Sydney (> 1000 /km²) are modelled to have contributions of 10 – 30% and the population-weighted exposure is18%.

Australian Government
Bureau of Meteorology

The Centre for Australian Weather and Climate Research
A partnership between CSIRO and the Bureau of Meteorology

CSIRO

Martin Cope

Phone: 03 9239 4647
Email: martin.cope@csiro.au
Web: www.cawcr.gov.au

A6. POSTER AND ORAL PRESENTATIONS

Two posters shown at the International Global Atmospheric Chemistry (IGAC) Beijing, September 2012

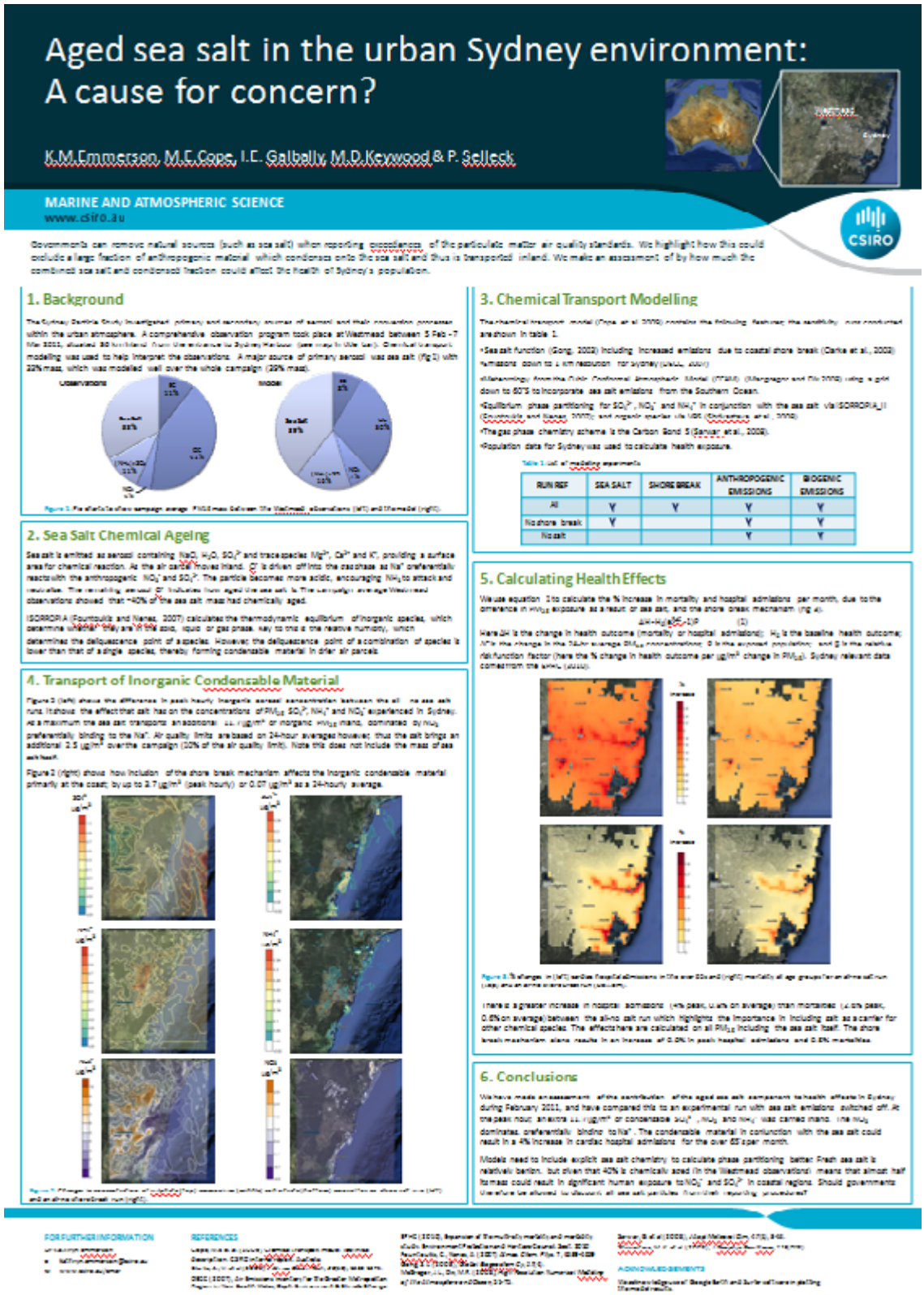

Secondary Organic Aerosol: biogenic vs anthropogenic

Team: Melita Keywood[1], Ian Galbally[1], Martin Cope[1], Kate Boast[1], Scott Chambers[2], Min Cheng[1], Suzanne Crumeyrolle[1,4], Erin Dunne[1], Kathryn Emmerson[1], Rosemary Fedele[1], Rob Gillett[1], Alan Griffiths[2], Sarah Lawson[1], Branka Miljevic[3], Suzie Molloy[1], Jennifer Powell[1], Fabienne Reisen[1], Zoran Ristovski[3], Paul Selleck[1], Jason Ward[1], Chuanfu Zhang[5], Jianrong Zeng[5]

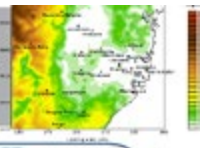

Development of a long term control strategy for particles in urban centres can be informed through the use of comprehensive three-dimensional simulations of the atmosphere, sources and multi-phase chemistry.

Such an approach requires a good understanding of the contribution made by local and remote particle sources to the total particle exposure within the region, and is informed by detailed and high quality experimental studies

Sydney Particle Study

A combined modelling and observation project that includes an intensive field campaign of aerosol and aerosol precursor measurements carried out in Sydney (Westmead) during February 2011.

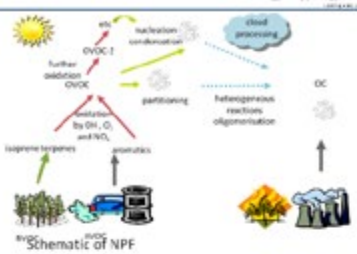

Schematic of NPF

Observations

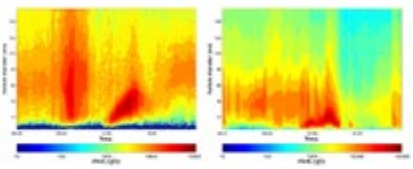

Typical particle size distributions, left 24 February 2012, right 9 February 2012. NPF events were observed on 50% of the afternoons during the measurement campaign. These events took the form of prolonged aerosol growth or bursts of short duration.

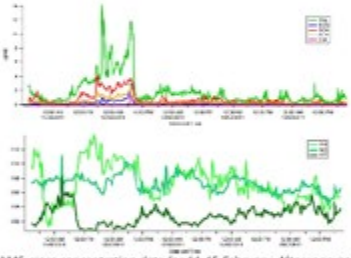

AMS mass concentration data for 11-15 February. Afternoon particle growth was associated with elevated oxygenated organics and sulfate concentrations.

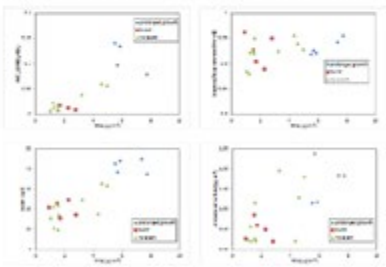

Relationships between SOA determined from integrated PM2.5 high volume samples and oxidation metrics for the different NPF event types. SOA shows a clear relationship with prolonged aerosol growth NPF events as does the metric of oxidation $HNO_3/(HNO_3+NO_3)$ and ozone. The isoprene oxidation metric isoprene/(isoprene + methacrolein +mvk) shows no clear relationship with NPF events. These observations suggest that while photochemistry may occur frequently, the partitioning of oxidized VOC compounds to the aerosol phase is NO_x limited.

Modelling

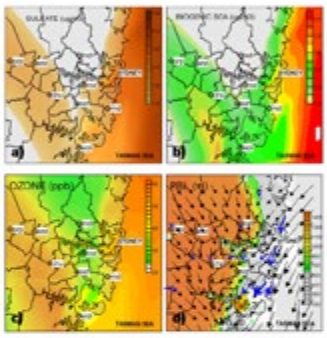

Modelled ground level concentrations of sulfate, a biogenic SOA component and ozone at 12 pm 11th February. All of the concentration fields show the presence of a plume being transported over Westmead from the north-west: here a power station plume in the model. Elevated concentrations of O_3 and SOA in the plume result from the interaction of plume NO_x and biogenic VOC emissions. The chemical transport occurred in a moderately deep boundary layer associated with the north-westerly flow.

Time series of observed and modeled SOA and modeled biogenic SOA. At the time of the peak SOA concentrations, 60-80% of the SOA mass has a biogenic origin.

Breakdown of the modelled organic aerosol into primary anthropogenic, secondary anthropogenic and biogenic; non-volatile background aerosol.

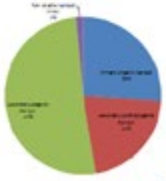

This research was supported by NSW Office of Environment and Heritage and CSIRO Marine and Atmospheric Research. Special thanks are given to Suzanne Quigley.

1 CSIRO Marine and Atmospheric Research, 2 ANSTO, 3 Queensland University of Technology, 4 now at NASA, 5 SINAP

Australian Government Bureau of Meteorology

The Centre for Australian Weather and Climate Research
A partnership between CSIRO and the Bureau of Meteorology

CSIRO

Talks given by Kathryn Emmerson and Martin Cope at the Aerosol Workshop in Murramarang, November 2012.

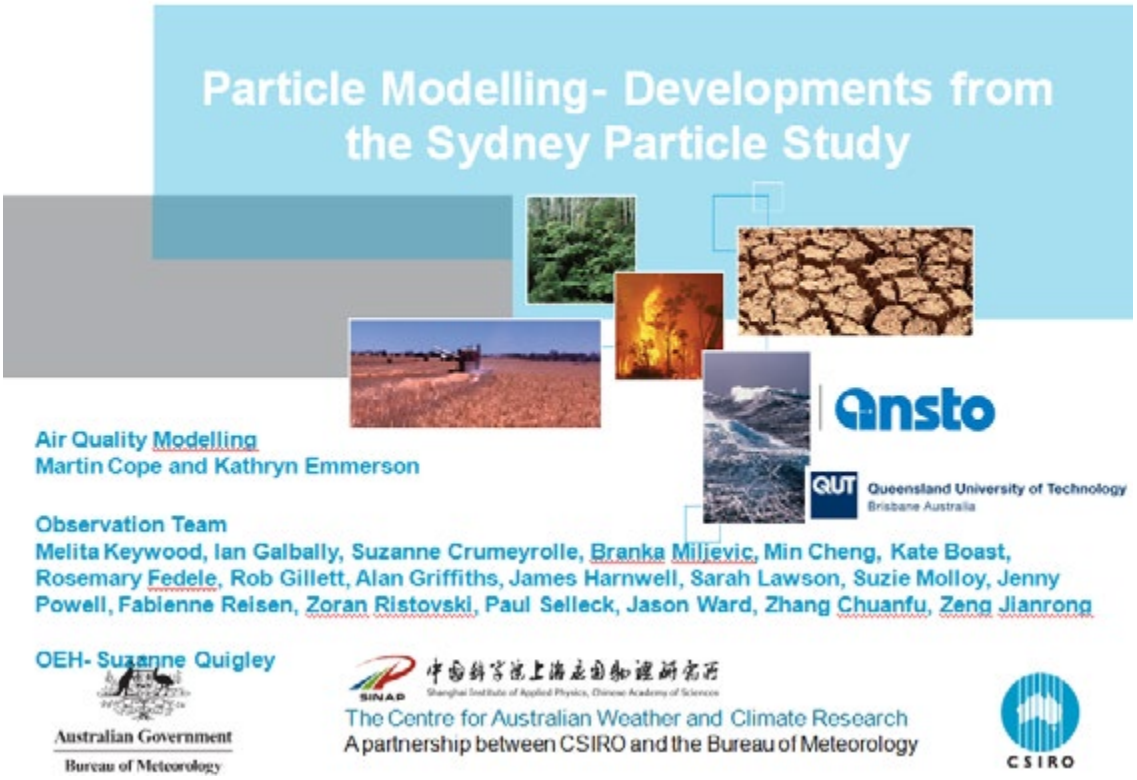

A7. GLOSSARY AND ABBREVIATIONS

Simple definitions of various technical terms are given here to assist the reader. If required, the reader should look to other sources for more formal and technical definitions.

ABL	Atmospheric Boundary Layer. The ABL is the lowest 100 to 3000 m of the atmosphere modified by the earth's surface. The ABL responds to surface forcings (i.e. heating, cooling, and roughness) with a time scale of about an hour or less, and its extent is deeper in the daytime and shallower in the nighttime. It is often turbulent and is capped by a temperature inversion (see definition below). Also called the Planetary Boundary Layer
Adsorbent tube	Tube holding material for trapping atmospheric VOCs that are subsequently released by thermal desorption and analysed.
Aerosol	A suspension of fine solid, liquid or mixed-phase particles in air.
AGL	Height Above Ground Level
ALD	Carbon Bond 5 lumped organic species
ALDX	Carbon Bond 5 lumped organic species
AM	Used in this report to represent the sampling time 05:00 to 10:00 h.
AMDAR data	Automated weather reports obtained from commercial aircraft
AMS	Aerosol Mass Spectrometer
ANSTO	Australian Nuclear Science and Technology Organisation
AQMS	Air Quality Monitoring System
AAQS	Ambient Air Quality Standards
AVOCs	VOCs (see entry) of anthropogenic origin, generally either fossil fuel products or unburnt and partially burnt products of combustion of fossil fuels
Background air	Background concentrations in this context refer to those concentrations observed in the air when the air is not under the direct influence of anthropogenic emissions. Background air contains concentrations of constituents that arise from natural sources, and from anthropogenic sources that are so distant that their contribution is already well mixed within the airmass by the time the air reaches the point of measurement.

Biogenic	In this report the term is used to indicate gases and aerosol that arise from emissions from biological activities in the soil, oceans, plants and animals.
Biomass Burning	Burning of vegetation in prescribed burns, wildfires and woodheaters
bVOCs	VOCs (see entry) of biological origin
Carbon Bond 5	A kinetic mechanism used to model the chemical transformation of gas-phase species
Carbonyls	The group of organic compounds that include the aldehydes and the ketones
CCAM	A global stretched grid atmospheric simulation model which has been used extensively to downscale from synoptic to the mesoscale
Chemical species	Chemical species is a common name for atoms, molecules, molecular fragments, free radicals and ions as entities being subjected to a chemical process or to a measurement.
Chemical transformation	Used in this context to describe the processes in the atmosphere where two or more chemical compounds react together producing new compounds.
CMAR	CSIRO Marine and Atmospheric Research (http://www.cmar.csiro.au).
CO	Carbon monoxide
CO_2	Carbon dioxide
Continuous monitoring	Ongoing, (unbroken in time except for standard instrument checks) measurements of the concentration of air pollutant(s) over a time which is typically any period between days and years. This monitoring is often undertaken to establish compliance with licence conditions.
CSIRO	Commonwealth Scientific and Industrial Research Organisation (http://www.csiro.au)
CTM	The CTM is a three-dimensional Eulerian chemical transport model with the capability of modelling the emission, transport, chemical transformation, wet and dry deposition of a coupled gas and aerosol phase atmospheric system.

C4Bz	C4 substituted benzene compounds e.g. 1,4-diethylbenzene
C5Bz	C5 substituted benzene compounds e.g. 1-butyl-2-methylbenzene
DECCW	Department of Environment, Climate Change and Water, NSW
Diffusion	In air pollution meteorology the words dispersion and diffusion are often used interchangeably. This is also the case in this report. However, strictly speaking the two words mean different things. Diffusion refers to dilution of pollutants by turbulent eddies in the atmosphere whose dimensions are smaller than that of a pollutant plume or a puff (see also Dispersion).
Dispersion	Dispersion refers to the movement or transport of pollutants horizontally or vertically by the wind field and their dilution by atmospheric turbulence. Dispersion includes both transport and diffusion of pollutants (see also Diffusion).
DNPH	2,4-Dinitrophenylhydrazine (used for trapping carbonyls)
EC	Elemental carbon (generally in aerosol). The suffix pri indicates that the aerosol is primary aerosol.
Enhancement	This term is applied to the concentration of compounds during events and indicates the increase in concentration above background levels at some time during the event
ETHA	Carbon Bond 5 lumped organic species
Fractional Bias	Used in Figure 7 Martin to add explanation
glc	Ground level concentration
GMR	Greater Metropolitan Region, Sydney
h	Hour of the day
HDD	Heating Degree Days
HNO_3	Nitric acid
IOLE	Carbon Bond 5 lumped organic species
Index Of Agreement	Used in Figure 10. IOA = $1-\frac{\sum_{i=1}^{N}(P_i-O_i)^2}{\sum_{i=1}^{N}(\lvert P_i-O_{mean}\rvert+\lvert O_i-O_{mean}\rvert)^2}$

	Where P_i is the model prediction and O_i is the observed concentration.
Inversion	An atmospheric layer in which potential temperature increases with altitude (e.g. Nocturnal Inversion). These layers are stable and resistant to vertical mixing and hence may restrict the vertical dispersion of pollutants. Properly described as a temperature inversion. The term is often used to refer to the bottom of an inversion layer, i.e. the lowest altitude at which the potential temperature starts increasing.
ISORROPIA-iia	A model framework that calculates the composition and phase state of an ammonia-sulfate-nitrate-chloride-sodium-(calcium-potassium-magnesium)-water inorganic aerosol in thermodynamic equilibrium with gas phase precursors
LOD	Limit Of Detection. The smallest concentration detectable by a measurement system as the concentration of the substance being measured approaches zero.
MDL	Minimum Detectable Limit. The lowest measured concentration in a sample that can be regarded as statistically significant.
mg	Milligram (1 mg = 10^{-3} gram = 0.001 gram). One thousandth of a gram
mg/m^3	Milligram per cubic metre. 1 mg/m^3 = 1000 $\mu g/m^3$
n/a	Not applicable
NH_3	ammonia
NH_4^+	ammonium
NH4	ammonium
NHx	$NH_3 + NH_4^+$
n/r	Not recorded
ng	Nanogram (1 ng = 10^{-9} gram = 0.000000001 gram). One billionth of a gram
ng/m^3	Nanogram per cubic metre. 1 ng/m^3 = 0.001 $\mu g/m^3$
NBL	Neutral Boundary Layer. A type of atmospheric boundary layer (ABL) that forms when winds are strong and/or when there is negligible heating or cooling of the ground (e.g. overcast

	conditions). The turbulence responsible for pollutant mixing under these conditions is generated by wind shear.
NEPM	National Environment Protection Measure see http://www.ephc.gov.au/nepms
NIT	Nitrate
NITx	NO_x + Nitrate
nm	Nanometre (1 nm = 10^{-9} metre = 0.000000001 metre). One billionth of a metre
Nm^3	Normal cubic metres. Volume of a gas sample in cubic metres expressed at 0 degrees Celsius and 1.0 atmosphere (101.325 kilopascals).
NO	Nitric oxide
Nocturnal Inversion	A layer of stable air (see Inversion) of the order of 10m to several 100m depth adjacent to the earth's surface that can form at night over land due to infrared radiative cooling of the surface particularly under the meteorological conditions of a cloudless sky and light winds, and typically erodes quickly after sunrise.
NO_x	Oxides of nitrogen (commonly $NO_x = NO + NO_2$)
NO_y	Oxides of nitrogen (commonly $NO_y = NO + NO_2 + HNO_3$ + Inorganic Nitrate + Organic Oxidised nitrogen containing compounds)
NO_2	Nitrogen dioxide
NPI	National Pollutant Inventory (see http://www.npi.gov.au/)
OC	Organic carbon (generally in aerosol)
OEH	Office of Environment and Heritage, NSW
OLE	Carbon Bond 5 lumped organic species
OVOCs	Partially oxidised VOCs (see entry)
O_3	Ozone
PAR	Carbon Bond 5 lumped organic species
PBL	Planetary Boundary Layer, see ABL.

PM	Used in this report to represent the sampling time 11:00 to 21:00 h.
$PM_{2.5}$	Particulate matter in the air, with an aerodynamic diameter of 2.5 µm (micrometres) or less.
PM_{10}	Particulate matter in the air, with an aerodynamic diameter of 10 µm (micrometres) or less.
Potential Temperature	Potential temperature is a useful measure of the stability of the atmosphere. The potential temperature of a parcel of air at pressure P is the temperature that the parcel would acquire if the parcel of air is brought to a standard reference pressure P_0, usually 1013 hPa adiabatically, that is without heat being either added to or taken from the parcel of air. Potential temperature accounts for the changes in air density due to pressure changes. If the potential temperature increases with height, vertical motions are suppressed and the atmosphere is said to be stably stratified. If the potential temperature decreases with height, a rising parcel of air will continue to rise, generating convective motion and mixing the atmosphere; it is said to be unstable. If the potential temperature remains constant with increasing height, the atmosphere is said to be neutrally stratified. The potential temperature is usually denoted by θ and defined as $q = T(P_0/P)^{0.286}$ where *T* is the temperature in degrees Kelvin of the air at pressure *P* and P_0 is a standard reference pressure (usually 1013 hPa).
ppb	Parts per billion (by volume): 1 ppb = 1/1000 ppm.
ppm	Parts per million (by volume): a unit for the concentration of a gas in the atmosphere based on the mixing ratio approach. A concentration of 1 ppm is equivalent to a volume of 1 cubic metre of pure undiluted gas in 1 million cubic metres of air. The expression ppm (or ppb) is without dimensions. The ppm (or ppb) unit is useful because its value is unaffected by changes in temperature and pressure, and also because many sampling techniques are based on volume concentrations. Concentrations of gaseous compounds can be converted from mixing ratio units, e.g. ppm units (volumetric), to density units, e.g. mg/m^3 (mass/volume), using the following formula: $$C(\mathrm{mg\ m^{-3}}) = \frac{273.15 \times M_w \times C(\mathrm{ppm})}{22.4136 \times (273.15 + T)},$$ where C is the concentration, M_w is the molecular weight of the gas, and T is the ambient temperature in degrees Celsius.

	At a temperature of 0 degrees Celsius, the conversion factors from 1 ppm to mg/m^3 are: benzene (C_6H_6) 3.490; carbon monoxide (CO) 1.250; formaldehyde (HCHO) 1.340; nitrogen dioxide (NO_2) 2.050; nitric oxide (NO) 1.340; ozone (O_3) 2.140; sulfur dioxide (SO_2) 2.860; toluene (C_7H_8) 4.113; xylene (C_8H_{10}) 4.740.
ppt	Parts per trillion (by volume): 1 ppt = 1/1000 ppb.
Primary air pollutant	Pollutant entering the atmosphere directly from a source. A primary air pollutant may react to form a secondary air pollutant (see definition below).
PTR-MS	Proton Transfer Reaction Mass Spectrometer: an instrument used to measure those volatile organic compounds and other chemical species that have a proton affinity greater than water
Quantiles	The fraction (or percent) of points below the given value. That is, the 0.3 (or 30%) quantile is the point at which 30% percent of the data fall below and 70% fall above that value. Certain quantiles have special names. The 0.25-, 0.50-, and 0.75-quantiles are called the first, second and third quartiles. The 0.01-, 0.02-, 0.03, … , 0.98-, 0.99-quantiles are called the first, second, third, … , ninety-eighth, and ninety-ninth percentiles.
QUT	Queensland University of Technology
Rn	Radon
RH	Relative Humidity
RMSE	Root Mean Square Error (the suffixes s and u used in the report represent Systematic and Unsystematic).
SBL	Stable Boundary Layer. A type of atmospheric boundary layer (ABL) that develops during the night when the ground is substantially cooler than the air above it, thus forming a stable temperature gradient with height in the air that opposes vertical motions of air and resulting in little ambient turbulence.
sccm	Standard cubic centimetres (of gas) per minute
Secondary air pollutant	Secondary pollutants are not directly emitted from a process. Rather, secondary air pollutants are formed by physical processes and/or chemical reactions of primary pollutants in the surrounding air. Ozone and many aerosols are usually secondary air pollutants.

Sequencer	The adsorbent tube VOC (ATD-VOC) and Carbonyl Sequencer is an automatic air sampler for sampling of VOCs and Carbonyls using tubes and cartridges simultaneously.
SIA	Secondary Inorganic Aerosol
SINAP	Shanghai Institute of Applied Physics, Chinese Academy of Sciences
SO_x	Sulfur oxides, the sum of SO_2 and SO_3 and Sulfate
SO_2	Sulfur dioxide
SO_4	Sulfate
SOA	Secondary Organic Aerosol
SPS	Sydney Particle Study, conducted in two phases, SPS1 in Summer 2011 and SPS2 in Autumn 2012
SVOCs	Semi-Volatile Organic Compounds These organic compounds co-exist in the gas and liquid or solid phase in the atmosphere under ambient atmospheric conditions. (see also VOCs).
Subsidence Inversion	A temperature inversion that develops aloft as a result of air gradually sinking over a wide area and being warmed by adiabatic compression, usually associated with subtropical high pressure areas.
TAPM	The Air Pollution Model. A prognostic meteorological and air pollution dispersion model developed by CSIRO Atmospheric Research (http://www.dar.csiro.au/tapm). The meteorological component of TAPM predicts the local-scale flow, such as sea breezes and terrain-induced circulations, given the larger-scale synoptic meteorology. The air pollution component uses the model-predicted three-dimensional meteorology and turbulence, and consists of a set of chemical species conservation equations and an optional particle trajectory module.
Temperature inversion	see Inversion
TEOM	Tapered Element Oscillating Microbalance. A device for measuring the mass concentration of aerosol in the air. Aerosol is collected on a Teflon coated borosilicate glass filter vibrating on a hollow tapered element. As the mass collected on the vibrating filter increases the frequency decreases, and is measured and recorded by an electronic circuit. The mass concentration is determined from the relationship between particulate mass and the measured vibration frequency and reported in $\mu g/m^3$ after correction for

	temperature and pressure. Size selective inlets are used to measure PM_{10}, $PM_{2.5}$ etc.
TVOC	Total VOCs. The sum of the concentrations of the speciated VOCs measured.
Ultrafine Particles	Particles with an aerodynamic diameter less than 1 micron.
US EPA	United States Environmental Protection Agency (http://www.epa.gov)
UTC	Coordinated Universal Time
µg	Microgram (1 µg = 10^{-6} gram = 0.000001 gram). One millionth of a gram
µm	Micrometre (1 µm = 10^{-6} metre = 0.000001 metre). One millionth of a metre
µg/m^3	Microgram per cubic metre: a unit for the concentration of a gas or particulate matter in the atmosphere based on the density approach (mass per unit volume of air). Concentrations of gaseous compounds can be converted from density units, e.g. mg/m^3 (mass/volume), to mixing ratio units, e.g. ppm units (volumetric), using the following formula: $$C(\text{ppm}) = \frac{22.4136 \times (273.15 + T) \times C(mg/m^3)}{273.15 \times M_w},$$ where C is the concentration, M_w is the molecular weight of the gas, and T is the ambient temperature in degrees Celsius.
	At a temperature of 0 degrees Celsius, the conversion factors from 1 mg/m^3 to ppm are: benzene (C_6H_6) 0.287; carbon monoxide (CO) 0.800; formaldehyde (HCHO) 0.746; nitrogen dioxide (NO_2) 0.488; nitric oxide (NO) 0.746; ozone (O_3) 0.467; sulfur dioxide (SO_2) 0.350; toluene (C_7H_8) 0.243; xylene (C_8H_{10}) 0.211.
VOCs	Volatile Organic Compounds. These organic compounds have relatively low boiling points and, therefore, readily evaporate into the atmosphere under conditions of normal temperature and pressure.

A8. REFERENCES

Agapides, N.: Methodology used to estimate woodheater emissions for the 2008 NSW Greater Metropolitan Region air emissions inventory, http://www.casanz.org.au/branches/NSWACT%20Documents/Wood%20Smoke%20Transcripts/Agapides_OEH_Wood_Smoke_Workshop_Sept_2012.pdf, 2012.

Alfarra, M. R., Coe, H., Allan, J. D., Bower, K. N., Boudries, H., Canagaratna, M. R., Jimenez, J. L., Jayne, J. T., Garforth, A. A., Li, S.-M., and Worsnop, D. R.: Characterization of urban and rural organic particulate in the Lower Fraser Valley using two Aerodyne Aerosol Mass Spectrometers, Atmos. Environ., 38, 5745-5758, 2004.

Ayers, G. P., Bigg, E. K., Turvey, D. E., and Manton, M. J.: Urban Influence on Condensation Nuclei over a Continent, Atmospheric Environment, 16, 951-954, Doi 10.1016/0004-6981(82)90180-9, 1982.

Azzi, M., Cope, M., and Rae, M.: Sustainable Energy Deployment within the Greater Metropolitan Region. NSW- Environmental Trust 2012.

BoM: Monthly Weather Review, New South Wales, February 2011. Bureau of Meterology, Australia, 2011.

Brunekreef, B., and Forsberg, B.: Epidemiological evidence of effects of coarse airborne particles on health, Eur Respir J, 26, 309-318, Doi 10.1183/09031936.05.00001805, 2005.

Chen, L. C., and Lippmann, M.: Effects of Metals within Ambient Air Particulate Matter (PM) on Human Health, Inhal Toxicol, 21, 1-31, Pii 902580759

Doi 10.1080/08958370802105405, 2009.

Chow, J. C., Watson, J. G., Chen, L. W. A., Chang, M. C. O., Robinson, N. F., Trimble, D., and Kohl, S.: The IMPROVE-A temperature protocol for thermal/optical carbon analysis: maintaining consistency with a long-term database, Journal of the Air & Waste Management Association, 57, 1014-1023, 10.3155/1047-3289.57.9.1014, 2007.

Clarke, A., Kapustin, V., Howell, S., Moore, K., Lienert, B., Masonis, S., Anderson, T., and Covert, D.: Sea-salt size distributions from breaking waves: Implications for marine aerosol production and optical extinction measurements during SEAS, J Atmos Ocean Tech, 20, 1362-1374, 2003.

Cohen, D. D.: Applications of simultaneous IBA techniques to aerosol analysis, Nuclear instruments & methods in physics research. Section B, Beam interactions with materials and atoms, 79, 385-388, 1993.

Cohen, D. D.: Elemental analysis by PIXE and other IBA techniques and their application to source fingerprinting of atmospheric fine particle pollution, Nuclear instruments & methods in physics research. Section B, Beam interactions with materials and atoms, 109-110, 218-226, 10.1016/0168-583x(95)00912-4, 1996.

Cohen, D. D.: Characterisation of atmospheric fine particles using IBA techniques, Nuclear instruments & methods in physics research. Section B, Beam interactions with materials and atoms, 136-138, 14-22, 1998.

Cope, M. E., Hess, G. D., Lee, S., Tory, K., Azzi, M., Carras, J., Lilley, W., Manins, P. C., Nelson, P., Ng, L., Puri, K., Wong, N., Walsh, S., and Young, M.: The Australian Air Quality Forecasting System. Part I: Project description and early outcomes, J Appl Meteorol, 43, 649-662, Doi 10.1175/2093.1, 2004.

DECCW: Air emissions inventory for the Greater Metropolitan Region in New South Wales; Calendar year 2003, 2007.

Donahue, N. M., Robinson, A. L., Stanier, C. O., and Pandis, S. N.: Coupled partitioning, dilution, and chemical aging of semivolatile organics, Environ Sci Technol, 40, 2635-2643, Doi 10.1021/Es052297c, 2006.

Duffy, B. L., Nelson, P. F., Ye, Y., Weeks, I. A., and Galbally, I. E.: Emissions of Benzene, Toluene, Xylenes and 1,3 Butadiene from a Representative Portion of the Australian Car Fleet, Atmospheric Environment, 32, 2693-2704, 1998.

EA: Environment Australia. Technical Report No. 5: Emissions from Domestic Solid Fuel Burning Appliances. Canberra, Australia, Consultancy by CSIRO Atmospheric Research authors: Gras J.L., Meyer C. P., Weeks I. A., Gillett R. W., Galbally I. E., Todd, J., Carnovale F., Joynt R. C., Hinwood A., Berko H., Brown S. 95 p + appendices, 2002.

Fountoukis, C., and Nenes, A.: ISORROPIA II: a computationally efficient thermodynamic equilibrium model for K+-Ca2+-Mg2+-Nh(4)(+)-Na+-SO42--NO3--Cl--H2O aerosols, Atmos Chem Phys, 7, 4639-4659, 2007.

Goldstein, A. H., and Galbally, I. E.: Known and unexplored organic constituents in the earth's atmosphere, Environ Sci Technol, 41, 1514-1521, Doi 10.1021/Es072476p, 2007.

Gong, S. L., Barrie, L. A., Prospero, J. M., Savoie, D. L., Ayers, G. P., Blanchet, J. P., and Spacek, L.: Modeling sea-salt aerosols in the atmosphere .2. Atmospheric concentrations and fluxes, J Geophys Res-Atmos, 102, 3819-3830, Doi 10.1029/96jd03401, 1997.

Gong, S. L.: A parameterization of sea-salt aerosol source function for sub- and super-micron particles, Global Biogeochem Cy, 17, Artn 1097

Doi 10.1029/2003gb002079, 2003.

Grahame, T. J., and Schlesinger, R. B.: Evaluating the health risk from secondary sulfates in eastern North American regional ambient air particulate matter, Inhal Toxicol, 17, 15-27, Doi 10.1080/08958370590885672, 2005.

Harrison, R. M., Smith, D. J. T., and Kibble, A. J.: What is responsible for the carcinogenicity of PM2.5?, Occup Environ Med, 61, 799-805, DOI 10.1136/oem.2003.010504, 2004.

Hennigan, C. J., Sullivan, A. P., Collett, J. L., and Robinson, A. L.: Levoglucosan stability in biomass burning particles exposed to hydroxyl radicals, Geophysical Research Letters, 37, Artn L09806

Doi 10.1029/2010gl043088, 2010.

Hildemann, L. M., Markowski, G. R., Jones, M. C., and Cass, G. R.: Submicrometer Aerosol Mass Distributions of Emissions from Boilers, Fireplaces, Automobiles, Diesel Trucks, and Meat-Cooking Operations, Aerosol Sci Tech, 14, 138-152, 1991.

Hoffmann, D., Tilgner, A., Iinuma, Y., and Herrmann, H.: Atmospheric Stability of Levoglucosan: A Detailed Laboratory and Modeling Study, Environ Sci Technol, 44, 694-699, Doi 10.1021/Es902476f, 2010.

Hurley, P. J.: TAPM V4. Part 1. Technical description, CSIRO Marine and Atmospheric Research Internal Report, 2008.

Janssen, N. A. H., Hoek, G., Simic-Lawson, M., Fischer, P., van Bree, L., ten Brink, H., Keuken, M., Atkinson, R. W., Anderson, H. R., Brunekreef, B., and Cassee, F. R.: Black Carbon as an Additional Indicator of the Adverse Health Effects of Airborne Particles Compared with PM10 and PM2.5, Environ Health Persp, 119, 1691-1699, Doi 10.1289/Ehp.1003369, 2011.

Kessler, S. H., Smith, J. D., Che, D. L., Worsnop, D. R., Wilson, K. R., and Kroll, J. H.: Chemical Sinks of Organic Aerosol: Kinetics and Products of the Heterogeneous Oxidation of Erythritol and Levoglucosan, Environ Sci Technol, 44, 7005-7010, Doi 10.1021/Es101465m, 2010.

Keywood, M., Guyes, H., Selleck, P., and Gillett, R.: Quantification of secondary organic aerosol in an Australian urban location, Environ Chem, 8, 115-126, Doi 10.1071/En10100, 2011.

Keywood, M. D., Galbally, I., Suzanne Crumeyrolle, Branka Miljevic, Kate Boast, Scott Chambers, Min Cheng, Erin Dunne, Rosemary Fedele, Rob Gillett, Alan Griffiths, James Harnwell, Sarah Lawson, Suzie Molloy, Jenny Powell, Fabienne Reisen, Zoran Ristovski, Paul Selleck, Jason

Ward, Chuanfu Zhang, Zen, J., Cope, M., and Emmerson, K.: Sydney Particle Study- Stage-I: Executive Summary, 2012.
Kulmala, M., Dal Maso, M., Makela, J. M., Pirjola, L., Vakeva, M., Aalto, P., Miikkulainen, P., Hameri, K., and O'Dowd, C. D.: On the formation, growth and composition of nucleation mode particles, Tellus B, 53, 479-490, 2001.
Kulmala, M.: How particles nucleate and grow, Science, 302, 1000-1001, 2003.
Kumar, P., Robins, A., Vardoulakis, S., and Britter, R.: A review of the characteristics of nanoparticles in the urban atmosphere and the prospects for developing regulatory controls, Atmospheric Environment, 44, 5035-5052, DOI 10.1016/j.atmosenv.2010.08.016, 2010.
Kumar, P., Ketzel, M., Vardoulakis, S., Pirjola, L., and Britter, R.: Dynamics and dispersion modelling of nanoparticles from road traffic in the urban atmospheric environment-A review, J Aerosol Sci, 42, 580-603, DOI 10.1016/j.jaerosci.2011.06.001, 2011.
Laden, F., Neas, L. M., Dockery, D. W., and Schwartz, J.: Association of fine particulate matter from different sources with daily mortality in six US cities, Environ Health Persp, 108, 941-947, Doi 10.1289/Ehp.00108941, 2000.
Linfoot, S., and Freeman, K.: Measurement of ambient levels of selected air toxics in the greater Sydney region. Proceedings of the 14th International Clean Air and Environment Conference, Melbourne, Australia. Clean Air Society of Australia and New Zealand, p. 324-330., 1998.
Lu, H., and Shao, Y. P.: A new model for dust emission by saltation bombardment, J Geophys Res-Atmos, 104, 16827-16841, Doi 10.1029/1999jd900169, 1999.
Mann, G. W., Carslaw, K. S., Spracklen, D. V., Ridley, D. A., Manktelow, P. T., Chipperfield, M. P., Pickering, S. J., and Johnson, C. E.: Description and evaluation of GLOMAP-mode: a modal global aerosol microphysics model for the UKCA composition-climate model, Geosci Model Dev, 3, 519-551, DOI 10.5194/gmd-3-519-2010, 2010.
McGregor, J. L., and Dix, M. R.: An updated description of the Conformal-Cubic atmospheric model, High Resolution Numerical Modelling of the Atmosphere and Ocean, 51-75, 2008.
Meyer, C. P., Luhar, A. K., and Mitchell, R. M.: Biomass burning emissions over northern Australia constrained by aerosol measurements: I—Modelling the distribution of hourly emissions, Atmospheric Environment, 42, 1629-1646, 10.1016/j.atmosenv.2007.10.089, 2008.
Meyer, C. P., Reisen, F., Keywood, M. D., and Crumeyrolle, S.: Impacts of smoke from regeneration burning on air quality in the Huon Valley, Tasmania, 2011.
Ng, N. L., Canagaratna, M. R., Jimenez, J. L., Zhang, Q., Ulbrich, I. M., and Worsnop, D. R.: Real-Time Methods for Estimating Organic Component Mass Concentrations from Aerosol Mass Spectrometer Data, Environ. Sci. Technol., 45, 910-916, 10.1021/es102951k, 2011.
Norris, G., Vedantham, R., Wade, K., Brown, S., Prouty, J., and Foley, C.: EPA Positive matrix factorization (PMF) 3.0 - Fundamentals and User Guide, 2008.
Ostro, B., Tobias, A., Cluerol, X., Alastuey, A., Amato, F., Pey, J., Perez, N., and Sunyer, J.: The Effects of Particulate Matter Sources on Daily Mortality: A Case-Crossover Study of Barcelona, Spain, Environ Health Persp, 119, 1781-1787, Doi 10.1289/Ehp.1103618, 2011.
Pehkonen, S. O., and Lin, C. J.: Aqueous photochemistry of mercury with organic acids, J Air Waste Manage, 48, 144-150, 1998.
Pope, C. A., Burnett, R. T., Thun, M. J., Calle, E. E., Krewski, D., Ito, K., and Thurston, G. D.: Lung cancer, cardiopulmonary mortality, and long-term exposure to fine particulate air pollution, Jama-J Am Med Assoc, 287, 1132-1141, DOI 10.1001/jama.287.9.1132, 2002.
Pope, C. A., and Dockery, D. W.: Health effects of fine particulate air pollution: Lines that connect, J Air Waste Manage, 56, 709-742, 2006.
Pope, C. A., Ezzati, M., and Dockery, D. W.: Fine-Particulate Air Pollution and Life Expectancy in the United States., New Engl J Med, 360, 376-386, Doi 10.1056/Nejmsa0805646, 2009.

Radhi, M., Box, M. A., Box, G. P., Mitchell, R. M., Cohen, D. D., Stelcer, E., and Keywood, M. D.: Optical, physical and chemical characteristics of Australian continental aerosols: results from a field experiment, Atmospheric Chemistry and Physics, 10, 5925-5942, 10.5194/acp-10-5925-2010, 2010.

Ruckerl, R., Schneider, A., Breitner, S., Cyrys, J., and Peters, A.: Health effects of particulate air pollution: A review of epidemiological evidence, Inhal Toxicol, 23, 555-592, Doi 10.3109/08958378.2011.593587, 2011.

Sarwar, G., Luecken, D., Yarwood, G., Whitten, G. Z., and Carter, W. P. L.: Impact of an updated carbon bond mechanism on predictions from the CMAQ modeling system: Preliminary assessment, J Appl Meteorol Clim, 47, 3-14, Doi 10.1175/2007jamc1393.1, 2008.

Sarwar, G., Appel, K. W., Carlton, A. G., Mathur, R., Schere, K., Zhang, R., and Majeed, M. A.: Impact of a new condensed toluene mechanism on air quality model predictions in the US, Geosci Model Dev, 4, 183-193, DOI 10.5194/gmd-4-183-2011, 2011.

Seigneur, C., Karamchandani, P., Lohman, K., Vijayaraghavan, K., and Shia, R. L.: Multiscale modeling of the atmospheric fate and transport of mercury, J Geophys Res-Atmos, 106, 27795-27809, Doi 10.1029/2000jd000273, 2001.

Seinfeld, J. H., and Pandis, S. N.: Atmospheric chemistry and physics : from air pollution to climate change, Wiley, New York, xxvii, 1326 p. pp., 1998.

Song, C. H., and Carmichael, G. R.: The aging process of naturally emitted aerosol (sea-salt and mineral aerosol) during long range transport, Atmospheric Environment, 33, 2203-2218, 1999.

Torre, P., Eriksen, P., and Bardsley, T.: 'Volatile Organic Compound analysis in an industrial location in Melbourne', Proceedings of the 13th International Clean Air and Environment Conference, Adelaide, Australia. Clean Air Society of Australia and New Zealand, p. 256-261., 2000.

Tsai, F. C., Apte, M. G., and Daisey, J. M.: An exploratory analysis of the relationship between mortality and the chemical composition of airborne particulate matter, Inhal Toxicol, 12, 121-135, 2000.

Tsimpidi, A. P., Karydis, V. A., Zavala, M., Lei, W., Molina, L., Ulbrich, I. M., Jimenez, J. L., and Pandis, S. N.: Evaluation of the volatility basis-set approach for the simulation of organic aerosol formation in the Mexico City metropolitan area, Atmos Chem Phys, 10, 525-546, 2010.

The Centre for Australian Weather and Climate Research is a partnership between CSIRO and the Bureau of Meteorology.